

© 2008

TAMMY J. SICILIANO

ALL RIGHTS RESERVED

A STABILITY COMPARISON AND ANTIMICROBIAL EVALUATION OF GOLD  
N-HETEROCYCLIC CARBENES AND THEIR SILVER PRECURSORS

A Dissertation

Presented to

The Graduate Faculty of The University of Akron

In Partial Fulfillment

of the Requirements for the Degree

Doctor of Philosophy

Tammy J. Siciliano

August, 2008

A STABILITY COMPARISON AND ANTIMICROBIAL EVALUATION OF GOLD  
N-HETEROCYCLIC CARBENES AND THEIR SILVER PRECURSORS

Tammy J. Siciliano

Dissertation

Approved:

Accepted:

---

Advisor  
Dr. Wiley J. Youngs

---

Department Chair  
Dr. Kim C. Calvo

---

Co-Advisor  
Dr. Claire A. Tessier

---

Dean of the College  
Dr. Ronald F. Levant

---

Committee Member  
Dr. Christopher Ziegler

---

Dean of the Graduate School  
Dr. George R. Newkome

---

Committee Member  
Dr. Michael Taschner

---

Date

---

Committee Member  
Dr. Amy Milsted

## ABSTRACT

The synthesis of the first metal N-heterocyclic carbene (NHC) complexes by Öfele and Wanzlick started an exciting new class of coordination chemistry. The isolation of the first free carbene by Arduengo provided a novel route from which numerous NHC metal complexes have been made. Among their many applications, the potential for therapeutic use has been an area of growing interest and a topic of this review. The first gold NHC complex synthesized from its silver NHC precursor by Lin revolutionized the frontier for simple gold NHC generation to which this review is rooted.

Chapter 1 provides a review on past and current routes by which gold(I) and gold(III) NHC complexes have been synthesized. The discussion focuses on their structural comparisons and a detailed history of the medicinal use of gold is presented before exploring their current role in the field. In Chapter 2, the stability of gold-(bis)NHC complexes in aqueous and physiological solution is discussed in comparison to their silver-(bis)NHC precursors. Silver has been used as an antimicrobial agent for thousands of years and the antimicrobial properties of both are explored. Chapter 3 focuses further on water stability and antimicrobial properties as it is applied to silver acetate NHC complexes in comparison to silver- and gold-(bis)NHC analogues.

Imidazolium salts, NHC precursors, have been shown to possess antimicrobial properties. Chapter 4 investigates these properties on synthesized imidazolium salts with a variety of functional groups on varying positions of the imidazole ring. There are several different types of silver dressings commercially available. Chapter 5 evaluates the antimicrobial effectiveness of eight such dressings and comparisons are made.

## DEDICATION

To my wonderful husband and adorable children,  
Dave Siciliano and Nicholas and Madelyn

## ACKNOWLEDGEMENTS

I would like to take this time to extend my deepest gratitude to everyone responsible in contributing their time, service and friendship for making this degree possible. I would first like to thank my advisor, Professor Wiley J. Youngs for his continued support and guidance over the last 5 years. He always had many words of wisdom for me and I will always watch what shoes I wear on a boat and will eat the steak dinner served when I ordered a hamburger. I would also like to acknowledge my co-advisor, Professor Claire A. Tessier for all of her invaluable help, knowledge and kindness. She is an incredible role model and I have appreciated her continued support. I would like to acknowledge Professors William Donovan and Kim Calvo for their guidance and assistance in helping me to complete my first year of teaching freshman chemistry. I would also like to extend a thank you to Dr. Amy Milsted for her assistance with antimicrobial studies. I would also like to thank Dr. Venkat Dudipala for his assistance with NMR studies.

I would like to thank the members of Youngs group: Dr. Doug Medvetz, Dr. Khadijah Hindi, Paul Custer, Amanda Knapp, Supat Moolsin, Sujeewani Ekanayake, Michael Deblock, Brian Wright and Nikki Robishaw. Our daily interactions have made my graduate life much more fun. I would also like to

thank our current group post doc, Dr. Matthew Panzner for all of his helpful guidance. I also want to acknowledge past group members: Dr. Jered Garrison and Dr. Semih Durmus for their kindness and continued friendship, and a special thank you to Dr. Abdulkareem Melaiye for all his help in teaching me the antimicrobial testing. An extra special thank you to the girls, Khadijah and Nikki, I will always value our friendship and will miss our lunches. I hope you keep in touch. The sincerest thank you to my friend, Sarah Walton, the hardships she has endured have helped me to appreciate my accomplishments and her continued courage and fighting spirit have been an inspiration.

I would especially like to thank the members of my family for all of their love and unconditional support. My grandmother, Jeannine Morrison for always loving and caring for me and my children. My mother, Patti Paul for her loving and giving nature. My cousin, Carrie Rogan for her friendship and early morning conversations. My father, Ray Paul for his humor and concern, although he has no understanding of what it is I do. I have truly been blessed with a loving and supporting family and there are too many of you to list, but take note that you have all influenced me and I thank you for your assistance in my accomplishments.

Finally I would like to thank my amazing husband, Dave Siciliano. He is my best friend and love of my life. His love and encouragement have meant the world to me. I cannot even begin to express how grateful to God I am for having him in my life. I would also like to thank my two beautiful children, Nicholas and Madelyn. They are my life and I thank God for them every day.



## TABLE OF CONTENTS

	Page
LIST OF TABLES.....	xvi
LIST OF FIGURES.....	xviii
LIST OF SCHEMES.....	xxii
LIST OF EQUATIONS.....	xxiv
CHAPTER	
I. GOLD N-HETEROCYCLIC CARBENE COMPLEXES OF THE IMIDAZOLYL TYPE AND EXPLORATION OF THE MEDICINAL APPLICATIONS OF GOLD .....	1
1.1 Introduction.....	1
1.2 Synthesis of Gold(I) N-Heterocyclic Carbene Complexes .....	3
1.2.1 Cleavage of Electron-Rich Olefins .....	3
1.2.2 Generation from the Free Carbene .....	4
1.2.3 Deprotonation ( <i>In Situ</i> ) of Imidazolium Salts .....	6
1.2.4 Protonation or Alkylation of Imidazolyl Aurate Compounds .....	10
1.2.5 Transfer from Tungsten-NHC Complexes.....	12
1.2.6 Transfer from Manganese-NHC Complexes .....	13
1.2.7 Transmetallation from NHC-Silver(I) Complexes .....	14

1.2.8 A Comparison of Synthesis Methods and Select Characterization Data for Similar NHC-Gold(I) Complexes .....	20
1.3 Synthesis of Gold(III) N-Heterocyclic Carbenes .....	23
1.4 Characterizational Comparison of Gold(III) N-Heterocyclic Carbenes with Their NHC-Gold(I) Precursors .....	26
1.5 Medicinal Applications of Gold .....	27
1.5.1 History of Gold Use.....	27
1.5.2 Biological Activity of Gold.....	29
1.5.3 The Use of Gold as an Antiarthritic .....	30
1.5.4 The Use of Gold as an Anticancer Agent .....	37
1.5.5 Gold as an Antimicrobial Agent.....	41
1.6 Medicinal Applications of NHC-Gold Complexes.....	45
1.6.1 Anticancer Properties of Gold NHC Complexes .....	45
1.6.2 Antimicrobial Properties of Gold NHCs .....	48
1.7 Toxicity of Gold and Gold-Containing Compounds.....	50
1.7.1 Metallic Gold Toxicity .....	50
1.7.2 Gold Toxicity Associated with Rheumatoid Arthritis Treatment.....	51
1.8 Conclusion.....	53
II. SYNTHESIS, WATER STABILITY AND ANTIMICROBIAL PROPERTIES OF GOLD-NHC COMPLEXES AND THEIR SILVER-NHC PRECURSORS .....	55
2.1 Introduction.....	55

2.2	Synthesis and Characterization of Silver(I)-(bis)NHC Complexes .....	56
2.3	Water Stability of Silver(I)-(bis)NHC Complexes .....	64
2.4	Synthesis and Characterization of Gold(I)-(bis)NHC Complexes .....	70
2.5	Water Stability of Gold(I)-(bis)NHC Complexes.....	78
2.5.1	Stability of Select Gold-NHC Complexes in an Aqueous Environment.....	78
2.5.2	Stability of Gold Complex 2.9 in Physiological Sodium Chloride Solution .....	83
2.6	Antimicrobial Comparison of Gold(I)-NHC Complexes and Their Silver(I)-NHC Precursors .....	87
2.6.1	Minimum Inhibitory Concentration.....	87
2.6.2	Minimum Bactericidal Concentration.....	89
2.7	Conclusion.....	91
2.8	Experimental Section .....	91
2.8.1	General Considerations .....	91
2.8.2	X-Ray Crystallographic Structure Determination Details.....	93
2.8.3	Synthesis of <b>2.1</b> (C <sub>5</sub> H <sub>9</sub> N <sub>3</sub> O <sub>3</sub> ) .....	93
2.8.4	Synthesis of <b>2.2</b> (C <sub>5</sub> H <sub>3</sub> N <sub>3</sub> Cl <sub>2</sub> O <sub>3</sub> ) .....	94
2.8.5	Synthesis of <b>2.3</b> (C <sub>5</sub> H <sub>8</sub> N <sub>2</sub> ClI).....	94
2.8.6	Synthesis of <b>2.4</b> (C <sub>5</sub> H <sub>8</sub> N <sub>3</sub> O <sub>3</sub> Cl) .....	95
2.8.7	Synthesis of <b>2.5</b> (C <sub>10</sub> H <sub>16</sub> N <sub>5</sub> O <sub>3</sub> Ag) .....	96

2.8.8 Synthesis of <b>2.6</b> ( $C_{10}H_{12}N_5O_3Cl_4Ag$ ) .....	97
2.8.9 Synthesis of <b>2.7</b> ( $C_{10}H_{16}N_6O_6Ag_2$ ) .....	97
2.8.10 Synthesis of <b>2.8</b> ( $C_{10}H_{14}N_6O_6Cl_2Ag_2$ ) .....	98
2.8.11 Synthesis of <b>2.9</b> ( $C_{10}H_{16}N_5O_3Au$ ) .....	99
2.8.12 Synthesis of <b>2.10</b> ( $C_{10}H_{12}N_5O_3Cl_4Au$ ) .....	100
2.8.13 Synthesis of <b>2.12</b> ( $C_{10}H_{12}N_6O_6Cl_4AuAg$ ) .....	101
2.8.14 Synthesis of <b>2.13</b> ( $C_{10}H_{14}N_5O_3Cl_2Au$ ) .....	102
2.8.15 Antimicrobial Testing.....	102
2.8.16 Determination of MIC .....	103
2.8.17 Determination of MBC.....	103
 III. SYNTHESIS AND COMPARISON OF WATER STABILITY AND ANTIMICROBIAL PROPERTIES OF SILVER ACETATE N-HETEROCYCLIC CARBENE COMPLEXES .....	     104
3.1 Introduction.....	104
3.2 Synthesis and characterization of silver acetate NHC complexes.....	105
3.3 Water Stability of Silver Complexes .....	111
3.3.1 Water Stability of Silver Acetate NHC Complexes .....	111
3.3.2 Water Stability Comparison of Silver Acetate NHC Complexes with Their (bis)NHC-Silver and –Gold Analogs .....	 116
3.4 Antimicrobial Properties of Silver Acetate NHC Complexes in Comparison with Gold(I)-NHC Complexes and Their Silver(I)-NHC Precursors.....	117

3.4.1 Antimicrobial Properties of Silver Acetate NHC Complexes .....	117
3.4.2 Antimicrobial Comparison of Silver Acetate NHC Complexes with (bis)NHC-Gold(I) Complexes and Their (bis)NHC-Silver(I) Precursors .....	120
3.5 Conclusion.....	121
3.6 Experimental Section .....	121
3.6.1 General Considerations .....	122
3.6.2 X-Ray Crystallographic Structure Determination Details.....	123
3.6.3 Synthesis of <b>3.3</b> (C <sub>5</sub> H <sub>9</sub> I) .....	123
3.6.4 Synthesis of <b>3.4</b> (C <sub>7</sub> H <sub>11</sub> N <sub>2</sub> O <sub>2</sub> Ag) .....	124
3.6.5 Synthesis of <b>3.5</b> (C <sub>14</sub> H <sub>11</sub> Cl <sub>2</sub> N <sub>3</sub> O <sub>2</sub> ).....	125
3.6.6 Synthesis of <b>3.6</b> (C <sub>15</sub> H <sub>14</sub> Cl <sub>2</sub> N <sub>3</sub> O <sub>2</sub> I).....	126
3.6.7 Synthesis of <b>3.7</b> (C <sub>17</sub> H <sub>16</sub> Cl <sub>2</sub> N <sub>3</sub> O <sub>2</sub> Ag) .....	127
3.6.8 Antimicrobial Testing.....	128
3.6.9 Determination of MIC .....	128
3.6.10 Determination of MBC.....	128
IV. THE SYNTHESIS AND EXPLORATION OF ANTIMICROBIAL PROPERTIES OF IMIDAZOLIUM SALTS.....	129
4.1 Introduction.....	129
4.2 Synthesis and Characterization of Imidazolium Salts .....	132
4.3 Antimicrobial Properties of Imidazolium Salts.....	138

4.3.1	Minimum Inhibitory Concentration.....	138
4.3.2	Minimum Bactericidal Concentration.....	141
4.4	Conclusion.....	143
4.5	Experimental Section .....	143
4.5.1	General Considerations .....	143
4.5.2	X-Ray Crystallographic Structure Determination Details.....	144
4.5.3	Synthesis of <b>4.1</b> ( $C_6H_{11}N_2OI$ ) .....	145
4.5.4	Synthesis of <b>4.2</b> ( $C_7H_{13}N_2O_2I$ ).....	146
4.5.5	Synthesis of <b>4.3</b> ( $C_8H_{15}N_2O_3Br$ ) .....	146
4.5.6	Synthesis of <b>4.4</b> ( $C_{31}H_{31}N_2O_2B$ ) .....	147
4.5.7	Synthesis of <b>4.5</b> ( $C_{15}H_{16}N_3O_2Br$ ).....	148
4.5.8	Synthesis of <b>4.6</b> ( $C_{15}H_{16}N_3O_2PF_6$ ).....	148
4.5.9	Antimicrobial Testing.....	149
4.5.10	Determination of MIC .....	150
4.5.11	Determination of MBC.....	150
V.	COMPARISON OF THE ANTIMICROBIAL ACTIVITY OF SILVER DRESSINGS USING MIC, MBC AND KIRBY BAUER METHODS .....	151
5.1	Introduction.....	151
5.2	Description of Silver Dressings.....	152
5.3	Kirby Bauer Disc Diffusion Method .....	153

5.4 MIC Method Evaluation .....	155
5.5 MBC Method Evaluation.....	158
5.6 Conclusion.....	159
5.7 Experimental Section .....	160
5.7.1 General Considerations .....	160
5.7.2 Kirby Bauer Testing .....	160
5.7.3 Antimicrobial Testing.....	161
5.7.4 Determination of MIC .....	162
5.7.5 Determination of MBC.....	162
VI. CONCLUSION AND FUTURE DIRECTIONS .....	163
BIBLIOGRAPHY.....	166
APPENDICES .....	175
APPENDIX A: SUPPLEMENTARY MATERIAL FOR THE X-RAY CRYSTAL STRUCTURE OF $C_5H_8N_3O_3Cl$ ( <b>2.4</b> ).....	176
APPENDIX B: SUPPLEMENTARY MATERIAL FOR THE X-RAY CRYSTAL STRUCTURE OF $C_{10}H_{16}N_5O_3Ag$ ( <b>2.5</b> ).....	180
APPENDIX C: SUPPLEMENTARY MATERIAL FOR THE X-RAY CRYSTAL STRUCTURE OF $C_{10}H_{12}N_5O_3Cl_4Ag$ ( <b>2.6</b> ) .....	185
APPENDIX D: SUPPLEMENTARY MATERIAL FOR THE X-RAY CRYSTAL STRUCTURE OF $C_{10}H_{16}N_6O_6Ag_2$ ( <b>2.7</b> ).....	190
APPENDIX E: SUPPLEMENTARY MATERIAL FOR THE X-RAY CRYSTAL STRUCTURE OF $C_{10}H_{14}N_6O_6Cl_2Ag_2$ ( <b>2.8</b> ).....	194

APPENDIX F: SUPPLEMENTARY MATERIAL FOR THE X-RAY CRYSTAL STRUCTURE OF $C_{10}H_{16}N_5O_3Au$ (2.9) .....	198
APPENDIX G: SUPPLEMENTARY MATERIAL FOR THE X-RAY CRYSTAL STRUCTURE OF $C_{10}H_{12}N_5O_3Cl_4Au$ (2.10) .....	203
APPENDIX H: SUPPLEMENTARY MATERIAL FOR THE X-RAY CRYSTAL STRUCTURE OF $C_5H_9N_2Cl_4Au$ (2.11) .....	209
APPENDIX I: SUPPLEMENTARY MATERIAL FOR THE X-RAY CRYSTAL STRUCTURE OF $C_{10}H_{12}N_6O_6Cl_4AuAg$ (2.12) .....	213
APPENDIX J: SUPPLEMENTARY MATERIAL FOR THE X-RAY CRYSTAL STRUCTURE OF $C_7H_{11}N_2O_2Ag$ (3.4) .....	221
APPENDIX K: SUPPLEMENTARY MATERIAL FOR THE X-RAY CRYSTAL STRUCTURE OF $C_{14}H_{11}N_3O_2Cl_2$ (3.5) .....	228
APPENDIX L: SUPPLEMENTARY MATERIAL FOR THE X-RAY CRYSTAL STRUCTURE OF $C_{15}H_{14}N_3O_2Cl_2I$ (3.6) .....	234
APPENDIX M: SUPPLEMENTARY MATERIAL FOR THE X-RAY CRYSTAL STRUCTURE OF $C_{17}H_{16}N_3O_2Cl_2Ag$ (3.7) .....	239
APPENDIX N: SUPPLEMENTARY MATERIAL FOR THE X-RAY CRYSTAL STRUCTURE OF $C_6H_{11}N_2OI$ (4.1) .....	248
APPENDIX O: SUPPLEMENTARY MATERIAL FOR THE X-RAY CRYSTAL STRUCTURE OF $C_{31}H_{31}N_2O_2B$ (4.4) .....	252
APPENDIX P: SUPPLEMENTARY MATERIAL FOR THE X-RAY CRYSTAL STRUCTURE OF $C_{15}H_{16}N_3O_2PF_6$ (4.6) .....	259
APPENDIX Q: ABBREVIATIONS AND ACCRONYMS .....	265



## LIST OF TABLES

Table	Page
Table 1-1 A yield (%) synthesis method comparison for the R <sub>2</sub> ImAuCl structure. Prepared in part from a table in reference 21 .....	20
Table 1-2 A comparison of selected <sup>13</sup> C NMR spectra resonances (ppm), bond distances (Å) and bond angles (°) for the R <sub>2</sub> ImAuCl structure. Combined table from those in references 17, 21 and 33. ....	21
Table 1-3 A comparison of selected <sup>13</sup> C NMR spectra resonances (ppm), <sup>31</sup> P NMR spectra resonances, bond distances (Å) and bond angles (°) for (mono)NHC-gold(I) phosphine complexes. Prepared in part from a table in reference 21. ....	22
Table 1-4 A comparison of selected <sup>13</sup> C NMR spectra resonances (ppm), bond distances (Å) and yields (%) for NHC-gold(III) complexes. Combined table from those in references 13 and 40. ....	25
Table 1-5 A comparison of selected <sup>13</sup> C NMR spectra resonances (ppm) for NHC-gold(III) complexes and NHC-gold(I) precursors <sup>40</sup> .....	26
Table 2-1 Selected bond distances (Å) and angles (°) for <b>2.5-2.8</b> .....	63
Table 2-2 A comparison of selected <sup>13</sup> C NMR spectra resonances (ppm), bond distances (Å) and angles (°) for <b>2.5, 2.6, 2.9</b> and <b>2.10</b> .....	73
Table 2-3 Selected bond distances (Å) and angles (°) for <b>2.12, 2.10, 2.7</b> and <b>2.8</b> .....	77
Table 2-4 MIC values of <b>2.1, 2.2, 2.4-2.10</b> and <b>2.13</b> in mmol/L .....	88
Table 2-5 MBC results for <b>2.5-2.10</b> and <b>2.13</b> in mmol/L .....	90
Table 3-1 A comparison of selected <sup>13</sup> C NMR spectra resonances (ppm), bond distances (Å) and angles (°) for <b>3.2, 3.4, 3.7, 3.8</b> and <b>3.9</b> .....	111
Table 3-2 Stability of complexes <b>3.2, 3.4, 3.8</b> and <b>3.9</b> in D <sub>2</sub> O.....	112

Table 3-3 MIC values of <b>3.1-3.4</b> and <b>3.6-3.11</b> in mmol/L .....	118
Table 3-4 MBC values of <b>3.2,3.4</b> and <b>3.7-3.9</b> in mmol/L.....	119
Table 4-1 MIC values of imidazole, <b>4.1-4.5</b> and <b>4.7-4.11</b> in mmol/L.....	139
Table 4-2 MBC values of imidazole, <b>4.1-4.5</b> and <b>4.7-4.11</b> in mmol/L .....	142
Table 5-1 Properties of the evaluated eight commercially available dressings .....	153
Table 5-2 Zone of Inhibition (cm).....	154
Table 5-3 MIC results for silver dressings (+) turbidity or (-) no turbidity .....	156
Table 5-4 MIC results for silver dressings (+) turbidity or (-) no turbidity .....	157
Table 5-5 MIC results for silver dressings (+) turbidity or (-) no turbidity .....	157
Table 5-6 MBC results of silver dressings (S) bacteriostatic or (C) bactericidal .....	159

## LIST OF FIGURES

Figure	Page
Figure 1-1 Imidazole .....	2
Figure 1-2 (bis)NHC-gold(I) complex from the free carbene <sup>16</sup> .....	5
Figure 1-3 Neutral gold(I) complexes from the free carbene <sup>17</sup> .....	6
Figure 1-4 (tetra)NHC-dinuclear gold complexes from the free carbene <sup>19</sup> .....	6
Figure 1-5 NHC-gold phosphine complex <sup>20</sup> .....	7
Figure 1-6 (bis)NHC-gold complexes via deprotonation <sup>22</sup> .....	9
Figure 1-7 Dinuclear gold(I) complexes <sup>23</sup> .....	10
Figure 1-8 Chloro derivatives of 43 <sup>31</sup> .....	15
Figure 1-9 Dinuclear NHC-gold complexes via silver transmetallation <sup>34,35</sup> .....	19
Figure 1-10 The R <sub>2</sub> ImAuCl structure .....	20
Figure 1-11 (bis)NHC-gold(III) complexes and NHC-gold(I) precursors <sup>13</sup> .....	23
Figure 1-12 Gold sodium thiosulfate .....	29
Figure 1-13 Simplified formulation of sodium aurothiopropanol sulfonate <sup>45</sup> .....	31
Figure 1-14 Simplified formulations of gold sodium thiomalate (a) and gold thioglucose (b) <sup>8</sup> .....	32
Figure 1-15 Polymeric ring structure for gold(I) thiolate complexes <sup>45</sup> .....	32
Figure 1-16 Auranofin <sup>8</sup> .....	33
Figure 1-17 The gold(dppe) complex evolution <sup>9</sup> .....	38

Figure 1-18 Gold(III) damp complexes <sup>9</sup> .....	39
Figure 1-19 Folic acid .....	41
Figure 1-20 Evaluated gold phosphorus ylide compounds .....	44
Figure 1-21 NHC-gold(I) auranofin analogues <sup>21</sup> .....	46
Figure 1-22 (bis)NHC-gold(I) ferrocenylphenyl complex <sup>87</sup> .....	47
Figure 1-23 NHC-gold(I) chloro complex <sup>88</sup> .....	49
Figure 1-24 Bucillamine and DMPS .....	52
Figure 2-1 Thermal ellipsoid plot of <b>2.4</b> shown at 50% probability .....	58
Figure 2-2 Thermal ellipsoid plot of cationic portion of <b>2.5</b> shown at 50% probability .....	59
Figure 2-3 Thermal ellipsoid plot of cationic portion of <b>2.6</b> shown at 50% probability .....	60
Figure 2-4 Thermal ellipsoid plot of dinuclear silver complex <b>2.7</b> shown at 50% probability .....	61
Figure 2-5 Thermal ellipsoid plot of silver complex <b>2.8</b> shown at 50% probability .....	63
Figure 2-6 <sup>1</sup> H NMR spectra of <b>2.5</b> in DMSO- <i>d</i> <sub>6</sub> (a) and in D <sub>2</sub> O, initially (b) and after 16 hours (c) .....	66
Figure 2-7 <sup>1</sup> H NMR spectra of <b>2.8</b> in DMSO- <i>d</i> <sub>6</sub> (a) and in D <sub>2</sub> O, initially (b) and after 16 hours (c) .....	67
Figure 2-8 <sup>1</sup> H NMR spectrum of <b>2.6</b> in DMSO- <i>d</i> <sub>6</sub> .....	68
Figure 2-9 <sup>1</sup> H NMR spectra of <b>2.6</b> in and D <sub>2</sub> O, initially (a) and after 16 hours (b) .....	69
Figure 2-10 Thermal ellipsoid plots of the cationic portions of <b>2.9</b> (a) and <b>2.10</b> (b) shown at 50% probability .....	72
Figure 2-11 Thermal ellipsoid plot of imidazolium gold(III) salt <b>2.11</b> shown at 50% probability .....	74

Figure 2-12 Thermal ellipsoid plot of gold-silver complex <b>2.12</b> shown at 50% probability.....	75
Figure 2-13 Proposed structure of <b>2.13</b> .....	78
Figure 2-14 $^1\text{H}$ NMR spectra of <b>2.9</b> in $\text{D}_2\text{O}$ , initially (a), and after 2 (b) and 3 (c) years .....	80
Figure 2-15 $^1\text{H}$ NMR spectra of <b>2.13</b> in $\text{D}_2\text{O}$ , initially (a) and after 2 weeks (b).....	81
Figure 2-16 $^1\text{H}$ NMR spectra of <b>2.10</b> in $\text{D}_2\text{O}$ , initially (a) and after 2 weeks (b).....	82
Figure 2-17 $^1\text{H}$ NMR spectrum of <b>2.9</b> in $\text{D}_2\text{O}$ before NaCl addition .....	84
Figure 2-18 $^1\text{H}$ NMR spectra of <b>2.9</b> after NaCl addition taken on days 1 (a) and .....	85
Figure 2-19 $^1\text{H}$ NMR spectra of <b>2.9</b> after NaCl addition taken on days 3 (a) and .....	86
Figure 3-1 Thermal ellipsoid plot of <b>3.4</b> shown at 50% probability.....	106
Figure 3-2 Thermal ellipsoid plot of <b>3.5</b> shown at 50% probability.....	107
Figure 3-3 Thermal ellipsoid plot of cationic portion of <b>3.6</b> shown at 50% probability with hydrogen atoms omitted for clarity .....	108
Figure 3-4 Thermal ellipsoid plot of <b>3.7</b> shown at 50% probability.....	109
Figure 3-5 Silver acetate NHC complexes <b>3.8</b> and <b>3.9</b> .....	110
Figure 3-6 $^1\text{H}$ NMR spectra of <b>3.4</b> in $\text{DMSO}-d_6$ (a) and $\text{D}_2\text{O}$ (b) .....	113
Figure 3-7 $^1\text{H}$ NMR spectra of <b>3.4</b> in $\text{DMSO}-d_6$ with water additions of 20 $\mu\text{L}$ (a), 40 $\mu\text{L}$ (b) and 60 $\mu\text{L}$ (c).....	114
Figure 3-8 $^1\text{H}$ NMR spectra of <b>3.4</b> in $\text{DMSO}-d_6$ with water additions of 80 $\mu\text{L}$ (a) and 100 $\mu\text{L}$ (b).....	115
Figure 3-9 Imidazolium iodide salts <b>3.10</b> and <b>3.11</b> .....	117
Figure 4-1 Quaternary ammonium salts BAC and CPC .....	129

Figure 4-2 Alkylthiomethyl (a) and alkoxymethyl (b) imidazolium salt derivatives .....	130
Figure 4-3 Alkyl (a) and alkyl-hydroxyethyl-(b) methylimiazolium salt derivatives .....	131
Figure 4-4 Thermal ellipsoid plot of <b>4.1</b> shown at 50% probability.....	132
Figure 4-5 Imidazolium <sup>1</sup> H NMR resonances in the synthesis of cationic <b>4.4</b> with [I <sup>+</sup> ] and zwitterion (a) and [BPh <sub>4</sub> <sup>-</sup> ] (b).....	135
Figure 4-6 Thermal ellipsoid plot of cationic portion of <b>4.4</b> shown at 50% probability.....	136
Figure 4-7 Thermal ellipsoid plot of cationic portion of <b>4.6</b> shown at 50% probability.....	138
Figure 4-8 Imidazole and various imidazolium salts .....	139
Figure 4-9 Antimicrobial activity of the dimethyl imidazolium series .....	140
Figure 5-1 Silver sulfadiazine .....	151

## LIST OF SCHEMES

Scheme	Page
Scheme 1-1 Generation of (mono)NHC-gold(I) complexes via deprotonation <sup>21</sup> .....	8
Scheme 1-2 Generation of (bis)NHC-gold complexes via protonation or alkylation <sup>24</sup> .....	11
Scheme 1-3 Generation of NHC-gold(I) complex via transfer from manganese <sup>12</sup> .....	13
Scheme 1-4 Generation of (mono) and (bis)NHC-gold(I) via silver transmetallation <sup>29</sup> .....	15
Scheme 1-5 Synthesis of derivatives of <b>46</b> and <b>47</b> <sup>30,31</sup> .....	16
Scheme 1-6 Generation of (mono)NHC-gold(I) chloro complexes via silver transmetallation <sup>17,21,33</sup> .....	17
Scheme 1-7 Synthesis of structural variations of <b>26</b> <sup>33</sup> .....	18
Scheme 1-8 Synthesis of (mono)NHC-gold(III) complexes by oxidative addition <sup>40</sup> .....	24
Scheme 2-1 Synthesis of imidazolium nitrate salts <b>2.1</b> and <b>2.2</b> .....	57
Scheme 2-2 Synthesis of nitrate salt <b>2.4</b> .....	57
Scheme 2-3 Synthesis of gold-NHC complexes <b>2.9</b> and <b>2.10</b> .....	70
Scheme 3-1 Generation of a caffeine-based silver acetate complex .....	104
Scheme 3-2 Synthesis of silver acetate complex <b>3.4</b> .....	106
Scheme 3-3 Synthesis of phthalimide imidazole derivative <b>3.5</b> .....	107
Scheme 4-1 Synthesis of imidazolium salts <b>4.2</b> and <b>4.3</b> .....	133

Scheme 4-2 Imidazolium carboxylic acid salt derivative <b>4.4</b> .....	136
Scheme 4-3 Imidazolium bromide phthalimide derivative <b>4.5</b> .....	137



## LIST OF EQUATIONS

Equation	Page
1-1.....	4
1-2.....	12
1-3.....	12
2-1.....	58
2-2.....	59
2-3.....	60
2-4.....	62
3-1.....	105
3-2.....	108
3-3.....	109
4-1.....	132
4-2.....	136
-	

# CHAPTER I

## GOLD N-HETEROCYCLIC CARBENE COMPLEXES OF THE IMIDAZOLYL TYPE AND EXPLORATION OF THE MEDICINAL APPLICATIONS OF GOLD

### 1.1 Introduction

Carbenes were first introduced into inorganic and organometallic chemistry by Fischer in 1964.<sup>1</sup> Öfele and Wanzlick synthesized the first metal-N-heterocyclic carbene (NHC) complexes in 1968, but a free NHC was not isolated until 1991 by Arduengo.<sup>1,2</sup> Since that time, a wide variety of NHC-metal complexes have been synthesized involving both transition and main group metals.<sup>3,4,5</sup> NHCs have been compared with phosphines for the way they bond to metals. However, some evidence has suggested that NHCs tend to bind the metal more tightly.<sup>6</sup> Paired with easier preparation methods, NHCs have become a field of growing interest.

The interest in NHC-metal complexes for medicinal applications has increased in recent years. Gold, a metal with a long medicinal history, has been documented for its therapeutic effects as far back as 2500 BC.<sup>7</sup> The modern day use of gold was sparked by the discovery that gold salts exhibited bacteriostatic activity. Today, it's most prominent medicinal application has been in the treatment chrysotherapy, of the disease, rheumatoid arthritis, a chronic

autoimmune disease in which no causative agent has yet to have been identified. The success rate of treatment has been weighed against the adverse side-effects and a less toxic, although somewhat less effective alternative has been implemented into treatment regimes. An exact mechanism of action has not been isolated but several theories have been supported.<sup>8</sup> Because of the beneficial effects seen with chrysotherapy in the treatment of rheumatoid arthritis, studies have been directed towards other areas of the medical field. Current studies have focused mainly on the use of gold-based therapeutics for their potential as anticancer agents.<sup>9</sup> Several gold(I)-NHC complexes have been synthesized to target the mitochondrial membrane in cancerous cells, modeled after results from a chrysotherapy agent that showed disruption of membrane permeability.<sup>10</sup>

There have been many synthetic routes for gold NHC compounds. NHCs of the imidazolyl type have been incorporated into a multitude of gold compounds, as described within.<sup>11</sup> Imidazole (Figure 1-1) has been easily converted into imidazolium salts by attachment of a wide variety of functional groups onto positions 1 and 3 of the imidazole ring. Currently, seven different methods have been used to synthesize a wide variety of gold(I)-NHCs.<sup>11,12</sup> In comparison, very few gold(III)-NHC complexes have been reported and only one basic method has been described.<sup>13</sup>

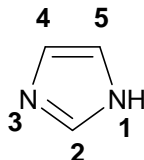


Figure 1-1 Imidazole

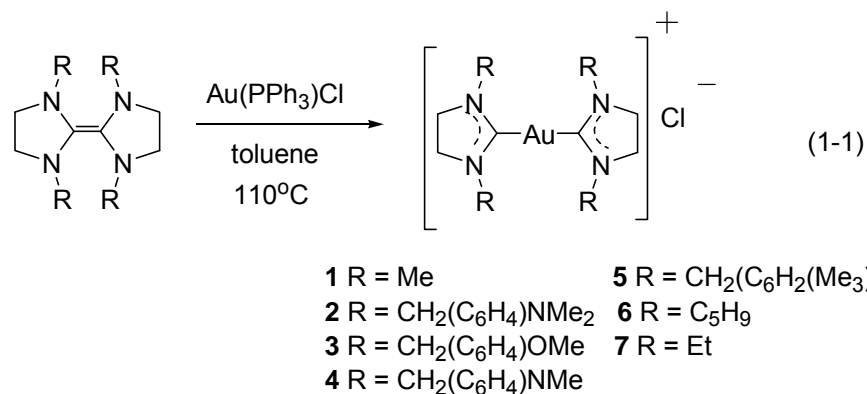
This review focuses on the synthesis of both gold(I) and gold(III) NHC complexes of the imidazolyl type and the medicinal applications of gold, as well as gold NHCs. This review has been divided into six categories: (1) the synthesis of gold(I) NHCs with an emphasis on structural comparisons; (2) the synthesis of gold(III) NHCs; (3) a structural comparison of gold(I) and gold(III) NHCs; (4) medicinal applications of gold; (5) medicinal applications of gold NHCs, and (6) gold toxicity.

## 1.2 Synthesis of Gold(I) N-Heterocyclic Carbene Complexes

To date, seven separate methods have been reported for the synthesis of gold(I) N-heterocyclic carbene complexes: (1) cleavage of electron-rich olefins; (2) generation from the free carbene; (3) deprotonation (*in situ*) of imidazolium salts; (4) protonation or alkylation of imidazolyl aurate compounds; (5) transfer from tungsten-NHC complexes; (6) transfer from manganese-NHC complexes, and (7) transmetalation from silver(I)-NHC complexes. Sections 1.2.1-1.2.7 describe the various synthetic routes. Section 1.2.8 compares and contrasts the characterizational data.

### 1.2.1 Cleavage of Electron-Rich Olefins

The isolation of transition metal-NHC derivatives via electron-rich olefin cleavage was introduced by Çetinkaya *et al.* in 1974.<sup>14</sup> Reactions were conducted with a mixture of the olefin with Au(PPh<sub>3</sub>)Cl in refluxing toluene for 5-20 minutes. A large variety of transition metal-NHC complexes were synthesized by this route including the hygroscopic gold(I) complex **1** in 84% yield (eq 1-1).

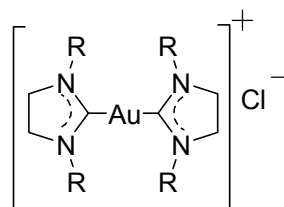


The method was repeated, with slight alteration, by Seckin and co-workers in 2003. The reaction was run in a 2:1 ratio with the olefin in excess in refluxing toluene for 2 hours for a 96% yield of gold compound **2** (eq. 1-1), which was later polymerized.<sup>15</sup> Özdemir *et al.* also repeated the process in 2004, with the olefin in only slight excess, for the generation of gold metal complexes **3-7** (eq. 1-1), which were later evaluated for their antimicrobial properties as discussed in section 1.6.2.<sup>16</sup> Reactions were run with the olefin in excess and yields of greater than 70% were obtained. The <sup>13</sup>C NMR spectras showed that the carbene carbon resonances for complexes **2-7** were all between approximately 203-205 ppm, in close agreement.

### 1.2.2 Generation from the Free Carbene

Several NHC-gold(I) complexes have been synthesized from reactions starting with the free carbene. Özdemir *et al.* synthesized a (bis)NHC-gold complex **8** (Figure 1-2), of the saturated type (C4-C5 single bond), by interaction of Au(PPh<sub>3</sub>)Cl with the free carbene in boiling toluene for 2 hours.<sup>16</sup> This compound appears to be the only saturated gold-NHC complex to have been

synthesized by this method. A yield of 73% was obtained and the carbene carbon resonance was observed at 206.8 ppm in the  $^{13}\text{C}$  NMR spectrum.



**8** R = Mes

Figure 1-2 (bis)NHC-gold(I) complex from the free carbene<sup>16</sup>

A series of neutral (mono)NHC-gold chloro complexes (Figure 1-3) were synthesized by de Frémont and co-workers, in which  $\text{Au}(\text{SMe}_2)\text{Cl}$  was mixed with the free NHC in THF for 12 hours.<sup>17</sup> Free carbenes used to generate the complexes varied at the C4 and C5 positions of the imidazole ring with hydrogen (**9-11**), methyl or isopropyl (**12-13**) or four hydrogen atoms in the case of the saturated complex (**14**). NHC-gold complexes **9-11** had yields ranging from 67-78% and carbene carbon resonances between approximately 166-175 ppm in the  $^{13}\text{C}$  NMR spectra. Gold complexes **12-13** had lower yields in comparison, both at 58%, and  $^{13}\text{C}$  NMR spectrum resonances of the carbene carbon observed at 168.4 ppm and 166.0 ppm, respectively. Complex **14** displayed the highest yield at 81% and the furthest downfield resonance at 196.1 ppm in the  $^{13}\text{C}$  NMR spectrum, attributed to the more electron rich environment of the saturated NHC carbene.<sup>18</sup> Crystallographic information was reported for all six complexes and all C2-Au bond distances were between 1.942(3)-1.996(12) Å. The C2-Au-C2 bond angles were also reported between approximately 177-180°, close to linearity.

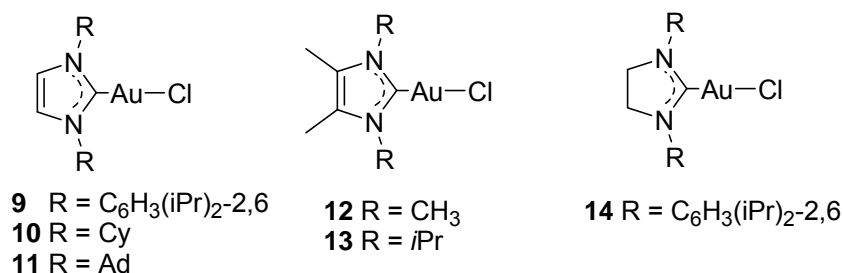


Figure 1-3 Neutral gold(I) complexes from the free carbene<sup>17</sup>

Several (tetra)NHC-dinuclear gold complexes **15-17** were synthesized by Fehlhammer *et al.* in 2001 from reaction of Au(PPh<sub>3</sub>)Cl with the free carbene in THF at -78°C (Figure 1-4).<sup>19</sup> All gold complexes had yields between 82-86%. The <sup>13</sup>C NMR spectral resonances for the carbene carbon were all within good agreement to each other between 187.1-188.2 ppm. A crystal structure of **16** was obtained and a C2-Au bond distance of 2.032(9) Å was given. A C2-Au-C2 bond angle of 174.6(4)° was also reported, deviating slightly from linearity.

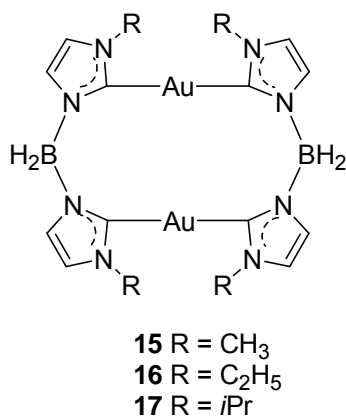


Figure 1-4 (tetra)NHC-dinuclear gold complexes from the free carbene<sup>19</sup>

### 1.2.3 Deprotonation (*In Situ*) of Imidazolium Salts

The *in situ* deprotonation of imidazolium salts for generation of a gold(I) complex can be achieved using either a strong or a weak base. Böhler and co-

workers synthesized a (mono)NHC-gold phosphine complex **18** using Au(PPh<sub>3</sub>)Cl in the presence of KO<sup>t</sup>Bu in THF (Figure 1-5).<sup>20</sup> The product was isolated in a 61% yield. A crystal structure was obtained and the C2-Au bond distance was 2.111(7) Å and the P-Au bond distance was 2.299(2) Å. The C2-Au-P angle was reported at 173.8(2)°, a small deviation from linearity. The carbene carbon resonance was noted at 207.3 ppm in the <sup>13</sup>C NMR spectrum and the phosphine resonance was observed at 40.2 ppm in the <sup>31</sup>P NMR spectrum.

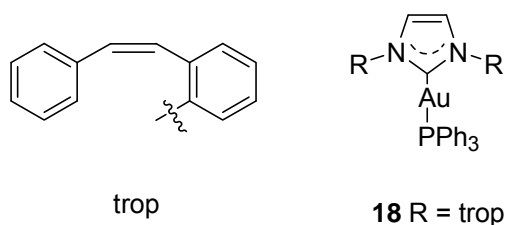
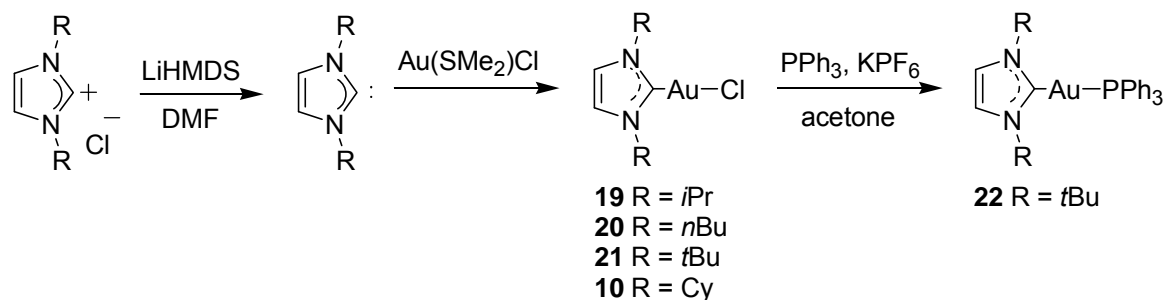


Figure 1-5 NHC-gold phosphine complex<sup>20</sup>

A series of (mono)NHC-gold(I) complexes bearing the chloro group was synthesized by Baker *et al.* in 2005 by using Au(SMe<sub>2</sub>)Cl.<sup>21</sup> The imidazolium salts were deprotonated by means of lithium hexamethyldisilazide (LiHMDS) in DMF. The solution was mixed in equal molar equivalents with Au(SMe<sub>2</sub>)Cl for 1 hour resulting in gold complexes **10** and **19-21** (Scheme 1-1). The products were obtained in relatively lower yields ranging from 31-51%. The carbene carbon resonance was observed between approximately 166-170 ppm for each compound by <sup>13</sup>C NMR spectra. Crystal structures were obtained for **10**, **19** and **21**. The average C2-Au bond distance was approximately 1.99 Å and average C2-Au-Cl bond angle was close to linearity at approximately 177°.





Scheme 1-1 Generation of (mono)NHC-gold(I) complexes via deprotonation<sup>21</sup>

Interestingly, an NHC-gold phosphine complex was obtained upon treatment of **21** with PPh<sub>3</sub> in the presence of KPF<sub>6</sub> in acetone (Scheme 1-1) to afford **22** in 88% yield. The <sup>13</sup>C NMR spectrum showed the carbene carbon resonance at 184.67 ppm and the <sup>31</sup>P NMR spectrum showed the phosphine resonance at 39.67 ppm. A crystal structure was obtained and a C2-Au bond distance of 2.044(4) Å was observed as well as a P-Au distance of 2.274(1) Å, similar to **18**.

Several (bis)NHC-gold(I) complexes were also synthesized by Baker *et al.* in 2006 by using a method analogous to Scheme 1-2. Using the gold reagent Au(SMe<sub>2</sub>)Cl and various imidazolium salts, in the presence LiHMDS in DMF for 4 hours, resulted in products **23-28** (Figure 1-6).<sup>22</sup> Complexes **23**, **26** and **28** had yields between 73-82%, while complexes **24**, **25** and **27** only had yields ranging from 33-50%. The carbene carbon resonances observed in the <sup>13</sup>C NMR spectra were all between 177.2-183.3 ppm. All compounds were crystallographically characterized and the C2-Au distances reported were between 1.97-2.05 Å. All C2-Au-C2 bond angles were close to linearity at an average of 179°.

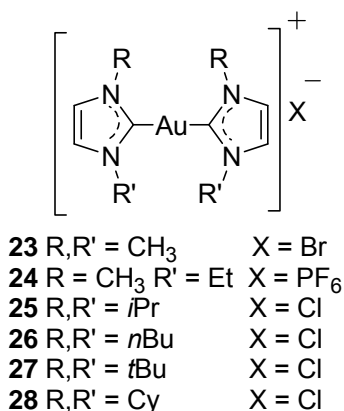


Figure 1-6 (bis)NHC-gold complexes via deprotonation<sup>22</sup>

Barnard and co-workers generated a series of dinuclear gold NHC complexes **29-35** using Au(SMe<sub>2</sub>)Cl in the presence of a weak carboxylate salt (NaOAc, LiOAc or LiOBu) in DMF for 30 minutes at 120°C (Figure 1-7).<sup>23</sup> Compounds **29**, **30** and **33-35** all had low yields between 23-44%, whereas **31** and **32** were higher at 64% and 70%, respectively. All carbene carbon resonances were between 183.2-188.1 ppm in the <sup>13</sup>C NMR spectra, which was in close agreement to the range of 187.1-188.2 ppm obtained for dinuclear gold complexes **15-17**. Crystal structures were obtained for six complexes (**29-32** and **34-35**). The average C2-Au bond distance was approximately 2.02 Å and the average C2-Au-C2 bond angle was approximately 176°. The average of these bond distances and angles were close to that reported for **16** at 203.2(9) Å and 174.6(4)°, respectively.

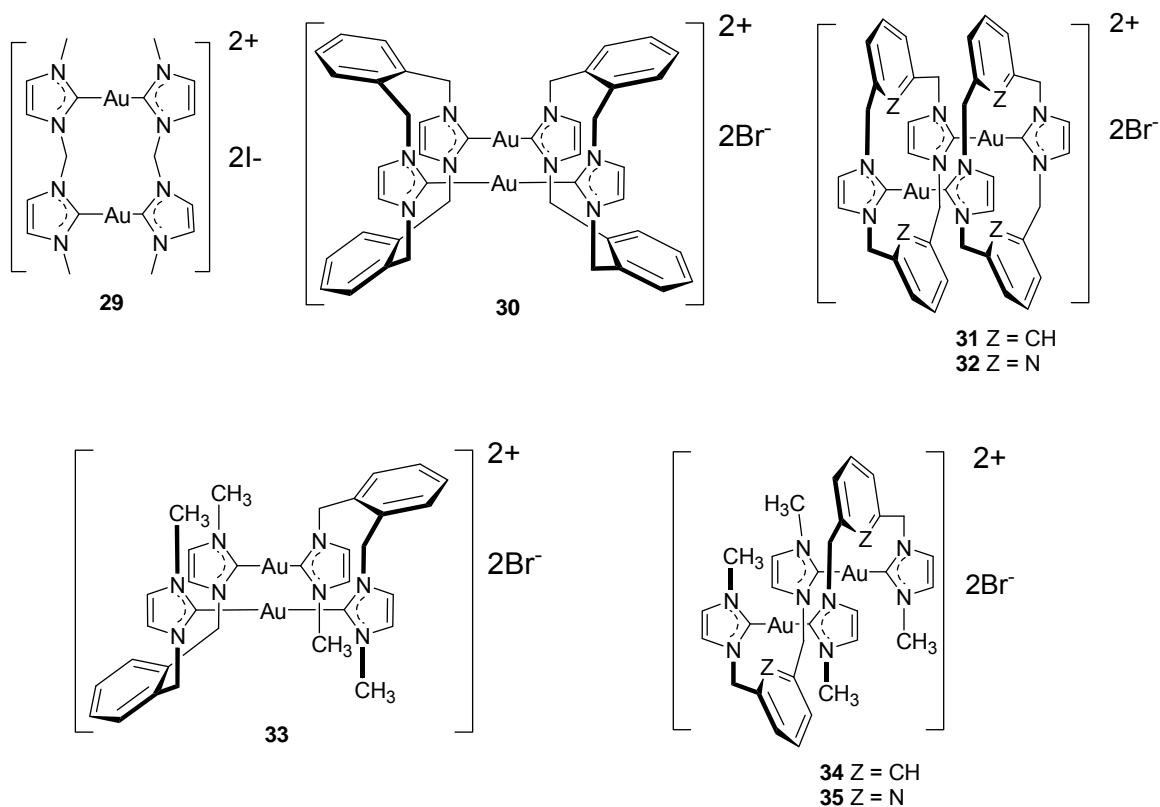
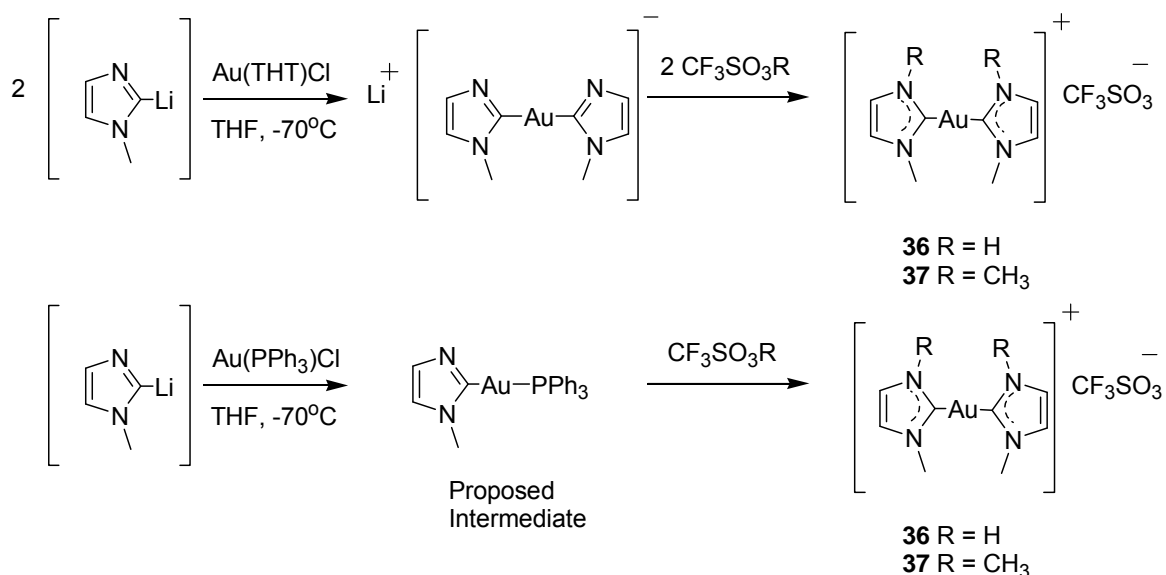


Figure 1-7 Dinuclear gold(I) complexes<sup>23</sup>

#### 1.2.4 Protonation or Alkylation of Imidazolyl Aurate Compounds

The generation of (bis)NHC-gold(I) complexes has been reported via protonation or alkylation of imidazolyl aurate intermediates. This type of reaction was studied by Raubenheimer *et al.* in 1996, based on earlier work by Burini and co-workers.<sup>24,25</sup> For the synthesis of complexes **36** and **37**, two different methods were used with the same products obtained for both (Scheme 1-2).



Scheme 1-2 Generation of (bis)NHC-gold complexes via protonation or alkylation<sup>24</sup>

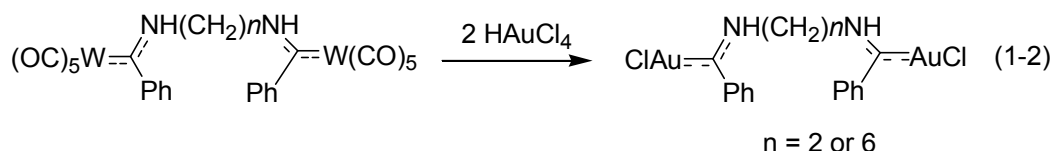
The difference between the two reactions was the gold starting material and the molar equivalents used. The top reaction of Scheme 1-2 proceeds by the formation of the (bis)imidazolyl aurate intermediate with Au(THT)Cl in THF at -70°C, followed by protonation with CF<sub>3</sub>SO<sub>3</sub>H or alkylation with CF<sub>3</sub>SO<sub>3</sub>CH<sub>3</sub> to afford **36** and **37**. The bottom reaction uses the gold starting material Au(PPh<sub>3</sub>)Cl and proceeds by what has been proposed as a neutral phosphine intermediate. Subsequent protonation or alkylation as stated above again leads to the generation of complexes **36** and **37**.

The first route produced yields of 80% and 88% for **36** and **37**, respectively. No yield information was reported for the alternate route. The nitrogen-bound proton of **36** was observed at a resonance of 12.02 ppm by <sup>1</sup>H NMR spectrum, consistent with the structure. The carbene carbon resonances were noted at 182.8 ppm for **36** and at 185.7 for **37** in the <sup>13</sup>C NMR spectra,

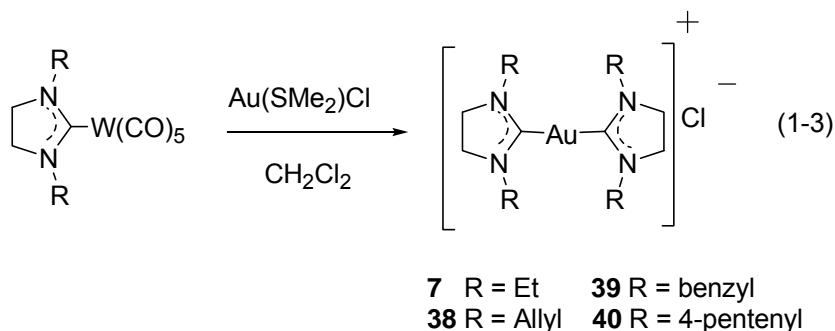
consistent with similar (bis)NHC-gold complex **23**, the bromide salt, at 183.3 ppm.

### 1.2.5 Transfer from Tungsten-NHC Complexes

Carbene transfer from tungsten to gold was first studied by Fischer *et al.* in 1984. Carbene transfer took place from dinuclear tungsten pentacarbonyl complexes to dinuclear gold chloro complexes (eq 1-2).<sup>26</sup>



This type of reaction was applied for NHC-tungsten complexes by Liu and co-workers in 1998 and 1999 to generate NHC-gold complexes **7-10** (eq. 1-3).<sup>27,28</sup>

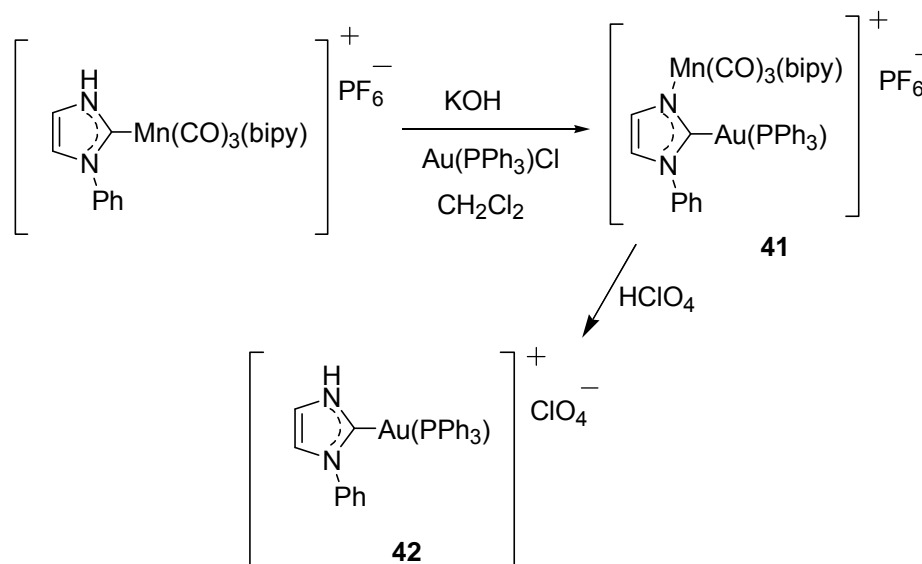


The resulting gold(I) complexes were formed by direct reaction of  $\text{W(CO)}_5\text{-NHC}$  complexes with chloro(dimethylsulfide)gold in dichloromethane. The reactions were run using a 2:1 ratio, with the ligand in excess, and yields between 56-77% were observed. These appear to be the only gold-NHC compounds to have been synthesized from this method. The  $^{13}\text{C}$  NMR spectral resonances for the carbene carbon were all observed between 204-205 ppm for complexes **7** and **38-40**.

Complex **7** was also synthesized via electron-rich olefin cleavage, as described above in section 1.2.1. No yield for **7** was reported via tungsten transfer,<sup>27,28</sup> but a yield of 85% has been reported for generation from cleavage of electron-rich olefins.<sup>16</sup> A <sup>13</sup>C NMR spectral resonance for the carbene carbon was observed in CDCl<sub>3</sub> at 204.2 ppm via the cleavage route and 203.8 ppm via tungsten transfer.

### 1.2.6 Transfer from Manganese-NHC Complexes

The NHC transfer from a manganese(I) complex to a gold(I) complex was reported by Ruiz and Perandones in 2007.<sup>12</sup> An NHC-manganese complex in dichloromethane was mixed with Au(PPh<sub>3</sub>)Cl in the presence of excess KOH generating an isolable mixed metal NHC-gold(C bound)-manganese(N-bound) intermediate **41**, which afforded the NHC-gold(I) complex **42**, upon treatment with HClO<sub>4</sub> (Scheme 1-3).

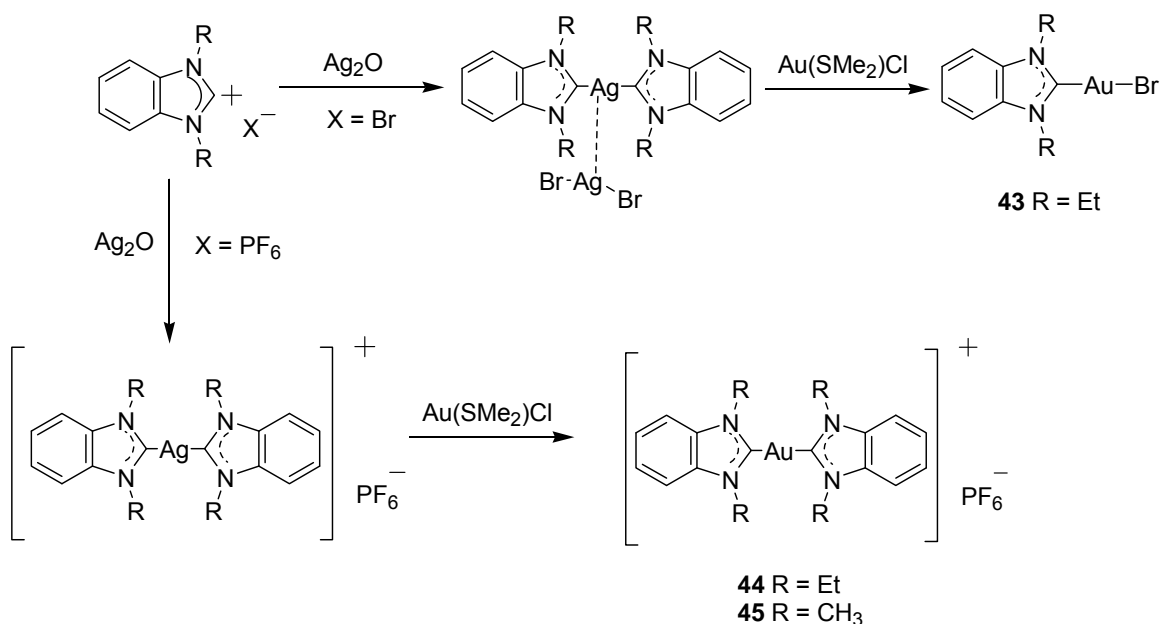


Scheme 1-3 Generation of NHC-gold(I) complex via transfer from manganese<sup>12</sup>

These were the only two gold-NHC compounds to have been generated by this method. A crystal structure of **41** was reported with a C2-Au distance of 2.035(4) Å, a P-Au distance of 2.283(1) Å and a C2-Au-P angle close to linearity at 173.7(2)°. The  $^{13}\text{C}$  NMR spectrum showed a resonance at 190.4 ppm for the carbene carbon and the  $^{31}\text{P}$  NMR spectrum showed a shift of 40.3 ppm for the phosphine in **41**. No  $^{13}\text{C}$  NMR data was given for **42** and no crystallographic information was mentioned. A resonance was reported for the phosphine at 40.5 ppm in the  $^{31}\text{P}$  NMR spectrum.

### 1.2.7 Transmetallation from NHC-Silver(I) Complexes

Of all the preparation methods employed for NHC-gold(I) complexes, transmetallation from NHC-silver(I) complexes has been the most widely used thus far. Silver complexes can be easily isolated or used *in situ*. This method was introduced by Lin *et al.* in 1998 when they successfully synthesized NHC-gold complexes **43** and **44**, after using  $\text{Ag}_2\text{O}$  to synthesize the NHC-silver precursor (Scheme 1-4).<sup>29</sup> Both **43** and **44** were obtained in good yield at 91% and 89%, respectively. A crystal structure of **44** was later reported and a C2-Au bond distance of 2.024(12) Å and C2-Au-C2 bond angle of 175.0(14)° was given.<sup>30</sup> The dimethyl complex **45** was obtained in 85% yield and a C2-Au distance of 2.054(10) Å, C2-Au-C2 bond angle of 180.0(2)° and a carbene carbon resonance of 183.7 ppm by  $^{13}\text{C}$  NMR spectrum was given.



Scheme 1-4 Generation of (mono) and (bis)NHC-gold(I) via silver transmetalation<sup>29</sup>

In 1999, Lin and co-workers modified **43** by substituting the bromide with a chloride.<sup>31</sup> Several derivatives **46-48** were synthesized (Figure 1-8).<sup>31,32</sup> All three compounds were obtained in good yields of 71%-91%. Crystal structures were also reported for each and they were similar. The average C2-Au distance and C2-Au-Cl bond angle were approximately 1.99 Å and 179°, respectively.

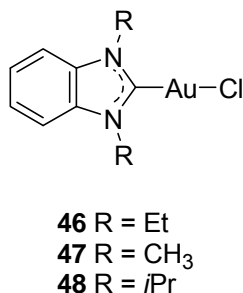
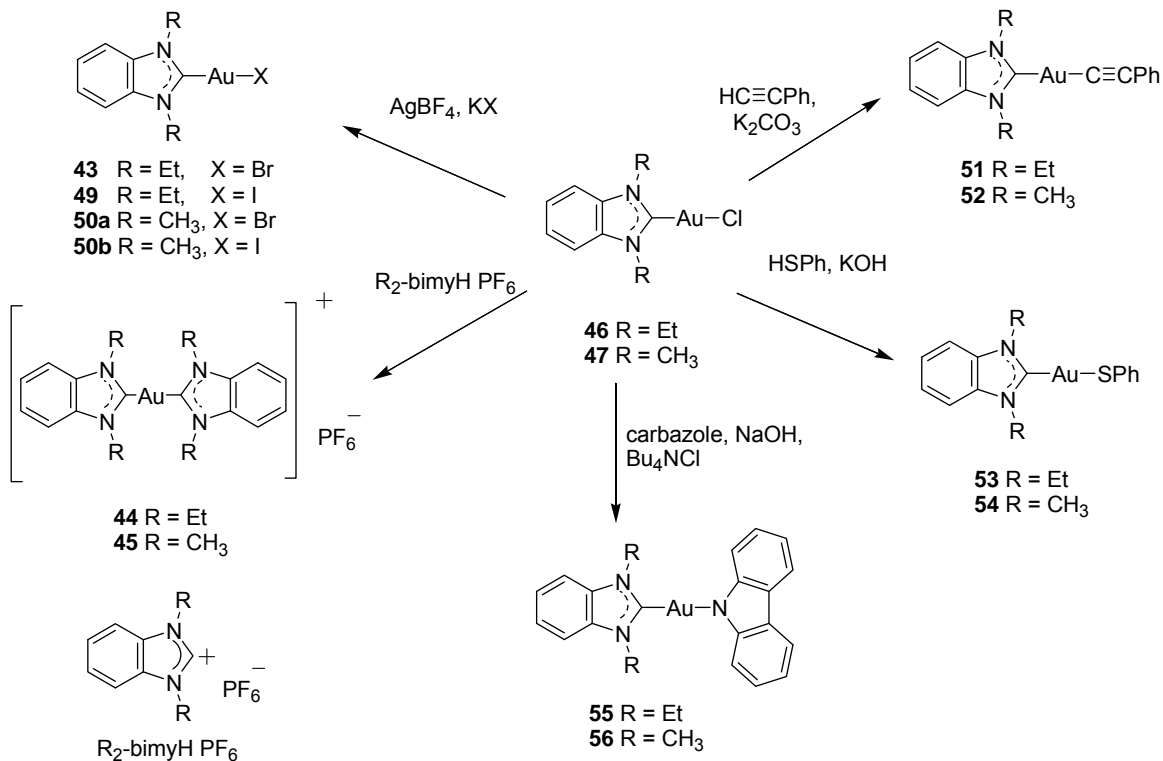


Figure 1-8 Chloro derivatives of **43**<sup>31</sup>

Complexes **46** and **47** were further investigated and it was found that the chloride group could be displaced easily generating a series of derivatives **49-56**



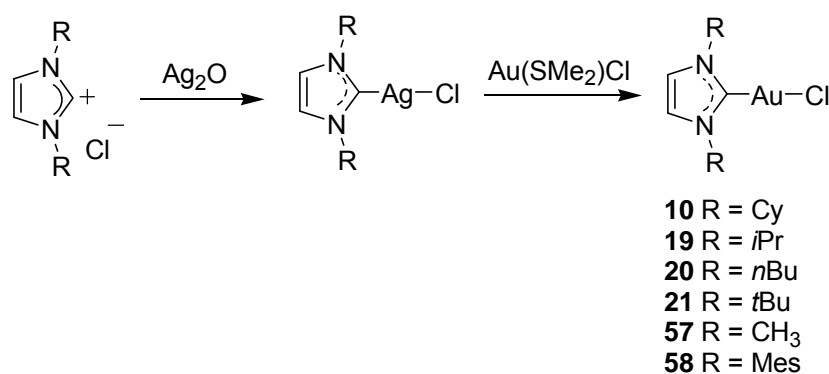
(Scheme 1-5).<sup>31</sup> All compounds were characterized by elemental analysis and <sup>1</sup>H NMR spectroscopy. A crystal structure of **56** was obtained and a C2-Au bond distance of 1.986(6) Å and a C2-Au-N (cbz) bond angle of 179.2(2)<sup>o</sup> was reported, similar to that observed in the parent compound **47** at 1.985(11) Å and 178.1(3)<sup>o</sup>, respectively.



Scheme 1-5 Synthesis of derivatives of **46** and **47**<sup>30,31</sup>

Generation of the (mono)NHC-gold(I) chloro complexes was also conducted via the silver transmetalation method, with success noted in several independent studies (Scheme 1-6).<sup>17,21,33</sup> Compounds **10** (Figure 1-3) and **19-21** (Scheme 1-1), previously reported by alternate methods described above, were generated in yields ranging from 60-89%, with characterization in agreement with literature values. A crystal structure of **21** was obtained and the

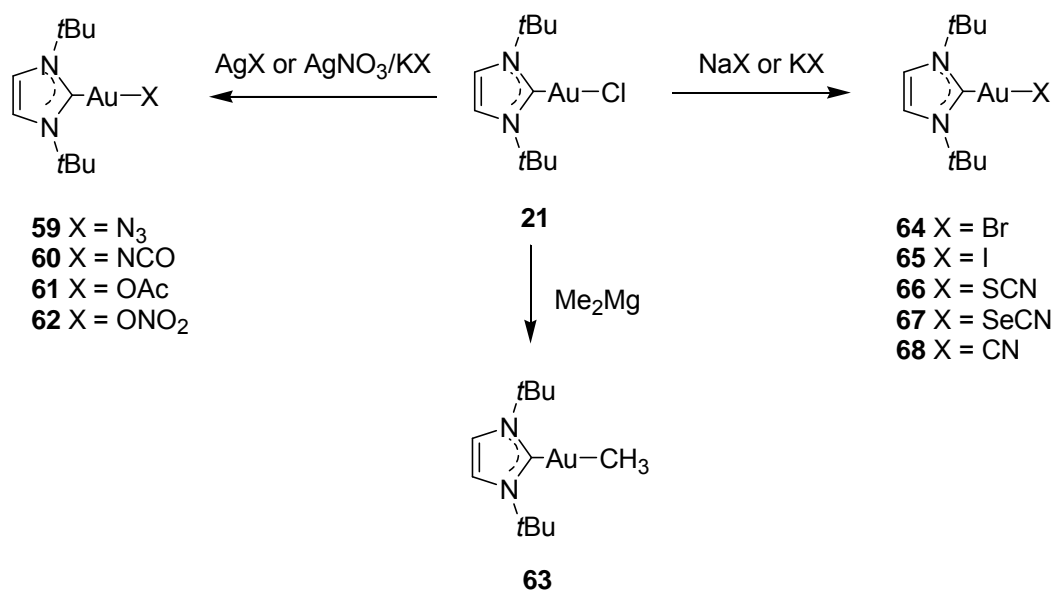
C2-Au bond distance was observed at 2.018(3) Å and the C2-Au-Cl bond angle was reported at approximately 180°. Complexes **57** and **58** were obtained in 93% and 82% yields, respectively. Both **57** and **58** were also crystallographically characterized and C2-Au bond distances were reported at 1.95(2) Å and 1.999(5) Å, respectively. Bond angles of the C2-Au-Cl were close to linearity with an average value of approximately 180°.



Scheme 1-6 Generation of (mono)NHC-gold(I) chloro complexes via silver transmetalation<sup>17,21,33</sup>

In a similar manner to chemistry seen for the manipulation of the chloro group on complexes **46** and **47** (Scheme 1-5), further experiments were performed on **21**.<sup>33</sup> It was shown that the chloride group could be exchanged, thereby generating another series of structurally diverse compounds **59-68** (Scheme 1-7). All compounds were characterized by <sup>13</sup>C NMR spectra and a broad range was observed for the carbene carbon resonances. The differences were attributed to the properties of the X atom. The parent compound **21** had a carbene carbon resonance of 168.2 ppm. Downfield shifts were observed when X was a halogen (**64** or **65**), a carbon (**63** or **68**), a sulfur (**66**), or selenium (**67**).

Differences in the position of the resonance from **21** ranged from +4.2 ppm in **64** to +30.5 ppm for **63**. Upfield shifts were reported when X was a nitrogen (**59** or **60**) or an oxygen (**61** or **62**). Variation in the position of the resonance from **21** ranged from -1.8 in **59** to -11.9 observed in **62**. These differences were explained by the  $\sigma$ -donor ability of the exchanged ligand, those being more  $\sigma$ -donating or electron-rich would cause a downfield shift by decreasing the Lewis acidity of the metal and vice versa. The link between the carbene carbon's chemical shift and the Lewis acidity of the metal was reported by Herrmann *et al.* in 1995 and supported by Raubenheimer in 1997 when upfield shifts were observed in the oxidation of NHC-gold(I) complexes to NHC-gold(III) systems.<sup>13,18</sup> Crystal structures were also obtained for all compounds and although the exchanged ligands were very different, all C2-Au distances and C2-Au-X angles were within normally observed parameters, ranging between 1.97-2.03 Å and 172-179°, respectively.



Scheme 1-7 Synthesis of structural variations of **26**<sup>33</sup>

Some interesting dinuclear NHC-gold complexes have also been synthesized via the route of silver transmetallation. Independent studies by Ghosh *et al.* and Catalano and Moore found that, by using Au(SMe<sub>2</sub>)Cl or Au(tht)Cl, the corresponding NHC-gold(I) complexes **69-71** were afforded (Figure 1-9).<sup>34,35</sup> In the generation of **69** and **70**, Au(SMe<sub>2</sub>)Cl was used in a 2:1 ratio with the silver complex in dichloromethane at room temperature for 4 hours.

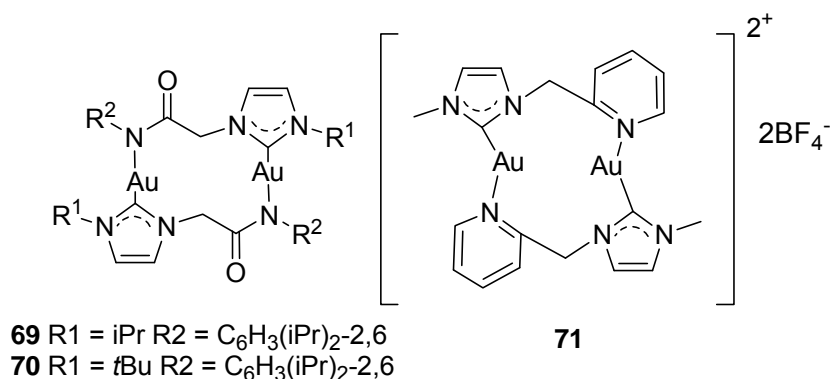


Figure 1-9 Dinuclear NHC-gold complexes via silver transmetallation<sup>34,35</sup>

Crystal structures were obtained for **69** and **70** and C2-Au distances of approximately 1.95 Å and C2-Au-N angles of approximately 175° were reported. Upfield shifts were observed in the <sup>13</sup>C NMR spectra with a resonance for carbene carbon at approximately 169.9 ppm, as expected from the Au-N bond.

For **71**, the gold reagent Au(tht)Cl was used in a 1:1 ratio in dichloromethane at room temperature for 10 minutes. Compound **71** was crystallographically characterized and the C2-Au bond distances were approximately 2.00 Å and the C2-Au-N bond angles were approximately linear at 179°. The same upfield shift was observed in the <sup>13</sup>C NMR spectrum for the

carbene carbon resonance at 166.53 ppm, again as expected due to the Au-N bond.

### 1.2.8 A Comparison of Synthesis Methods and Select Characterization Data for Similar NHC-Gold(I) Complexes

Generation of the (mono)NHC-gold(I) chloro complexes has been attempted successfully via three different synthesis methods: from the free carbene, deprotonation of the imidazolium *in situ* and by transmetallation from metal-NHC precursors. Several complexes have been synthesized by 2 or all 3 of these routes. Based on the R<sub>2</sub>ImAuCl structure (Figure 1-10), a yield comparison has been provided in Table 1-1. The silver transmetallation method produced the most consistently higher yields for compounds that the methods had in common. Although the free carbene route had the higher yield for the cyclohexyl derivative, the extra care, inconvenience and preparation may not be worth the 7% difference.

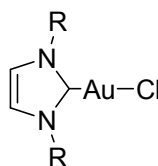


Figure 1-10 The R<sub>2</sub>ImAuCl structure

Table 1-1 A yield (%) synthesis method comparison for the R<sub>2</sub>ImAuCl structure. Prepared in part from a table in reference 21

Compound	<b>10</b>	<b>19</b>	<b>20</b>	<b>21</b>
R Group	Cy	<i>i</i> Pr	<i>n</i> Bu	<i>t</i> Bu
Free Carbene	67			
Deprotonation	42	31	51	45
Ag Transmetallation	60	70	73	89

There have also been many other compounds based on the R<sub>2</sub>ImyAuCl structure (Figure 1-10). For this reason, a characterizational comparison of the <sup>13</sup>C NMR spectroscopy carbene carbon resonance, C2-Au bond distance and C2-Au-Cl bond angle have been made available in Table 1-2.

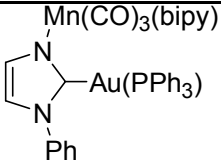
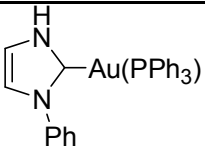
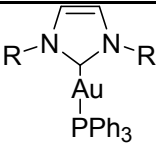
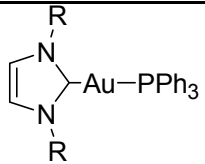
Table 1-2 A comparison of selected <sup>13</sup>C NMR spectra resonances (ppm), bond distances (Å) and bond angles (°) for the R<sub>2</sub>ImAuCl structure. Combined table from those in references 17, 21 and 33.

Compound	R Group	<sup>13</sup> C NMR C2-Au	Bond distance C2-Au	Bond angle C2-Au-Cl
<b>9</b>	C <sub>6</sub> H <sub>3</sub> ( <i>i</i> Pr) <sub>2</sub> -2,6	175.1	1.942(3)	177.0(4)
<b>10</b>	Cy	168.0	1.990(13)	178.2(4)
<b>11</b>	Ad	166.3	1.989(2)	178.07(7)
<b>19</b>	<i>i</i> Pr	168.7	1.964(6)	175.0(2)
<b>20</b>	<i>n</i> Bu	169.9		
<b>21</b>	<i>t</i> Bu	168.2	2.018(3)	180
<b>57</b>	CH <sub>3</sub>	171.9	1.95(2)	178.9(6)
<b>58</b>	Mes	173.6	1.999(5)	180

All <sup>13</sup>C NMR spectra resonances for the carbene carbon were in close proximity to each other with a range of 166.3-175.1 ppm. Bond distances for the C2-Au bond had a range of 1.94-2.02 Å and bond angles for the C2-Au-Cl were between 175° and 180°. The data would suggest that the R group had little bearing on the carbene-gold center for the R<sub>2</sub>ImyAuCl structure.

There were three different (mono)NHC-gold(I) phosphine complexes synthesized and one gold(I) NHC isolated intermediate that also contained a nitrogen-bound manganese complex. A collection of available relevant characterization information has been reported in Table 1-3 for easy comparison.

Table 1-3 A comparison of selected  $^{13}\text{C}$  NMR spectra resonances (ppm),  $^{31}\text{P}$  NMR spectra resonances, bond distances (Å) and bond angles ( $^\circ$ ) for (mono)NHC-gold(I) phosphine complexes. Prepared in part from a table in reference 21.

Compound				
	<b>41</b>	<b>42</b>	<b>18 R = trop</b>	<b>22 R = tBu</b>
$^{13}\text{C}$ NMR				
C2-Au	190.4		207.3	184.7
$^{31}\text{P}$ NMR				
PPh <sub>3</sub>	40.3	40.5	40.2	39.7
Bond distance				
C2-Au	2.035(4)		2.111(7)	2.044(4)
P-Au	2.283(1)		2.299(2)	2.274(1)
Bond Angle				
C2-Au-P	173.7(2)		173.8(2)	177.3(1)

Unfortunately, not much supporting information was given for **12**, but the  $^{31}\text{P}$  NMR spectra resonances for the PPh<sub>3</sub> ligands seem to be in close agreement with one another. For the other three, given the fact that the same phosphine was attached to the gold, it would appear that choice in R group has direct bearing on the carbene-gold center. The  $^{13}\text{C}$  NMR spectra for the carbene carbon resonance for **18** is the furthest downfield, indicating more  $\sigma$ -donation. This would suggest some sort of interaction between the trop substituent and the imidazole ring. It was noted that the solid state structure showed the tropyliene rings turned away from the gold center, toward the NHC ring.<sup>20</sup>

The C2-Au bond distances for the compounds in Table 1-3 were slightly elongated in comparison to data obtained for the R<sub>2</sub>ImAuCl structure above. The greatest distance was also observed in **18**, so steric effects could be a plausible

explanation. All C2-Au-P bond angles noted were similar with each other and deviated from linearity at approximately 175°.

### 1.3 Synthesis of Gold(III) N-Heterocyclic Carbenes

Gold(III) NHC complexes have been formed by oxidative addition of respective gold(I) NHC complexes. The chemistry of gold(III) carbene systems was explored in the 1970s, but very little focus has been given to this area.<sup>36,37,38,39</sup> By adopting the oxidative addition approach used in earlier gold(III) carbene studies, Raubenheimer *et al.* synthesized a series of (bis)NHC-gold(III) complexes **72a-73c** from their NHC-gold(I) precursors **72** and **73** (Figure 1-11).<sup>13</sup>

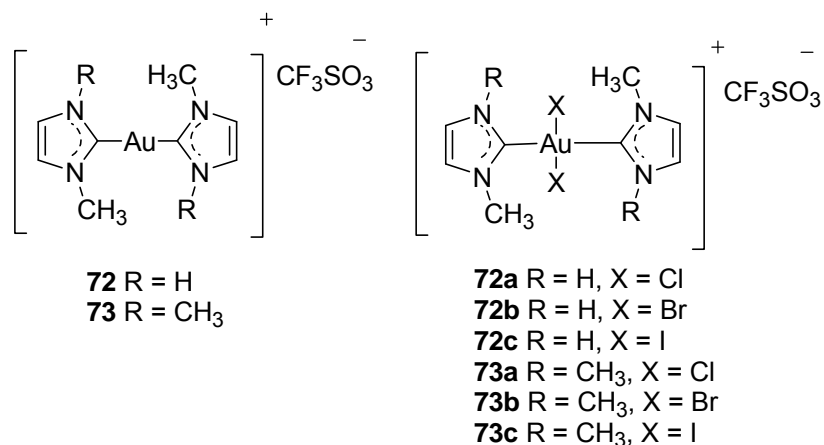


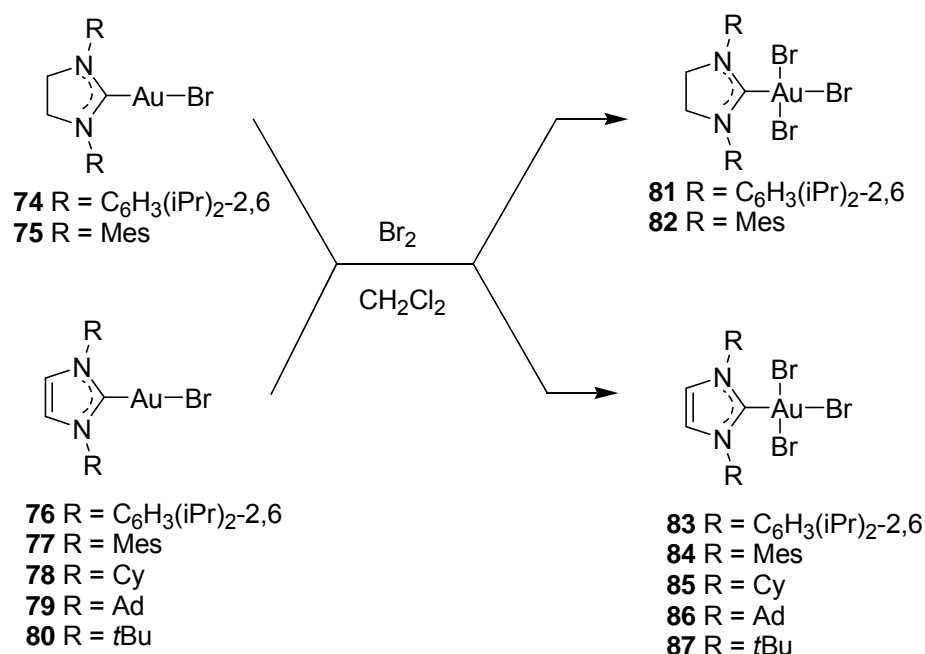
Figure 1-11 (bis)NHC-gold(III) complexes and NHC-gold(I) precursors<sup>13</sup>

A solution of a (bis)NHC-gold(I) complex in cooled dichloromethane was oxidized by the bubbling through of Cl<sub>2</sub> or dropwise addition of Br<sub>2</sub> or I<sub>2</sub>. Reaction temperatures were approximately -40°C for a time of 30 minutes. The resulting gold(III) compounds showed retention of both carbene carbon bonds and a crystal structure of **72a** showed square planar coordination about the gold center.



$^{13}\text{C}$  NMR spectroscopic data, C2-Au bond distances and yield information have been compiled in Table 1-4 and will be discussed thereafter.

A series of mono(NHC)-gold(III) complexes was synthesized recently in a detailed publication by de Frémont and co-workers, which incorporated the use of saturated and unsaturated NHCs.<sup>40</sup> The NHC-gold(I) bromide starting materials **74-80** were generated by a method analogous to Scheme 1-7, with the use of LiBr. The oxidative addition of  $\text{Br}_2$  in slight excess was carried out at room temperature for 1 hour (both IMes analogues proceeded at  $-78^\circ\text{C}$  for 20 minutes) to yield the corresponding gold(III) compounds **81-87** (Scheme 1-8).



Scheme 1-8 Synthesis of (mono)NHC-gold(III) complexes by oxidative addition<sup>40</sup>

Crystal structures were obtained for the seven complexes **81-87** and all showed square planar coordination about the gold center. No NHC bond cleavage or rearrangement was observed.  $^{13}\text{C}$  NMR spectroscopy data, C2-Au

bond distances and yield information have been compiled in Table 1-4 and will be discussed thereafter.

Table 1-4 A comparison of selected  $^{13}\text{C}$  NMR spectra resonances (ppm), bond distances (Å) and yields (%) for NHC-gold(III) complexes. Combined table from those in references 13 and 40.

Compound	Yield	$^{13}\text{C}$ NMR C2-Au	<i>Bond distances</i> C2-Au
<b>72a</b>	90	154.5	2.13(2)
<b>72b<sup>a</sup></b>	63	154.1	
<b>72c</b>	84	145.6	
<b>73a</b>	68	160.6	
<b>73b<sup>a</sup></b>	65	150.6	
<b>73c</b>	89	144.1	
<b>81</b>	57	174.1	2.042(13)
<b>82</b>	72	172.3	2.052(13)
<b>83</b>	84	146.2	2.048(19)
<b>84</b>	94	144.4	2.009(8)
<b>85</b>	89	136.8	2.04(2)
<b>86</b>	95	132.9	2.052(6)
<b>87</b>	93	134.2	2.015(5)

<sup>a</sup> Br analogue

Based on data presented in Table 1-4, (bis)NHC-gold(III) systems had  $^{13}\text{C}$  NMR spectrum resonances more downfield than the mono systems, with the exception of the saturated complexes **81** and **82**. This is not surprising because the (bis)NHC system would have more  $\sigma$ -donation, due to the second NHC versus the bromide. All C2-Au distances for the mono gold series were in close agreement with each other between the range of 2.01-2.05 Å and slightly shorter than reported for bis gold complex **72a** at 2.13(2) Å.

## 1.4 Characterizational Comparison of Gold(III) N-Heterocyclic Carbenes with Their NHC-Gold(I) Precursors

During the oxidative addition of halogens to gold(I) NHCs, the metal center undergoes a change in geometry from a virtually linear two-coordinate arrangement to that of a square planar four-coordinate system isoelectronic to  $d^8$  metal systems, like that observed for cisplatin. These complexational changes can also be observed by  $^{13}\text{C}$  NMR spectroscopy. Detailed  $^{13}\text{C}$  NMR spectroscopy information between NHC-gold(III) complexes and gold(I) analogues has been gathered in Table 1-5.

Table 1-5 A comparison of selected  $^{13}\text{C}$  NMR spectra resonances (ppm) for NHC-gold(III) complexes and NHC-gold(I) precursors<sup>40</sup>

NHC-Au(III)	C2-Au	NHC-Au(I)	C2-Au
<b>72a</b>	154.5	<b>72</b>	185.7
<b>72b</b>	154.1	<b>72</b>	185.7
<b>72c</b>	145.6	<b>72</b>	185.7
<b>73a</b>	160.6	<b>73</b>	182.8
<b>73b</b>	150.6	<b>73</b>	182.8
<b>73c</b>	144.1	<b>73</b>	182.8
<b>81</b>	174.1	<b>74</b>	199.0
<b>82</b>	172.3	<b>75</b>	198.1
<b>83</b>	146.2	<b>76</b>	179.0
<b>84</b>	144.4	<b>77</b>	176.7
<b>85</b>	136.8	<b>78</b>	172.1
<b>86</b>	132.9	<b>79</b>	170.2
<b>87</b>	134.2	<b>80</b>	172.4

A comparison of the data from the  $^{13}\text{C}$  NMR spectroscopy supports the theory by Herrmann *et al.* that the metal as a Lewis acid would be more acidic in the higher oxidation state, as seen here for gold(III), and therefore would have

less electron density.<sup>18</sup> This correlates to the upfield shift observed for the gold(III) NHCs in comparison with their gold(I) NHC precursors.

The only gold(I) NHC with crystallographic information was **76**. The C2-Au bond distance was reported at approximately 1.98 Å and the Au-Br distance was approximately 2.38 Å. The corresponding gold(III) NHC complex **83** had a C2-Au distance of 2.048(19) Å and Au-Br distances of 2.384(3) Å, 2.386(4) Å and 2.397(3) Å.

### 1.5 Medicinal Applications of Gold

Gold has a rich medicinal history. It has been used as early as 2500<sub>BC</sub> and is still in use for therapeutic applications today. The information covered in this section consists of five different topics: (1) history of gold use; (2) biological activity of gold; (3) gold as an antiarthritic agent; (4) gold as an anticancer agent and, (5) gold as an antimicrobial agent.

#### 1.5.1 History of Gold Use

The earliest use of gold as a medicinal agent can be traced back to China in the year 2500<sub>BC</sub> where it was used to cure sickness. It was speculated that this was probably in the form of gold flakes or dust as Au(0).<sup>41</sup> It was also ingested by alchemists and those seeking to increase longevity.<sup>7</sup> This practice was based on the premise of metallic gold's low chemical reactivity. Based on its popularity, gold was highly sought after and coveted. This led to the development of gold elixirs also known as "potable gold". It was later discovered that these elixirs actually contained very little gold.<sup>7</sup>

The early Chinese had a variety of uses for gold drugs.<sup>7</sup> They were ground into powder and placed into open wounds during surgical procedures and in skin ulcers. A gold foil could be warmed and placed on the skin to remove mercury from the ear or flesh. It was noted that gold could calm the heart by relaxing palpitations and stop one from coughing. The “Bencao Zaixin” was one of the first to record that gold drugs were beneficial for the joints.<sup>7</sup>

The use of gold drugs became popular in medieval Europe also in the form of elixirs. Once again, many of these contained little gold.<sup>9</sup> In the 1600s, the dedicated apothecary and herbalist Nicholas Culpeper introduced the use of gold cordials. These were medicinal drinks that were said to lift the spirit and cure such ailments as melancholy, fainting and fevers. Gold therapeutics were introduced into the modern age in 1890 when Robert Koch discovered the bacteriostatic activity of a gold cyanide complex,  $K[Au(CN)_2]$ , against *tubercle bacillus*. His *in vitro* testing involved diluting the gold(I) salt to a concentration much too dilute for the cyanide to show any anti-tubercular activity.<sup>8</sup> However, his compound failed to show any activity in animal models. This prompted the synthesis and testing of new gold salts and in 1924 gold sodium thiosulfate **88** (Figure 1-12) was used in the treatment of tuberculosis. Although gold therapy was proved ineffective against tuberculosis, it was used as a treatment option until the 1930s.

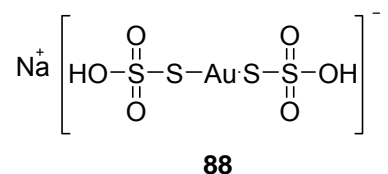


Figure 1-12 Gold sodium thiosulfate

Since that time, gold drugs have been used as treatment options for rheumatoid arthritis and have been continually investigated for antimicrobial and antitumor properties and in other therapeutic applications. The use of gold as a therapeutic agent has been termed chrysotherapy based on the Greek word for gold, *chrysos*.

#### 1.5.2 Biological Activity of Gold

Of the different oxidation states of gold, only gold(0), gold(I) and gold(III) have shown stability in biological environments.<sup>8,41</sup> Gold(I) predominantly forms 2-coordinate linear complexes<sup>42</sup> and has a preference for soft ligands including those with S-donor atoms, whereas gold(III) forms predominantly square planar complexes and stabilized complexes with hard ligands, specifically those with N- or O-donor atoms. An equilibrium between the three states *in vivo* has been observed.<sup>41</sup> Gold(III) can be reduced by thiols, thioethers or disulfide bonds to gold(I) and, both gold(III) and gold(I) can be reduced in the presence of mild reducing agents or in the absence of stabilizing ligands to gold(0).<sup>8</sup> Evidence has been presented that supports the oxidation of gold(I) to gold(III) by both *in vitro* and *in vivo* studies.<sup>43,44</sup> Gold(0), although predominately inert, can eventually dissolve at very small levels in the presence of thiol-containing compounds and

oxidized to gold(I).<sup>41</sup> Gold(I) has been noted as being more thermodynamically stable than gold(III) and the primary form found *in vivo*.<sup>8</sup>

Gold salts bind largely to albumin and globulin, which carry them through the plasma where they remain for months. They accumulate in tissues such as the kidneys, liver, spleen, bone marrow and to a lesser extent in the hair and nails.<sup>41</sup> Large amounts of gold salts also accumulate within phagolysosomes termed aurosomes when in conjunction with chrysotherapy, which are lysosomes that experience morphological changes after gold buildup.<sup>8</sup> Any gold not stored in the tissues is excreted in the urine but in relatively small amounts to gold content in initial drug administration.<sup>41</sup>

### 1.5.3 The Use of Gold as an Antiarthritic

Rheumatoid arthritis (RA) has been termed an autoimmune disease, meaning the body mounts an immune response against itself. RA has been characterized by the progression of erosion of the joints resulting in deformities, causing disability and an immense amount of pain that can lead to increased mortality if not treated efficiently.<sup>45</sup> It consists of abnormal growth of the synovial cells, cells lining the joints, infiltration of the joint space and production of immunoglobulin proteins known as rheumatoid factors. The worsening inflammatory response has been associated with increased levels of chemical mediators dealing with the immune system and muscle contraction. Although studies and research has been numerous, a causative agent has yet to be found. Considerable evidence presented suggests the involvement of reactive oxygen

species (ROS), oxygen ions, free radicals and peroxides that can damage cells at increased levels.<sup>46</sup>

The benefits from the use of gold on the joints had been recorded in ancient times but it wasn't until 1929 when Jacque Forestier used sodium aurothiopropanol sulfonate **89** termed Allochrysine™ (Figure 1-13) to treat RA that gold therapeutic agents received notoriety. Injections were given weekly starting with small doses of 0.05 cc and increased until a total of 1.5-2.0 g had been given. There was recorded improvement in 80% of patients.<sup>47</sup>

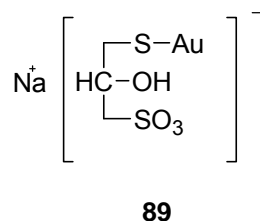


Figure 1-13 Simplified formulation of sodium aurothiopropanol sulfonate<sup>46</sup>

Two early compounds tested, still in clinical use today, were gold sodium thiomalate **90** (Figure 1-14) termed Myochrysine™ and gold thioglucose **91** (Figure 1-14) termed Solgonal™. Both hydrophilic compounds have been found to differ from their solid state structure in solution by forming polymeric rings **92** (Figure 1-15), with the exact structure dependent on various parameters.<sup>46</sup>



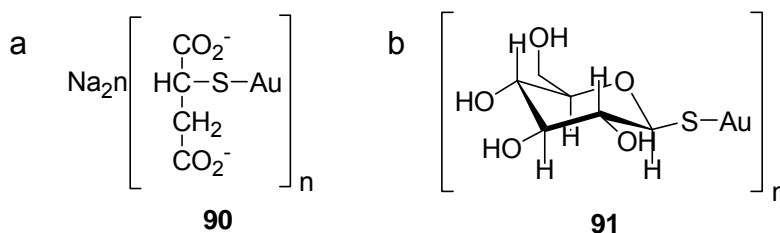


Figure 1-14 Simplified formulations of gold sodium thiomalate (a) and gold thioglucose (b)<sup>8</sup>

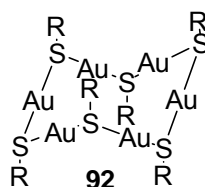


Figure 1-15 Polymeric ring structure for gold(I) thiolate complexes<sup>46</sup>

The hydrophilic nature of these complexes restricts them to cell surface interactions. This new class of gold(I) thiolate drugs halted the progression of the disease but also caused adverse affects, which will be discussed in section 1.7.

Both drugs must be administered via intramuscular injection. The treatment regimen consists of weekly injections with initial dosing of 10 mg. The dose increases to the amount of 50 mg until the onset of remission occurs, to which it is then reduced.<sup>9</sup> This form of treatment usually occurs over a period of three to six months before the benefits of anti-inflammatory action are seen.<sup>43</sup>

Gold from these compounds undergoes rapid absorption with maximum gold levels in the blood reached within two hours.<sup>48</sup> Serum albumin has been identified as the principle carrier in the blood stream with 85-90% of the gold bound to the tissues where it accumulates.<sup>49</sup> The identification of a gold(I)-albumin metabolite from gold sodium thiomalate was determined by Synchrotron

X-ray studies with albumin in excess, as it would be *in vivo*, and found to be (thiomalate) S-Au-S (Cys-34).<sup>49</sup> Once taken up by the lysosomes, myeloperoxidase via hypochlorous acid generation during oxidative burst can oxidize the gold(I) to gold(III).<sup>41,43</sup> It has been proposed that this change in oxidation occurs rapidly at inflamed sites followed by the slower process of reduction to gold(I) by thiols, thioethers and disulfides.<sup>8</sup> This redox cycle is associated with the beneficial immunological effect of anti-inflammatory action.

There were no changes in RA treatment regimens until a gold(I) oral alternative, auranofin **93** termed Ridaura™ (Figure 1-16), was introduced in 1985. A 6 mg dose per day over the course of 12 to 24 months equates to the average seen in most patients.<sup>50</sup> Although the treatment plans were more convenient and adverse effects were minimized in comparison with injectable gold(I) thiolates, auranofin has been considered a somewhat less effective option.<sup>44</sup> This has been related to the lower gold levels in the blood and therefore, lower retention in the body.<sup>8</sup>

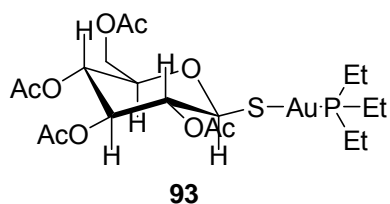


Figure 1-16 Auranofin<sup>8</sup>

Unlike its gold(I) counterparts, this molecule shows lipophilicity due to the phosphine ligand and has been found to be monomolecular in solution, with lipophilicity being key for cellular uptake.<sup>43</sup> Evidence from Synchrotron X-ray

studies and  $^{31}\text{P}$  NMR spectroscopy shows that auranofin binds to the sulfhydryl of Cys-34 with the phosphine ligand intact via ligand exchange of the acetylglucose.<sup>49,51</sup> Studies conducted mimicking *in vivo* conditions demonstrated that auranofin has a very short lifetime with the presence of excess albumin in the blood. Once acetylthiogluconate was displaced, the  $\text{Et}_3\text{PAu}^+$  moiety was taken up by the cells via a sulfhydryl shuttle mechanism.<sup>52,53</sup> Triethylphosphine can be displaced by physiological glutathione and irreversibly oxidized to  $\text{Et}_3\text{P}=\text{O}$ .<sup>54,55</sup> These displacements were consistent with radiolabeled studies that reported the excretion time of the phosphine ligand to be eight hours and the acetylglucose to be sixteen hours.<sup>8</sup>

The exact mechanism of action for which gold(I) drugs exert their anti-inflammatory action has gone unknown but evidence of several pathways connected to the gold *in vivo* redox cycle has been postulated. Although gold(I) was found to be the primary form of gold present *in vivo*, T-cells have been sensitized to gold(III) rather than the gold(I) drugs administered.<sup>8</sup> An *in vivo* study conducted in mice analyzed the oxidation of gold(I) to gold(III) using T-lymphocytes sensitized to gold(III). Three separate mechanisms were purposed: 1) generation of gold(III) scavenges ROS, 2) gold(III) irreversibly denatures proteins that enhance inflammation and 3) gold(III) may interfere with antigen processing.<sup>56</sup> During an inflammatory response,  $\text{O}_2^-$  and  $\text{H}_2\text{O}_2$  are released by inflammatory cells. The generation of gold(III) in phagocytes relies on the presence of hypochlorous acid requiring the need of ROS.<sup>8</sup> Gold(III) is a strong oxidizing agent. It can oxidize cysteine and can also cleave disulfide bonds in

proteins, hence denaturing them.<sup>52</sup> During the oxidation to gold(III), the oxidation of proteins can occur as well which could account for clinical improvements of the disease. Alteration of proteins already detected as non-self antigens could lead to their inhibition of T-cell recognition.<sup>45</sup> If anti-inflammatory effects were operating within the proposed *in vivo* gold redox system, the time period of prolonged beneficial effects and consequent adverse effects would be explained.<sup>8,54</sup>

Although both types of gold(I) anti-arthritis have different metabolisms *in vivo*, they share the dicyanogold(I),  $[\text{Au}(\text{CN})_2]^-$ , metabolite.<sup>57</sup> Patients undergoing chrysotherapy have similar levels of gold in their bloodstreams but vary in the amount of gold in the red blood cells. High levels are associated with patients who smoke while receiving treatment, which was shown to be facilitated by reactions between gold and cyanide in the blood due to hydrocyanic inhalation.<sup>58</sup> Although auranofin can interact with cyanide, it was considered of lesser importance to its cellular uptake due to the lipophilicity of the molecule.<sup>8</sup> *In vitro* studies have indicated that gold undergoes rapid uptake into the red blood cells during incubation with dicyanogold.<sup>59</sup> While these findings were void of a mechanism for gold uptake from dicyanogold, it was reported that dicyanogold did not enter cells through the anion channel and that excess cyanide did not block gold uptake, implicating loss of a cyanide ligand. The active metabolite was generated at inflamed sites through reaction with cyanide released during phagocytosis.<sup>60</sup> It formed primarily albumin adducts over ligand exchange due to gold's strong affinity for cyanide.<sup>53</sup> Evidence indicated that it entered the cell and

limited oxidative burst, rapid release of ROS.<sup>61</sup> The inhibition of oxidative burst may contribute to slowing the progression of RA observed in chrysotherapy patients.<sup>53</sup> Although the major site of action for inhibition was not identified, several potential sites could be excluded.<sup>58</sup> In the presence of excess cyanide, the gold(III) species tetracyanoaurate,  $[\text{Au}(\text{CN})_4]^-$ , will form.<sup>8</sup> This follows the same redox pattern as described above with rapid oxidation and slower reduction contributing to suspected method of anti-inflammatory action.<sup>43</sup>

It has been suggested that auranofin has an anti-inflammatory mechanism of action different from that of gold(I) thiolate drugs. Although aurocyanide was identified as a common metabolite to both types of gold drugs administered, its cellular interaction was different from that seen in auranofin. Auranofin irreversibly binds polymorphonuclear leukocytes responsible for oxidative burst and at concentrations of 1  $\mu\text{M}$ , inhibition was immediate.<sup>58</sup> Evidence also suggested that it targeted macrophages, cells responsible for initiating rheumatoid synovitis, inflammation associated with swelling of the joint.<sup>52</sup> It was apparent that the phosphine ligand, being lipophilic, along with sulfhydryl shuttle transport into cells, affects cytotoxicity and contributes to the possibility of an alternate mechanism of action in comparison to gold(I) thiolates.

Although significant, the anti-inflammatory response was not credited as the only means of chrysotherapy effectiveness. Antimicrobial activity, which will be discussed in section 1.5.5, reduction of immune response activity and enzyme inhibition have all been considered mechanisms of action that may contribute separately or in parallel to gold(I) anti-arthritis efficacy.<sup>8</sup> It has been noted that

patients treated with gold show decreased rheumatoid factor synthesis.<sup>62</sup> Based on *in vivo* results, auranofin reduced antibody levels thereby depressing humoral immunity.<sup>63</sup> It has also been suggested that gold(I) or gold(III) may interact with the major histocompatibility complex protein inhibiting T-cell response associated with the disease.<sup>64</sup> *In vitro* studies have shown that inhibition of enzymes occurs in large part in the lysosomes, where gold concentrations have been identified as greatest, consistent with the reported area of tissue damage in those suffering with RA.<sup>61</sup>

#### 1.5.4 The Use of Gold as an Anticancer Agent

The discovery of cisplatin's antitumor activity in 1969 prompted the search for other metal-containing complexes possessing similar activity. Substantial lower malignancy rates of RA patients undergoing chrysotherapy had been reported.<sup>65</sup> Gold(I) thiolates were shown to have no activity, whereas auranofin showed cytotoxic effects toward HeLa cells and *in vivo* activity against P388 leukemia. Despite promising results, it had no effect on solid tumors.<sup>66</sup>

Many auranofin (Figure 1-16) derivatives were designed to try and combat the lack of solid tumor activity.<sup>67</sup> Versions were synthesized that modified or replaced the sugar, the phosphine or both. Both *in vitro* (B16 melanoma and P388 leukemia) and *in vivo* (P388 leukemia inoculated mice) studies were conducted and several conclusions were drawn. Activity was increased in the presence of phosphine ligands and reduced in their absence. Tumor activity was limited, with the most active compound containing a  $\text{PEt}_2\text{Me}$  ligand. The importance of this study was a new development in drug screening.<sup>68</sup> Based on

these results, it was concluded that *in vitro* activity does not also mean *in vivo* activity, and that inactivity *in vitro* would likely be inactive *in vivo*. A mechanism of action different to that of cisplatin was also suggested and will be discussed in section 1.6.1.

A promising class of gold(I) tertiary phosphine complexes was prepared incorporating the (diphenylphosphine)ethane (dppe) ligand system **94** (Figure 1-17). The uncomplexed dppe ligand had been known to possess antitumor activity.<sup>9</sup> The most important compound that emerged was [dppe(AuCl)] **95** (Figure 1-17). These types of complexes were shown to rearrange in biological media, giving the tetrahedral [Au(dppe)<sub>2</sub>]<sup>+</sup> **96** (Figure 1-17).<sup>66</sup>

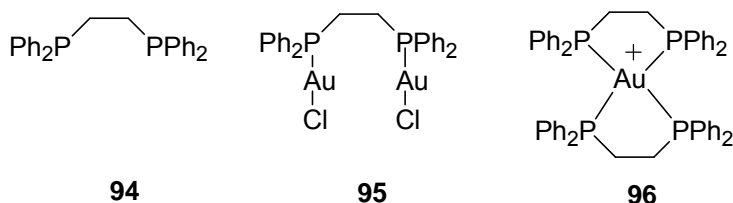


Figure 1-17 The gold(dppe) complex evolution<sup>9</sup>

The complex **96** showed activity toward peritoneal cancer cells. The gold was thought to protect the ligand from oxidation and aid in the active species delivery.<sup>9</sup> The identified rearrangement of the structure was also thought to further stabilize the compound through the chelate effect and guard even more against substitution of the phosphine ligand. Unfortunately, the toxicity of the compound prevented its use in clinical trials.

The investigation of gold(III) complexes has showed promising results. A series centered around coordination of gold to the (dimethylamino)methylphenyl (damp) ligand was synthesized (Figure 1-18). The first compound of interest **97** [AuCl<sub>2</sub>(damp)] included the *cis*-oriented positions of the chlorides, similar to the arrangement in cisplatin. When tested against a panel of human tumor lines, activity was shown to be similar to the cytotoxicity of cisplatin.<sup>69</sup> For breast, rectum and bladder tumor lines, activity was close to that seen in cisplatin, however, activity against ovarian had an IC<sub>50</sub> of 18 versus the 14 observed for cisplatin.

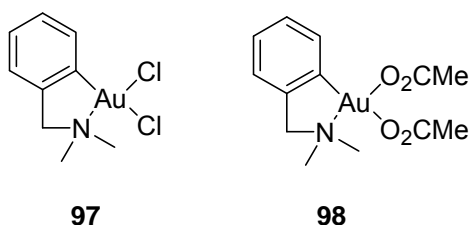


Figure 1-18 Gold(III) damp complexes<sup>9</sup>

A major drawback was the lack of water solubility. A derivative was synthesized bearing acetate groups in replacement of the chlorides **98** (Figure 1-18). *In vitro* testing again showed similar activity in comparison with cisplatin.<sup>70</sup> Results of *in vivo* testing in nude mice indicated that **98** had activity similar to cisplatin against bladder-type tumors. An interesting correlation was the ability of **98** to hydrolyze in aqueous solution, much like cisplatin, for which the resulting product has been suspected to interact with DNA.<sup>71</sup> Studies were conducted to investigate if there was a similar mechanism of action. Interstrand cross-linking was detected after incubation with ovarian cells for cisplatin. No similar effect



was observed for **98**. NMR spectroscopy studies done with biological ligands also showed a S-binding preference and reported no N-binding.<sup>70</sup> Based on these results, an alternate mode of action seems apparent.

An area of cancer research gaining more interest has been the applications surrounding the use of gold nanoparticles. One of the first major advancements in this area was the reduction of tumor growth in mice with the combination of gold nanoparticle injection and X-ray radiation.<sup>72</sup> It was also observed that one without the other showed no effect on tumor growth. An *in vitro* study conducted using a human lung carcinoma cell line revealed that gold nanoparticles lead to apoptosis by themselves.<sup>73</sup> Importantly, other cell lines have not exhibited the same results.

An experiment was also conducted on human cells to assess cytotoxicity and cellular uptake.<sup>74</sup> The presence of gold in the cells was confirmed by transmission electron microscopy (TEM) and although gold precursors may have exhibited toxicity, no adverse effects were seen in cellular function. A gold(0) nanoparticle stabilized by 5-aminovaleric acid [ $\text{NH}_2\text{-(CH}_2\text{)}_4\text{-COOH}$ ] showed selectivity to a leukemia cancer cell line by penetration rather than injection.<sup>75</sup> The selectivity efficiency of the gold nanoparticle has been attributed to the larger absorption cross-section found to reduce the laser energy required to kill by more than half.<sup>76</sup>

Folic acid receptors (FR) have been identified in large numbers on cancer cells and have limited expression on healthy cells. Folic acid **99** (Figure 1-19) was attached to gold nanoparticles by noncovalent interaction.<sup>77</sup> The

nanoparticles were tested *in vitro* against various strains of ovarian and multiple myeloma cell lines with different degrees of FR to assess targeted ability and subsequent cellular uptake. As expected, maximum uptake was seen in cells with the higher amount of FR, indicating successful targeting of cancer cells.

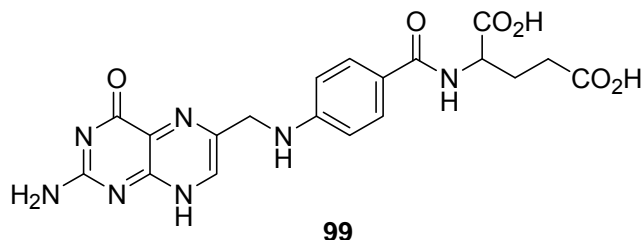


Figure 1-19 Folic acid

Based on the multitude of drug design and screening, gold complexes have become an area of interest for anticancer applications. Ongoing research in the area of gold nanoparticles has shown great promise in targeting and cytotoxic effects of cancer cells. Although no gold drug has entered clinical trials in this area, promising *in vitro* and *in vivo* results suggest the future possibility of such a complex. There have been many indications in recent years that NHC-gold(I) complexes possess anticancer properties and act by an alternate mode of action than that of cisplatin. These studies and findings will be discussed in detail in section 1.6.1.

#### 1.5.5 Gold as an Antimicrobial Agent

Infection was once thought to play a primary role in the cause of RA, to which no specific microorganism has yet to be identified.<sup>47</sup> The early work performed by Robert Koch, in which efficacy for gold salts against the strain of

*tubercle bacillus* had been shown, prompted investigations over the course of a decade into the antimicrobial properties of numerous gold compounds.

Koch had indicated that gold compounds were bacteriostatic toward *t. bacillus* in concentrations of 1 ppm.<sup>62</sup> *In vitro* testing done in the 1930s and 40s was conducted against a multitude of both gram positive and gram negative bacteria. Concentrations between  $10^{-3}$  and  $10^{-5}$  M were sufficient at inhibiting or preventing microorganism growth.<sup>62</sup> A discovery had also been made that blood from patients undergoing chrysotherapy had inhibited growth of a *streptococci* strain.<sup>78</sup> However, a study conducted using a microorganism known to induce polyarthritis in mice failed to show any link towards bacteriostatic ability of gold compounds, even at a higher dose of  $10^{-2}$  M.<sup>79</sup> An explanation for this difference was based on the suggestion that gold may have altered the pH of the culture media by precipitating proteins.<sup>80</sup>

Several *in vivo* studies were also conducted at this time. It was discovered that mice receiving a sodium gold thiomalate injection showed no signs of infection after being injected with a lethal dose of a *streptococcus* strain.<sup>81</sup> Another study was performed in mice with mycoplasma strain-induced arthritis. Various types of gold compounds were used as treatment options. Contrary to previous results, effectiveness was seen for doses injected up to 1 week after arthritis onset.<sup>79</sup> If treatment was continued for 3 weeks, 94% of infected mice had disappearance of arthritis as opposed to only 7% of a non-infected, non-injected (gold) control group. A separate study confirmed the inactivity of sodium

thiomalate under similar circumstances, indicating that gold was necessary for beneficial effects.<sup>82</sup>

An *in vitro* study was conducted using auranofin, in which 2 strains of *Pseudomonas putida* (one being gold resistant) were grown in its presence.<sup>83</sup> Radiolabeled <sup>195</sup>Au was also used to follow the uptake of gold into the cells. Several relevant observations were noted. Auranofin, at a dose of 50  $\mu$ M was able to reduce the amount of viable cells to only 16% within the first hour and 0% after 6 hours, whereas the resistant strain showed 58% viable cells after 16 hours. The determination of the rate of oxygen consumption by the cells was also made. Auranofin was able to limit O<sub>2</sub> uptake in the non-resistant strain to only 16% over a course of 20 minutes. Importantly, auranofin tested without the phosphine moiety present only inhibited 5% of O<sub>2</sub> uptake under the same conditions, indicating a role for its presence. Radiolabeled studies indicated a gradual uptake of gold over a 3 hour period, whereas little change was seen during the same time period for the resistant strain. Results showed that uptake is not rapid and suggest that resistance may be linked to the ability of uptake control.<sup>83</sup>

A few gold phosphorus ylide compounds **99-101** (Figure 1-20) from a broad metal complex search were found to have some promising antibacterial activity against a methicillin-resistant strain of *Staphylococcus aureus* (MRSA). Minimum inhibitory concentrations (MIC), standard microbiological test used to determine the bacteriostatic activity of antimicrobial agents with low values

reflecting efficacy, revealed that concentrations as low as 1.0 µg/mL inhibited 50% of bacterial growth.<sup>84</sup>

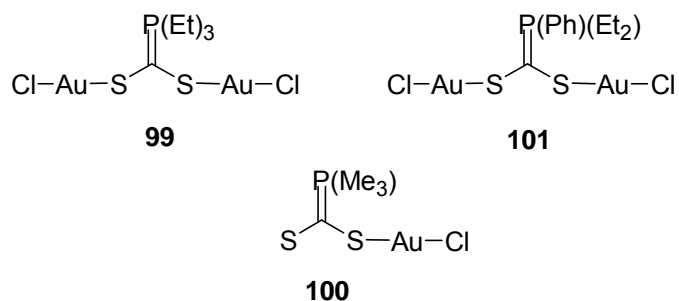


Figure 1-20 Evaluated gold phosphorus ylide compounds

Another gold compound, [Au(SCN)(PMe<sub>3</sub>)], also showed encouraging results against the same methicillin-resistant strain of *Staphylococcus aureus*. An MIC<sub>50</sub> (minimum concentration inhibiting 50% of bacterial growth) of 0.33 µg/cm<sup>3</sup> was observed.<sup>66</sup> It was later tested against laboratory strains of various other organisms and was found less active against *Pseudomonas aeruginosa* and *Candida albicans*, suggesting gram positive sensitivity was favored.<sup>85</sup> *In vivo* studies conducted also showed a reduction in bacterial growth for treatment on pairs of hairless-obese mice inoculated with cultures on the skin.

A few of the Au(damp) derivatives (Figure 1-18) studied for antitumor properties were also tested against a series of gram positive and gram negative bacteria. Broad spectrum activity was reported.<sup>9</sup> However, the same gram positive selectivity trend was observed, although to a lesser degree.<sup>66,71</sup>

Although gold complexes vary in effectiveness for gram positive or negative bacteria, their efficacy has warranted further evaluation. A specific mechanism of action has not been determined at this time. Some more recent

studies involving gold-NHC complexes have been conducted with encouraging results, which may help to shed light on a possible mechanism of action. These studies will be discussed in section 1.6.2.

## 1.6 Medicinal Applications of NHC-Gold Complexes

The medicinal applications of gold-NHC complexes are reviewed in this section. The two areas of application include anticancer and antimicrobial studies.

### 1.6.1 Anticancer Properties of Gold NHC Complexes

Early anticancer evaluations on auranofin showed the complex's ability to disrupt regulation of mitochondrial membrane permeability (MMP), resulting in MMP transition, swelling and loss of permeability.<sup>86</sup> Action was found to be concentration-dependent and maximum rate and swelling extent was observed at 1  $\mu$ M. A release of cytochrome c was also induced, indicating the possible link of initiating apoptosis. The replacement of phosphine ligands by NHCs in gold(I) has been investigated and a series of NHC-gold(I) auranofin analogues **102-106** (Figure 1-21) was synthesized.<sup>21</sup> However, at the time of this review, results on mitochondrial function were still in progress.<sup>10</sup>

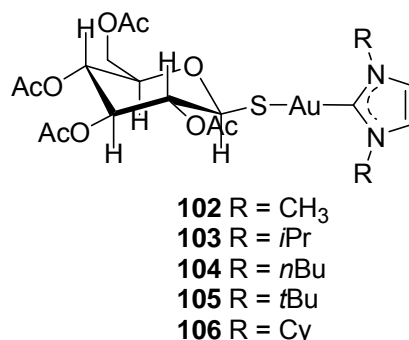


Figure 1-21 NHC-gold(I) auranofin analogues<sup>21</sup>

A series of dinuclear gold(I) NHCs **29-35** (Figure 1-7) were also tested for MMP disruption.<sup>87</sup> At concentrations of 10  $\mu$ M and in the presence of calcium (25  $\mu$ M), **30-35** induced significant swelling, however, **29**, which differed structurally, inducing swelling at a lower level. It was also determined that the amount of gold uptake in the cells had no correlation with the rate of swelling induction.

Complex **30** was used to further investigate the role of calcium. In the presence of calcium, **30** induced swelling at concentrations as low as 0.5  $\mu$ M, although at a slower rate. If the concentration of **30** was increased, the rate increased as well. If calcium was absent, induced-swelling from **30** was completely blocked at 0.5  $\mu$ M and was inhibited at concentrations between 5-10  $\mu$ M. If the concentration of **30** was increased to 40  $\mu$ M, significant swelling did occur but at a slower rate observed for when calcium was present.

A series of (bis)NHC-gold(I) complexes **23, 25-28** (Figure 1-6) were investigated for their ability to induce swelling and subsequent loss of MMP.<sup>22</sup> The substituents were varied so as to generate differences in lipophilicity. Lipophilicity had a direct bearing on the induction of swelling and the order increased as expected by **23 < 25 < 26 < 27 < 28**.<sup>10</sup> At concentrations of 1 and

10  $\mu\text{M}$  and in the presence of calcium (25  $\mu\text{M}$ ), each induced dose-dependent, swelling assessed by standard assay, with **28** showing the most rapid onset.

Recently a (bis)NHC-gold(I) complex with a ferrocene moiety **107** (Figure 1-22) was synthesized and tested for cytotoxic activity.<sup>88</sup> The compound was tested against various human cell lines and the viability of cells was determined by MTT assay. In HeLa and Jurkat cells, **107** had  $\text{IC}_{50}$ s averaging approximately 0.413  $\mu\text{M}$ , lower values than cisplatin for each with an approximate average value of 0.711  $\mu\text{M}$ . Importantly, **107** also showed selectivity for cancer cells.

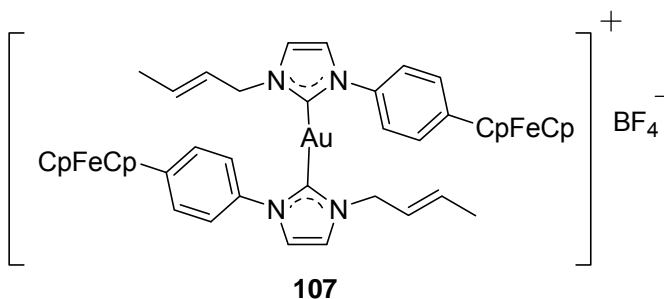


Figure 1-22 (bis)NHC-gold(I) ferrocenylphenyl complex<sup>88</sup>

Based on current evidence, gold(I)-NHC complexes possess antitumor properties and appear to have a mechanism of action separate from that of cisplatin. Their ability to disrupt MMP and induce swelling leads to a direct loss of permeability. The lipophilicity of the complex affects the rate of cell uptake and can be manipulated by substituent choice, thereby targeting cancer cells. The addition of a ferrocene moiety appears to enhance anticancer activity *in vitro*, indicating the need for further studies.



### 1.6.2 Antimicrobial Properties of Gold NHCs

Based on the multitude of antimicrobial studies done with various gold phosphine compounds, testing of NHC derivatized gold compounds was a logical next step. A study was conducted by Özdemir *et al.* in 2004, in which a series of saturated (bis)NHC-gold(I) chloride complexes **3-7** (eq. 1-1) and **8** (Figure 1-2) were synthesized and analyzed *in vitro* for their potential antimicrobial properties.<sup>16</sup> Various strains of *Escherichia coli*, *Staphylococcus epidermidis* and *S. aureus*, *Enterococcus faecalis*, *Enterobacter cloacae*, *Pseudomonas aeruginosa* and *Candida albicans* were evaluated. The compounds were dissolved in DMSO and diluted with water and serial dilutions were performed. The MICs were assessed visually by growth.

No compound showed any consistency across both gram positive and gram negative bacteria. Compound **3** was the most effective with a concentration of 3.12 µg/mL against *S. aureus* and *E. faecalis* and the only gold(I) NHC to show any activity against *P. aeruginosa* at the aforementioned value.<sup>16</sup> The closest compound structurally to **3** was **4** and it only showed activity towards *E. coli* at the same concentration of 3.12 µg/mL. The mechanism of action remains unclear but the presence of substituted benzyls on the nitrogen atom of the imidazole ring seems to enhance the compounds ability to affect gram negative bacteria.

A gold(I) NHC complex was synthesized bearing nitrogen-bound methylbenzyl and *t*-butyl substituents on the imidazole ring **108** (Figure 1-23).<sup>89</sup> This complex was tested for its antimicrobial activity against *Bacillus subtilis* and

*Escherichia coli*. Microorganisms were treated with different concentrations of **108** and the growth of the bacteria was measured over multiple time intervals. After 12 hours of incubation, 80% of *B. subtilis* growth had been inhibited, however, no effect was seen on *E. coli* growth at the same concentrations. This finding was in agreement with other gold complexes tested in that there appears to be a selectivity to gram positive bacteria over gram negative types.

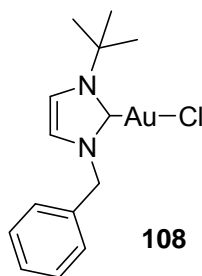


Figure 1-23 NHC-gold(I) chloro complex<sup>89</sup>

Further evaluation was done to examine the morphology of the *B. subtilis* cells after 4 hours of incubation time with **108**. A control was also used with no gold compound present for comparison. The cells increased in length, seen by differential interference contrast (DIC) microscopy, by 3.5 fold in the presence of 4  $\mu$ M of **108**. These results and the absence of any cell morphology in the control, suggested that the gold complex inhibited cell proliferation by blocking cytokinesis. The explanation seems plausible since FtsZ, a tubulin-like protein, is equally distributed within the cell. Given gold's strong ability to bind sulfur sites in biological media and previous findings of gradual uptake of gold into bacterial cells, cellular protein binding could be present.

The results of both studies indicate further investigation for the use of NHC-gold complexes as antimicrobial agents is warranted. The ongoing trend with gold complexes evaluated for antimicrobial use has been the observation of a gram positive bacteria selectivity. The efficacy of **3** against *P. aeruginosa*, a gram negative bacteria, was an encouraging finding. It was suspected that the presence of a substituted benzyl group on the nitrogen of the imidazole ring enhanced antimicrobial activity. Further testing is needed to investigate which types of benzyl derivatives equate to the greatest increase in effectiveness of the antimicrobial agent. Based on the cell morphology of *B. subtilis* induced by incubation with **108**, an inhibition with cell proliferation was suggested.<sup>89</sup> Studies have proven the interaction of gold with sulfur sites in biological media.<sup>8,49</sup> A possible mechanism for the antimicrobial activity could be through interaction with cellular proteins.

### 1.7 Toxicity of Gold and Gold-Containing Compounds

The toxicity associated with gold is reviewed in this section. Both gold(0) and gold(I) oxidation states are evaluated.

#### 1.7.1 Metallic Gold Toxicity

Metallic gold generally has low toxicity and the average person has a total of 0.2 mg throughout their body.<sup>90</sup> Its use in the food industry has included gold(0) powder incorporated into pastries, chocolate and liquors with virtually no direct-link response. There have been rare instances of allergic reactions due to contact.<sup>41</sup> Very few cases of toxicity have been associated with the use of

metallic gold or gold alloys in dental applications. There has been some allergic response seen in patients receiving gold optical implants. Inflammation has been reported several weeks post operation and testing indicated exaggerated lymphocytic infiltrations.<sup>41</sup>

#### 1.7.2 Gold Toxicity Associated with Rheumatoid Arthritis Treatment

Rheumatoid arthritis has been classified as a chronic autoimmune disease that can have serious long-term outcomes. The course of action for those suffering with this disease has been early intervention with the most effective medications. All drugs associated with treatment of this disease, including gold-based pharmaceuticals, have adverse effects associated with their use.

Currently, three gold compounds have been approved in the United States for the treatment of RA, gold thiomalate (Figure 1-14), gold thioglucose (Figure 1-14) and auranofin (Figure 1-16). The gold thiolates are administered through intramuscular injection and auranofin is administered orally. Approximately half of patients undergoing chrysotherapy experienced some sort of adverse effect. The most common adverse effect amongst all three has been identified as diverse forms of dermatitis, a blanket term for inflammation of the skin.<sup>41</sup> Dermatitis accounts for roughly two-thirds of all reported side-effect cases, however it was not based on gold concentrations in the skin. Symptoms reported include painful itching, rash and hypersensitivity of mucous membranes. More severe, but less frequent manifestations include blood disorders affecting blood cells and platelets, pneumonia and nephrotoxicity. Patients receiving a cumulative dose of less than 250 mg rarely reported any adversity and many receiving 1000 mg or

more were adverse-free. Dermal reactions were categorized as dosage-related because most eruptions disappeared within 3 months of stopping treatment.<sup>41</sup> Many were also able to resume treatment without side-effects reoccurring.

A major area of concern has been critical concentrations in the organs. Based on the bioactivity of these gold compounds, tissue uptake has been reported as cumulative.<sup>48</sup> To help combat tissue accumulation, various chelated agents have been used to assist in clearance from the body. Bucillamine **109** and 2,3-dimercaptopropane sulphonate (DMPS) **110** (Figure 1-24) have been shown to improve renal damage and decrease gold concentration in the kidneys.<sup>91</sup>

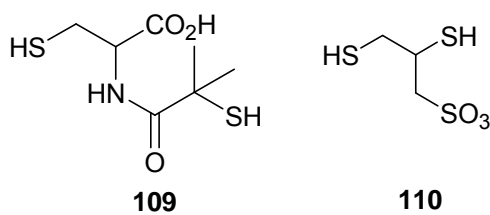


Figure 1-24 Bucillamine and DMPS

Patients receiving gold thiolate treatment options must endure large weekly injectable doses in order to sustain the therapeutic effect, frequently experiencing pain. This has been managed by using smaller needles or the incorporation of lidocaine.<sup>50</sup> In the late 1960s, 17 deaths in the United Kingdom were recorded with gold listed as the probable cause of death. It was later reported that these incidences may have been overestimated. Patients receiving aurothiomalate had higher reported side-effects associated to poor sulfoxidation capacity.<sup>50</sup>

Auranofin has been considered the safest option of the three. The same side-effects have been observed but were considerably milder, with the most reported condition being bowel changes.<sup>50</sup> Perhaps, the most important difference shown for auranofin was the binding of only 35% of total gold in the blood to albumin, versus the 90% of total gold in the blood for aurothiomalate.<sup>48</sup> After 6 months of treatment, auranofin was found 58% bound to blood cells as opposed to 3% for aurothiomalate.<sup>63</sup> For this reason, auranofin retention in the body and hence critical organs has been found to be small in comparison to gold thiolate drugs.<sup>48</sup>

## 1.8 Conclusion

NHC gold chemistry has seen a variety of methods used in the synthesis of gold(I) NHC compounds, with the most popular being silver transmetallation reactions. The methods used to synthesize gold(III) NHCs have been less plentiful, with oxidative addition of halogens being the only method reported. Both types of gold NHC complexes differ structurally, with gold(I) NHCs being 2-coordinate, linear systems and gold(III) NHCs being 4-coordinate, square planar complexes.

The area of gold chemistry and its potential for medicinal use has had a rich history that continues to grow. Documented since 2500 BC, gold has shown a wide variety of therapeutic applications from an anti-infective to anti-arthritic and recently investigated for anti-cancer properties. The use of gold NHC compounds for antimicrobial and antimitochondrial activity has recently gained attention. Although further investigation is needed, results would indicate that

these gold NHC compounds showed effectiveness in both areas and the use of other gold NHCs may show promise.

## CHAPTER II

### SYNTHESIS, WATER STABILITY AND ANTIMICROBIAL PROPERTIES OF GOLD-NHC COMPLEXES AND THEIR SILVER-NHC PRECURSORS

#### 2.1 Introduction

The use of silver oxide as a means to synthesize silver-NHCs has been used since 1998 when it was first applied by Lin and co-workers as a transmetallation agent to generate a gold-NHC complex.<sup>29</sup> Since that time, carbene transfer has become a popular technique that has been applied to a variety of metals. Our area of interest in silver-NHCs has been broadened to explore their use as potential antimicrobial agents.<sup>92,93,94,95</sup> Our reported research has shown their efficacy and even versatility as silver-NHC impregnated nanofibers.<sup>96</sup> Previously reported work by our group has also shown that varying the substituents off the backbone of the imidazole ring can have varying effects on the stability of silver acetate NHC systems, as will be discussed in section 3.3.<sup>95</sup> When electron-withdrawing groups were placed at the 4- and 5-positions, the metal system showed enhanced stability in aqueous solution. Our purpose was to explore the use of electron-withdrawing groups placed at the 4- and 5-positions of



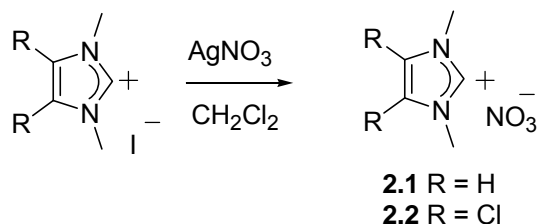
silver-(bis)NHC and subsequent gold-(bis)NHC systems to see if the same trends were observed.

Robert Koch was the first to have demonstrated the antibacterial activity of gold(I) salts.<sup>41</sup> The activities of these salts against *tubercle bacillus* lead to the use of various gold compounds in the treatment of tuberculosis for 40 years. Although a wide variety of microbe testing was performed on numerous gold complexes between the 1930s and 1940s with some positive outcomes, little has been reported since that time. The antimicrobial activity of several gold(I)-NHC complexes of the saturated type (single bond between C<sub>4</sub> and C<sub>5</sub> of imidazole ring) was investigated by Özdemir and co-workers in 2004.<sup>16</sup> They reported that the placement of mesityl or para-substituted benzyl groups on the nitrogen atoms lead to encouraging activity against several bacteria strains. Our intent was to explore the antimicrobial properties of gold(I)-NHC complexes synthesized and compare them to those of their silver(I)-NHC precursors.

## 2.2 Synthesis and Characterization of Silver(I)-(bis)NHC Complexes

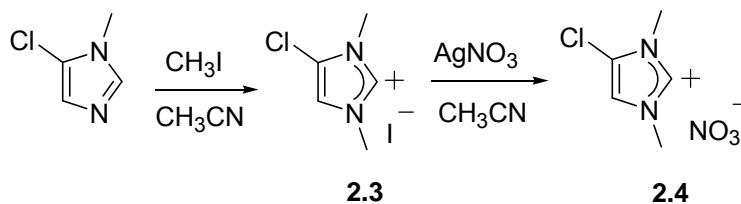
Anion exchange of 1,3-dimethylimidazolium iodide and 4,5-dichloro-1,3-dimethylimidazolium iodide was easily achieved by adding equal equivalents of silver nitrate and stirring in dichloromethane for 20-30 minutes (Scheme 2-1). Upon filtration and evaporation of the volatiles, a hygroscopic solid, 1,3-dimethylimidazolium nitrate **2.1** was obtained in 97% from the dihydrogen-NHC analog. Upon filtration and evaporation of the volatiles, the salt 4,5-dichloro-1,3-dimethylimidazolium nitrate **2.2** was obtained in 72% yield from the dichloro-NHC analog. The <sup>1</sup>H and <sup>13</sup>C NMR spectras were consistent with the structures, with

the imidazolium protons observed at 9.08 ppm for **2.1** and 9.39 ppm for **2.2** in the  $^1\text{H}$  NMR and the imidazolium carbons observed at 137.5 ppm for **2.1** and 136.8 ppm for **2.2** in the  $^{13}\text{C}$  NMR.



Scheme 2-1 Synthesis of imidazolium nitrate salts **2.1** and **2.2**

The iodide salt of the monochloro-analog **2.3** can be generated by refluxing 5-chloro-1-methylimidazole in acetonitrile with excess iodomethane (Scheme 2-2). The imidazolium proton resonance can be seen in the  $^1\text{H}$  spectrum at 9.20 ppm and the imidazolium carbon resonance was observed in the  $^{13}\text{C}$  NMR spectrum at 137.4 ppm.



Scheme 2-2 Synthesis of nitrate salt **2.4**

The nitrate salt **2.4** was synthesized by anion exchange using silver nitrate in acetonitrile (Scheme 2-2). Slight shifts of the imidazolium peaks can be seen in both  $^1\text{H}$  and  $^{13}\text{C}$  NMR spectra at 9.22 ppm and 137.5 ppm, respectively. A crystal structure of **2.4** was also obtained by slow evaporation from a concentrated solution of dichloromethane and the thermal ellipsoid plot is shown in Figure 2-1.

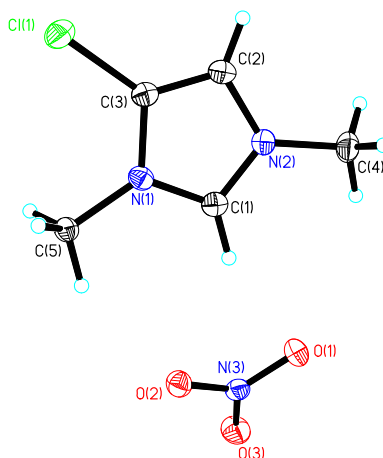
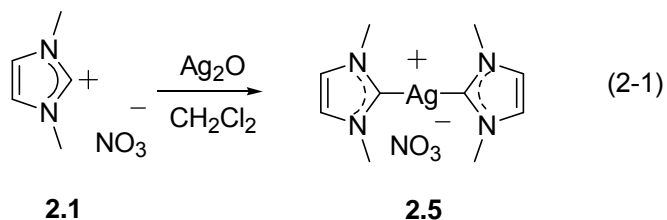


Figure 2-1 Thermal ellipsoid plot of **2.4** shown at 50% probability

To the nitrate salt **2.1**, 2 molar equivalents of silver oxide were added and stirred in dichloromethane for 4 hours to afford silver complex **2.5** (eq. 2-1). This complex was prepared by Lee and co-workers in 2002 by an alternate method.<sup>97</sup> However, only melting point (mp), <sup>1</sup>H NMR and elemental analysis were reported.



The <sup>1</sup>H NMR spectrum was in agreement with the protons of the 4- and 5-positions showing a single resonance at 7.43 ppm and the methyl protons, also showing a single resonance at 3.81 ppm. Elemental analysis was within close agreement with the expected values for nitrogen and hydrogen, with differences between 1-2%. However, carbon analysis deviated by approximately 16%. The <sup>13</sup>C NMR spectrum of **2.5** shows the resonance of the carbene carbon at 180.1

ppm. A crystal structure of **2.5** was obtained to unambiguously identify the complex. Single crystals were grown from a concentrated dichloromethane solution and the thermal ellipsoid plot is shown in Figure 2-2.

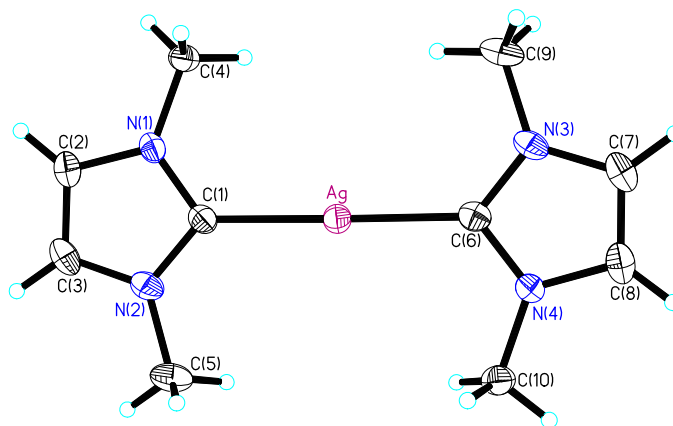
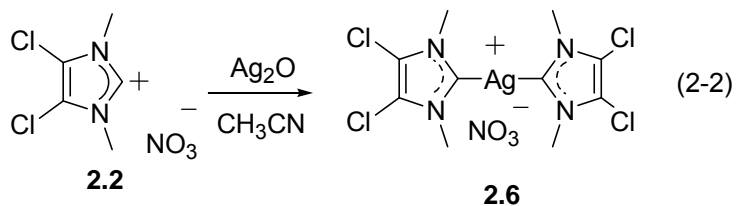


Figure 2-2 Thermal ellipsoid plot of cationic portion of **2.5** shown at 50% probability

A reaction between the nitrate salt **2.2** and silver oxide was run in a 1:1 ratio in acetonitrile for 3 hours to synthesize silver complex **2.6** (eq. 2-2). The  $^{13}\text{C}$  NMR spectrum of **2.6** shows the carbene carbon resonance at 181.3 ppm similar to that observed for complex **2.5** at 180.1 ppm. Single crystals suitable for X-ray diffraction were grown from a concentrated acetonitrile solution and the thermal ellipsoid plot is shown in Figure 2-3.



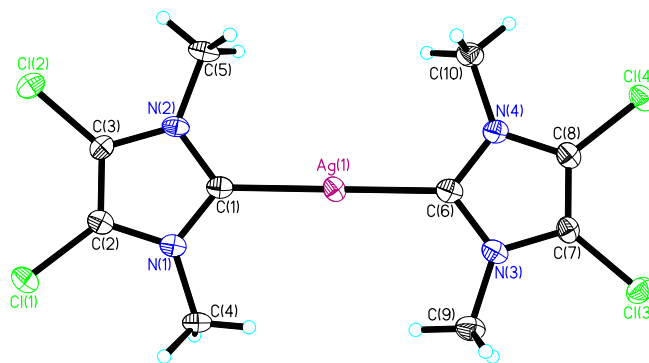
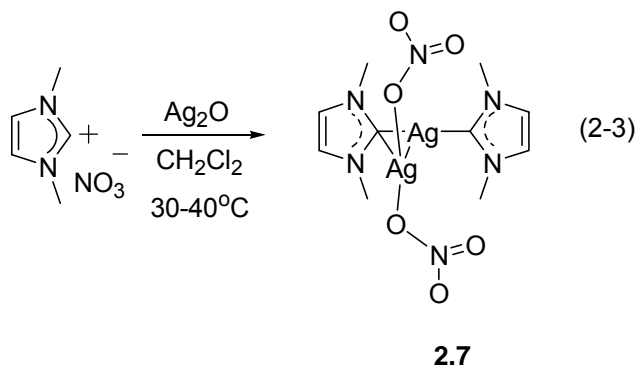


Figure 2-3 Thermal ellipsoid plot of cationic portion of **2.6** shown at 50% probability

Upon reaction of **2.1** with 4 molar equivalents of silver oxide in dichloromethane under reflux between 30-40°C for 4 hours, the dinuclear silver complex **2.7** was obtained (eq. 2-3). The reaction was similar to that of **2.5** except the silver oxide ratio was increased by two and the mixture was stirred at reflux. Importantly, if only one of the reaction conditions were changed, silver complex **2.5** was achieved.



The  $^{13}\text{C}$  NMR spectrum revealed a single carbene carbon resonance at 180.2 ppm, similar to that of **2.5** (180.1 ppm) and **2.6** (181.3 ppm). The structure of **2.7** was determined by single crystal X-ray diffraction (Figure 2-4). Crystals

suitable for X-ray diffraction were obtained from slow evaporation of a saturated dichloromethane solution. Complex **2.7** crystallized in the monoclinic space group P2(1)/m. It had a Z value of two indicating the molecule sitting on a reflection plane.

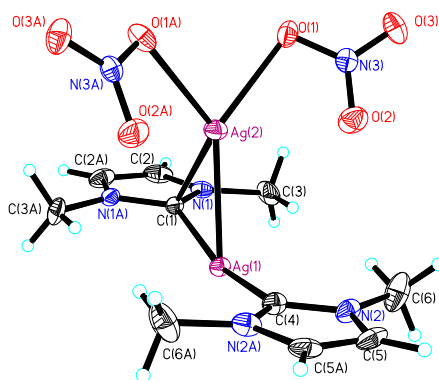
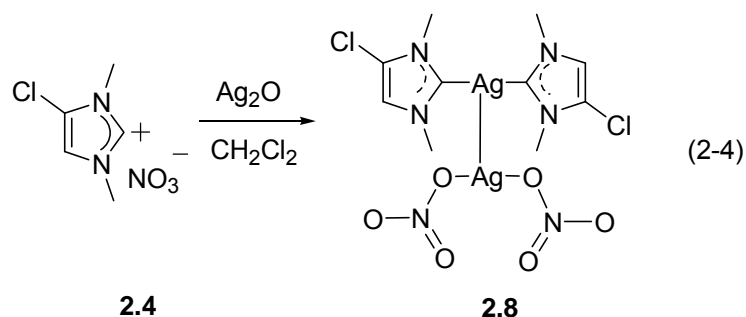


Figure 2-4 Thermal ellipsoid plot of dinuclear silver complex **2.7** shown at 50% probability

The nitrate salt **2.4** was stirred with 1 molar equivalent of silver oxide for 2 hours in dichloromethane and dinuclear silver complex **2.8** was obtained (eq. 2-4). The same product was obtained with equivalents greater than one of silver oxide, reaction times ranging from 2-4 hours or acetonitrile as the solvent.



The carbene carbon resonance was observed at 181.6 ppm in the  $^{13}\text{C}$  NMR spectrum. The resonance was similar to those observed for **2.5** (180.1 ppm), **2.6** (181.3 ppm) and **2.7** (180.2 ppm).

Single crystals suitable for X-ray diffraction were grown by slow evaporation from a concentrated dichloromethane solution and the thermal ellipsoid plot is shown in Figure 2-5. Selected bond distances and angles of silver complexes **2.5**, **2.6**, **2.7** and **2.8** have been collected in Table 2-1. The carbon-silver bond distances for the monosilver complexes were within experimental error of each other in agreement at an average of 2.08 Å. The carbon-silver bond distances for the dinuclear silver complexes differed significantly. Complex **2.7** had three carbon-silver bonds with distances of 2.145(5) Å, 2.102(5) Å and 2.467(5) Å. Complex **2.8** had two carbon-silver bonds, both with distances of 2.100(2) Å. The dinuclear silver complexes also showed oxygen-silver bonds with distances of 2.409(3) Å for **2.7** and 2.446(2) Å for **2.8**. These complexes also displayed silver-silver bond distances of 2.6717(7) Å for **2.7** and 2.6806(10) Å for **2.8**, which are both shorter than that observed in elemental silver at 2.889 Å. Similar (bis)NHC-silver(I) complexes of silver halide salts have also been

reported with silver-silver interactions of 3.189(4) Å ( $\text{AgCl}_2$ )<sup>-</sup> and 3.2082(4) Å ( $\text{AgBr}_2$ )<sup>-</sup>.<sup>97</sup>

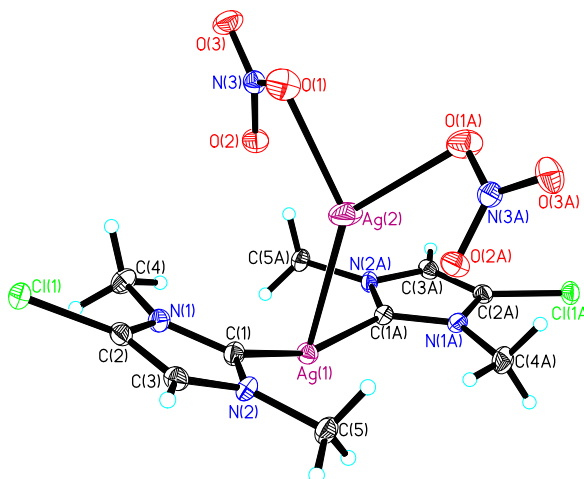


Figure 2-5 Thermal ellipsoid plot of silver complex **2.8** shown at 50% probability

Table 2-1 Selected bond distances (Å) and angles (°) for **2.5**, **2.6**, **2.7** and **2.8**

Compound	<b>2.5</b>	<b>2.6</b>	<b>2.7</b>	<b>2.8</b>
			dinuclear	dinuclear
<i>Bond lengths</i>				
Carbene-Ag1	2.073(3)	2.075(5)	2.145(5)	2.100(2)
	2.077(3)	2.074(5)	2.102(5)	2.100(2)
Carbene-Ag2			2.467(5)	
Ag1-Ag2			2.6717(7)	2.6806(10)
O1-Ag2			2.409(3)	2.446(2)
O1A-Ag2			2.409(3)	2.446(2)
<i>Bond angles</i>				
C-Ag1-C	178.92(11)	179.51(19)	162.6(2)	158.29(12)
C-Ag1-Ag2			60.45(14)	79.14(6)
			102.18(14)	79.14(6)
O1-Ag2-O1A			82.32(13)	82.82(9)



The carbon-silver-carbon bond angle for the monosilver complexes was essentially linear with  $178.92(11)^{\circ}$  observed for **2.5** and  $179.51(19)^{\circ}$  observed for **2.6**. The carbon-silver-carbon bond angle for the dinuclear silver complexes deviated from linearity with  $162.6(6)^{\circ}$  observed for **2.7** and  $158.29(12)^{\circ}$  observed for **2.8**. The oxygen-silver-oxygen bond angle was similar in both dinuclear silver complexes at  $82.32(13)^{\circ}$  observed for **2.7** and  $82.82(9)^{\circ}$  for **2.8**.

### 2.3 Water Stability of Silver(I)-(bis)NHC Complexes

$^1\text{H}$  NMR experiments of complexes **2.5**, **2.6** and **2.8** were conducted in  $\text{D}_2\text{O}$  to determine water stability by monitoring the NMR spectra as a function of time. A sample of each compound was placed into an NMR tube and  $\text{D}_2\text{O}$  was added immediately before insertion into the NMR instrument. The experiment ran for 16 hours. A scan was taken initially and then every subsequent hour. For complexes **2.5** and **2.8**, stability was determined by observing the proton integration of the backbone region of the imidazole ring. The stability of complex **2.6** was determined by observing the proton integration of the N-methyl group of the imidazole ring.

Of the three silver-(bis)NHC systems analyzed, **2.5** was the least stable in an aqueous environment. Although this compound was stable in  $\text{DMSO-}d_6$  (Figure 2-6a), approximately 39% degraded upon initial dilution in  $\text{D}_2\text{O}$  (Figure 2-6b) and only approximately 7% remained intact after 16 hours (Figure 2-6c). Monochloro analog **2.8**, also stable in  $\text{DMSO-}d_6$  (Figure 2-7a), showed greater stability than **2.5** with approximately 39% degradation upon initial dilution in  $\text{D}_2\text{O}$  (Figure 2-7b) and approximately 45% remaining intact after 16 hours (Figure 2-

7c). The dichloro analog **2.6**, which was DMSO-*d*6 stable (Figure 2-8), demonstrated the most water stability in comparison to **2.5** and **2.8** with approximately 34% degradation upon initial dilution in D<sub>2</sub>O (Figure 2-9a) and approximately 64% remaining intact after 16 hours (Figure 2-9b).

The above results further supported the same water stability trend observed for corresponding silver acetate NHC systems of the dihydro and dichloro analogues.<sup>95</sup> The enhanced water stability of the dichloro system has been attributed to the presence of electron withdrawing groups at the 4- and 5-positions of the imidazole ring, thereby withdrawing electron density from the carbene carbon rendering it less susceptible to proton attack in aqueous solution.<sup>95</sup>

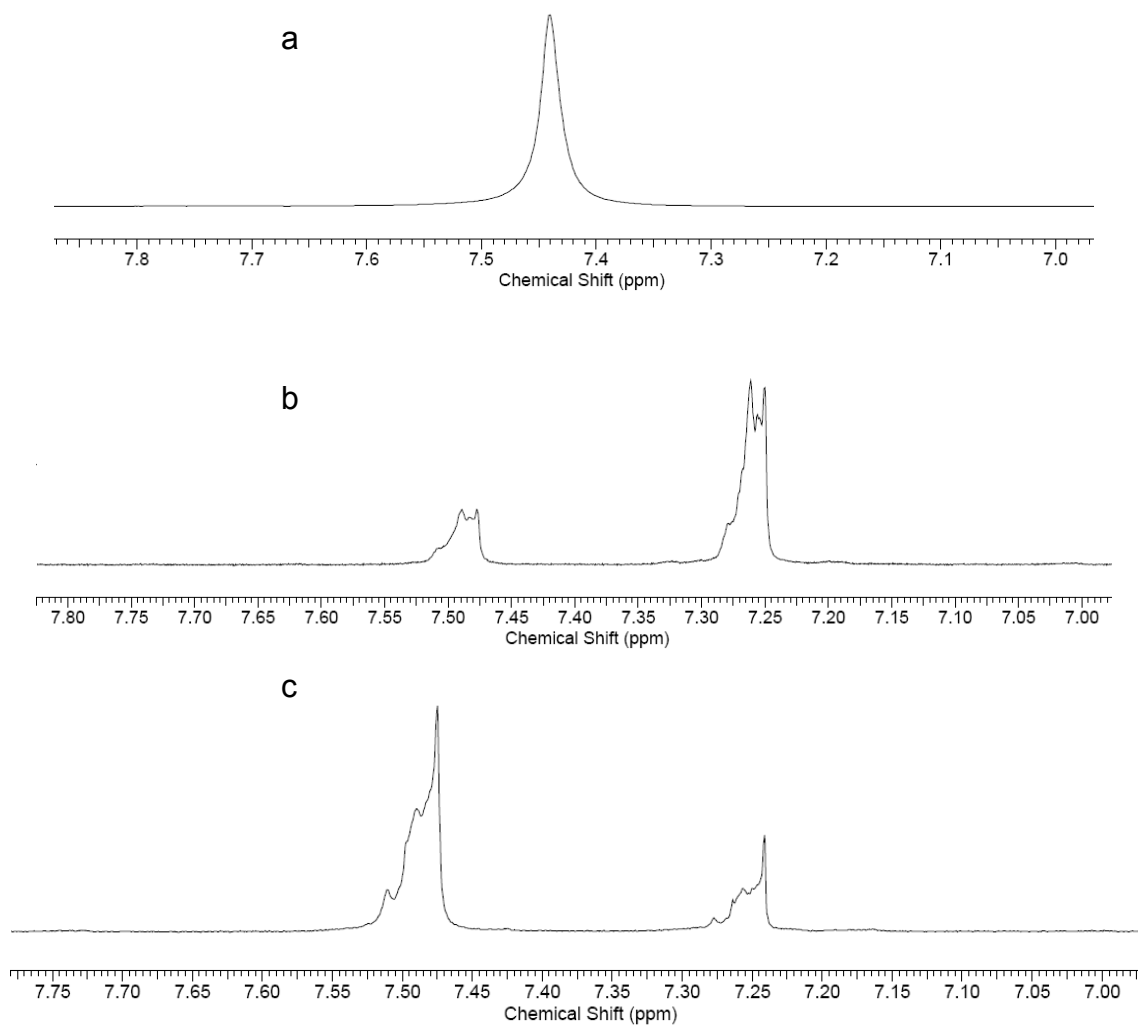


Figure 2-6  $^1\text{H}$  NMR spectra of **2.5** in DMSO- $d_6$  (a) and in  $\text{D}_2\text{O}$ , initially (b) and after 16 hours (c)

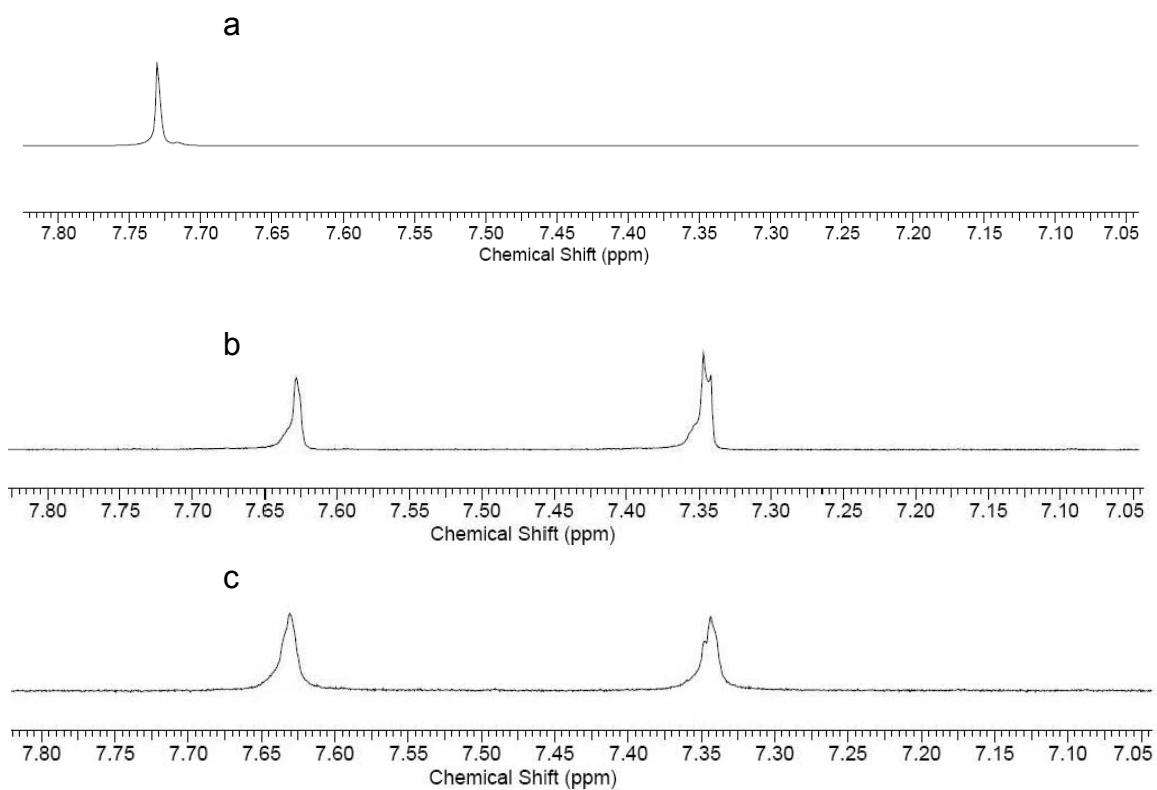


Figure 2-7  $^1\text{H}$  NMR spectra of **2.8** in  $\text{DMSO}-d_6$  (a) and in  $\text{D}_2\text{O}$ , initially (b) and after 16 hours (c)

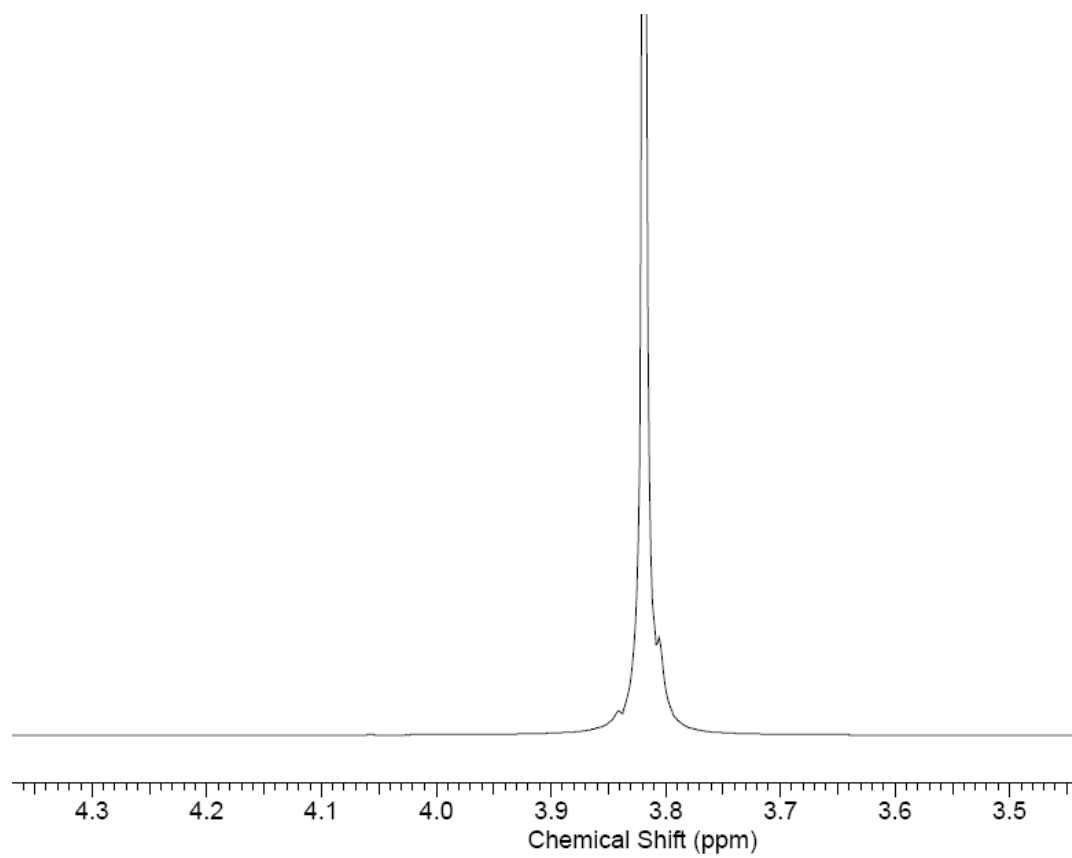


Figure 2-8  $^1\text{H}$  NMR spectrum of **2.6** in  $\text{DMSO-}d_6$

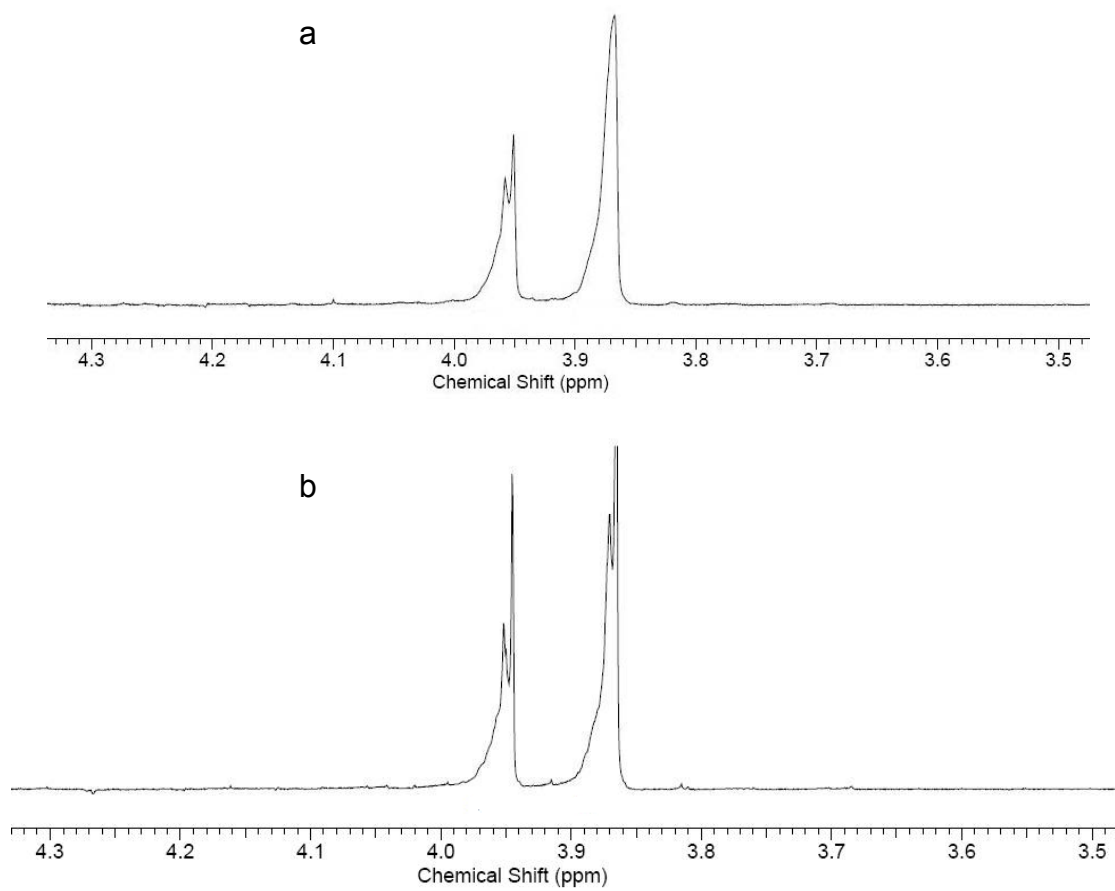
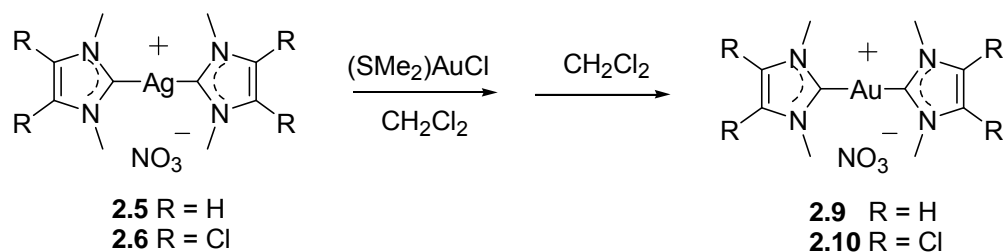


Figure 2-9  $^1\text{H}$  NMR spectra of **2.6** in  $\text{D}_2\text{O}$ , initially (a) and after 16 hours (b)

## 2.4.Synthesis and Characterization of Gold(I)-(bis)NHC Complexes

The syntheses of gold(I)-(bis)NHC complexes were achieved via transmetallation reactions from their silver(I)-(bis)NHC analogues. The reaction was run in dichloromethane with a 1:1 ratio of silver-NHC complex to chloro dimethylsulfide gold (Scheme 2-3). When starting with silver complexes **2.5** and **2.6** the subsequent sequence was followed. Upon filtration of the precipitate, assumed to be silver chloride, and evaporation of the volatiles, a white solid formed. The solid was recrystallized from dichloromethane and after slow evaporation a white solid formed which turned dark brown, possibly from the disproportionation of gold.<sup>98</sup> The resulting solid was stirred in dichloromethane and any solid not in solution was removed by filtration. Upon evaporation of the volatiles, gold-NHC complexes **2.9** and **2.10** were afforded, respectively.



Scheme 2-3 Synthesis of gold-NHC complexes **2.9** and **2.10**

The gold complexes were characterized by NMR spectroscopy. The carbene carbon resonance at 201.9 ppm in the  $^{13}\text{C}$  NMR spectrum of gold complex **2.9** differed from that of **2.10** at 182.1 ppm. It was assumed that the dihydrogen analog would show more  $\sigma$ -donation to the metal than the dichloro analog because of the difference in electron withdrawing capabilities

corresponding to a more downfield shift in the  $^{13}\text{C}$  NMR spectra, as seen with **2.9** in comparison to **2.10**. In comparison with silver complexes **2.5** (180.1 ppm) and **2.6** (181.3 ppm), it would appear that the trend was more easily distinguished for the gold complexes **2.9** (201.9 ppm) and **2.10** (182.1 ppm). NMR spectral data has been collected in Table 2-2.

Single crystals suitable for X-ray diffraction were grown by slow evaporation from a concentrated dichloromethane solution for **2.9** and **2.10** and the thermal ellipsoid plots are shown in Figure 2-10. Carbon-gold bond distances of 2.011(5) Å and 2.024(5) Å were observed for **2.9** and similar to those of **2.10** at 2.001(4) Å and 2.028(4) Å. These distances were shorter in comparison with the corresponding silver analogs **2.5** with 2.073(3) Å and 2.077(3) Å observed and **2.6** with 2.075 Å and 2.074(5) Å observed due to the relativistic effects of gold. Both gold-NHC complexes and their silver precursors have carbon-metal-carbon bond angles close to linearity. The carbon-gold-carbon bond angle seen in **2.9** and **2.10** at  $177.33(15)^\circ$  and  $178.43(15)^\circ$ , respectively, were similar to silver analogs **2.5** and **2.6**, with the corresponding carbon-silver-carbon angle seen at  $178.92(11)^\circ$  and  $179.51(19)^\circ$ , respectively. The above mentioned comparisons have been compiled in Table 2-2.



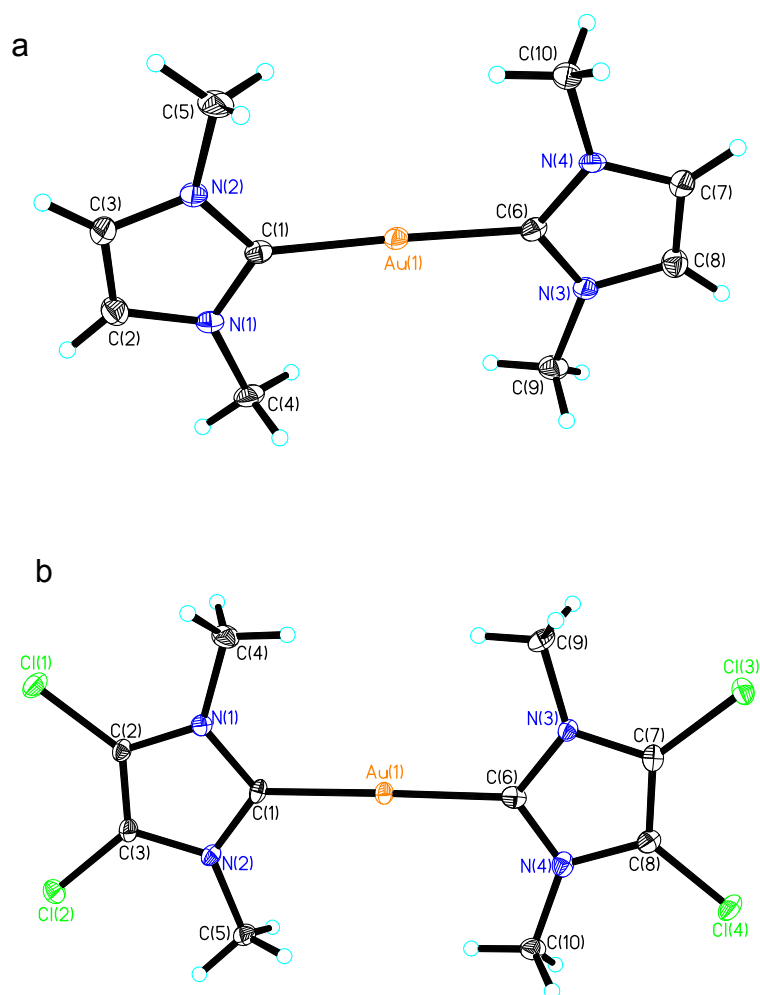


Figure 2-10 Thermal ellipsoid plots of the cationic portions of **2.9** (a) and **2.10** (b) shown at 50% probability

Table 2-2 A comparison of selected  $^{13}\text{C}$  NMR spectra resonances (ppm), bond distances (Å) and angles ( $^\circ$ ) for **2.5**, **2.6**, **2.9** and **2.10**

Compound	<b>2.5</b>	<b>2.6</b>	<b>2.9</b>	<b>2.10</b>
$^{13}\text{C}$ NMR				
Carbene-Metal	180.1	181.3	201.9	182.1
<i>Bond lengths</i>				
Carbene-Metal	2.073(3)	2.075(5)	2.011(5)	2.001(4)
Carbene-Metal	2.077(3)	2.074(5)	2.024(5)	2.028(4)
<i>Bond angles</i>				
C-Metal-C	178.92(11)	179.51(19)	177.33(15)	178.43(15)

An alternate method for the synthesis of **2.9** was attempted for the purpose of characterizing the dark brown solid which did not go back into solution after recrystallization. The reaction was run in a 1:1 ratio of **2.5** to  $\text{AuCl}(\text{SMe}_2)$  in dichloromethane for 2 hours at room temperature. After filtration of the precipitate, assumed to be silver chloride, and evaporation of the volatiles, the resulting solid was washed three times with diethyl ether. The solid was redissolved in dichloromethane and the volume was reduced to approximately 10 mL. Hexane was then added to the concentrated solution and a precipitate formed and was filtered.  $^1\text{H}$  NMR spectra of the resulting precipitate showed a mix of an imidazolium salt and likely gold complex **2.9**. Crystals suitable for X-ray diffraction, collected from the sides of the filter flask, showed the imidazolium salt to be the gold(III) salt **2.11**, 1,3-dimethylimidazolium tetrachloroaurate (Figure 2-11). The oxidation to gold(III) could be from disproportionation or due in part to the concentrated dichloromethane-hexane solution.<sup>98</sup> Roulet and co-workers

indicated that oxidation to gold(III) was quicker in dichloromethane as compared to acetonitrile or acetone.<sup>99</sup> A redox reactive intermediate was suspected whose stability would be facilitated by the solvents' coordinative interaction with the gold.

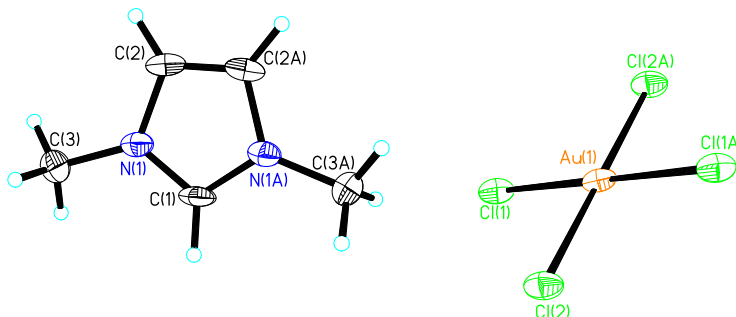


Figure 2-11 Thermal ellipsoid plot of imidazolium gold(III) salt **2.11** shown at 50% probability

Another possible explanation could be based on the ligand's potential to affect the HOMO-LUMO separation. Mohamed and co-workers reiterated that complexes with ligands that are strongly donating will decrease the HOMO-LUMO separation, thereby increasing the favorability of oxidation.<sup>100</sup> Ligand **2.1**, in this case having only hydrogen at the 4- and 5-positions of the imidazole ring, would show no  $\sigma$ -donor reduction in comparison to ligand **2.2** that has chlorine substituents at both of the corresponding positions. Peris and co-workers found that chlorine substituents at the noted positions lead to a reduction in  $\sigma$ -donor capability in comparison with nonchlorinated substituents.<sup>101</sup> This finding was later supported by our group and will be discussed in section 3.3.<sup>95</sup> Ligand **2.1**, being a better  $\sigma$ -donor than **2.2**, would generate smaller HOMO-LUMO

separation making oxidation more favorable. No such redox-type product has been observed during the synthesis of **2.10**, corresponding gold complex of ligand **2.2**, which is discussed further below.

In an attempt to isolate and characterize the dark brown solid that did not go back into solution after recrystallization of **2.10**, a reaction was run in a 1:1 ratio of **2.6** to AuCl(SMe<sub>2</sub>) in dichloromethane for 3.5 hours at room temperature. The flask was warmed and the mixture was filtered producing a yellow solution, which was allowed to slowly evaporate. The resulting solid was redissolved in dichloromethane and stirred and any solid not in solution was filtered. The resulting solution was allowed to slowly evaporate. This process was repeated and upon dissolving in dichloromethane, any solid that did not go back into solution was filtered and collected. The resulting crystals were characterized by X-ray diffraction and identified as gold-silver complex **2.12** (Figure 2-12). Complex **2.12** crystallized in the monoclinic space group C2/m. It had a Z value of six, indicating one and a half molecules present in the unit cell.

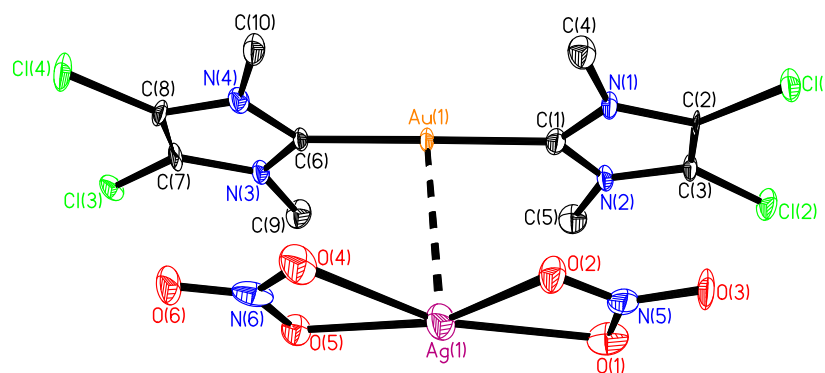


Figure 2-12 Thermal ellipsoid plot of gold-silver complex **2.12** shown at 50% probability

The gold-silver distance for **2.12** was observed to be 3.1350(7) Å, well within the sum of the van der waals radii, 3.38 Å. Previously reported NHC gold(I) complexes containing silver have been noted with gold-silver interactions of 3.219(9) Å and 2.8635(15) Å.<sup>102,103</sup> The carbon-gold-carbon bond angle had an average of 180°. Interestingly, the carbon-silver-carbon bond angle of the dinuclear silver complexes **2.7** and **2.8** deviated from linearity at 162.6(2)° and 158.29(12)°, respectively in comparison. Selected bond distances and angles for complexes **2.12**, **2.10**, **2.7** and **2.8** have been tabulated in Table 2-3 for easy comparison.

Table 2-3 Selected bond distances (Å) and angles (°) for **2.12**, **2.10**, **2.7** and **2.8**

Compound	<b>12</b>	<b>10</b>	<b>7</b>	<b>8</b>
<i>Bond lengths</i>				
Carbene-Metal	2.019(8)	2.001(4)	2.145(5)	2.100(2)
	2.016(8)	2.028(4)	2.102(5)	2.100(2)
	1.997(9)			
	1.997(9)			
Au1-Ag1	3.1350(7)			
	3.1350(7)			
	3.1350(7)			
Au2-Ag2	3.1046(6)			
	3.1046(6)			
	3.1046(6)			
Ag1-Ag2			2.6717(7)	2.6806(10)
<i>Bond angles</i>				
C-Metal-C	179.0(3)	178.43(15)	162.6(2)	158.29(12)
	180.0(4)			
C-Au1-Ag1	82.055(16)			
	82.055(16)			
	97.958(16)			
	97.958(16)			
C-Au2-Ag2	90.0			
	90.0			
	90.000(1)			
	90.000(1)			
C-Ag1-Ag2			60.45(14)	79.14(6)
			102.18(14)	79.14(6)

A reaction between dinuclear silver complex **2.8** and AuCl(SMe<sub>2</sub>) in dichloromethane was conducted. The experiment was run using the same 1:1 ratio with stirring at room temperature for 2 hours. The precipitate, assumed to be silver chloride, was filtered and the volatiles were evaporated to yield a white solid, likely gold complex **2.13** (Figure 2-9).

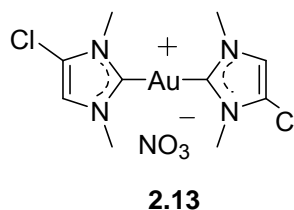


Figure 2-13 Proposed structure of **2.13**

The solid was recrystallized from dichloromethane but after many attempts, the crystals were too small for X-ray diffraction. The  $^{13}\text{C}$  NMR spectrum showed the resonance for the carbene carbon-metal shift at 184.0 ppm in comparison to 181.6 ppm observed in **2.8**. Elemental analysis also supported the structure proposed as **13** versus an Au-Ag structure similar to **2.12** or **2.8**.

## 2.5 Water Stability of Gold(I)-(bis)NHC Complexes

The water stability of complexes **2.9**, **2.10** and **2.13** was assessed and compared with their silver NHC precursors. The stability of complex **2.9** was further evaluated in a physiological sodium chloride solution.

### 2.5.1 Stability of Select Gold-NHC Complexes in an Aqueous Environment

$^1\text{H}$  NMR experiments of complexes **2.9**, **2.10** and **2.13** were conducted in  $\text{D}_2\text{O}$  to determine water stability. A sample of each compound was placed into an NMR tube and  $\text{D}_2\text{O}$  was added immediately before insertion into the NMR instrument. An initial scan was taken. The tube was stored in the dark and scanned at various time intervals over the course of weeks or years, as in the case of **2.9**. For complexes **2.9** and **2.13**, stability was determined by observing the proton resonance of the backbone region of the imidazole ring. The stability

of complex **2.10** was determined by observing the proton resonance of the N-methyl groups of the imidazole ring.

Because there was no degradation of **2.9** in D<sub>2</sub>O after several days (Figure 2-14a), a long term study was begun. After 2 years, the complex appeared to have remained stable (Figure 2-14b). Upon testing the sample at approximately 3 years, **2.9** seems to have remained intact (Figure 2-14c). The only noticeable difference between the scans appears to have been the slight broadening at the base of the peak.

The D<sub>2</sub>O solutions of complexes **2.13** and **2.10** were scanned initially and again 2 weeks later to assess water stability. Complex **2.13** was stable upon initial addition (Figure 2-15a) and appeared to remain stable with slight broadening at the base of the resonance (Figure 2-15b), at week 2. The same trend was observed for **2.10** with stability upon initial addition (Figure 2-16a) and slight broadening at the base of the resonance (Figure 2-16b) at week 2. As all three complexes showed water stability within parameters of the tests, assessment of the stabilizing effects of electron withdrawing groups at the 4- and 5-positions of the imidazole ring could not be made at this time on the gold-NHC analogs. A correlation for this trend would be possible if the same long term studies could be applied to **2.10** and **2.13**, as had been done with **2.9**. All three complexes also showed far superior water stability than their silver-NHC precursors.



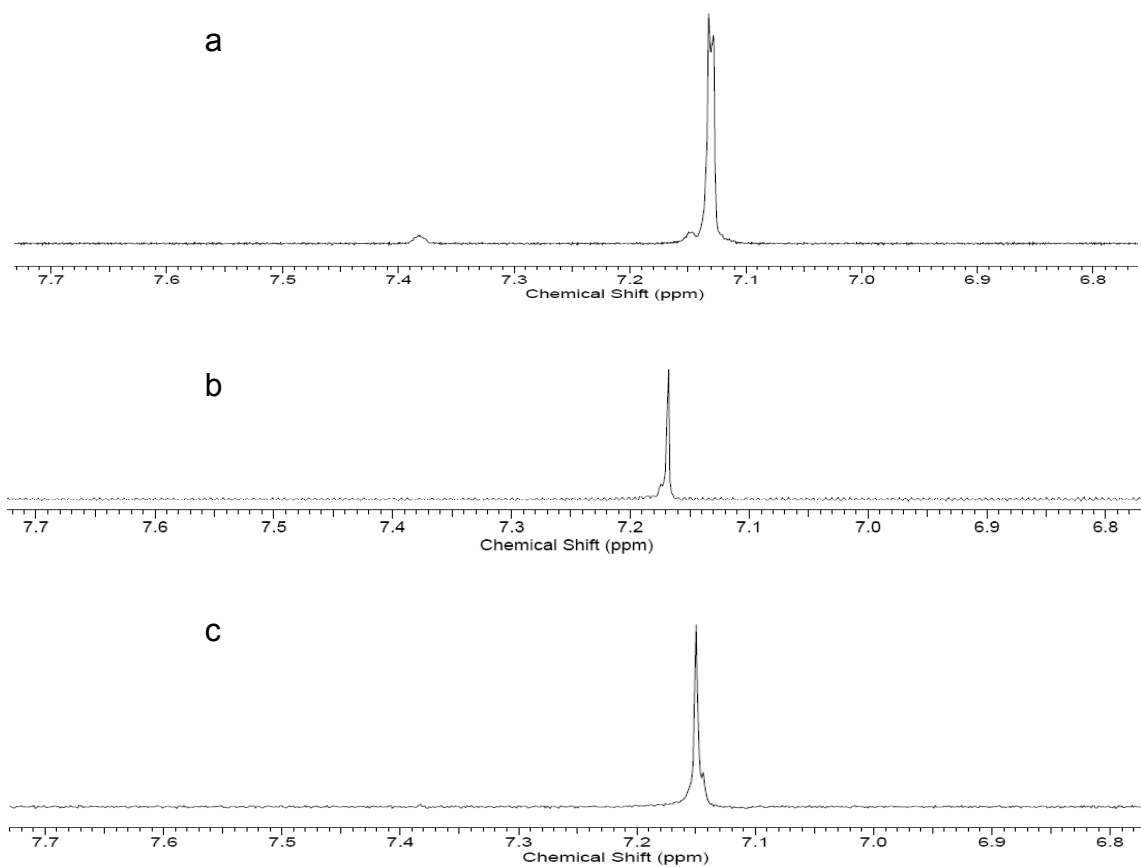


Figure 2-14  $^1\text{H}$  NMR spectra of **2.9** in  $\text{D}_2\text{O}$ , initially (a), and after 2 (b) and 3 (c) years

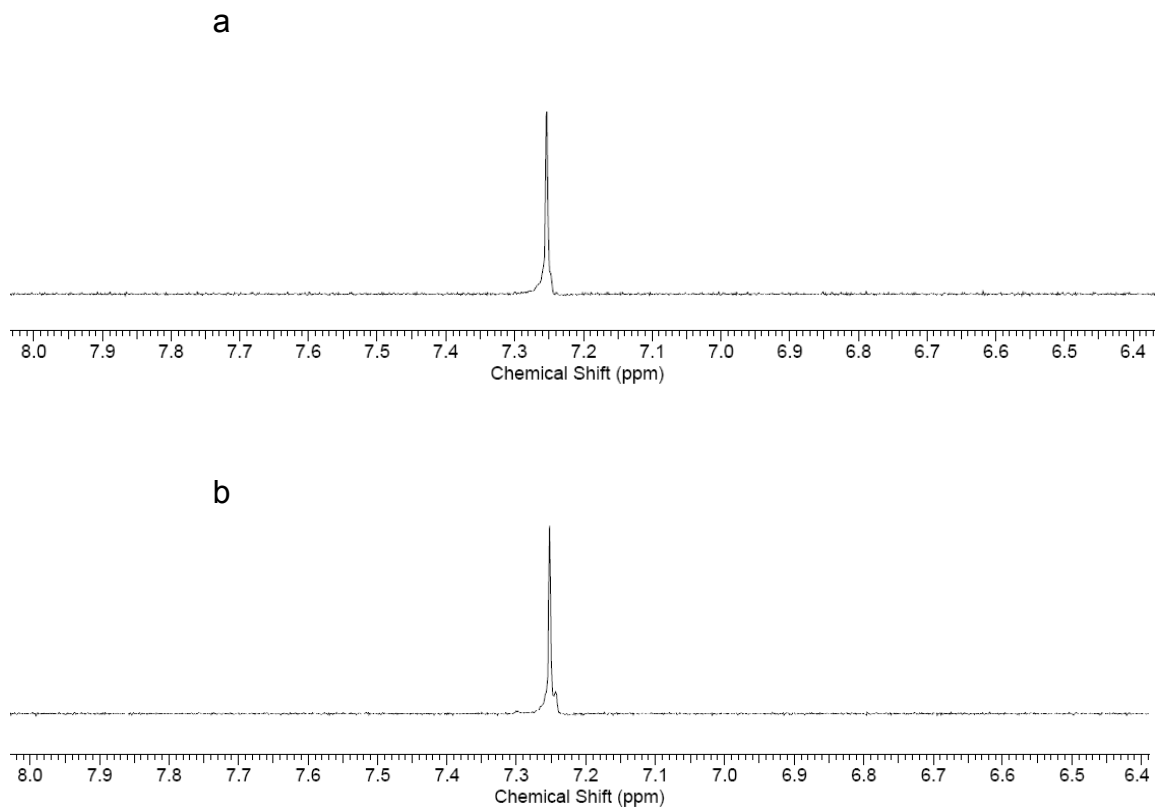


Figure 2-15  $^1\text{H}$  NMR spectra of **2.13** in  $\text{D}_2\text{O}$ , initially (a) and after 2 weeks (b)

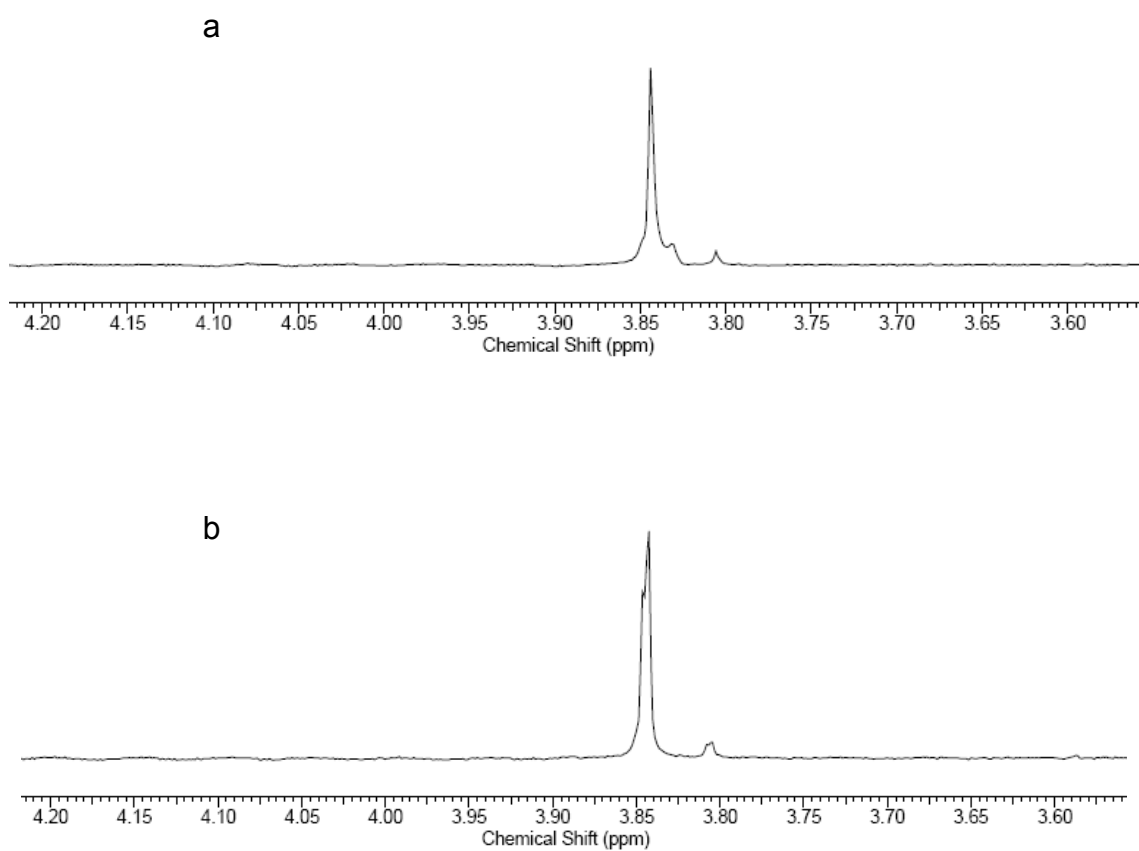


Figure 2-16  $^1\text{H}$  NMR spectra of **2.10** in  $\text{D}_2\text{O}$ , initially (a) and after 2 weeks (b)

### 2.5.2 Stability of Gold Complex **2.9** in Physiological Sodium Chloride Solution

The stability of **2.9** in the presence of physiological sodium chloride was tested in D<sub>2</sub>O by <sup>1</sup>H NMR spectroscopy. It was determined by observing the proton resonance of the methyl groups off the nitrogen positions of the imidazole ring, as it gave a clearer view. A sample of **2.9** was dissolved in 0.73 mL of D<sub>2</sub>O in an NMR tube and an initial scan was taken (Figure 2-17). A total of 0.20 mL of a 0.9% NaCl solution was added to the sample tube for an approximate 32% by weight of the total solution. A scan was taken of the sample and 48% decomposition could be seen on the first day (Figure 2-18a). The decomposition product was assumed to be the imidazolium salt. A scan was taken on day 2 and approximately 65% had degraded (Figure 2-18b). Further scans were taken on days 3 (Figure 2-19a) and 4 (Figure 2-19b) and approximately 35% and 31% of **2.9** remained, respectively.

As demonstrated by this experiment, gold complex **2.9** sustained stability of approximately 52% the first day upon exposure to a 32% by weight physiological sodium chloride solution. Further degradation was seen on day 2 but then the relative amount of **2.9** remained fairly constant through day 4 with approximately 33% remaining intact. Results of this test would suggest that an *in vivo* application for this complex may be possible.

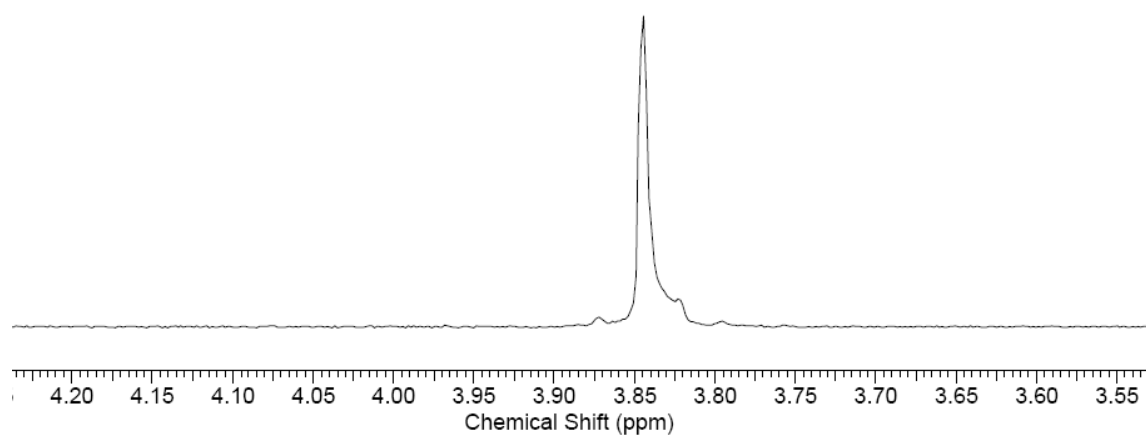


Figure 2-17  $^1\text{H}$  NMR spectrum of **2.9** in  $\text{D}_2\text{O}$  before NaCl addition

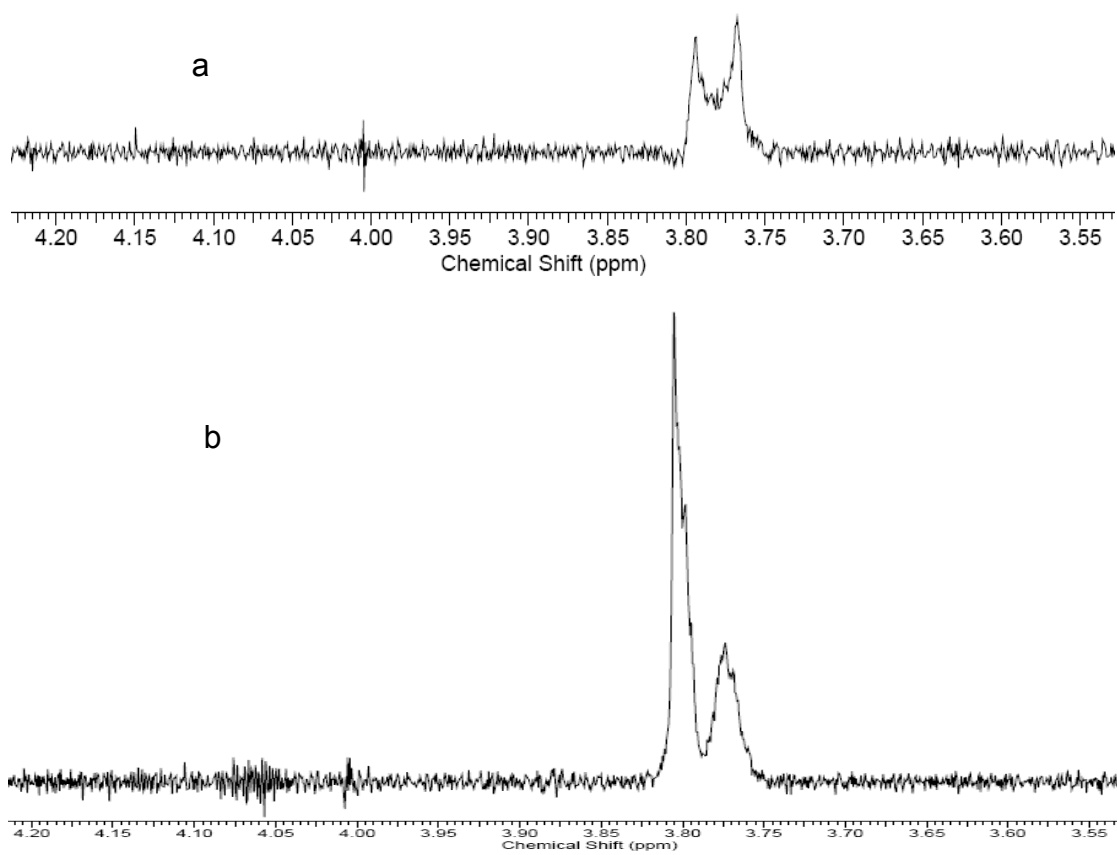


Figure 2-18  $^1\text{H}$  NMR spectra of 2.9 after NaCl addition taken on days 1 (a) and 2 (b)

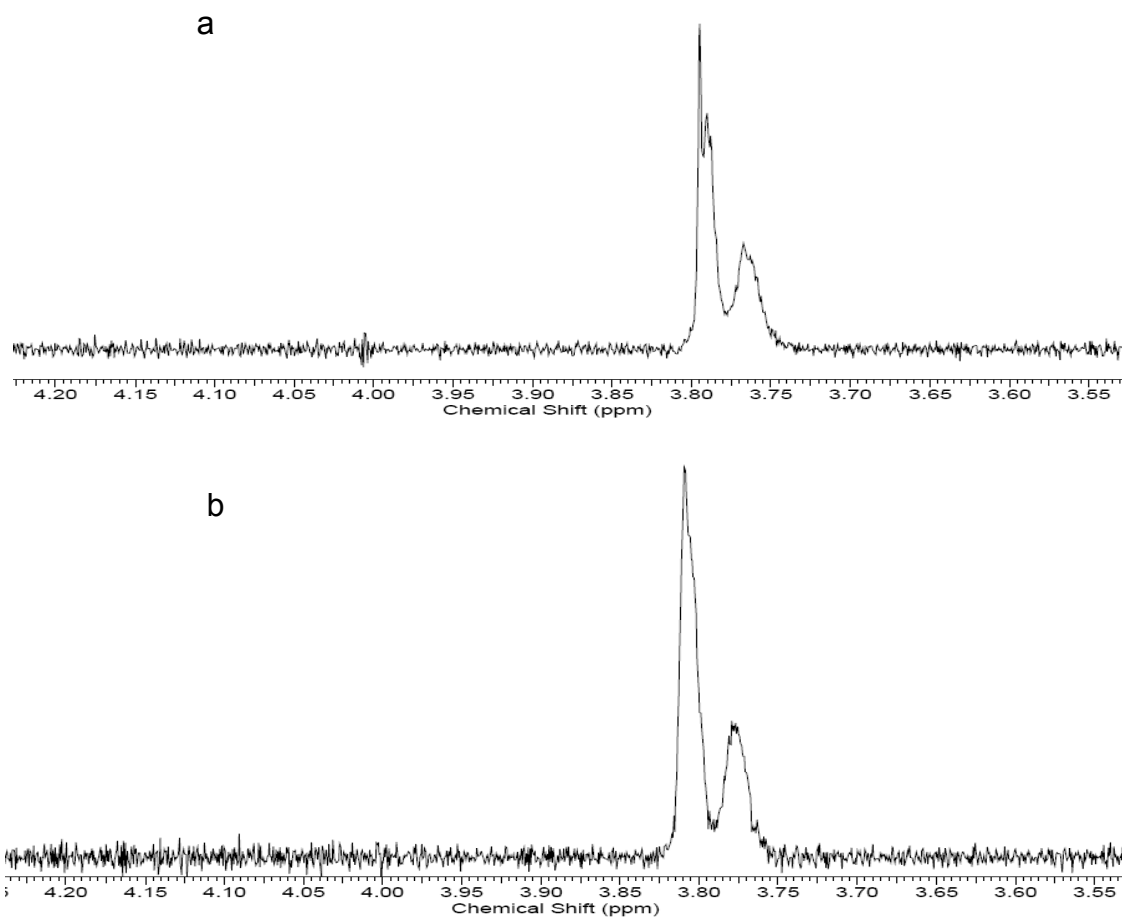


Figure 2-19  $^1\text{H}$  NMR spectra of **2.9** after NaCl addition taken on days 3 (a) and 4 (b)

## 2.6 Antimicrobial Comparison of Gold(I)-NHC Complexes and Their Silver(I)-NHC Precursors

The antimicrobial properties of the synthesized silver and gold NHC complexes were evaluated using two standard microbiological tests. The activity of the gold NHC complexes was compared to their silver precursors.

### 2.6.1 Minimum Inhibitory Concentration

An antimicrobial study of **2.1**, **2.2**, **2.4**, **2.5-2.10** and **2.13** was conducted in order to compare the activity of gold and silver complexes to the imidazolium precursors. Silver nitrate was used as a control. The antimicrobial properties were evaluated using the minimum inhibitory concentration (MIC) and minimum bactericidal concentration (MBC) methods. The MIC, a standard microbiological test, has been used to determine the bacteriostatic activity of antimicrobial agents. The lower the MIC value, the more effective the compound will be as an antimicrobial agent. All compounds were tested against laboratory strains of test organisms *Escherichia coli*, *Staphylococcus aureus*, and *Pseudomonas aeruginosa*. The MIC was obtained by visual inspection of the turbidity of the solution. Results for MIC are reported in Table 2-4.

All imidazolium nitrate salts displayed no antimicrobial activity at the same molar concentrations as the silver- and gold-NHC complexes. The dinuclear silver complexes **2.7** and **2.8** and the (bis)dichloro NHC-silver analog **2.6** all showed greater activity than silver nitrate and the other synthesized complexes against all three organism strains tested, whereas silver complex **2.5** showed



activity equal to silver nitrate. Gold complex **2.9** showed activity equal to silver nitrate and its silver complex analogue **2.5**, but only against *E.coli*. With that exception, the gold compounds were not as active as silver nitrate or their silver-NHC analogues. Gold complexes **2.10** and **2.13** were more active against *S.aureus* and *P.aeruginosa* than *E.coli*. Dinuclear silver complex **2.8** was the most active compound tested with MIC values of 0.11 mmol/L against all three organism strains, whereas gold complex **2.9** was the least active against *S.aureus* and *P.aeruginosa* at MIC values of 0.45 mmol/L and gold complex **2.13** was the least active against *E.coli* with an MIC value of 0.93 mmol/L.

Table 2-4 MIC values of **2.1**, **2.2**, **2.4-2.10** and **2.13** in mmol/L ( $\pm 0.3$ )

Compound	<i>E. coli</i>	<i>S. aureus</i>	<i>P. aeruginosa</i>
<b>2.1</b>	>4.1	>4.1	>4.1
<b>2.2</b>	>3.9	>3.9	>3.9
<b>2.4</b>	>3.9	>3.9	>3.9
AgNO <sub>3</sub>	0.15	0.15	0.15
<b>2.5</b>	0.15	0.15	0.15
<b>2.6</b>	0.13	0.13	0.13
<b>2.7</b>	0.13	0.13	0.13
<b>2.8</b>	0.11	0.11	0.11
<b>2.9</b>	0.15	0.45	0.45
<b>2.10</b>	0.78	0.26	0.26
<b>2.13</b>	0.93	0.31	0.31

Based on the above results, it was demonstrated that the presence of a second silver atom only slightly increased antimicrobial activity. The presence of a chlorine atom on the 4- and 5-positions of the imidazole ring showed little difference in antimicrobial properties in comparison with hydrogen atoms at said positions, within the silver-NHC complexes. The same pattern was also observed within the gold-NHC complexes, with the exception of activity against *E.coli*. Once the exact structure of **2.13** can be determined or the monosilver analogue of **2.8** can be synthesized, a better evaluation can be made amongst the three ligand variations.

#### 2.6.2 Minimum Bactericidal Concentration

A sample from each of the complexes containing no growth (clear) MIC tubes tested from above was taken and evaluated for the minimum bactericidal concentration (MBC). The MBC determines the lowest concentration of antimicrobial that will kill an organism. MBC differs from the MIC by providing evidence that an antimicrobial actually prevents organism growth by killing microorganisms (MBC) rather than merely inhibiting growth (MIC). Results for the MBC have been reported in Table 2-5.

Table 2-5 MBC results for **2.5-2.10** and **2.13** in mmol/L L ( $\pm 0.3$ )

Compound	<i>E. coli</i>	<i>S. aureus</i>	<i>P. aeruginosa</i>
AgNO <sub>3</sub>	0.15	>0.45	>0.45
<b>2.5</b>	0.15	>0.45	>0.45
<b>2.6</b>	>0.40	0.40	>0.40
<b>2.7</b>	0.13	0.13	0.13
<b>2.8</b>	0.11	>0.33	>0.33
<b>2.9</b>	0.45	1.4	1.4
<b>2.10</b>	0.78	0.78	>0.78
<b>2.13</b>	0.93	0.93	>0.93

Dinuclear silver complex **2.7** was the most effective complex at preventing organism growth against all microorganism strains tested, having an MBC value of 0.13 mmol/L. Dinuclear silver complex **2.8** was the most effective at preventing organism growth against *E.coli*, at an MBC value of 0.11 mmol/L, also lower than silver nitrate. Silver complex **2.5** prevented organism growth against *E.coli* with an MBC value of 0.15 mmol/L, the same as silver nitrate. The gold complexes all had MBC values higher than those observed for silver nitrate and their silver-NHC precursors.

Based on the above results, it was determined that silver-NHC complexes were more effective at preventing microorganism growth of *Escherichia coli*, *Staphylococcus aureus*, and *Pseudomonas aeruginosa* than corresponding gold-NHC complexes at the same molar concentrations.

## 2.7 Conclusion

A series of (bis)NHC-silver(I) nitrate complexes were synthesized by varying the substituents on the 4- and 5-positions of the imidazole ring with hydrogen atoms, chlorine atoms or a combination of both. These complexes were evaluated for the stability in an aqueous environment and it was determined that the series increased in stability as H, H < H, Cl < Cl, Cl, with respect to the substituent on the 4- and 5-position of the imidazole ring, respectively. The presence of two electron withdrawing groups confers water stability. Corresponding (bis)NHC-gold(I) nitrate complexes were synthesized from their silver(I) precursors, although the exact structure for the monochloro analogue **2.13** was not unambiguously determined. The gold complexes were also evaluated for their water stability with superiority in comparison to their silver precursors. The antimicrobial properties of all complexes were determined and the silver precursors were found to be much more efficacious than corresponding gold analogs.

## 2.8 Experimental Section

The general considerations and X-ray information have been explained below. The experimental procedures for compounds **2.1-2.10**, **2.12** and **2.13** have been compiled in this section.

### 2.8.1 General Considerations

All reactions were carried out under aerobic conditions. All silver and gold reactions were conducted in the absence of light. The reagents 5-chloro-1-

methylimidazole, 4,5-dichloroimidazole, iodomethane and silver(I) oxide were purchased from Alfa Aesar; chloro(dimethylsulfide)gold(I) and Hyflo Super Cel® were purchased from Aldrich; silver nitrate was purchased from VWR and potassium hydroxide was purchased from Fisher Scientific. All reagents were used as received. 1,3-Dimethylimidazolium iodide was prepared using a modified literature procedure as described in section 3.5.3 and 4,5-dichloro-1,3-dimethylimidazolium iodide was prepared in accordance with literature procedures.<sup>104,95</sup> The synthesis of imidazolium salt **2.3** was developed by Dr. Matthew J. Panzner. The synthesis of silver complex **2.6** was developed by Dr. Khadijah Hindi and prepared with slight modifications. LB Broth Miller (DIFCO) and Bacto-agar (DIFCO) were prepared according to manufacturer's instruction and sterilized before use. All solvents were purchased from Fisher Scientific and used as received. <sup>1</sup>H and <sup>13</sup>C NMR spectral data were collected on a Varian Gemini 300 MHz instrument and referenced to the residual protons of the deuterated solvents and the solvent resonances, respectively. <sup>1</sup>H NMR stability studies done in D<sub>2</sub>O for complexes **2.5**, **2.6** and **2.8** were collected on a Varian INOVA 400 MHz instrument. <sup>109</sup>Ag NMR data was collected on a Varian INOVA 750 MHz instrument. Elemental analyses were performed at the Microanalysis Laboratory at The University of Illinois. Mass spectrometric analysis of **2.1**, **2.7** and **2.9** was performed at the mass spectrometry facility at The University of Akron and analysis of **2.2-2.6**, **2.8**, **2.10**, **2.12** and **2.13** was performed at the CCIC Mass Spectrometry and Proteomics Facility at The Ohio State University.

### 2.8.2 X-Ray Crystallographic Structure Determination Details

The crystal structure of **2.4** was solved by Brian Wright. The crystal structures of **2.5**, **2.6**, **2.10**, **2.11** and **2.12** were solved by Dr. Matthew Panzner. The crystal structure of **2.7** was solved by Dr. Doug Medvetz and the crystal structure of **2.8** was solved by Paul Custer. The crystal structure of **2.9** was solved by Dr. Semih Durmus. Crystals of **2.4-2.12** were coated in paraffin oil and mounted on a CryoLoop™ and placed on the goniometer head under a stream of nitrogen cooled to 100K. The data was collected on a Bruker APEX CCD diffractometer with graphite-monochromated Mo K $\alpha$  radiation ( $\lambda$  = 0.71073 Å). The unit cell was determined by using reflections from three different orientations. The data was integrated using SAINT.<sup>105</sup> An empirical absorption correction and other corrections were applied to the data using multi-scan SADABS.<sup>105</sup> Structure solution, refinement, and modeling were accomplished by using the Bruker SHELXTL package.<sup>106</sup> The structure was determined by full-matrix least-squares refinement of  $F^2$  and the selection of the appropriate atoms from the generated difference map. Hydrogen atom positions were calculated and  $U_{iso}(H)$  values were fixed according to a riding model.

### 2.8.3 Synthesis of **2.1** (C<sub>5</sub>H<sub>9</sub>N<sub>3</sub>O<sub>3</sub>)

The salt 1,3-dimethylimidazolium iodide (0.945 g, 4.22 mmol) was placed in a 125 mL flask with dichloromethane (45 mL) with stirring and AgNO<sub>3</sub> (0.725 g, 4.22 mmol) was added. The mixture was stirred at room temperature for 20 minutes. The mixture was filtered and the volatiles were evaporated. The resulting solid was rinsed with diethyl ether (10 mL) two times and stirred for 10

minutes on the third time to yield white hygroscopic solid **2.1**. Yield: 0.55 g, 3.5 mmol, 82%. Mp: 60-62°C. Anal. Calcd for C<sub>5</sub>H<sub>9</sub>N<sub>3</sub>O<sub>3</sub>: C, 37.74; H, 5.70; N, 26.41. Found: C, 36.28; H, 5.52; N, 24.60. <sup>1</sup>H NMR (300 MHz, DMSO-*d*<sub>6</sub>): δ 9.08 (s, 1H, NCHN), 7.68 (s, 2H, CH), 3.84 (s, 6H, CH<sub>3</sub>). <sup>13</sup>C NMR (75 MHz, DMSO-*d*<sub>6</sub>): δ 137.5 (s, NCHN), 123.7 (s, C=C), 35.8 (s, CH<sub>3</sub>). ESI-MS (*m/z*): Calcd for C<sub>5</sub>H<sub>9</sub>N<sub>2</sub> [M-NO<sub>3</sub>]<sup>+</sup>: 97.14, found 97.1.

#### 2.8.4 Synthesis of **2.2** (C<sub>5</sub>H<sub>3</sub>N<sub>3</sub>Cl<sub>2</sub>O<sub>3</sub>)

The salt 4,5-dichloro-1,3-dimethylimidazolium iodide (2.25 g, 7.68 mmol) was placed in a 125 mL flask with dichloromethane (50 mL). AgNO<sub>3</sub> (1.31 g, 7.70 mmol) was added and the mixture was stirred at room temperature for 30 minutes. The mixture was filtered and the volatiles were evaporated. The resulting solid was rinsed with diethyl ether (10 mL) three times to yield dark yellow solid **2.2**. Yield: 1.3 g, 5.5 mmol, 72%. Mp: 147-149°C. Anal. Calcd for C<sub>5</sub>H<sub>7</sub>N<sub>3</sub>Cl<sub>2</sub>O<sub>3</sub>: C, 26.34; H, 3.09; N, 18.43. Found: C, 26.45; H, 3.07; N, 17.47. <sup>1</sup>H NMR (300 MHz, DMSO-*d*<sub>6</sub>): δ 9.39 (s, 1H, NCHN), 3.83 (s, 6H, CH<sub>3</sub>). <sup>13</sup>C NMR (75 MHz, DMSO-*d*<sub>6</sub>): δ 136.8 (s, NCHN), 118.9 (s, C=C), 34.8 (s, CH<sub>3</sub>). ESI-MS (*m/z*): Calcd for C<sub>5</sub>H<sub>6</sub>N<sub>2</sub>Cl<sub>2</sub> [M-HNO<sub>3</sub>]<sup>+</sup>: 165.02, found 165.0.

#### 2.8.5 Synthesis of **2.3** (C<sub>5</sub>H<sub>8</sub>N<sub>2</sub>ClI)

Acetonitrile (10 mL) was added to a 100 mL round bottom flask containing 5-chloro-1-methylimidazole (1.73 g, 14.8 mmol). Iodomethane (3 mL) was added to the flask and the solution was refluxed at 80°C overnight. Diethyl ether (20 mL) was added to the flask and a precipitate formed. The precipitate was filtered and

dried yielding yellow solid **2.3**. Yield: 3.6 g, 14 mmol, 94%. Mp: 172-174°C. Anal. Calcd for C<sub>5</sub>H<sub>7</sub>N<sub>3</sub>Cl<sub>2</sub>O<sub>3</sub>: C, 23.23; H, 3.12; N, 10.84. Found: C, 23.48; H, 2.89; N, 10.87. <sup>1</sup>H NMR (300 MHz, DMSO-*d*<sub>6</sub>): δ 9.20 (s, 1H, NCHN), 8.02 (s, 1H, CH), 3.85 (s, 3H, CH<sub>3</sub>), 3.78 (s, 3H, CH<sub>3</sub>). <sup>13</sup>C NMR (75 MHz, DMSO-*d*<sub>6</sub>): δ 137.4 (s, NCHN), 121.1 (s, C=C), 120.6 (s, C=C), 36.6 (s, CH<sub>3</sub>), 33.7 (s, CH<sub>3</sub>). ESI-MS (*m/z*): Calcd for C<sub>5</sub>H<sub>8</sub>N<sub>2</sub>Cl [M-I]<sup>+</sup>: 131.6, found 131.0.

#### 2.8.6 Synthesis of **2.4** (C<sub>5</sub>H<sub>8</sub>N<sub>3</sub>O<sub>3</sub>Cl)

The salt **2.3** (1.18 g, 4.56 mmol) was placed in a 50 mL flask with acetonitrile (20 mL). AgNO<sub>3</sub> (0.775 g, 4.56 mmol) was added and the mixture was stirred at room temperature for 30 minutes. The mixture was filtered and the volatiles were evaporated. The resulting solid was stirred in diethyl ether (20 mL) for 30 minutes and filtered to yield white solid **2.4**. Yield: 0.78 g, 4.0 mmol, 88%. Mp: 116-118°C. Anal. Calcd for C<sub>5</sub>H<sub>7</sub>N<sub>3</sub>Cl<sub>2</sub>O<sub>3</sub>: C, 31.02; H, 4.17; N, 21.71. Found: C, 31.15; H, 4.08; N, 21.25. <sup>1</sup>H NMR (300 MHz, DMSO-*d*<sub>6</sub>): δ 9.22 (s, 1H, NCHN), 8.01 (CH), 3.84 (s, 6H, CH<sub>3</sub>), 3.8(s, 6H, CH<sub>3</sub>). <sup>13</sup>C NMR (75 MHz, DMSO-*d*<sub>6</sub>): δ 137.5 (s, NCHN), 121.1 (s, C=C), 120.6 (s, C=C), 36.5 (s, CH<sub>3</sub>), 33.6 (s, CH<sub>3</sub>). ESI-MS (*m/z*): Calcd for C<sub>5</sub>H<sub>8</sub>N<sub>2</sub>Cl [M-NO<sub>3</sub>]<sup>+</sup>: 131.6, found 131.0.

X-ray crystal structure analysis of **2.4**: formula C<sub>5</sub>H<sub>8</sub>ClN<sub>3</sub>O<sub>3</sub>, *MW* = 193.59, colorless crystal 0.39 x 0.17 x 0.08 mm<sup>3</sup>, *a* = 8.608(4) Å, *b* = 9.977(4) Å, *c* = 9.726(4) Å, α = 90°, β = 100.313(7)°, γ = 90°, *V* = 821.8(6) Å<sup>3</sup>, *D*<sub>calc</sub> = 1.565 Mg m<sup>-3</sup>, μ = 0.436 mm<sup>-1</sup>, *Z* = 4, monoclinic, space group P2(1)/n, λ = 0.71073 Å, *T* = 100 K, ω and φ scans, 6398 reflections collected, 1677 independent (*R*<sub>int</sub> = 0.0309), 111 refined parameters, *R*<sub>1</sub>/*wR*<sub>2</sub> (*I* ≥ 2σ(1)) = 0.0353/0.0963 and



R1/wR2 (all data) = 0.0400/0.0997, maximum (minimum) residual electron density 0.392 (-0.212) e/Å<sup>3</sup>.

### 2.8.7 Synthesis of **2.5** (C<sub>10</sub>H<sub>16</sub>N<sub>5</sub>O<sub>3</sub>Ag)

Ag<sub>2</sub>O (7.34 g, 31.7 mmol) was added to **2.1** (2.52 g, 15.8 mmol) in dichloromethane (45 mL) and stirred at room temperature for 4 hours. A clear solution was obtained after filtration. The volatiles were removed and resulting solid was washed with diethyl ether three times (10 mL) to yield white solid **2.5**. Yield: 2.3 g, 6.3 mmol, 47%). Mp: 151-153 °C (dec) (lit. 188 °C (dec)). Anal. Calcd for C<sub>10</sub>H<sub>16</sub>N<sub>5</sub>O<sub>3</sub>Ag: C, 33.16; H, 4.45; N, 19.34. Found: C, 27.48; H, 4.53; N, 18.34. <sup>1</sup>H NMR (300 MHz, DMSO-*d*<sub>6</sub>): δ 7.43 (s, 4H, CH), 3.81 (s, 12H, CH<sub>3</sub>). <sup>13</sup>C NMR (75 MHz, DMSO-*d*<sub>6</sub>): δ 180.1 (s, C-Ag), 123.0 (s, C=C), 38.0 (s, CH<sub>3</sub>). <sup>109</sup>Ag (35 MHz, DMSO-*d*<sub>6</sub>): δ 318.6 (s). ESI-MS (*m/z*): Calcd for C<sub>10</sub>H<sub>16</sub>N<sub>4</sub>Ag [M-NO<sub>3</sub>]<sup>+</sup>: 299.04 and 301.04, found 298.80 and 300.80.

X-ray crystal structure analysis of **2.5**: formula C<sub>10</sub>H<sub>16</sub>AgN<sub>5</sub>O<sub>3</sub>, *MW* = 362.15, colorless crystal 0.40 x 0.32 x 0.06 mm<sup>3</sup>, *a* = 13.7005(15) Å, *b* = 6.9793(8) Å, *c* = 15.8626(18) Å, α = 90°, β = 114.105(2)°, γ = 90°, *V* = 1384.5(3) Å<sup>3</sup>, *D*<sub>calc</sub> = 1.737 Mg m<sup>-3</sup>, μ = 1.468 mm<sup>-1</sup>, *Z* = 4, monoclinic, space group P2(1)/c, λ = 0.71073 Å, *T* = 100 K, ω and φ scans, 11417 reflections collected, 3270 independent (*R*<sub>int</sub> = 0.0282), 176 refined parameters, R1/wR2 (*I* ≥ 2σ(1)) = 0.0358/0.0770 and R1/wR2 (all data) = 0.0417/0.0792, maximum (minimum) residual electron density 1.363 (-0.578) e/Å<sup>3</sup>.

### 2.8.8 Synthesis of **2.6** (C<sub>10</sub>H<sub>12</sub>N<sub>5</sub>O<sub>3</sub>Cl<sub>4</sub>Ag)

Ag<sub>2</sub>O (0.33 g, 1.4 mmol) was added to **2.2** (0.32 g, 1.4 mmol) in acetonitrile (30 mL) and stirred at room temperature for 3 hours. A clear solution was obtained after filtration through Hyflo Super Cel. The volatiles were removed and resulting solid was stirred in diethyl ether (20 mL) for 30 minutes to yield white solid **2.6**. Yield: 0.42 g, 0.85 mmol, 61%). Mp: 169 °C. Anal. Calcd for C<sub>10</sub>H<sub>12</sub>N<sub>5</sub>O<sub>3</sub>Cl<sub>4</sub>Ag: C, 24.03; H, 2.42; N, 14.01. Found: C, 20.40; H, 1.97; N, 12.80. <sup>1</sup>H NMR (300 MHz, DMSO-*d*<sub>6</sub>): δ 3.82 (s, 12H, CH<sub>3</sub>). <sup>13</sup>C NMR (75 MHz, DMSO-*d*<sub>6</sub>): δ 181.3 (s, C-Ag), 117.0 (s, C=C), 37.5 (s, CH<sub>3</sub>). ESI-MS (*m/z*): Calcd for C<sub>5</sub>H<sub>6</sub>N<sub>2</sub>Cl<sub>2</sub>Ag [M-(C<sub>5</sub>H<sub>6</sub>N<sub>2</sub>Cl<sub>2</sub>)NO<sub>3</sub>]<sup>+</sup>: 272.88, found 272.9.

X-ray crystal structure analysis of **2.6**: formula C<sub>10</sub>H<sub>12</sub>AgCl<sub>4</sub>N<sub>5</sub>O<sub>5</sub>, *MW* = 531.92, colorless crystal 0.27 x 0.15 x 0.03 mm<sup>3</sup>, *a* = 6.5183(12) Å, *b* = 13.808(2) Å, *c* = 14.542(3) Å, α = 72.205(3)°, β = 79.989(3)°, γ = 73.465(3)°, *V* = 930.9(3) Å<sup>3</sup>, *D*<sub>calc</sub> = 1.898 Mg m<sup>-3</sup>, μ = 1.688 mm<sup>-1</sup>, *Z* = 2, triclinic, space group P-1, λ = 0.71073 Å, *T* = 100 K, ω and φ scans, 8161 reflections collected, 4279 independent (*R*<sub>int</sub> = 0.0331), 230 refined parameters, *R*<sub>1</sub>/*wR*<sub>2</sub> (*I* ≥ 2σ(1)) = 0.0574/0.1356 and *R*<sub>1</sub>/*wR*<sub>2</sub> (all data) = 0.0655/0.1401, maximum (minimum) residual electron density 2.085 (-1.549) e/Å<sup>3</sup>.

### 2.8.9 Synthesis of **2.7** (C<sub>10</sub>H<sub>16</sub>N<sub>6</sub>O<sub>6</sub>Ag<sub>2</sub>)

Ag<sub>2</sub>O (5.43 g, 23.4 mmol) was added to a solution of **2.1** (0.80 g, 5.0 mmol) in dichloromethane (50mL) and refluxed at 30-40 °C for 4 hours. A clear solution was obtained following filtration and the volatiles were evaporated to give a white solid. The solid was washed with diethyl ether (10 mL) three times to

yield **2.7**. Yield: 0.99 g, 1.9 mmol, 38%. Mp: 169-170 °C (dec). Anal. Calcd for  $C_{10}H_{16}N_6O_6Ag_2$ : C, 22.64; H, 3.04; N, 15.85. Found: C, 23.44; H, 3.05; N, 15.73.  $^1H$  NMR (300 MHz, DMSO- $d_6$ ):  $\delta$  7.44 (s, 4H, CH), 3.81 (s, 12H, CH<sub>3</sub>).  $^{13}C$  NMR (75 MHz, DMSO- $d_6$ ):  $\delta$  180.2 (s, C-Ag), 122.9 (s, C=C), 37.9 (s, CH<sub>3</sub>). ESI-MS ( $m/z$ ): Calcd for  $C_{10}H_{16}N_4Ag [M-Ag(NO_3)_2]^+$ : 299.04 and 301.04, found 299.00 and 301.00.

X-ray crystal structure analysis of **2.7**: formula  $C_{10}H_{16}Ag_2N_6O_6$ ,  $MW = 529.92$ , colorless crystal  $0.35 \times 0.17 \times 0.03 \text{ mm}^3$ ,  $a = 6.5678(9) \text{ \AA}$ ,  $b = 15.329(2) \text{ \AA}$ ,  $c = 8.2587(11) \text{ \AA}$ ,  $\alpha = 90^\circ$ ,  $\beta = 106.712(2)^\circ$ ,  $\gamma = 90^\circ$ ,  $V = 796.35(18) \text{ \AA}^3$ ,  $D_{\text{calc}} = 2.018 \text{ Mg m}^{-3}$ ,  $\mu = 2.489 \text{ mm}^{-1}$ ,  $Z = 2$ , monoclinic, space group  $P2(1)/m$ ,  $\lambda = 0.71073 \text{ \AA}$ ,  $T = 100 \text{ K}$ ,  $\omega$  and  $\varphi$  scans, 6272 reflections collected, 1983 independent ( $R_{\text{int}} = 0.0519$ ), 117 refined parameters,  $R1/wR2$  ( $I \geq 2\sigma(1)$ ) = 0.0492/0.1549 and  $R1/wR2$  (all data) = 0.0509/0.1592, maximum (minimum) residual electron density 1.234 (-1.192)  $e/\text{\AA}^3$ .

#### 2.8.10 Synthesis of **2.8** ( $C_{10}H_{14}N_6O_6Cl_2Ag_2$ )

$Ag_2O$  (0.50 g, 2.2 mmol) was added to a solution of **2.4** (0.34 g, 1.7 mmol) in dichloromethane (30 mL). The mixture was stirred for 2 hours at room temperature. A clear solution was obtained after filtration through Hyflo Super Cel®. The volatiles were evaporated and the resulting solid was stirred in diethyl ether (20 mL) for 30 minutes. The mixture was filtered to yield white solid **2.8**. Yield: 0.17 g, 0.30 mmol, 17%. Mp: 168-170 °C (dec). Anal. Calcd for  $C_{10}H_{14}N_6O_6Cl_2Ag_2$ : C, 19.99; H, 2.35; N, 13.99. Found: C, 22.80; H, 2.61; N, 13.96.  $^1H$  NMR (300 MHz, DMSO- $d_6$ ):  $\delta$  7.73 (s, 2H, CH), 3.80 (s, 6H, CH<sub>3</sub>),

3.78 (s, 6H, CH<sub>3</sub>). <sup>13</sup>C NMR (75 MHz, DMSO-*d*<sub>6</sub>): δ 181.6 (s, C-Ag), 120.0 (s, C=C), 119.5 (s, C=C), 39.1 (s, CH<sub>3</sub>), 36.0 (s, CH<sub>3</sub>). ESI-MS (*m/z*): Calcd for C<sub>10</sub>H<sub>14</sub>N<sub>4</sub>Cl<sub>2</sub>Ag [M-Ag(NO<sub>3</sub>)<sub>2</sub>]<sup>+</sup>: 369.02, found 369.0.

X-ray crystal structure analysis of **2.8**: formula C<sub>10</sub>H<sub>14</sub>Ag<sub>2</sub>Cl<sub>2</sub>N<sub>6</sub>O<sub>6</sub>, *MW* = 600.91, colorless crystal 0.09 x 0.08 x 0.07 mm<sup>3</sup>, *a* = 18.017(6) Å, *b* = 6.786(2) Å, *c* = 16.465(6) Å, α = 90°, β = 122.812(5)°, γ = 90°, *V* = 1692.0(10) Å<sup>3</sup>, *D*<sub>calc</sub> = 2.359 Mg m<sup>-3</sup>, μ = 2.674 mm<sup>-1</sup>, *Z* = 4, monoclinic, space group C2/c, λ = 0.71073 Å, *T* = 100 K, ω and φ scans, 7056 reflections collected, 1978 independent (*R*<sub>int</sub> = 0.0277), 121 refined parameters, *R*<sub>1</sub>/*wR*<sub>2</sub> (*I* ≥ 2σ(1)) = 0.0231/0.0568 and *R*<sub>1</sub>/*wR*<sub>2</sub> (all data) = 0.0271/0.0576, maximum (minimum) residual electron density 0.975 (-0.888) e/Å<sup>3</sup>.

#### 2.8.11 Synthesis of **2.9** (C<sub>10</sub>H<sub>16</sub>N<sub>5</sub>O<sub>3</sub>Au)

Silver complex **2.5** (0.12 g, 0.34 mmol) was dissolved in dichloromethane (20 mL) and (SMe<sub>2</sub>)AuCl (0.99 g, 0.34 mmol) was added and stirred at room temperature for 2 hours. A clear solution was obtained after filtration. The volatiles were evaporated to give a white solid. The solid was recrystallized from dichloromethane to yield a brown solid. Dichloromethane (10 mL) was added and stirred for 10 minutes. The mixture was filtered and the volatiles were evaporated to yield a white solid. The solid was washed three times with diethyl ether (10 mL) to yield **2.9**. Yield: 0.12 g, 0.28 mmol, 83%. Mp: 162-164 °C. Anal. Calcd for C<sub>10</sub>H<sub>16</sub>N<sub>5</sub>O<sub>3</sub>Au: C, 26.62; H, 3.57; N, 15.52. Found: C, 27.13; H, 3.68; N, 14.88. <sup>1</sup>H NMR (300 MHz, D<sub>2</sub>O): δ 7.16 (s, 4H, CH), 3.84 (s, 12H, CH<sub>3</sub>). <sup>13</sup>C NMR (75

MHz, D<sub>2</sub>O):  $\delta$  201.9 (s, C-Au), 122.7 (s, C=C), 37.2 (s, CH<sub>3</sub>). ESI-MS ( $m/z$ ):

Calcd for C<sub>10</sub>H<sub>16</sub>N<sub>4</sub>Au [M-NO<sub>3</sub>]<sup>+</sup> : 389.2, found 388.8.

X-ray crystal structure analysis of **2.9**: formula C<sub>10</sub>H<sub>16</sub>AuN<sub>5</sub>O<sub>3</sub>,  $MW = 469.26$ , colorless crystal 0.38 x 0.31 x 0.15 mm<sup>3</sup>,  $a = 6.9373(6)$  Å,  $b = 9.9372(9)$  Å,  $c = 11.2032(10)$  Å,  $\alpha = 108.9990(10)^\circ$ ,  $\beta = 99.3050(10)^\circ$ ,  $\gamma = 97.1970(10)^\circ$ ,  $V = 707.41(11)$  Å<sup>3</sup>,  $D_{\text{calc}} = 2.203$  Mg m<sup>-3</sup>,  $\mu = 10.419$  mm<sup>-1</sup>,  $Z = 2$ , triclinic, space group P-1,  $\lambda = 0.71073$  Å,  $T = 100$  K,  $\omega$  and  $\phi$  scans, 6044 reflections collected, 3240 independent ( $R_{\text{int}} = 0.0336$ ), 185 refined parameters,  $R1/wR2$  ( $I \geq 2\sigma(1)$ ) = 0.0311/0.0793 and  $R1/wR2$  (all data) = 0.0322/0.0801, maximum (minimum) residual electron density 3.298 (-2.428) e/Å<sup>3</sup>.

#### 2.8.12 Synthesis of **2.10** (C<sub>10</sub>H<sub>12</sub>N<sub>5</sub>O<sub>3</sub>Cl<sub>4</sub>Au)

Silver complex **2.6** (0.21 g, 0.43 mmol) was dissolved in dichloromethane (20 mL) and (SMe<sub>2</sub>)AuCl (0.13 g, 0.43 mmol) was added and stirred at room temperature for 2 hours. A clear solution was obtained after filtration. The volatiles were evaporated to give a white solid. The solid was recrystallized from dichloromethane to yield a brown solid. Dichloromethane (10 mL) was added and stirred for 10 minutes. The mixture was filtered and the volatiles were evaporated to yield a white solid. The solid was washed three times with diethyl ether (10 mL) to yield **2.10**. Yield: 0.15 g, 0.25 mmol, 59%. Mp: 172-173 °C. Anal. Calcd for C<sub>10</sub>H<sub>12</sub>N<sub>5</sub>O<sub>3</sub>Cl<sub>4</sub>Au: C, 20.39; H, 2.05; N, 11.89. Found: C, 22.89; H, 2.66; N, 9.83. <sup>1</sup>H NMR (300 MHz, D<sub>2</sub>O):  $\delta$  3.88 (s, 12H, CH<sub>3</sub>). <sup>13</sup>C NMR (75 MHz, DMSO-*d*<sub>6</sub>):  $\delta$  182.1 (s, C-Au), 117.8 (s, C=C), 36.9 (s, CH<sub>3</sub>). Calcd for C<sub>10</sub>H<sub>12</sub>N<sub>4</sub>Cl<sub>4</sub>Au [M-NO<sub>3</sub>]<sup>+</sup> : 527.01, found 527.0.

X-ray crystal structure analysis of **2.10**: formula  $C_{10}H_{12}AuCl_4N_5O_3$ ,  $MW = 589.01$ , colorless crystal  $0.50 \times 0.22 \times 0.13 \text{ mm}^3$ ,  $a = 7.656(3) \text{ \AA}$ ,  $b = 8.850(3) \text{ \AA}$ ,  $c = 12.903(5) \text{ \AA}$ ,  $\alpha = 98.774(6)^\circ$ ,  $\beta = 96.074(6)^\circ$ ,  $\gamma = 106.662(6)^\circ$ ,  $V = 817.4(5) \text{ \AA}^3$ ,  $D_{\text{calc}} = 2.393 \text{ Mg m}^{-3}$ ,  $\mu = 9.673 \text{ mm}^{-1}$ ,  $Z = 2$ , triclinic, space group P-1,  $\lambda = 0.71073 \text{ \AA}$ ,  $T = 100 \text{ K}$ ,  $\omega$  and  $\varphi$  scans, 6542 reflections collected, 3291 independent ( $R_{\text{int}} = 0.0311$ ), 212 refined parameters,  $R1/wR2$  ( $I \geq 2\sigma(1)$ ) = 0.0248/0.0577 and  $R1/wR2$  (all data) = 0.0264/0.0584, maximum (minimum) residual electron density 1.322 (-1.067)  $\text{e/\AA}^3$ .

### 2.8.13 Synthesis of **2.12** ( $C_{10}H_{12}N_6O_6Cl_4AuAg$ )

Silver complex **2.6** (0.29 g, 0.59 mmol) was placed in a 125 mL flask containing dichloromethane (30 mL).  $(SMe_2)AuCl$  (0.17 g, 0.59 mmol) was added and stirred at room temperature for 3.5 hours. The flask was warmed and a yellow solution was obtained after filtration. The volatiles were evaporated slowly to yield a solid. Dichloromethane (35 mL) was added and stirred for 10 minutes and filtered. The volatiles were slowly evaporated and the process was repeated once more. The resulting solid was redissolved in dichloromethane (25 mL) and filtered to yield grey crystalline solid **2.12**. Yield: 0.02 g, 0.02 mmol, 4%. Mp: 208-211°C. Anal. Calcd for  $C_{10}H_{12}N_6O_6Cl_4AuAg$ : C, 15.83; H, 1.60; N, 11.07. Found: C, 17.74; H, 1.47; N, 10.92.  $^1H$  NMR (300 MHz,  $DMSO-d_6$ ):  $\delta$  3.88 (s, 12H,  $CH_3$ ).  $^{13}C$  NMR (75 MHz,  $DMSO-d_6$ ):  $\delta$  182.1 (s, C-Au), 117.8 (s, C=C), 36.8 (s,  $CH_3$ ). Calcd for  $C_{10}H_{12}N_4Cl_4Au [M-Ag(NO_3)_2]^+$ : 527.01, found 527.0.

X-ray crystal structure analysis of **2.12**: formula  $C_{10}H_{12}AgAuCl_4N_6O_6$ ,  $MW = 758.89$ , colorless crystal  $0.27 \times 0.11 \times 0.09 \text{ mm}^3$ ,  $a = 37.071(8) \text{ \AA}$ ,  $b =$

6.2092(13) Å,  $c = 12.900(3)$  Å,  $\alpha = 90^\circ$ ,  $\beta = 100.532(4)^\circ$ ,  $\gamma = 90^\circ$ ,  $V = 2919.4(11)$  Å<sup>3</sup>,  $D_{\text{calc}} = 2.590$  Mg m<sup>-3</sup>,  $\mu = 9.127$  mm<sup>-1</sup>,  $Z = 6$ , monoclinic, space group C2/m,  $\lambda = 0.71073$  Å,  $T = 100$  K,  $\omega$  and  $\varphi$  scans, 11643 reflections collected, 3231 independent ( $R_{\text{int}} = 0.0458$ ), 255 refined parameters,  $R1/wR2$  ( $I \geq 2\sigma(1)$ ) = 0.0364/0.0835 and  $R1/wR2$  (all data) = 0.0423/0.0860, maximum (minimum) residual electron density 2.062 (-2.149) e/Å<sup>3</sup>.

#### 2.8.14 Synthesis of **2.13** (C<sub>10</sub>H<sub>14</sub>N<sub>5</sub>O<sub>3</sub>Cl<sub>2</sub>Au)

Silver complex **2.8** (0.09 g, 0.2 mmol) was dissolved in dichloromethane (20 mL) and (SMe<sub>2</sub>)AuCl (0.04 g, 0.2 mmol) was added and stirred at room temperature for 2 hours. A clear solution was obtained after filtration. The volatiles were evaporated to give a white solid. The solid was stirred in diethyl ether (20 mL) overnight and redissolved in dichloromethane. The mixture was filtered and the volatiles were evaporated to yield white solid **2.13**. Yield: 0.06 g, 0.09 mmol, 60%. Mp: 268 °C. Anal. Calcd for C<sub>10</sub>H<sub>14</sub>N<sub>5</sub>O<sub>3</sub>Cl<sub>2</sub>Au: C, 23.09; H, 2.71; N, 13.46. Found: C, 22.85; H, 2.65; N, 12.26. <sup>1</sup>H NMR (300 MHz, D<sub>2</sub>O):  $\delta$  7.80 (s, 2H, CH), 3.86 (s, 6H, CH<sub>3</sub>), 3.83 (s, 6H, CH<sub>3</sub>). <sup>13</sup>C NMR (75 MHz, DMSO-*d*<sub>6</sub>):  $\delta$  184.0 (s, C-Au), 121.1 (s, C=C), 120.7 (s, C=C), 39.1 (s, CH<sub>3</sub>), 36.1 (s, CH<sub>3</sub>). Calcd for C<sub>10</sub>H<sub>13</sub>N<sub>4</sub>Cl<sub>2</sub>Au [M-HNO<sub>3</sub>]<sup>+</sup>: 457.11, found 457.1.

#### 2.8.15 Antimicrobial Testing

Sterilized LB Broth was measured (5 mL) into a sterile culture tube. A constant volume of suspension culture of microorganisms (one sterilized loop), was added to the tube containing the LB Broth. The mixture was cultured

overnight at 37°C in a shaking incubator. An initial solution of each compound in LB Broth (10 mL) was prepared. A series of serial dilutions was performed by transferring 1mL of the initial solution into a sterile tube containing LB Broth (2 mL) marked D1. An aliquot of 1 mL of well mixed solution D1 was transferred to a second sterile tube containing LB Broth (2 mL) marked D2. The same process was repeated for D3-D6, with D6 containing an initial LB Broth volume of 1mL. All initial and transfer values for **2.10** were halved due to the decreased water solubility of the complex. Each tube was inoculated with microorganism suspension (25 µL). The test was performed three times.

#### 2.8.16 Determination of MIC

Growth/no growth of microorganisms was visually evaluated after incubation for 24 hours at 37°C in a shaking incubator. The lowest concentration with no visible growth (turbidity) was taken as the MIC.

#### 2.8.17 Determination of MBC

One sterilized loop from determined MIC clear (no growth) tube was cultured on an agar plate and incubated for 24 hours at 37°C. The concentration of each compound supporting no colony formation was taken as the MBC.



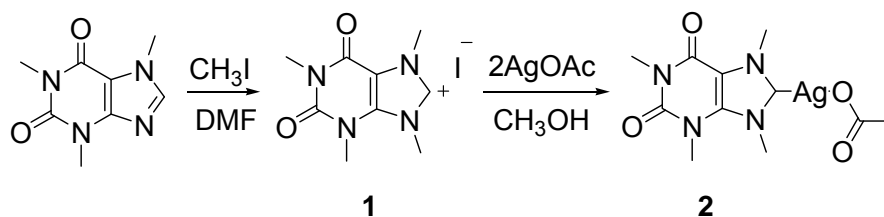
## CHAPTER III

### SYNTHESIS AND COMPARISON OF WATER STABILITY AND ANTIMICROBIAL PROPERTIES OF SILVER ACETATE N-HETEROCYCLIC CARBENE COMPLEXES

#### 3.1 Introduction

Bertrand and co-workers used silver acetate to generate a silver-NHC polymeric compound in 1997.<sup>107</sup> Since that time, our group has explored the use of silver acetate to synthesize a variety of NHC-silver acetate complexes.<sup>93,94,95</sup>

Typically, NHC-silver complexes show rapid decomposition in aqueous solution.<sup>3,96,108</sup> However, a caffeine-based silver acetate complex synthesized by our group showed stability in water for several days (Scheme 3-1). Our most recent research in this area has involved the addition of electron withdrawing groups at the 4- and 5-positions of the imidazole ring.<sup>95</sup> The observed effects on water stability are reported in section 3.3.

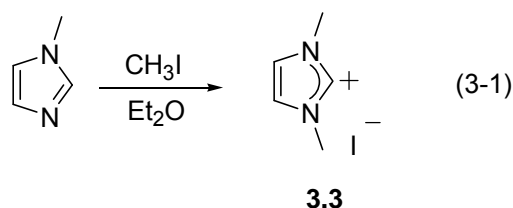


Scheme 3-1 Generation of a caffeine-based silver acetate complex

Because of silver's proven effectiveness as a broad spectrum antimicrobial agent, the properties of several NHC-silver acetate complexes synthesized were explored and reported in section 3.4. A comparison of both water stability and antimicrobial properties between said silver acetate NHC complexes and (bis)NHC-silver and -gold complexes from Chapter II has been included in sections 3.3 and 3.4, respectively.

### 3.2 Synthesis and characterization of silver acetate NHC complexes

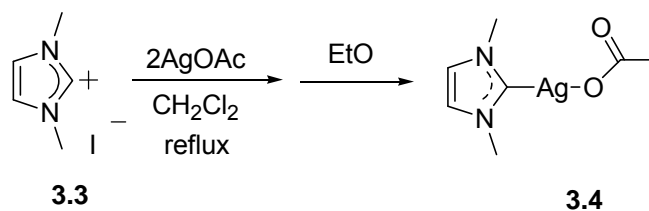
The salt 1,3-dimethylimidazolium iodide **3.3** was easily formed by the reaction between methylimidazole and excess iodomethane in diethyl ether using a modified literature procedure (eq. 3-1).<sup>104</sup>



Characterization in the literature procedure consisted only of <sup>1</sup>H NMR spectroscopy in D<sub>2</sub>O and elemental analysis. The <sup>1</sup>H and <sup>13</sup>C NMR spectra in DMSO-*d*<sub>6</sub> were consistent with the structure, with the imidazolium proton observed at 9.06 ppm in the <sup>1</sup>H NMR spectrum and the imidazolium carbon observed at 137.0 ppm in the <sup>13</sup>C NMR spectrum. The salt was obtained in 97% yield as compared to 88% in the literature.

The reaction of imidazolium salt **3.3** with 2 molar equivalents of silver acetate in refluxing dichloromethane for 40 hours afforded a white solid. The

solid was washed with diethyl ether and dried under vacuum to yield silver acetate NHC complex **3.4** (Scheme 3-2).



Scheme 3-2 Synthesis of silver acetate complex **3.4**

The carbene carbon was observed at 178.8 ppm in the  $^{13}\text{C}$  NMR spectrum in comparison to 186.2 ppm observed for the carbene carbon in **3.2**. Crystals suitable for X-ray diffraction were obtained from a saturated solution of dichloromethane. The solid state structure is shown in Figure 3-1. Complex **3.4** crystallized in the triclinic space group P-1. It had a Z value of six, indicating three molecules in the unit cell. One molecule also showed a disorder.

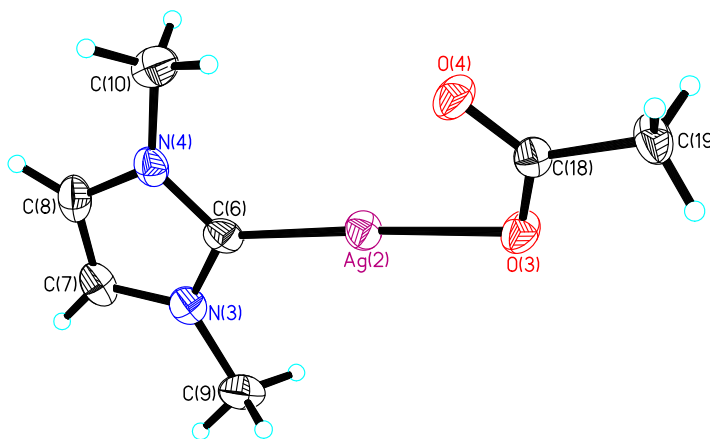
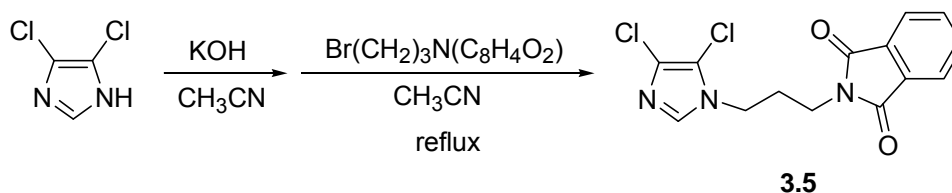


Figure 3-1 Thermal ellipsoid plot of **3.4** shown at 50% probability

A phthalimide derivative of imidazole was generated after deprotonation with potassium hydroxide in acetonitrile by adding 3-bromopropylphthalimide to the filtered solution and refluxing overnight (Scheme 3-3). Upon filtration of the precipitate and evaporation of the volatiles, compound **3.5** resulted in 87% yield.



Scheme 3-3 Synthesis of phthalimide imidazole derivative **3.5**

A resonance shift was observed in the  $^1\text{H}$  NMR spectrum from 3.70 ppm ( $\text{Br-CH}_2^-$ ) in the starting material to 4.04 ppm ( $\text{N-CH}_2^-$ ) in **3.5**. Crystals suitable for X-ray diffraction were grown from a concentrated acetonitrile solution. The solid structure is shown in Figure 3-2.

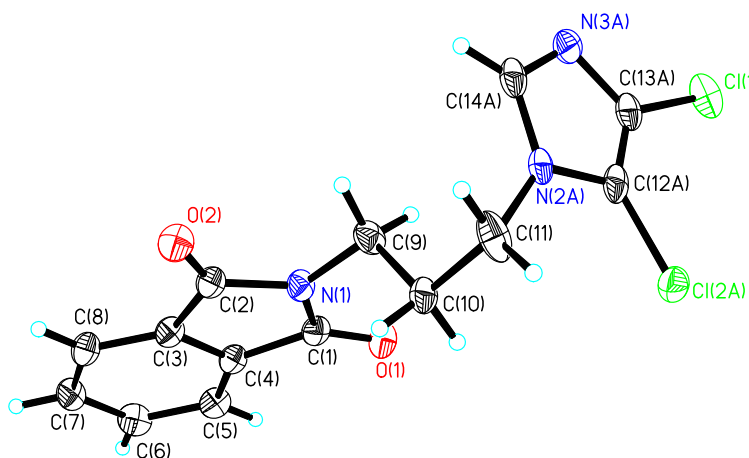
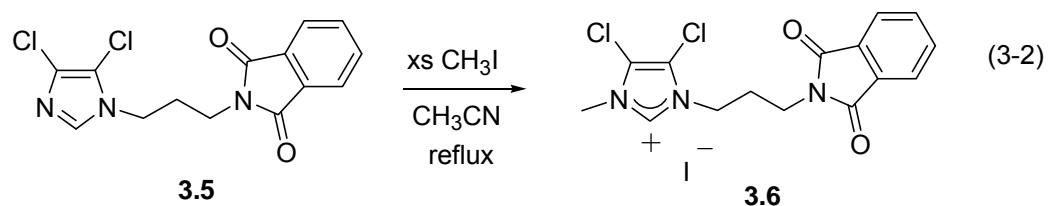


Figure 3-2 Thermal ellipsoid plot of **3.5** shown at 50% probability

The iodide salt of **3.5** was easily synthesized by methylation of the open nitrogen on the imidazole ring. Excess iodomethane was added to a solution of **3.5** in acetonitrile and refluxed overnight. Upon evaporation of the volatiles, complex **3.6** resulted in a 70% yield (eq. 3-2).



The imidazolium proton was observed at a resonance of 9.38 ppm in the  $^1\text{H}$  NMR spectrum and the imidazolium carbon was observed at a resonance of 136.5 ppm in the  $^{13}\text{C}$  NMR spectrum. Crystals suitable for X-ray diffraction were grown from a concentrated acetonitrile solution. The solid structure is shown in Figure 3-3.

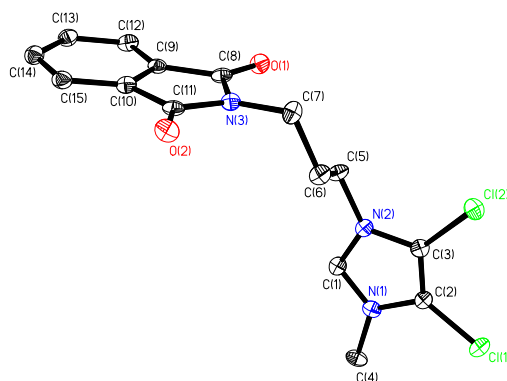
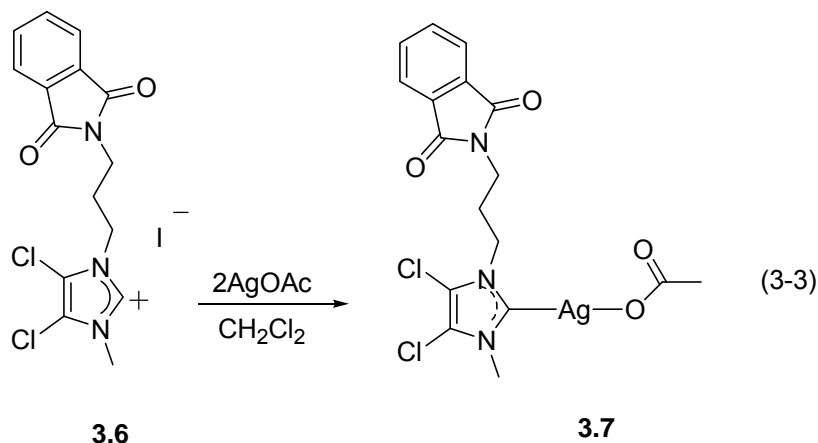


Figure 3-3 Thermal ellipsoid plot of cationic portion of **3.6** shown at 50% probability with hydrogen atoms omitted for clarity

The reaction of imidazolium salt **3.6** with 2 molar equivalents of silver acetate in dichloromethane at room temperature for 2 hours afforded silver

acetate NHC complex **3.7** (eq. 3-3). Upon filtration of the precipitate and evaporation of the volatiles, **3.7** resulted in 80% yield.



The carbene carbon resonance was observed at 174.5 ppm in the  $^{13}\text{C}$  NMR spectrum in comparison to 186.2 ppm observed for the carbene carbon in **3.2** and 178.8 observed in **3.4**. Crystal suitable for X-ray diffraction were obtained from a saturated solution of acetonitrile. The solid state structure is shown in Figure 3-4. Complex **3.7** crystallized in the triclinic space group P-1. It had a Z value of four, indicating two molecules in the unit cell.

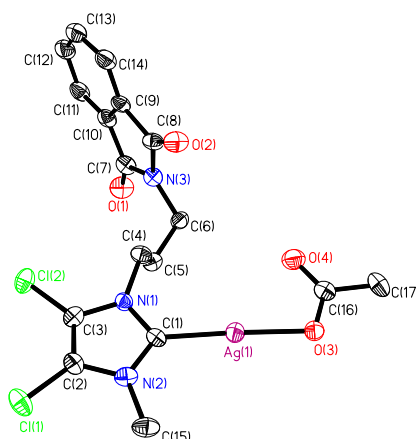


Figure 3-4 Thermal ellipsoid plot of **3.7** shown at 50% probability

The  $^{13}\text{C}$  NMR resonance of the carbene, Ag-C bond length and the C-Ag-O bond angle of **3.7** was compared to those reported **3.2**, **3.4** and two other silver acetate NHC analogs **3.8** and **3.9** (Figure 3-5). Complex **3.8** had chlorine atoms at the 4 and 5 positions of the imidazole ring and **3.9** had a methyl ester at the 4-position of the imidazole ring.<sup>93,95</sup>

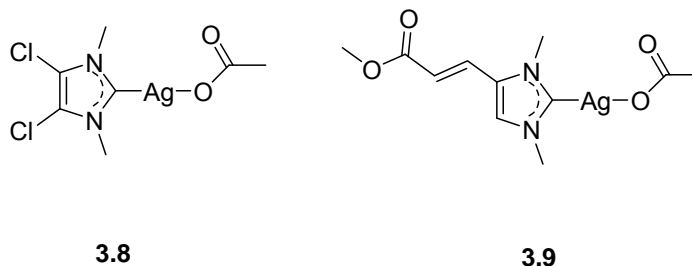


Figure 3-5 Silver acetate NHC complexes **3.8** and **3.9**

The  $^{13}\text{C}$  NMR spectral resonances for the carbene carbon were similar for **3.4**, **3.7** and **3.8** at 178.8 ppm, 174.5 ppm and 179.7 ppm, respectively. The  $^{13}\text{C}$  NMR spectral resonances for the carbene carbon shifts of **3.2** and **3.9** differed slightly from the others but were similar to each other at 186.2 ppm and 182.0 ppm, respectively.

The bond length of the carbon-silver bond for all five complexes was compared. Complexes **3.2** and **3.9** were experimentally identical at distances of 2.067(3) Å and 2.062(5) Å, respectively. Complexes **3.4** and **3.7** had average bond distances of 2.08 Å and 2.05 Å, respectively. Complex **3.8** had a distance slightly shorter in comparison at 2.030(8) Å. The carbon-silver-oxygen bond angle was closer to linearity for **3.4** and **3.7** with average values of 177° and 178°, respectively. For complexes **3.2**, **3.8** and **3.9** this angle deviated more from

linearity with values of 168.19(9)<sup>o</sup>, 168.9(2)<sup>o</sup> and 167.28(18)<sup>o</sup>, respectively. The above reported data has been compiled in Table 3-1.

Table 3-1 A comparison of selected <sup>13</sup>C NMR spectra resonances (ppm), bond distances (Å) and angles (°) for **3.2**, **3.4**, **3.7**, **3.8** and **3.9**

Compound	<b>3.2</b>	<b>3.4</b>	<b>3.7</b>	<b>3.8</b>	<b>3.9</b>
<i><sup>13</sup>C NMR</i>					
Carbene-Silver	186.2	178.8	174.5	179.7	182.0
<i>Bond lengths</i>					
C-Ag	2.067(3)	2.054(5) 2.064(6) 2.068(6) 2.120(6)	2.035(6) 2.067(6)	2.030(8)	2.062(5)
<i>Bond angles</i>					
C-Ag-O	168.19(9)	175.97(18) 176.0(2) 176.8(2) 177.35(17)	177.7(2) 178.1(2)	168.9(2)	167.28(18)

### 3.3 Water Stability of Silver Complexes

The water stability of complex **3.4** was assessed and compared with complexes **3.2**, **3.8** and **3.9**. The water stability of these complexes was compared to (bis)NHC-silver and gold analogs described in chapter 2.

#### 3.3.1 Water Stability of Silver Acetate NHC Complexes

The water stability of **3.2**, **3.4**, **3.8** and **3.9** were examined. The stability of each silver complex was assessed by noting the changes in the integration of <sup>1</sup>H NMR spectra. Complex **3.2** was reported to have stability in D<sub>2</sub>O for 3 days, **3.9** only showed stability for 1.5 hours but **3.8** showed increased stability with 66% of the compound remaining after 17 weeks.<sup>95</sup> Although stable in DMSO (Figure 3-6a), complex **3.4** degraded rapidly to the imidazolium salt in D<sub>2</sub>O, with only 5%



remaining after 2 hours (Figure 3-6b). Based on these results, it can be noted that the presence of electron withdrawing groups, particularly  $\sigma$ -withdrawing as in the chlorine groups of **3.8**, at the 4- and 5-positions of the imidazole ring enhance water stability. The presence of substituents with  $\pi$ -withdrawing capability, as in the methyl ester group of **3.9** at the 4-position of the imidazole ring, appeared to have no effect on the stability in aqueous environments. The findings have been compiled in Table 3-2.

Table 3-2 Stability of complexes **3.2**, **3.4**, **3.8** and **3.9** in D<sub>2</sub>O

Compound	<b>3.2</b>	<b>3.4</b>	<b>3.8</b>	<b>3.9</b>
Time	3 days	2 hours	17 weeks	1.5 hours

Because complex **3.4** proved to be stable in DMSO-*d*<sub>6</sub> (Figure 3-6a), a <sup>1</sup>H NMR experiment was performed to determine if DMSO stability would be affected by the addition of water. A series of 20  $\mu$ L water aliquots were added to an NMR tube containing a sample of complex **3.4** in DMSO-*d*<sub>6</sub>. After each addition, the <sup>1</sup>H NMR was taken after an interval of fifteen minutes. Upon the first water addition, approximately 83% of **3.4** remained intact (Figure 3-7a). With 40  $\mu$ L (Figure 3-7b) and 60  $\mu$ L (Figure 3-7c) of water, approximately 76% and 73% remained intact, respectively. At 80  $\mu$ L of water (Figure 3-8a), approximately 67% remained intact in comparison to only 8.3% remaining intact upon addition of 100  $\mu$ L of water (Figure 3-8b). The complex remained fairly stable with up to 80  $\mu$ L of water, suggesting that the NHC-silver acetate complex **3.4** can display some water stability with the presence of DMSO.

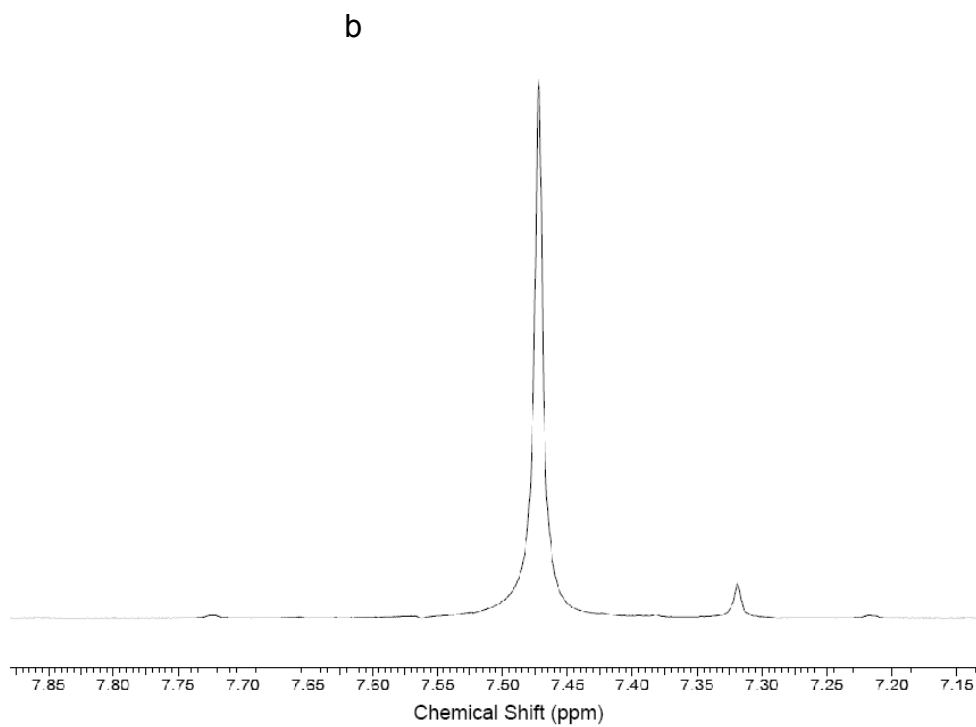
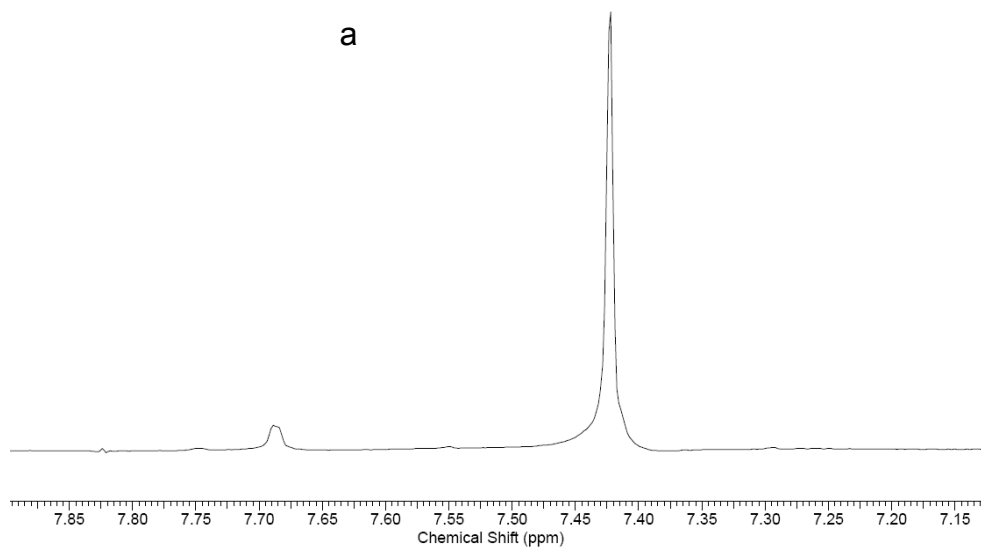


Figure 3-6  $^1\text{H}$  NMR spectra of **3.4** in  $\text{DMSO}-d_6$  (a) and  $\text{D}_2\text{O}$  (b)

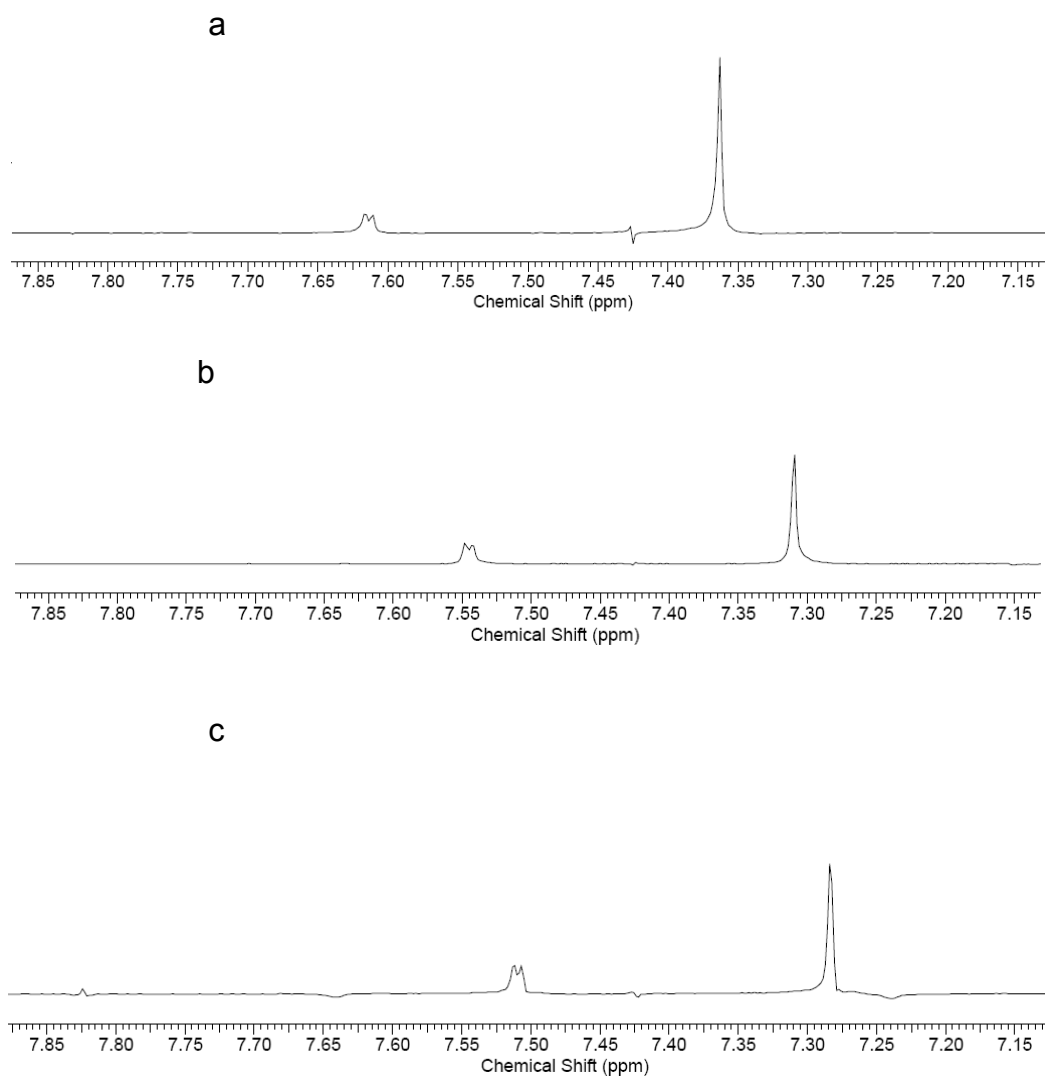


Figure 3-7  $^1\text{H}$  NMR spectra of **3.4** in  $\text{DMSO-}d_6$  with water additions of 20  $\mu\text{L}$  (a), 40  $\mu\text{L}$  (b) and 60  $\mu\text{L}$  (c)

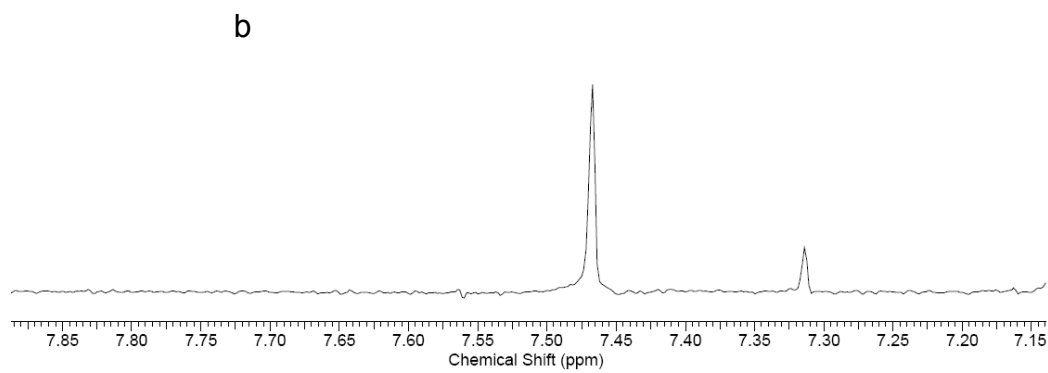
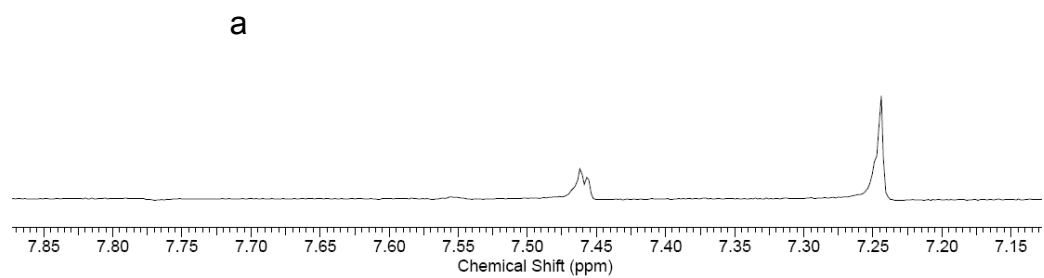


Figure 3-8  $^1\text{H}$  NMR spectra of **3.4** in  $\text{DMSO-}d_6$  with water additions of 80  $\mu\text{L}$  (a) and 100  $\mu\text{L}$  (b)

### 3.3.2 Water Stability Comparison of Silver Acetate NHC Complexes with Their (bis)NHC-Silver and –Gold Analogs

Based on results from the water stability studies conducted in section 2.3, it was shown that silver acetate NHC complex **3.8** had greater water stability than its bis(NHC)-silver counterpart. Only 34% of **3.8** had degraded in D<sub>2</sub>O in 17 weeks as opposed to the 36% that had degraded in 16 hours for the same (bis)NHC analogue. Complex **3.4** and (bis)NHC-silver counterpart both degraded rapidly. The results of these studies indicated that silver acetate NHC systems have superior stability in aqueous solution in comparison to the silver-(bis)NHC analogs.

Although **3.8** displayed marked improvement over bis(NHC)-silver analogue, an assessment could not be made concerning the water stability of the gold counterpart. Based on water stability studies conducted in section 2.5.1, 2 weeks of data had been compiled thus far on the dichloro-gold analog as compared to the 17 weeks worth on **3.8**. At the 2 week interval, the gold complex had remained stable. The bis(NHC)-gold complexes tested had proved to be far more stable than their bis(NHC)-silver precursors, thus the bis(NHC)-gold analog to **3.4** displayed better water stability in comparison. Based on results for the system with hydrogen at the 4- and 5-positions of the imidazole ring, evidence supported greatly enhanced stability in aqueous solution for gold-(bis)NHC complexes over both silver-(bis)NHC and silver acetate NHC complexes.

### 3.4 Antimicrobial Properties of Silver Acetate NHC Complexes in Comparison with Gold(I)-NHC Complexes and Their Silver(I)-NHC Precursors

The antimicrobial properties of the synthesized silver acetate NHC complexes were evaluated using two standard microbiological tests. The activity of these complexes was compared to (bis)NHC-silver and gold analogs described in chapter 2.

#### 3.4.1 Antimicrobial Properties of Silver Acetate NHC Complexes

The antimicrobial properties of silver acetate NHC complexes **3.2**, **3.4**, **3.7**, **3.8** and **3.9** were evaluated for their effectiveness by determining the minimum inhibitory concentration (MIC) against laboratory strains of test organisms *Escherichia coli*, *Staphylococcus aureus*, and *Pseudomonas aeruginosa* using silver nitrate as a control. The MIC, a standard microbiological test, has been used to determine the bacteriostatic activity of antimicrobial agents. The lower the MIC value, the more effective the compound will be as an antimicrobial agent. The corresponding iodide salts **3.1**, **3.3** and **3.6** were also tested along with **3.10** and **3.11** (Figure 3-9), imidazolium salts of **3.8** and **3.9**.

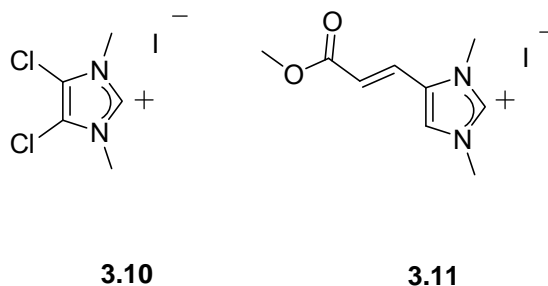


Figure 3-9 Imidazolium iodide salts **3.10** and **3.11**

Results for the MIC test have been reported in Table 3-3. The MIC was obtained by visual inspection of the turbidity of solution. The imidazolium iodide salts **3.1**, **3.3**, **3.6**, **3.10** and **3.11** displayed virtually no antimicrobial properties in comparison to the silver complexes. All silver compounds tested showed antimicrobial activity against the organisms. The MIC values for the silver complexes were similar, with **3.9** being most effective against *Escherichia coli* and *Pseudomonas aeruginosa* with MIC values of 0.16 mmol/L for both and **3.2** being most effective against *Staphylococcus aureus* with an MIC value of 0.12 mmol/L. Complex **3.7** had MIC values higher for all three microorganisms than the other silver acetate NHC systems tested at 0.45 mmol/L. All silver compounds were tested against silver nitrate and all except **3.7** were effective at concentrations lower than that of silver nitrate, indicating their effectiveness as antimicrobial agents.

Table 3-3 MIC values of **3.1-3.4** and **3.6-3.11** in mmol/L L ( $\pm 0.3$ )

Compound	<i>E. coli</i>	<i>S. aureus</i>	<i>P. aeruginosa</i>
<b>3.1</b>	>180	>180	>180
<b>3.3</b>	91	91	91
<b>3.6</b>	53	160	53
<b>3.10</b>	64	195	21
<b>3.11</b>	45	45	45
AgNO <sub>3</sub>	0.35	0.35	0.35
<b>3.2</b>	0.17	0.12	0.17
<b>3.4</b>	0.24	0.24	0.24
<b>3.7</b>	0.45	0.45	0.45
<b>3.8</b>	0.19	0.13	0.19
<b>3.9</b>	0.16	0.16	0.16

A sample from each of the silver no growth (clear) MIC tubes tested from above was taken and evaluated for the minimum bactericidal concentration (MBC). The MBC determines the lowest concentration of antimicrobial that will prevent the growth of an organism. MBC differs from the MIC by providing evidence that an antimicrobial actually prevents organism growth by killing microorganisms (MBC) rather than merely inhibiting growth (MIC).

Results for the MBC test have reported in Table 3-4. The MBC test was assessed by the prevention of microorganism colony growth. The MBC values reported reflect molar concentrations that supported no colony growth. All silver complexes evaluated were bactericidal at said concentrations, indicating the prevention of colony growth. All silver compounds were tested against silver nitrate and all except **3.7** were effective at concentrations lower than that of silver nitrate, again indicating their effectiveness as antimicrobial agents.

Table 3-4 MBC values of **3.2,3.4** and **3.7-3.9** in mmol/L L ( $\pm 0.3$ )

Compound	<i>E. coli</i>	<i>S. aureus</i>	<i>P. aeruginosa</i>
AgNO <sub>3</sub>	0.35	0.35	0.35
<b>3.2</b>	0.17	0.12	0.17
<b>3.4</b>	0.24	0.24	0.24
<b>3.7</b>	0.45	0.45	0.45
<b>3.8</b>	0.19	0.13	0.19
<b>3.9</b>	0.16	0.16	0.16



### 3.4.2 Antimicrobial Comparison of Silver Acetate NHC Complexes with (bis)NHC-Gold(I) Complexes and Their (bis)NHC-Silver(I) Precursors

Based on results from the antimicrobial studies conducted in section 2.6, the silver acetate systems proved to behave similarly in effectiveness of bacteriostatic activity in comparison to their (bis)NHC-silver counterparts with MIC values all between 0.11-0.19 mmol/L, except for **3.4** and **3.7**, which were 0.24 mmol/L and 0.45 mmol/L, respectively. However, the silver acetate systems proved to be more effective than the bis-silver systems in bactericidal activity at the concentrations tested, with the exception of the dinuclear silver complex noted in Figure 2-4, which had MBC values similar to the silver acetate NHC systems of 0.13 mmol/L for *Pseudomonas aeruginosa*, *Escherichia coli* and *Staphylococcus aureus*.

Based on results from the antimicrobial studies conducted in section 2.6, the silver acetate systems also proved to be more effective in bacteriostatic activity in comparison to the (bis)NHC-gold analogues with MIC values all between 0.11-0.24 mmol/L, in comparison to an average MIC value of 0.43 mmol/L for the NHC-gold complexes. Again, **3.7** was the exception with an MIC value of 0.45 mmol/L for all three microorganisms evaluated. The silver acetate NHC complexes were also far more effective in bactericidal activity as well, with MBC values all between 0.11-0.45 mmol/L, in comparison to 0.45-1.4 mmol/L for the NHC-gold complexes.

### 3.5 Conclusion

Silver acetate NHC complexes were synthesized varying at the 1- and 3-positions of the imidazole ring and compared with our previously reported silver acetate NHC systems varying at the 4- and 5-positions of the imidazole ring. Water stability studies indicated enhanced stability for the dichloro analog attributed to its electron withdrawing capability. These systems were compared with their (bis)NHC-silver and -gold counterparts synthesized in chapter II and showed superior stabilities in comparison with the silver complexes, with the exception of both dihydro silver systems being equally unstable. Early results would indicate that the (bis)NHC-gold complexes have the most stability in an aqueous environment with the dihydro gold system showing stability in D<sub>2</sub>O for approximately 3 years. All silver acetate NHC complexes were evaluated for their antimicrobial properties and compared against results from chapter 2 for both silver and gold (bis)NHC systems. The acetate systems showed superior results against the gold systems in terms of both bacteriostatic and bactericidal activity. They displayed equal bacteriostatic activity to the silver (bis)NHC systems but improved bactericidal activity.

### 3.6 Experimental Section

The general considerations and X-ray information have been explained below. The experimental procedures for compounds **3.3-3.7** have been compiled in this section.

### 3.6.1 General Considerations

All reactions were carried out under aerobic conditions. All silver reactions were performed in the absence of light. The reagents methylimidazole and silver acetate were purchased from Acros Organics. Iodomethane and *N*-(3-bromopropyl)phthalimide were purchased from Alfa Aesar. Silver nitrate was purchased from VWR and potassium hydroxide was purchased from Fisher Scientific. All reagents were used as received. Imidazolium iodide salt **3.3** was prepared using a modified literature procedure as described in 3.5.3.<sup>104</sup> Imidazolium salt **3.1** and silver complex **3.2** were provided by Dr. Aysegul Kascatan-Nebioglu.<sup>93</sup> Imidazolium salt **3.10** and silver complex **3.8** were provided by Dr. Khadijah Hindi.<sup>95</sup> Imidazolium salt **3.11** and silver complex **3.9** were provided by Dr. Semih Durmus.<sup>95</sup> LB Broth Miller (DIFCO) and Bacto-agar (DIFCO) were prepared according to manufacturer's instruction and sterilized before use. All solvents were purchased from Fisher Scientific and used as received. <sup>1</sup>H and <sup>13</sup>C NMR data were collected on a Varian Gemini 300 MHz instrument and referenced to the residual protons of the deuterated solvents and the solvent resonances, respectively. The <sup>1</sup>H NMR stability study done in D<sub>2</sub>O for complex **3.4** was collected on a Varian INOVA 400 MHz instrument. <sup>109</sup>Ag NMR data was collected on a Varian INOVA 750 MHz instrument. Elemental analyses were performed at the Microanalysis Laboratory at The University of Illinois. Mass spectrometric analysis of **3.3** and **3.4** was performed at the mass spectrometry facility at The University of Akron and analysis of **3.5-3.7** was

performed at the CCIC Mass Spectrometry and Proteomics Facility at The Ohio State University.

### 3.6.2 X-Ray Crystallographic Structure Determination Details

The crystal structure of **3.4** was solved by Dr. Matthew Panzner. The crystal structure of **3.5** was solved by Michael Deblock. The crystal structures of **3.6** and **3.7** were solved by Dr. Doug Medvetz. Crystals of **3.4-3.7** were coated in paraffin oil and mounted on a CryoLoop™ and placed on the goniometer head under a stream of nitrogen cooled to 100K. The data was collected on a Bruker APEX CCD diffractometer with graphite-monochromated Mo K $\alpha$  radiation ( $\lambda$  = 0.71073 Å). The unit cell was determined by using reflections from three different orientations. The data was integrated using SAINT.<sup>105</sup> An empirical absorption correction and other corrections were applied to the data using multi-scan SADABS.<sup>105</sup> Structure solution, refinement, and modeling were accomplished by using the Bruker SHELXTL package.<sup>106</sup> The structure was determined by full-matrix least-squares refinement of  $F^2$  and the selection of the appropriate atoms from the generated difference map. Hydrogen atom positions were calculated and  $U_{iso}(H)$  values were fixed according to a riding model.

### 3.6.3 Synthesis of **3.3** (C<sub>5</sub>H<sub>9</sub>I)

Methylimidazole (3.29 g, 40.1 mmol) was dissolved in diethyl ether (50 mL). Iodomethane (3 mL) was added dropwise to the solution and the mixture was stirred at room temperature for 24 hours. The solvent was decanted and white hygroscopic solid **3.3** was obtained. Yield: 8.7 g, 39 mmol, 97%. Mp: 80-82

°C. Anal. Calcd for C<sub>5</sub>H<sub>9</sub>N<sub>2</sub>I: C, 26.80; H, 4.05; N, 12.50. Found: C, 27.53; H, 4.32; N, 12.36. <sup>1</sup>H NMR (300 MHz, DMSO-*d*<sub>6</sub>): δ 9.06 (s, 1H, NCHN), 7.69 (s, 2H, CH), 3.85 (s, 6H, CH<sub>3</sub>). <sup>13</sup>C NMR (75 MHz, DMSO-*d*<sub>6</sub>): δ 137.0 (s, NCHN), 123.4 (s, C=C), 35.7 (s, CH<sub>3</sub>). FT IR (nujol solution, cm<sup>-1</sup>): 3458, 1731, 1615, 1573, 1285, 1170, 1084, 807. ESI-MS (*m/z*): Calcd for C<sub>5</sub>H<sub>9</sub>N<sub>2</sub> [M-I]<sup>+</sup>: 97.14, found 97.10.

#### 3.6.4 Synthesis of **3.4** (C<sub>7</sub>H<sub>11</sub>N<sub>2</sub>O<sub>2</sub>Ag)

Imidazolium salt **3.3** (0.91 g, 4.0 mmol) was dissolved in dichloromethane (50 mL), AgOAc (1.37 g, 8.21 mmol) was added and the mixture was refluxed for 40 hours. After filtration, a clear solution was obtained. The volatiles were evaporated to produce a white sticky solid. The solid was washed with diethyl ether (10 mL) three times and dried under vacuum for 7 hours to yield **3.4**. Yield: 0.67 g, 2.6 mmol, 64%. Mp: 109-111 °C. Anal. Calcd for C<sub>7</sub>H<sub>11</sub>N<sub>2</sub>O<sub>2</sub>Ag: C, 31.96; H, 4.22; N, 10.65. Found: C, 35.75; H, 5.24; N, 10.28. <sup>1</sup>H NMR (300 MHz, DMSO-*d*<sub>6</sub>): δ 7.42 (s, 2H, CH), 3.76 (s, 6H, CH<sub>3</sub>), 1.78 (s, 3H, CH<sub>3</sub>). <sup>13</sup>C NMR (75 MHz, DMSO-*d*<sub>6</sub>): δ 178.8 (s, C-Ag), 174.3 (s, C=O), 122.9 (s, C=C), 38.0 (s, CH<sub>3</sub>), 23.2 (s, CH<sub>3</sub>). <sup>109</sup>Ag (35 MHz, DMSO-*d*<sub>6</sub>): δ 343.6 (s). ESI-MS (*m/z*): Calcd for C<sub>5</sub>H<sub>8</sub>N<sub>2</sub>Ag [M-HOAc]<sup>+</sup>: 202.97, found 203.00.

X-ray crystal structure analysis of **3.4**: formula C<sub>7</sub>H<sub>11</sub>AgN<sub>2</sub>O<sub>2</sub>, *MW* = 263.05, colorless crystal 0.11 x 0.05 x 0.04 mm<sup>3</sup>, *a* = 10.508(2) Å, *b* = 10.521(2) Å, *c* = 12.881(3) Å, α = 95.984(4)°, β = 96.090(4)°, γ = 93.974(4)°, *V* = 1403.7(5) Å<sup>3</sup>, *D*<sub>calc</sub> = 1.867 Mg m<sup>-3</sup>, μ = 2.117 mm<sup>-1</sup>, *Z* = 6, triclinic, space group P-1, λ = 0.71073 Å, *T* = 100 K, ω and φ scans, 11234 reflections collected, 5611

independent ( $R_{\text{int}} = 0.0320$ ), 344 refined parameters,  $R1/wR2$  ( $I \geq 2\sigma(1)$ ) = 0.0486/0.1040 and  $R1/wR2$  (all data) = 0.0700/0.1091, maximum (minimum) residual electron density 1.001 (-0.787)  $\text{e}/\text{\AA}^3$ .

### 3.6.5 Synthesis of **3.5** ( $\text{C}_{14}\text{H}_{11}\text{Cl}_2\text{N}_3\text{O}_2$ )

KOH (2.27 g, 40.4 mmol) was added to a flask containing 4,5-dichloroimidazole (1.29 g, 9.49 mmol) and acetonitrile (50 mL). The mixture was stirred for 2 hours at room temperature. The excess KOH was filtered, the solution was transferred to a round bottom flask and *N*-(3-bromopropyl)phthalimide (2.52 g, 9.41 mmol) was added. The mixture was stirred at reflux overnight. Upon filtration, the volatiles were evaporated to yield orange solid **3.5**. Yield: 2.66 g, 8.21 mmol, 87.4%. Mp: 138-140°C. Anal. Calcd for  $\text{C}_{14}\text{H}_{11}\text{Cl}_2\text{N}_3\text{O}_2$ : C, 51.87; H, 3.42; N, 12.96. Found: C, 50.63; H, 3.23; N, 12.49.  $^1\text{H}$  NMR (300 MHz,  $\text{DMSO}-d_6$ ):  $\delta$  7.85 (m, 4H, CH), 4.04 (t, 2H,  $\text{NCH}_2$ ), 3.59 (t, 2H,  $\text{NCH}_2$ ), 2.06 (quintet, 2H,  $\text{CH}_2$ ).  $^{13}\text{C}$  NMR (75 MHz,  $\text{DMSO}-d_6$ ):  $\delta$  168.0 (s, C=O), 136.0 (s, NCN), 134.4 (s, C=C), 131.7 (s, C=C), 124.3 (s, C=C), 123.0 (s, C=C), 112.0 (s, C=C), 43.5 (s,  $\text{CH}_2$ ), 34.6 (s,  $\text{CH}_2$ ), 28.1 (s,  $\text{CH}_2$ ). ESI-MS ( $m/z$ ): Calcd for  $\text{C}_{14}\text{H}_{11}\text{Cl}_2\text{N}_3\text{O}_2$  [M]: 324.16, found 324.0.

X-ray crystal structure analysis of **3.5** formula  $\text{C}_{14}\text{H}_{11}\text{Cl}_2\text{N}_3\text{O}_2$ ,  $MW = 324.16$ , colorless crystal  $0.16 \times 0.08 \times 0.04 \text{ mm}^3$ ,  $a = 7.456(4) \text{ \AA}$ ,  $b = 7.891(4) \text{ \AA}$ ,  $c = 12.384(6) \text{ \AA}$ ,  $\alpha = 77.305(8)^\circ$ ,  $\beta = 76.147(8)^\circ$ ,  $\gamma = 84.852(8)^\circ$ ,  $V = 689.7(6) \text{ \AA}^3$ ,  $D_{\text{calc}} = 1.561 \text{ Mg m}^{-3}$ ,  $\mu = 0.478 \text{ mm}^{-1}$ ,  $Z = 2$ , triclinic, space group P-1,  $\lambda = 0.71073 \text{ \AA}$ ,  $T = 100 \text{ K}$ ,  $\omega$  and  $\varphi$  scans, 11406 reflections collected, 2959 independent ( $R_{\text{int}} = 0.0291$ ), 245 refined parameters,  $R1/wR2$  ( $I \geq 2\sigma(1)$ ) =

0.0463/0.1126 and R1/wR2 (all data) = 0.0534/0.1193, maximum (minimum) residual electron density 0.546 (-0.298) e/Å<sup>3</sup>.

### 3.6.6 Synthesis of **3.6** (C<sub>15</sub>H<sub>14</sub>Cl<sub>2</sub>N<sub>3</sub>O<sub>2</sub>I)

Acetonitrile (50 mL) was added to a round bottom flask containing **3.5** (0.75 g, 2.3 mmol). Iodomethane (2 mL) was added and the solution was refluxed overnight. The volatiles were evaporated to yield orange solid **3.6**. Yield: 0.75 g, 1.6 mmol, 69%. Mp: 178-180°C. Anal. Calcd for C<sub>15</sub>H<sub>14</sub>Cl<sub>2</sub>N<sub>3</sub>O<sub>2</sub>I: C, 38.65; H, 3.03; N, 9.02. Found: C, 37.79; H, 2.96; N, 8.83. <sup>1</sup>H NMR (300 MHz, DMSO-*d*<sub>6</sub>): δ 9.38 (s, 1H, NCHN), 7.87 (m, 4H, CH), 4.28 (t, 2H, NCH<sub>2</sub>), 3.82 (s, 3H, CH<sub>3</sub>), 3.70 (t, 2H, NCH<sub>2</sub>), 2.16 (quintet, 2H, CH<sub>2</sub>). <sup>13</sup>C NMR (75 MHz, DMSO-*d*<sub>6</sub>): δ 168.1 (s, C=O), 136.5 (s, NCN), 134.3 (s, C=C), 131.7 (s, C=C), 123.1 (s, C=C), 119.3 (s, C=C), 118.2 (s, C=C), 46.2 (s, CH<sub>2</sub>), 35.0 (s, CH<sub>3</sub>), 34.3 (s, CH<sub>2</sub>), 27.3 (s, CH<sub>2</sub>). ESI-MS (*m/z*): Calcd for C<sub>15</sub>H<sub>13</sub>Cl<sub>2</sub>N<sub>3</sub>O<sub>2</sub> [M-HI]<sup>+</sup>: 338.18, found 338.0.

X-ray crystal structure analysis of **3.6** formula C<sub>15</sub>H<sub>14</sub>Cl<sub>2</sub>N<sub>3</sub>O<sub>2</sub>I, MW = 466.09, colorless crystal 0.17 x 0.08 x 0.04 mm<sup>3</sup>, *a* = 8.056(2) Å, *b* = 8.669(2) Å, *c* = 13.128(3) Å, α = 108.092(4)°, β = 96.705(4)°, γ = 97.150(4)°, *V* = 852.9(4) Å<sup>3</sup>, *D*<sub>calc</sub> = 1.815 Mg m<sup>-3</sup>, μ = 2.202 mm<sup>-1</sup>, *Z* = 2, triclinic, space group P-1, λ = 0.71073 Å, *T* = 100 K, ω and φ scans, 7290 reflections collected, 3843 independent (*R*<sub>int</sub> = 0.0231), 209 refined parameters, R1/wR2 (*I* ≥ 2σ(1)) = 0.0283/0.0731 and R1/wR2 (all data) = 0.0340/0.0749, maximum (minimum) residual electron density 0.700 (-0.843) e/Å<sup>3</sup>.

### 3.6.7 Synthesis of **3.7** (C<sub>17</sub>H<sub>16</sub>Cl<sub>2</sub>N<sub>3</sub>O<sub>2</sub>Ag)

Dichloromethane (30 mL) was added to a flask containing **3.6** (0.78 g, 1.7 mmol). AgOAc (0.56 g, 3.4 mmol) was added and the mixture was stirred at room temperature for 2.5 hours. The precipitate, assumed to be silver iodide, was filtered and the volatiles were evaporated to yield a yellow solid. Diethyl ether (30 mL) was added to the flask and stirred for 10 minutes. The solid was filtered and dried resulting in yellow solid **3.7**. Yield: 0.67 g, 1.3 mmol, 80%. Mp: 161-164°C. Anal. Calcd for C<sub>17</sub>H<sub>16</sub>Cl<sub>2</sub>N<sub>3</sub>O<sub>2</sub>Ag: C, 40.42; H, 3.19; N, 8.32. Found: C, 39.71; H, 3.06; N, 7.68. <sup>1</sup>H NMR (300 MHz, DMSO-*d*<sub>6</sub>):  $\delta$  7.82 (s, 4H, CH), 4.25 (t, 2H, NCH<sub>2</sub>), 3.73 (s, 3H, CH<sub>3</sub>), 3.66 (t, 2H, NCH<sub>2</sub>), 2.09 (quintet, 2H, CH<sub>2</sub>), 1.76 (s, 3H, CH<sub>3</sub>). <sup>13</sup>C NMR (75 MHz, DMSO-*d*<sub>6</sub>):  $\delta$  174.5 (s, C-Ag), 167.9 (s, C=O), 134.3 (s, C=C), 131.6 (s, C=C), 123.0 (s, C=C), 117.3 (s, C=C), 116.2 (s, C=C), 48.4 (s, CH<sub>2</sub>), 37.6 (s, CH<sub>3</sub>), 34.8 (s, CH<sub>2</sub>), 28.8 (s, CH<sub>2</sub>), 22.8 (s, CH<sub>3</sub>). ESI-MS (*m/z*): Calcd for C<sub>15</sub>H<sub>13</sub>Cl<sub>2</sub>N<sub>3</sub>O<sub>2</sub> [M-AgOAc]<sup>+</sup>: 338.18, found 338.0.

X-ray crystal structure analysis of **3.7** formula C<sub>17</sub>H<sub>16</sub>Cl<sub>2</sub>N<sub>3</sub>O<sub>2</sub>Ag, *MW* = 505.10, colorless crystal 0.16 x 0.12 x 0.09 mm<sup>3</sup>, *a* = 11.897(4) Å, *b* = 12.585(5) Å, *c* = 14.912(5) Å,  $\alpha$  = 78.521(6)°,  $\beta$  = 68.000(6)°,  $\gamma$  = 66.388(6)°, *V* = 1893.7(12) Å<sup>3</sup>, *D*<sub>calc</sub> = 1.772 Mg m<sup>-3</sup>,  $\mu$  = 1.375 mm<sup>-1</sup>, *Z* = 4, triclinic, space group P-1,  $\lambda$  = 0.71073 Å, *T* = 100 K,  $\omega$  and  $\phi$  scans, 14988 reflections collected, 7561 independent (*R*<sub>int</sub> = 0.0400), 491 refined parameters, *R*<sub>1</sub>/*wR*<sub>2</sub> (*I* ≥ 2σ(1)) = 0.0576/0.1557 and *R*<sub>1</sub>/*wR*<sub>2</sub> (all data) = 0.0764/0.1688, maximum (minimum) residual electron density 1.610 (-1.008) e/Å<sup>3</sup>.



### 3.6.8 Antimicrobial Testing

Sterilized LB Broth was measured (5 mL) into a sterile culture tube. A constant volume of suspension culture of microorganisms (one sterilized loop), was added to the tube containing the LB Broth. The mixture was cultured overnight at 37°C in a shaking incubator. An initial solution of each ligand in LB Broth (5 mL) and corresponding silver compound in LB Broth (10 mL) was prepared. A series of serial dilutions was performed by transferring 1 mL of the initial solution into a sterile tube containing LB Broth (2 mL) marked D1. One mL of well mixed solution D1 was transferred to a second sterile tube containing LB Broth (2 mL) marked D2. The same process was repeated for D3-D6, with D6 containing an initial LB Broth volume of 1 mL. Each tube was inoculated with microorganism suspension (25 µL). The test was performed three times.

### 3.6.9 Determination of MIC

Growth/no growth of microorganisms was visually evaluated after incubation for 24 hours at 37°C in a shaking incubator. The lowest concentration with no visible growth (turbidity) was taken as the MIC.

### 3.6.10 Determination of MBC

One sterilized loop from each clear (no growth) tube was cultured on an agar plate and incubated for 24 hours at 37°C. The lowest concentration of each silver compound supporting no colony formation was taken as the MBC.

# CHAPTER IV

## THE SYNTHESIS AND EXPLORATION OF ANTIMICROBIAL PROPERTIES OF IMIDAZOLIUM SALTS

### 4.1 Introduction

Quaternary ammonium compounds (QACs) such as benzalkonium chloride (BAC) and cetylpyridinium chloride (CPC) (Figure 4-1) have been widely used as commercially available disinfectants because of their bactericidal properties. BAC consists of as a mixture of even numbered alkyl chains, with C<sub>12</sub>-C<sub>14</sub> having the greatest activity. The efficacious demonstration of bactericidal activity of QACs prompted investigations of various salts of the imidazolium type.<sup>109,110,111</sup>

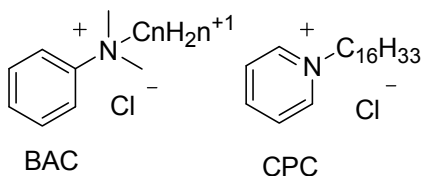


Figure 4-1 Quaternary ammonium salts BAC and CPC

Several different imidazolium salt systems were found to possess antimicrobial properties. One study focused on chloride salts containing N-ethyl and various N'-alkylthiomethyl derivatives ranging in even chain lengths of 4-14

carbon atoms (Figure 4-2a). It was determined that alkyl chain lengths of 10 or 12 carbons were sufficient to inhibit microorganism growth.<sup>109</sup> A separate study evaluated a series of 3-alkoxymethyl-1-methyl imidazolium salts of chloride, tetrafluoroborate and hexafluorophosphate, many of which were ionic liquids (Figure 4-2b). The alkoxy chain had a range in length of 3-12 or 14 and 16 carbon atoms. It was reported that chain lengths of 10-12 or 14 carbons displayed the most antimicrobial activity, with 12 being optimal.<sup>110</sup> Importantly, the anion had no affect on their activities.

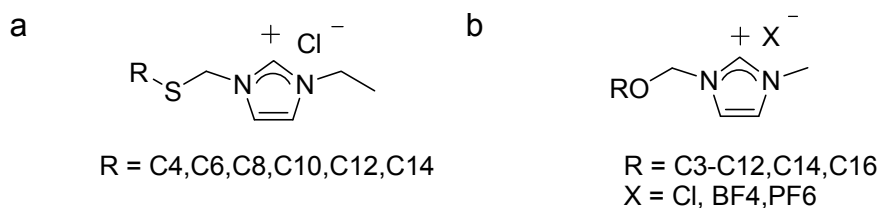


Figure 4-2 Alkylthiomethyl (a) and alkoxymethyl (b) imidazolium salt derivatives

A third study compared antimicrobial activity of two separate imidazolium types. A series of 1-alkyl-3-methylimidazolium chloride or bromide salts, ranging in even alkyl chain lengths of 8-16 carbon atoms (Figure 4-3a) and a series of 1-alkyl-3-hydroxyethyl-2-methylimidazolium chloride salts with alkyl chain lengths of either 14 or 16 carbon atoms (Figure 4-3b) were synthesized and analyzed. Both series were effective against a broad spectrum of microbes with the optimal range for the 1-alkyl-3-methylimidazolium series being 12-16 carbons.<sup>111</sup> Again, the anion had no affect on antimicrobial activity.

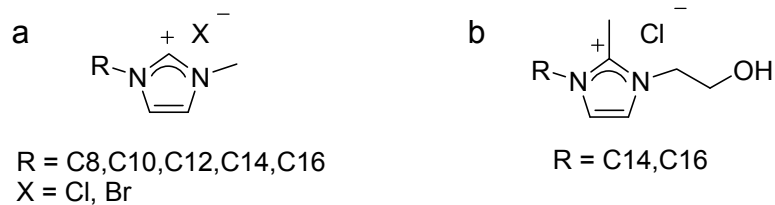


Figure 4-3 Alkyl (a) and alkyl-hydroxyethyl-(b) methylimiazolium salt derivatives

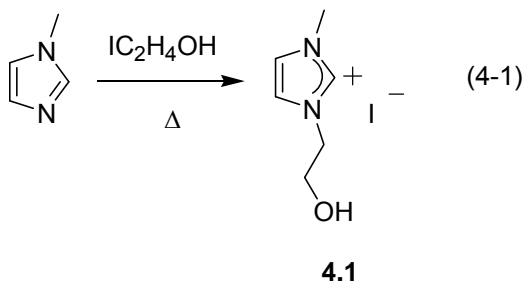
Based on these three separate studies, one could conclude that various substituents placed on different positions of the imidazole ring would affect the antimicrobial properties of the imidazolium salt if at least one nitrogen substituent would be a long alkyl chain consisting of at least 10-16 carbon atoms. It would also be expected that the choice of anion would have no bearing on antibacterial activity.

A significant discovery related to these types of salts was their ability to form micelles in aqueous solution, which has been linked to minimum inhibitory concentrations (MIC).<sup>109</sup> QACs were found to target the bacteria membrane by ionic interaction with phospholipids.<sup>112</sup> The mode of antimicrobial action was explained by these cytoplasmic interactions resulting in permeability loss and the disruption of respiration and ATP synthesis.<sup>111</sup>

The goal of the research discussed in this chapter was to synthesize a wide variety of imidazolium salts by varying the substituents on the nitrogen atoms and also on the 4- and 5-positions of the imidazole ring and test for any subsequent effect on antimicrobial properties.

## 4.2 Synthesis and Characterization of Imidazolium Salts

Generation of imidazolium salts with varying alkylhydroxy substituents was achieved by refluxing reagents in the absence of solvents. Methylimidazole was refluxed at 50°C with iodoethanol overnight yielding the hygroscopic imidazolium salt **4.1** (eq. 4-1).



The imidazolium proton resonance was observed at 9.10 ppm in the  $^1\text{H}$  NMR spectrum, consistent with acidic proton shifts of imidazolium salts ( $\delta$  8-10 ppm).<sup>1</sup> The corresponding imidazolium carbon resonance was observed at 136.7 ppm in the  $^{13}\text{C}$  NMR spectrum. Crystals suitable for X-ray diffraction were grown from a saturated ethanol solution. The crystal structure of **4.1** is shown in Figure 4-4. The complex crystallized in the monoclinic space group P2(1). Interestingly, the conformation was bent in the unit cell and displayed chirality.

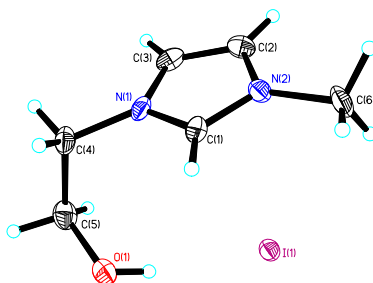
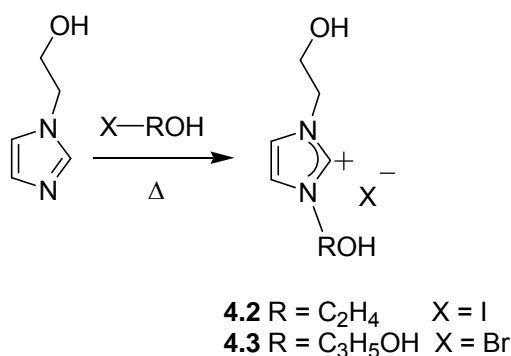


Figure 4-4 Thermal ellipsoid plot of **4.1** shown at 50% probability

The synthesis of imidazolium salts bearing 2 or 3 hydroxyl groups was also conducted in a similar manner by refluxing the reagents in the absence of solvents. By refluxing 2-hydroxyethylimidazole in the presence of iodoethanol, the ionic liquid imidazolium iodide salt **4.2** was formed (Scheme 4-1). 2-Hydroxyethylimidazole was refluxed in the presence of 3-bromo-1,2-propanediol followed by stirring in diethyl ether and imidazolium bromide salt **4.3** was provided (Scheme 4-1). The bromide salt **4.3** generated was in a semi-solid phase at room temperature.



Scheme 4-1 Synthesis of imidazolium salts **4.2** and **4.3**

The  $^1\text{H}$ MR spectrum for both compounds confirmed the structures by the observance of the imidazolium cation resonances at 9.12 ppm for iodide salt **4.2** and at 9.10 ppm for bromide salt **4.3**. The corresponding imidazolium carbon resonances at 136.5 ppm and 136.8 ppm in the  $^{13}\text{C}$  NMR spectra for **4.2** and **4.3** were consistent with the structures, respectively.

An imidazolium carboxylic acid derivative was synthesized by refluxing methylimidazole with iodopropionic acid in acetonitrile in the presence of acetic acid. Upon inspection of the resulting oil by  $^1\text{H}$  NMR, the presence of two

imidazolium cationic resonances were observed, one at 9.13 ppm for the iodide salt and one at 8.34 ppm, presumably to be from the zwitterion (Figure 4-5a).

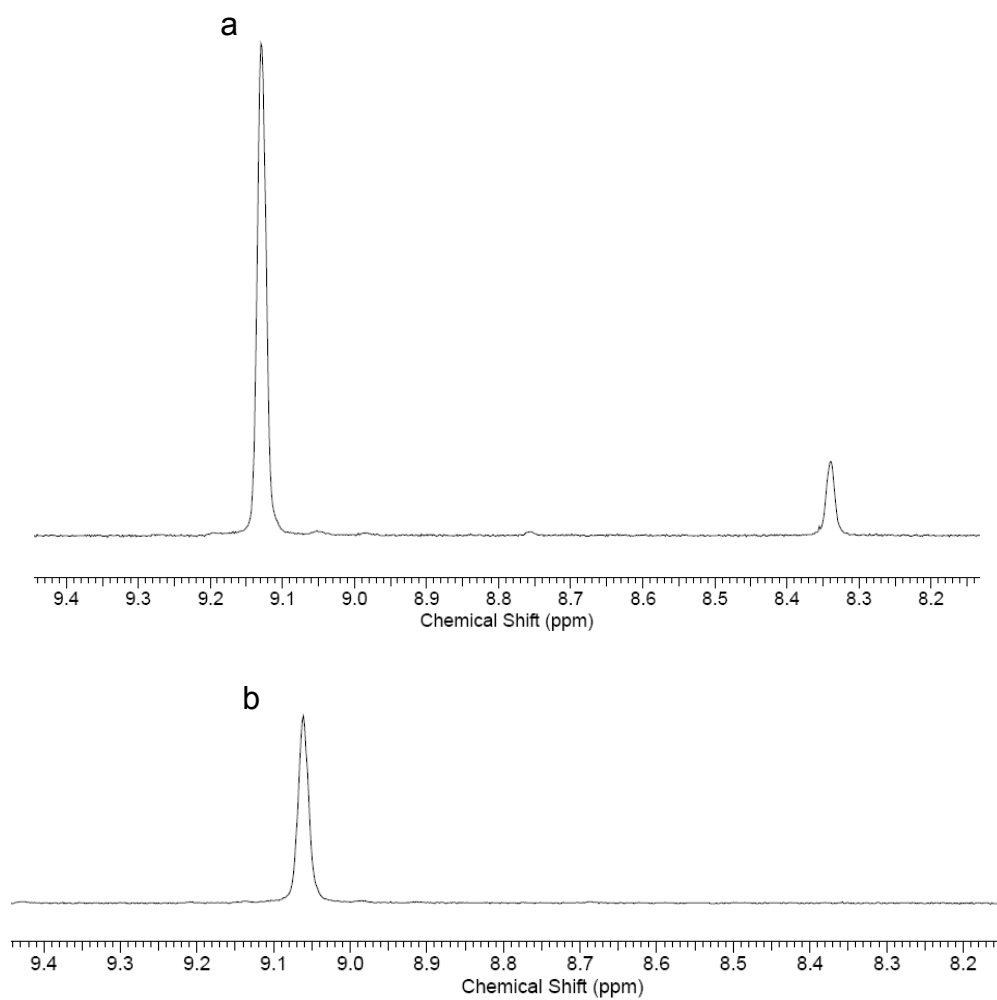
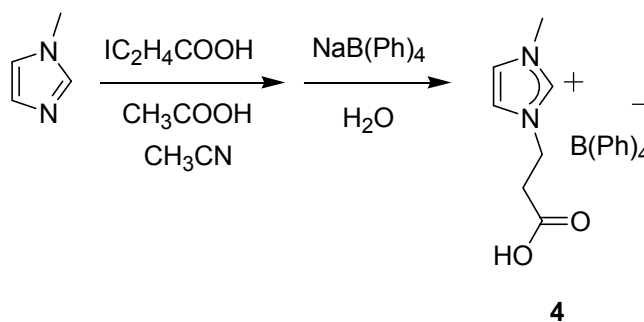


Figure 4-5 Imidazolium  $^1\text{H}$  NMR resonances in the synthesis of cationic **4.4** with  $[\text{I}^-]$  and zwitterion (a) and  $[\text{BPh}_4^-]$  (b)



The oil also contained acetic acid as indicated by  $^1\text{H}$  NMR that remained after stirring in THF. The oil was mixed with sodium tetraphenylborate in water to afford the single product imidazolium salt **4.4** (Scheme 4-2).



Scheme 4-2 Imidazolium carboxylic acid salt derivative **4.4**

The presence of the acidic proton was confirmed by the  $^1\text{H}$  NMR spectrum where the resonance was observed at 12.68 ppm. A carbonyl resonance was also observed in the  $^{13}\text{C}$  NMR spectrum at 172.7 ppm. The imidazolium cationic proton resonance was observed in the  $^1\text{H}$  NMR spectrum as well at 9.06 ppm (Figure 4-5b). The corresponding carbon resonance was observed at 137.5 ppm in the  $^{13}\text{C}$  NMR spectra. Crystals suitable for X-ray diffraction were grown from a concentrated solution of acetonitrile. The crystal structure is shown in Figure 4-6.

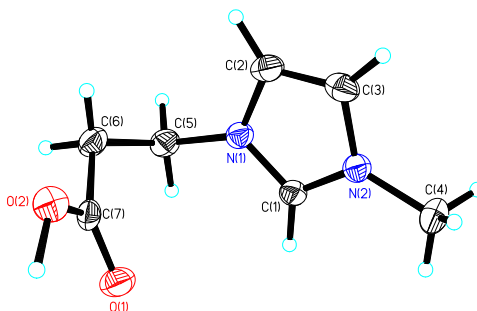
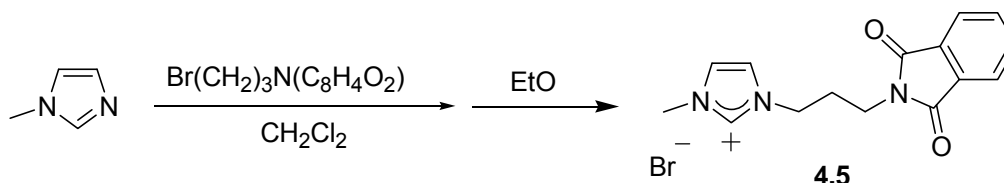


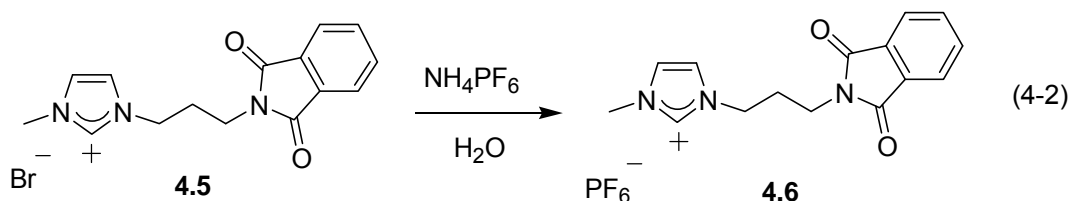
Figure 4-6 Thermal ellipsoid plot of cationic portion of **4.4** shown at 50% probability

A phthalimide derivative was generated by mixing methylimidazole and 3-bromopropylphthalimide in dichloromethane at room temperature overnight. Upon stirring in diethyl ether for 24 hours, the imidazolium bromide salt **4.5** was afforded (Scheme 4-3).



Scheme 4-3 Imidazolium bromide phthalimide derivative **4.5**

The  $^1\text{H}$  NMR spectrum showed the imidazolium proton resonance at 9.09 ppm. The  $^{13}\text{C}$  NMR spectra also showed the corresponding imidazolium carbon resonance at 136.7 ppm. Several attempts were made to crystallize **5** but no suitable crystals formed. An anion exchange of **5** with ammonium hexafluorophosphate in water yielded the imidazolium  $\text{PF}_6$  salt **6** (eq. 4-2). Crystals suitable for X-ray diffraction were grown from a concentrated solution of acetonitrile. The crystal structure is shown in Figure 4-7.



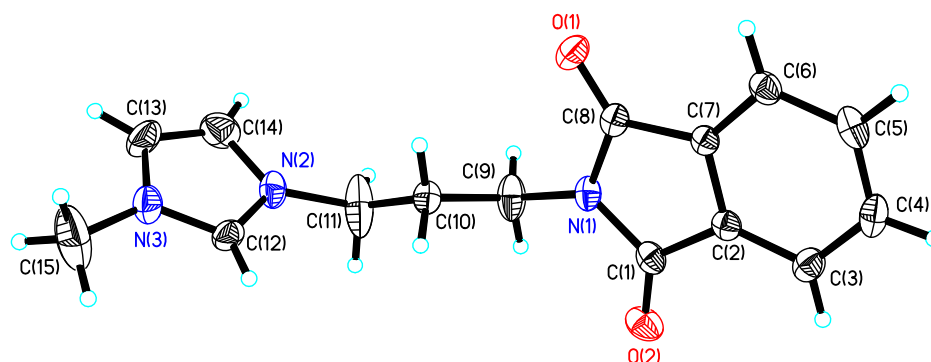


Figure 4-7 Thermal ellipsoid plot of cationic portion of **4.6** shown at 50% probability

### 4.3 Antimicrobial Properties of Imidazolium Salts

The antimicrobial properties of the synthesized imidazolium salts were evaluated using two standard microbiological tests. The activity of the imidazolium salts were compared against imidazole and literature values.

#### 4.3.1 Minimum Inhibitory Concentration

The antimicrobial properties of imidazolium salts **4.1-4.5** along with salts **4.7-4.13** (Figure 4-8) were evaluated for their effectiveness by determining the minimum inhibitory concentration (MIC) against laboratory strains of test organisms *Escherichia coli*, *Staphylococcus aureus*, and *Pseudomonas aeruginosa* using imidazole as a control.

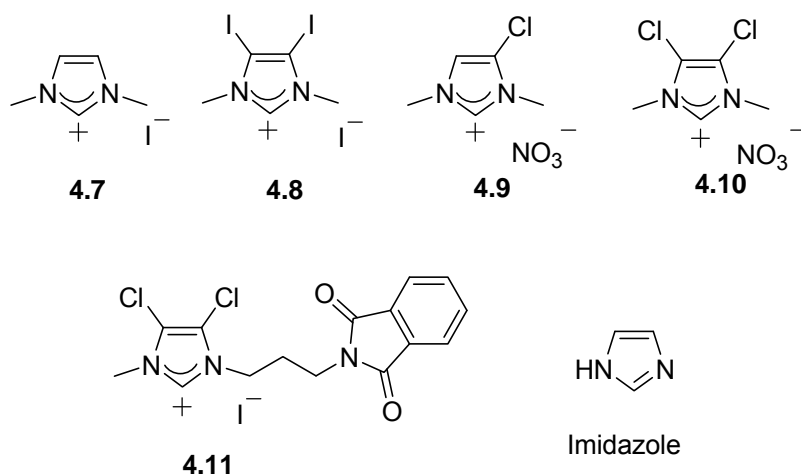


Figure 4-8 Imidazole and various imidazolium salts

The MIC, a standard microbiological test, has been used to determine the bacteriostatic activity of antimicrobial agents. The lower the MIC value, the more effective the compound will be as an antimicrobial agent. The MIC was determined visually by the turbidity of solution. Results for the MIC have been collected in Table 4-1.

Table 4-1 MIC values of imidazole, **4.1-4.5** and **4.7-4.11** in mmol/L L ( $\pm 0.3$ )

Compound	<i>E. coli</i>	<i>S. aureus</i>	<i>P. aeruginosa</i>
<b>4.1</b>	260	>260	85.8
<b>4.2</b>	232	>232	232
<b>4.3</b>	149	>450	>450
<b>4.4</b>	21.1	21.1	21.1
<b>4.5</b>	22.8	69.0	69.0
<b>4.7</b>	90.7	90.7	90.7
<b>4.8</b>	257 <sup>a</sup>	257 <sup>a</sup>	257 <sup>a</sup>
<b>4.9</b>	28.3	28.3	28.3
<b>4.10</b>	28.7	86.9	86.9
<b>4.11</b>	32.9	99.8	32.9
Imidazole	259	259	259

<sup>a</sup> Compound was only marginally soluble in LB Broth

Of the imidazolium salts tested, the carboxylic acid derivative **4.4** demonstrated the most activity against all microorganisms evaluated. An explanation of the improved bacteriostatic activity of **4.4** could be attributed to the fact that QACs target bacteria cell membranes by ionic interaction, thereby the possibility of multiple interaction sites would exist.

Among the dimethyl group types, the monochloro derivative **4.9** displayed the most effective activity and with values close to **4.4**. The observed activity trend was **4.9** > **4.10** > **4.7** > **4.8** (Figure 4-9). It should be mentioned that the diiodo derivate **4.8** displayed extremely low solubility in the LB Broth solution.

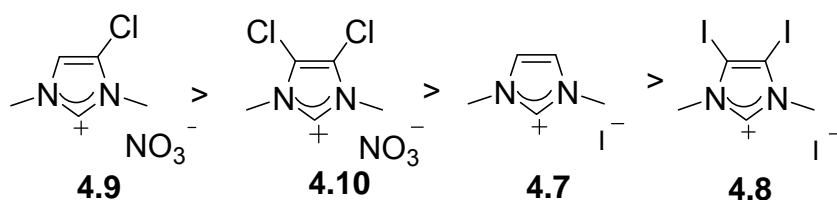


Figure 4-9 Antimicrobial activity of the dimethyl imidazolium series

The phthalimide derivatives differed structurally by the presence of two chloro groups. Dichloro derivative **4.11** was superior to dihydro derivative **4.5** only against *P. aeruginosa*. This finding was surprising because it did not follow the trend observed in the dimethyl series.

The hydroxy imidazolium derivative series **4.1-4.3** displayed virtually no antimicrobial activity. Each of these salts had high values indicating that the presence of hydroxy groups reduces antimicrobial activity in comparison to alkyl or carboxylic acid groups of similar chain length. Imidazole also showed high values, which were expected due to the absence of any nitrogen substituents.

Based on the above results, the bacteriostatic activity of imidazolium salts was greatly enhanced by the presence of a carboxylate group as a nitrogen substituent. The activity was also enhanced by the presence of a chloro group on the 4- and or 5-position of the imidazole ring but a decrease in effectiveness was seen when the nitrogen substituent contained a phthalimide group. Although different bacterial strains were used in comparison with published literature studies cited in section 4.1, it was evident that the above substituents demonstrated reduced activity. Average MIC values reported were between 0.02-0.09 mmol/L, indicating effectiveness at much lower molar concentrations than most active salt **4.4**, at 21.1 mmol/L.<sup>110,111</sup>

#### 4.3.2 Minimum Bactericidal Concentration

A sample from each no growth (clear) MIC tube tested from above was taken and evaluated for the minimum bactericidal concentration (MBC). The MBC determines the lowest concentration of antimicrobial that will prevent the growth of an organism. MBC differs from the MIC by providing evidence that an antimicrobial actually prevents organism growth by killing microorganisms (MBC) rather than merely inhibiting growth (MIC). Results for the MBC are reported in Table 4-2.

Table 4-2 MBC values of imidazole, **4.1-4.5** and **4.7-4.11** in mmol/ L ( $\pm 0.3$ )

Compound	<i>E. coli</i>	<i>S. aureus</i>	<i>P. aeruginosa</i>
<b>4.1</b>	>260	NA	85.8
<b>4.2</b>	>232	NA	>232
<b>4.3</b>	>149	NA	NA
<b>4.4</b>	>21.1	>21.1	>21.1
<b>4.5</b>	22.8	>69.0	>69.0
<b>4.7</b>	>90.7	90.7	>90.7
<b>4.8</b>	>257 <sup>a</sup>	>257 <sup>a</sup>	>257 <sup>a</sup>
<b>4.9</b>	>28.3	>28.3	>28.3
<b>4.10</b>	>28.7	>86.9	>86.9
<b>4.11</b>	>32.9	>99.8	>32.9
Imidazole	259	259	259

<sup>a</sup> Compound was only marginally soluble in LB Broth

The MBC was assessed by the prevention of microorganism colony growth. The MBC values reported reflected molar concentrations that supported no colony growth. Virtually none of the imidazolium salts that had low MIC values showed any bactericidal activity, indicating that they only inhibited growth. The only exception was the phthalimide imidazolium derivative **4.5** against *E. coli* that prevented growth at a concentration of 22.8 mmol/L. The dihydroxy derivative **4.1** was bactericidal against *P. aeruginosa* but only at the higher concentration of 85.8 mmol/L. Dimethyl derivative **4.7** prevented growth of *S. aureus* also at a higher concentration of 90.7 mmol/L.

Based on the above results, the substituents herein possessed only bacteriostatic properties. The molar concentrations were higher than the bactericidal values reported in the literature for long alkyl chain imidazolium salt derivatives.<sup>110</sup>

#### 4.4 Conclusion

Imidazolium salts with different substituents at the 1-, 3-, 4- and or 5-positions of the imidazole ring were synthesized. Imidazolium salts were evaluated for antimicrobial activity. A salt bearing a carboxylic acid at the 1-position of the imidazole ring showed the greatest bacteriostatic activity. Also, salts containing chlorides at the 4- and or 5- position(s) of the imidazole had positive results in comparison. However, all salts tested were not as active as reported imidazolium salt systems bearing long alkyl chain variations on at least one of the nitrogen atoms of the imidazole ring.

#### 4.5 Experimental Section

The general considerations and X-ray information have been explained below. The experimental procedures for compounds **4.1-4.6** have been compiled in this section.

##### 4.5.1 General Considerations

All reactions were carried out under aerobic conditions. The reagents methylimidazole, 3-bromo,1,2-propanediol and 3-iodopropionic acid were purchased from Acros Organics. Iodomethane, iodoethanol, sodium tetraphenylborate, ammonium hexafluorophosphate and *N*-(3-bromopropyl)phthalimide were purchased from Alfa Aesar. 2-Hydroxyethylimidazole was purchased from Oakwood Products Incorporated. Acetic acid and imidazole were purchased from Fisher Scientific. All chemicals



were used as received. Imidazolium iodide salt **4.7** was prepared using a modified literature procedure as described in 3.5.3.<sup>104</sup> Imidazolium salt **4.8** was provided by Dr. Doug Medvetz.<sup>113</sup> Imidazolium salts **4.9** and **4.10** were prepared as outlined in sections 2.7.6 and 2.7.4, respectively. Imidazolium salt **4.11** was prepared as outlined in section 3.5.6. LB Broth Miller (DIFCO) and Bacto-agar (DIFCO) were prepared according to manufacturer's instruction and sterilized before use. All solvents were purchased from Fisher Scientific and used as received. <sup>1</sup>H and <sup>13</sup>C NMR data were collected on a Varian Gemini 300 MHz instrument and referenced to the residual protons of the deuterated solvents and the solvent resonances, respectively. Mass spectrometric analysis was performed at the mass spectrometry facility at The University of Akron.

#### 4.5.2 X-Ray Crystallographic Structure Determination Details

The crystal structure of **4.1** was solved by Dr. Matthew Panzner. The crystal structures of **4.4** and **4.6** were solved by Dr. Semih Durmus. Crystals of **4.1**, **4.4** and **4.6** were coated in paraffin oil and mounted on a CryoLoop™ and placed on the goniometer head under a stream of nitrogen cooled to 100K. The data was collected on a Bruker APEX CCD diffractometer with graphite-monochromated Mo K<sub>α</sub> radiation ( $\lambda = 0.71073 \text{ \AA}$ ). The unit cell was determined by using reflections from three different orientations. The data was integrated using SAINT.<sup>105</sup> An empirical absorption correction and other corrections were applied to the data using multi-scan SADABS.<sup>105</sup> Structure solution, refinement, and modeling were accomplished by using the Bruker SHELXTL package.<sup>106</sup> The structure was determined by full-matrix least-squares refinement of  $F^2$  and the

selection of the appropriate atoms from the generated difference map. Hydrogen atom positions were calculated and  $U_{\text{iso}}(\text{H})$  values were fixed according to a riding model.

#### 4.5.3 Synthesis of **4.1** ( $\text{C}_6\text{H}_{11}\text{N}_2\text{OI}$ )

Methylimidazole (0.99 g, 12 mmol) was placed in a 100 mL round bottom flask. Iodoethanol (2.06 g, 12.0 mmol) was added dropwise and the mixture was refluxed at 53°C overnight. The white solid **4.1** was collected. Yield: 3.01 g, 11.8 mmol, 99.0%. Mp: 22.0°C.  $^1\text{H}$  NMR (300 MHz,  $\text{DMSO}-d_6$ ):  $\delta$  9.10 (s, 1H, NCHN), 7.74 (s, 1H, CH), 7.71 (s, 1H, CH), 5.11 (t, 1H, OH), 4.21 (t, 2H,  $\text{CH}_2$ ), 3.87 (s, 3H,  $\text{CH}_3$ ), 3.71 (q, 2H,  $\text{CH}_2$ ).  $^{13}\text{C}$  NMR (75 MHz,  $\text{DMSO}-d_6$ ):  $\delta$  136.7 (s, NCN), 123.3 (C=C), 122.6 (s, C=C), 59.2 (s, C-O), 51.6 (s, N-C), 38.8 (s,  $\text{CH}_3$ ). FT IR (nujol solution,  $\text{cm}^{-1}$ ): 3357, 1166, 1074, 722. ESI-MS ( $m/z$ ): Calcd for  $\text{C}_5\text{H}_9\text{N}_2$  [ $\text{M}-\text{I}$ ] $^+$ : 127.17, found 127.0.

X-ray crystal structure analysis of **4.1**: formula  $\text{C}_6\text{H}_{11}\text{N}_2\text{OI}$ ,  $MW = 254.07$ , colorless crystal  $0.35 \times 0.12 \times 0.10 \text{ mm}^3$ ,  $a = 7.5518(11) \text{ \AA}$ ,  $b = 7.2999(11) \text{ \AA}$ ,  $c = 8.6033(13) \text{ \AA}$ ,  $\alpha = 90.^\circ$ ,  $\beta = 106.635(2)^\circ$ ,  $\gamma = 90.^\circ$ ,  $V = 454.43(12) \text{ \AA}^3$ ,  $D_{\text{calc}} = 1.849 \text{ Mg m}^{-3}$ ,  $\mu = 3.467 \text{ mm}^{-1}$ ,  $Z = 2$ , monoclinic, space group  $\text{P2}(1)$ ,  $\lambda = 0.71073 \text{ \AA}$ ,  $T = 100 \text{ K}$ ,  $\omega$  and  $\varphi$  scans, 4006 reflections collected, 2022 independent ( $R_{\text{int}} = 0.0244$ ), 93 refined parameters,  $R1/wR2$  ( $I \geq 2\sigma(1)$ ) = 0.0277/0.0663 and  $R1/wR2$  (all data) = 0.0286/0.0669, maximum (minimum) residual electron density 1.387 ( $-1.042$ )  $\text{e/\AA}^3$ .

#### 4.5.4 Synthesis of **4.2** (C<sub>7</sub>H<sub>13</sub>N<sub>2</sub>O<sub>2</sub>I)

A 100 mL round bottom flask was charged with 2-hydroxyethylimidazole (1.09 g, 9.70 mmol). Iodoethanol (1.68 g, 9.73 mmol) was added and the mixture was refluxed at 55°C overnight to yield yellow ionic liquid **4.2**. Yield: 2.74 g, 9.63 mmol, 99.3%. <sup>1</sup>H NMR (300 MHz, DMSO-*d*<sub>6</sub>): δ 9.12 (s, 1H, NCHN), 7.75 (s, 2H, CH), 5.12 (s, 2H, OH), 4.23 (t, 4H, CH<sub>2</sub>), 3.73 (t, 4H, CH<sub>2</sub>). <sup>13</sup>C NMR (75 MHz, DMSO-*d*<sub>6</sub>): δ 136.5 (s, NCN), 122.5 (C=C), 59.3 (s, C-O), 51.6 (s, N-C). FT IR (nujol solution, cm<sup>-1</sup>): 3360, 3139, 3095, 1563, 1158, 1066, 872, 750. ESI-MS (*m/z*): Calcd for C<sub>7</sub>H<sub>13</sub>N<sub>2</sub>O<sub>2</sub> [M-I]<sup>+</sup>: 157.10, found 157.0.

#### 4.5.5 Synthesis of **4.3** (C<sub>8</sub>H<sub>15</sub>N<sub>2</sub>O<sub>3</sub>Br)

A 50 mL round bottom flask was charged with 3-bromo,1,2-propanediol (2.43 g, 15.7 mmol). 2-Hydroxyethylimidazole (0.93 g, 8.3 mmol) was added and the mixture was refluxed at 69°C overnight. Diethyl ether (20 mL) was added to the flask and allowed to stir for 2 days. The filtrate was decanted and the flask was dried *in vacuo* for 2 hours to yield semi-solid **4.3**. Yield: 1.52 g, 5.71 mmol, 68.7%. <sup>1</sup>H NMR (300 MHz, DMSO-*d*<sub>6</sub>): δ 9.10 (s, 1H, NCHN), 7.75 (s, 1H, CH), 7.71 (s, 1H, CH), 5.31 (d, 1H, OH), 5.16 (t, 1H, OH), 4.94 (s, 1H, OH), 4.35 (d, 2H, CH<sub>2</sub>), 4.30 (d, 2H, CH<sub>2</sub>), 4.23 (t, 2H, CH<sub>2</sub>), 4.10 (m, 2H, CH<sub>2</sub>), 3.73 (m, 1H, CHOH). <sup>13</sup>C NMR (75 MHz, DMSO-*d*<sub>6</sub>): δ 136.8 (s, NCN), 123.1 (C=C), 122.4 (s, C=C), 69.7 (s, C-O), 62.7 (s, C-O), 59.2 (s, C-O), 52.1 (s, N-C), 51.6 (s, CH<sub>3</sub>). FT IR (nujol solution, cm<sup>-1</sup>): 3345, 3105, 2360, 1165, 1061, 939, 872, 752. ESI-MS (*m/z*): Calcd for C<sub>8</sub>H<sub>15</sub>N<sub>2</sub>O<sub>3</sub>[M-Br]<sup>+</sup>: 187.22, found 187.11.

#### 4.5.6 Synthesis of **4.4** (C<sub>31</sub>H<sub>31</sub>N<sub>2</sub>O<sub>2</sub>B)

Methylimidazole (0.89 g, 10 mmol) was placed in a 250 mL round bottom flask with acetonitrile (50 mL). Iodopropanoic acid (0.21 g, 10 mmol) and acetic acid (4 drops) was added to the flask. The mixture was refluxed overnight and additional acetic acid (5 drops) was added. The mixture was refluxed for 24 hours and volatiles were removed under vacuum to yield an ionic liquid. The ionic liquid was stirred in THF for 2 hours and the volatiles were removed under vacuum. The ionic liquid was placed in a 125 mL flask with water (25 mL) and added to a 250 mL flask containing sodium tetraphenylborate (1.07 g, 3.13 mmol) and water (50 mL) while stirring. The mixture was stirred for 30 minutes and the precipitate was filtered and dried to yield white solid **4.4**. Yield: 0.79 g, 1.7 mmol, 53%). Mp: 194-196°C. <sup>1</sup>H NMR (300 MHz, DMSO-*d*<sub>6</sub>): δ 12.68 (s, 1H, COOH), 9.06 (s, 1H, NCHN), 7.73 (s, 1H, CH), 7.64 (s, 1H, CH), 7.19 (s, 4H, CH), 6.94 (t, 8H, CH), 6.80 (t, 8H, CH), 4.33 (t, 2H, CH<sub>2</sub>), 3.81 (s, 3H, CH<sub>3</sub>), 2.89 (t, 2H, CH<sub>2</sub>). <sup>13</sup>C NMR (75 MHz, DMSO-*d*<sub>6</sub>): δ 172.7 (s, C=O), 165.0 (s, C-B), 164.4 (s, C-B), 163.7 (s, C-B), 163.0 (s, C-B), 137.5 (s, NCN), 136.2 (s, C=C), 134.7 (s, C=C), 128.0 (s, C=C), 126.0 (d, C=C), 124.0 (s, C=C), 123.0 (s, C=C), 122.3 (s, C=C), 45.7 (s, CH<sub>2</sub>), 36.3 (s, CH<sub>2</sub>), 35.0 (s, CH<sub>3</sub>). ESI-MS (*m/z*): Calcd for C<sub>7</sub>H<sub>11</sub>N<sub>2</sub>O<sub>2</sub> [M-B(Ph)<sub>4</sub>]<sup>+</sup>: 155.18, found 155.0.

X-ray crystal structure analysis of **4.4**: formula C<sub>31</sub>H<sub>31</sub>N<sub>2</sub>O<sub>2</sub>B, *MW* = 474.39, colorless crystal 0.43 x 0.17 x 0.05 mm<sup>3</sup>, *a* = 9.2523(10) Å, *b* = 9.2082(10) Å, *c* = 30.191(3) Å, α = 90.°, β = 98.149(2)°, γ = 90.°, *V* = 2546.2(5) Å<sup>3</sup>, *D*<sub>calc</sub> = 1.238 Mg m<sup>-3</sup>, μ = 0.076 mm<sup>-1</sup>, *Z* = 4, monoclinic, space group P2(1)/n,

$\lambda = 0.71073 \text{ \AA}$ ,  $T = 100 \text{ K}$ ,  $\omega$  and  $\varphi$  scans, 22051 reflections collected, 6111 independent ( $R_{\text{int}} = 0.0925$ ), 449 refined parameters,  $R1/wR2$  ( $I \geq 2\sigma(1)$ ) = 0.0598/0.1019 and  $R1/wR2$  (all data) = 0.1006/0.1147, maximum (minimum) residual electron density 0.265 (-0.223)  $\text{e/\AA}^3$ .

#### 4.5.7 Synthesis of **4.5** ( $\text{C}_{15}\text{H}_{16}\text{N}_3\text{O}_2\text{Br}$ )

A flask was charged with 3-bromopropylphthalimide (4.71 g, 17.6 mmol) and dichloromethane (50 mL). Methylimidazole (1.44 g, 17.6 mmol) was added to the flask and the mixture was stirred at room temperature for 24 hours. The volatiles were removed under vacuum and the resulting solid was washed two times with diethyl ether (10 mL) and allowed to stir for 24 hours on the third addition. The mixture was filtered and dried to yield white solid **4.5**. Yield: 5.40 g, 15.4 mmol, 87.8%. Mp:  $198^\circ\text{C}$ .  $^1\text{H}$  NMR (300 MHz,  $\text{DMSO-}d_6$ ):  $\delta$  9.09 (s, 1H, NCHN), 7.88 (s, 2H, CH), 7.87 (s, 2H, CH), 7.78 (s, 1H, CH), 7.71 (s, 1H, CH), 4.23 (t, 2H,  $\text{CH}_2$ ), 3.84 (s, 3H,  $\text{CH}_3$ ), 3.62 (t, 2H,  $\text{CH}_2$ ), 2.15 (t, 2H,  $\text{CH}_2$ ).  $^{13}\text{C}$  NMR (75 MHz,  $\text{DMSO-}d_6$ ):  $\delta$  168.1 (C=O), 136.7 (s, NCN), 134.4 (s, C=C), 131.8 (s, C=C), 123.6 (s, C=C), 123.1 (s, C=C), 122.3 (s, C=C), 46.5 (s, C-N), 35.8 (s, C-N), 34.4 (s, C-N), 28.7 (s, C-C). ESI-MS ( $m/z$ ): Calcd for  $\text{C}_{15}\text{H}_{16}\text{N}_3\text{O}_2$   $[\text{M-Br}]^+$ : 270.31, found 269.9.

#### 4.5.8 Synthesis of **4.6** ( $\text{C}_{15}\text{H}_{16}\text{N}_3\text{O}_2\text{PF}_6$ )

The imidazolium salt **4.5** (1.54 g, 4.40 mmol) was dissolved in water (25 mL). Ammonium hexafluorophosphate was added until a white solid could be

seen. The precipitate was washed with water (10 mL) three times and dried to yield white solid **4.6**.

X-ray crystal structure analysis of **4.6**: formula  $C_{15}H_{16}N_3O_2PF_6$ ,  $MW = 415.27$ , colorless crystal  $0.41 \times 0.26 \times 0.05 \text{ mm}^3$ ,  $a = 8.1750(19) \text{ \AA}$ ,  $b = 12.680(3) \text{ \AA}$ ,  $c = 32.223(7) \text{ \AA}$ ,  $\alpha = 90.^\circ$ ,  $\beta = 90.^\circ$ ,  $\gamma = 90.^\circ$ ,  $V = 3340.2(13) \text{ \AA}^3$ ,  $D_{\text{calc}} = 1.652 \text{ Mg m}^{-3}$ ,  $\mu = 0.246 \text{ mm}^{-1}$ ,  $Z = 8$ , orthorhombic, space group  $Pbca$ ,  $\lambda = 0.71073 \text{ \AA}$ ,  $T = 100 \text{ K}$ ,  $\omega$  and  $\varphi$  scans, 27461 reflections collected, 4099 independent ( $R_{\text{int}} = 0.0765$ ), 297 refined parameters,  $R1/wR2$  ( $I \geq 2\sigma(1)$ ) = 0.0553/0.1338 and  $R1/wR2$  (all data) = 0.0947/0.1491, maximum (minimum) residual electron density 0.400 (-0.351)  $\text{e/\AA}^3$ .

#### 4.5.9 Antimicrobial Testing

Sterilized LB Broth was measured (5 mL) into a sterile culture tube. A constant volume of suspension culture of microorganisms (one sterilized loop), was added to the tube containing the LB Broth. The mixture was cultured overnight at  $37^\circ\text{C}$  in a shaking incubator. An initial solution of each compound in LB Broth (5 mL) was prepared. An initial solution of **11** was prepared in LB Broth (8 mL). A series of serial dilutions was performed by transferring 1mL of the initial solution into a sterile tube containing LB Broth (2 mL) marked D1. An aliquot of 1 mL of well mixed solution D1 was transferred to a second sterile tube containing LB Broth (2 mL) marked D2. The same process was repeated for D3-D6, with D6 containing an initial LB Broth volume of 1mL. Each tube was inoculated with microorganism suspension (25  $\mu\text{L}$ ).

#### 4.5.10 Determination of MIC

Growth/no growth of microorganisms was visually evaluated after incubation for 24h at 37°C in a shaking incubator. The lowest concentration with no visible growth (turbidity) was taken as the MIC.

#### 4.5.11 Determination of MBC

One sterilized loop from determined MIC clear (no growth) tube was cultured on an agar plate and incubated for 24h at 37°C. The concentration of each compound supporting no colony formation was taken as the MBC.

## CHAPTER V

### COMPARISON OF THE ANTIMICROBIAL ACTIVITY OF SILVER DRESSINGS USING MIC, MBC AND KIRBY BAUER METHODS

#### 5.1 Introduction

Silver has been used as a medicinal agent for thousands of years. Currently, much of the use of medicinal silver agents has been in the area of wound care. In the 1960's, a standard 0.5% silver nitrate solution was used in wound management with several drawbacks.<sup>114</sup> Silver nitrate caused discoloration of the wound bed and irritation and it induces hyponatremia or hypochloremia.<sup>115</sup> A 1% silver sulfadiazine cream emerged in 1968 as a topical treatment for wound infections (Figure 5-1).

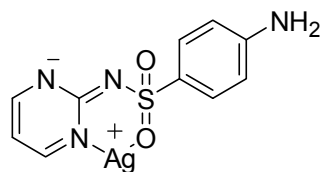


Figure 5-1 Silver sulfadiazine

Despite its wide use, silver sulfadiazine also caused discoloration of the wound bed and sulfonamides have been reported to act as allergens.<sup>115</sup> Cases of bacterial resistance to both treatment options has been reported.<sup>116</sup> Our group



has been at the forefront of developing new forms of silver-containing compounds exhibiting antimicrobial properties.<sup>93,94,95,96,96</sup>

There have been a multitude of silver-coated and silver impregnated dressings introduced in recent years. Studies have been conducted comparing various silver-containing dressings using assorted techniques.<sup>117, 118, 119, 120, 121</sup>

Antimicrobial activity of five such dressings has been noted by the reduction of bacteria over a 24 hour period.<sup>122</sup>

The first goal of this research was to determine a zone of bacterial inhibition for eight such commercially available silver dressings, providing a direct correlation for topical use. The second goal was to compare the initial and any continued activity of silver dressings by using minimum inhibitory concentration (MIC) and minimum bactericidal concentration (MBC) methods with multiple microorganism inoculations, indicating the sustained effect and plausible extended release of silver. The dressings were tested against laboratory strains of test organisms *Escherichia coli*, *Staphylococcus aureus*, and *Pseudomonas aeruginosa*.

## 5.2 Description of Silver Dressings

Antimicrobial evaluation was performed on eight commercial silver-containing dressings from five different manufactures. The form and amount of silver contained within each dressing were varied. The dressings comprised of different matrices, for example foam or hydrocolloids. The properties of each dressing have been compiled in Table 5-1.

Table 5-1 Properties of the evaluated eight commercially available dressings

Dressing (Manufacturer)	Matrix	Silver Content	Website
Acticoat (Smith and Nephew)	Polyethylene net	Nanocrystalline/ Coated	<a href="http://www.global.smith-nephew.com">http://www.global.smith-nephew.com</a>
Aquacel Ag (ConvaTec)	Hydrofiber®	Ionic/Impregnated 116.5 µg/cm <sup>2</sup>	<a href="http://www.convatec.com">http://www.convatec.com</a>
Contreet (Coloplast)	Foam	Ionic/Impregnated 926 µg/cm <sup>2</sup>	<a href="http://www.woundcare.coloplast.com">http://www.woundcare.coloplast.com</a>
Contreet HC (Coloplast)	Hydrocolloid	Ionic/Impregnated 280 µg/cm <sup>2</sup>	<a href="http://www.woundcare.coloplast.com">http://www.woundcare.coloplast.com</a>
PolyMem Silver (Ferris)	Quadra Foam	Ionic/Impregnated 124 µg/cm <sup>2</sup>	<a href="http://www.polymem.com">http://www.polymem.com</a>
Promogran Prisma (Johnson & Johnson Gateway)	Cellulose and Collagen	Ionic/Impregnated 0.25%	<a href="http://www.jnigateway.com">http://www.jnigateway.com</a>
SeaSorb Ag (Coloplast)	Alginate	Ionic/Impregnated 280 µg/cm <sup>2</sup>	<a href="http://www.woundcare.coloplast.com">http://www.woundcare.coloplast.com</a>
Silvercel (Johnson & Johnson Gateway)	Alginate	Elemental/Coated 8%	<a href="http://www.jnigateway.com">http://www.jnigateway.com</a>

### 5.3 Kirby Bauer Disc Diffusion Method

The Kirby Bauer disc diffusion method was used to determine the zone of inhibition for each silver dressing against laboratory strains of microorganisms *Escherichia coli*, *Staphylococcus aureus*, and *Pseudomonas aeruginosa* using a 0.5% silver nitrate solution as a control. This test was chosen for its direct correlation with topical dressing treatment. Dressings demonstrating a wider zone of inhibition would be more desirable for preventing infection around the

wound bed. Dressings were cut into 7.9 mm circles and placed in the center of an organism-inoculated agar plate. The plates were incubated at 37°C overnight and the zone of inhibition was measured. Results of the Kirby Bauer test were compiled in Table 5-2.

Table 5-2 Zone of Inhibition (cm)

Dressing	<i>P. aeruginosa</i>	<i>S. aureus</i>	<i>E. coli</i>
Acticoat	0.50	0.30	0.25
Aquacel Ag	0.50	0.40	0.20
Contreet	0.35	0.20	0.20
Contreet HC	0.60	0.50	0.30
Polymem Ag	No Value <sup>a</sup>	0.20	No Value <sup>a</sup>
Prisma	0.50	0.40	0.50
Seasorb Ag	0.30	0.30	0.30
Silvercel	0.50	0.25	0.10
0.5% AgNO <sub>3</sub> (aq)	0.50	0.50	0.40

<sup>a</sup> no measurable zone of inhibition

For *P. aeruginosa*, Contreet HC had the best zone of inhibition with 0.60 cm. Prisma, Aquacel Ag, Silvercel, Acticoat and AgNO<sub>3</sub> all had zones of inhibition measuring 0.50 cm. Contreet had a zone of inhibition of 0.35 cm while Seasorb Ag measured 0.30 cm. Polymem Silver showed no measurable zones of inhibition. For *S. aureus*, both Contreet HC and AgNO<sub>3</sub> displayed the best zones of inhibition with 0.50 cm. Prisma and Aquacel Ag each had a zone of inhibition of 0.40 cm. Seasorb Ag and Acticoat both measured zones of inhibition of 0.30 cm. Contreet, Polymem Silver, and Silvercel all had zones of inhibition less than 0.30 cm with 0.20 cm, 0.20 cm and 0.25 cm respectively. For *E. coli*, Prisma was the most effective with a zone of inhibition of 0.50 cm. AgNO<sub>3</sub> measured a zone of 0.40 cm followed by Seasorb Ag and Contreet HC all measuring 0.30 cm.

Acticoat, Contreet and Aquacel Ag all measured less than 0.30 cm at 0.25 cm, 0.20 cm and 0.20 cm respectively. Polymem Silver showed no measurable zone of inhibition.

Aquacel Ag and Silvercel were tested against different strains of the same bacteria used above in a previously published study. Inhibition zones reported were approximately 3 times larger.<sup>120</sup>

Based on the above results, Prisma had higher zones of inhibition the most consistently across the three types of microorganisms tested, indicating effectiveness for topical applications of bacteria inhibition. Contreet HC displayed large inhibition zones but only against *S. aureus* and *P. aeruginosa* and showed only a moderate zone for *E. coli*.

#### 5.4 MIC Method Evaluation

The antimicrobial properties of each silver dressing were evaluated for their effectiveness by determining the minimum inhibitory concentration (MIC) against laboratory strains of test organisms *Escherichia coli*, *Staphylococcus aureus*, and *Pseudomonas aeruginosa*. The MIC, a standard microbiological test, has been used to determine the bacteriostatic activity of antimicrobial agents. The lower the MIC, the more effective the dressing will be as an antimicrobial agent. Each dressing was cut into four different dimensions decreasing in size from D1-D4, as to mimic serial dilution, and placed into a sterilized culture tube containing sterilized LB Broth. Each tube was inoculated with microorganism suspension and incubated overnight in a shaking incubator at 37°C. Results for MIC are reported in Table 5-3.

Table 5-3 MIC results for silver dressings (+) turbidity or (-) no turbidity

Dressing	initial organism inoculation											
	P. aeruginosa				S. aureus				E.coli			
	D1	D2	D3	D4	D1	D2	D3	D4	D1	D2	D3	D4
Acticoat	-	-	-	-	-	-	-	-	-	-	-	-
Aquacel Ag	-	-	-	-	-	-	-	-	-	-	-	-
Contreet	-	-	-	-	-	-	-	+	-	-	+	+
Contreet HC	+	+	+	+	+	+	+	+	+	+	+	+
Polymem Silver	-	-	+	+	-	-	+	+	-	-	+	+
Prisma	-	-	-	-	-	-	-	-	-	-	-	-
Seasorb Ag	-	-	-	+	-	-	+	+	-	-	-	+
Silvercel	-	-	-	-	-	-	-	-	-	-	-	-
0.5% AgNO <sub>3</sub> (aq)	-	-	-	-	-	-	-	-	-	-	-	-

The MIC was obtained by visual inspection of the turbidity of solution.

Contreet HC showed turbidity across the board for all microorganism strains, so no MIC could be determined from the dimensions tested. Polymem Silver and Seasorb Ag showed very little effectiveness against *P. aeruginosa* and had low efficacy against *S. aureus* and *E. coli* along with Contreet. Prisma, Aquacel Ag, Silvercel, Acticoat and silver nitrate showed no turbidity for each microorganism type and no MIC was reached for the dimension at the volume of microorganism suspension tested. Contreet showed no turbidity only against *P. aeruginosa* so no MIC was reached.

Only tubes where turbidity was not observed and MIC was not reached, were subjected to an addition of microorganism suspension after a period of 20 days to evaluate any prolonged activity. Inoculated samples were incubated overnight in a shaking incubator at 37°C and checked for turbidity. Results for MIC have been reported in Table 5-4.

Table 5-4 MIC results for silver dressings (+) turbidity or (-) no turbidity

Dressing	1st organism addition											
	P. aeruginosa				S. aureus				E.coli			
	D1	D2	D3	D4	D1	D2	D3	D4	D1	D2	D3	D4
Acticoat	-	-	-	+	-	-	-	+	-	-	-	-
Aquacel Ag	-	-	-	-	-	-	-	-	-	-	-	-
Contreet	-	-	-	+								
Prisma	-	-	-	-	-	-	-	+	-	-	-	-
Silvercel	-	-	-	-	-	-	+	+	-	-	-	-
0.5% AgNO <sub>3</sub> (aq)	-	-	-	+	-	-	-	+	-	-	-	+

Contreet displayed turbidity against *P. aeruginosa*, whereas Prisma and Silvercel showed turbidity only against *S. aureus*. Acticoat displayed turbidity against *P. aeruginosa* and *S. aureus* only, while silver nitrate had turbidity across the board. Aquacel Ag showed no signs of turbidity after the organism addition, indicating prolonged antimicrobial effectiveness.

Only tubes where turbidity was not observed were subjected to a second addition of microorganism suspension after a two day period, to evaluate any further extended activity. The samples were incubated overnight in a shaking incubator at 37°C and checked for turbidity. Results for the MIC are reported in Table 5-5.

Table 5-5 MIC results for silver dressings (+) turbidity or (-) no turbidity

Dressing	2nd organism addition											
	P. aeruginosa				S. aureus				E.coli			
	D1	D2	D3	D4	D1	D2	D3	D4	D1	D2	D3	D4
Acticoat									-	-	+	+
Aquacel Ag	-	-	-	+	-	-	-	+	-	-	-	+
Prisma	-	+	+	+					-	-	+	+
Silvercel	-	-	-	+					-	-	-	+

The MIC was reached for each of the remaining dressings tested. Aquacel Ag was the most consistent across the board for all three microorganism types at the dimensions tested and more effective than the silver nitrate solution. Silvercel was also as effective against *P. aeruginosa* and *E. coli* at D3 after three organism suspension inoculations.

Based on the above results, Aquacel Ag showed superior sustained effects after a total of 24 days of testing and 3 microorganism inoculations. The findings indicated that properties relevant to the dispersal of silver rather than the amount of silver contained in the dressing were more important on subsequent antimicrobial activity.

#### 5.5 MBC Method Evaluation

A sample from each of the silver dressing no growth (clear) MIC tubes tested from above was taken and evaluated for the minimum bactericidal concentration (MBC). The MBC determines the lowest concentration of antimicrobial that will prevent the growth of an organism. MBC differs from the MIC by providing evidence that an antimicrobial actually prevents organism growth by killing microorganisms (MBC) rather than merely inhibiting growth (MIC). Results for the MBC have reported in Table 5-6.

Table 5-6 MBC results of silver dressings (S) bacteriostatic or (C) bactericidal

Dressing	Based on MIC of Microorganism Suspension		
	P. aeruginosa	S. aureus	E.coli
Acticoat	S <sup>b</sup>	S <sup>b</sup>	C <sup>c</sup>
Aquacel Ag	S <sup>c</sup>	S <sup>c</sup>	S <sup>c</sup>
Contreet	S <sup>b</sup>	S <sup>a</sup>	S <sup>a</sup>
Polymem Silver	S <sup>a</sup>	S <sup>a</sup>	S <sup>a</sup>
Prisma	S <sup>c</sup>	S <sup>b</sup>	S <sup>c</sup>
Seasorb Ag	S <sup>a</sup>	S <sup>a</sup>	S <sup>a</sup>
Silvercel	S <sup>c</sup>	S <sup>b</sup>	S <sup>c</sup>
0.5% AgNO <sub>3</sub> (aq)	S <sup>b</sup>	S <sup>b</sup>	C <sup>b</sup>

<sup>a</sup> Initial bacteria inoculation    <sup>b</sup> 1<sup>st</sup> bacteria addition    <sup>c</sup> 2<sup>nd</sup> bacteria addition

All silver dressings tested displayed bacteriostatic activity against the microorganism types at the dimensions tested, with the exception of Acticoat and the silver nitrate solution which showed bactericidal properties against *E. coli*. Of importance, the MIC for dressings obtained only after the second or third microorganism inoculation would have contained an increased number of bacteria colonies. For this reason, results based on this testing method may appear skewed due to the procedure followed from the MIC test.

## 5.6 Conclusion

Based on above results from the three different testing methods, several conclusions can be made. Although bacterial sensitivity can be shown as indicated by the Kirby Bauer disc diffusion method, it does not always correlate to overall antimicrobial activity. The MIC method can be a useful tool in evaluating antimicrobial activity of silver dressings. By extending test parameters, the determination of sustained bacteriostatic properties was able to be assessed. Although MBC results were obtained, consideration of the difference in



microorganism volume between inoculations must be made. Importantly, the testing methods used in the evaluation of these dressings were all *in vitro* assessments and their behavior may be different in animal models.

## 5.7 Experimental Section

The general considerations for the experiments have been outlined below. Detailed procedures have been compiled for each microbiological test used.

### 5.7.1 General Considerations

All silver dressing samples were obtained from the lab of Dr. Eliot Mostow, Akron Ohio. Silver nitrate was purchased from Harshaw Chemical Company. LB Broth Miller (DIFCO) and LB-agar (DIFCO) were prepared according to manufacturer's instruction and sterilized before use.

### 5.7.2 Kirby Bauer Testing

Sterilized LB Broth was measured (5 mL) into a sterile culture tube. A constant volume of suspension culture of microorganisms (one sterilized loop), was added to the tube containing the LB Broth. The mixture was cultured overnight at 37°C in a shaking incubator. Prisma, Aquacel Ag, Acticoat, Polymem, Contreet, Seasorb and Contreet HC were each excised into samples of 7.9 mm using a commercial hole punch. A 0.5% silver nitrate aqueous solution was prepared to use as a control. An aliquot (10 µL) of this solution was inoculated onto 3 excised circles of filter paper of 7.9 mm. An aliquot (25 µL) of each microorganism solution was injected onto separate agar plates for each dressing type and control and spread evenly over the plate. All samples were

placed into the middle of each organism-injected plate and incubated at 37°C overnight. The zone of inhibition was measured for each plate and recorded. The test was performed once.

### 5.7.3 Antimicrobial Testing

Sterilized LB Broth was measured (5 mL) into a sterile culture tube. A constant volume of suspension culture of microorganisms (one sterilized loop), was added to the tube containing the LB Broth. The mixture was cultured overnight at 37°C in a shaking incubator. Prisma was cut into three pieces each of the following dimensions D1-D4: 1.33 x 1cm, 2 x 0.66 cm, 1 x 0.66 cm and 1 x 0.50 cm. Aquacel Ag, Acticoat, Polymem Ag, Contreet, Seasorb Ag and Contreet HC were cut into three pieces each of the following dimensions D1-D4: 2 x 1.33 cm, 2 x 1cm, 2 x 0.66 cm and 1 x 1cm. Sterilized LB Broth (3 mL) was measured into sterile culture tubes. The said dimensions of each dressing were placed into tubes labeled D1-D4 for each microorganism type. Each tube was inoculated with the microorganism solutions (25 µL) from above and incubated at 37°C overnight in a shaking incubator.

A 0.5% (by weight) silver nitrate aqueous solution was prepared to use as a control in the following manner. A 1 mL aliquot of the solution was placed in a vial and mixed with LB Broth (10 mL). A series of serial dilutions was performed by transferring 1 mL of the initial solution into a sterile tube containing LB Broth (2 mL) marked D1. Serial dilutions were performed by taking a 1mL aliquot of the AgNO<sub>3</sub>/LB solution and adding it to the 1<sup>st</sup> tube with mixing. A 1 mL aliquot of this solution was added to the 2<sup>nd</sup> tube and so on until all 4 tubes contained 2 mL of

solution. All tubes were inoculated with microorganism suspension (25 µL) from above and incubated at 37°C overnight in a shaking incubator. The test was performed once.

#### 5.7.4 Determination of MIC

Growth/no growth of microorganisms was visually evaluated after incubation for 24 hours at 37°C in a shaking incubator. The lowest concentration with no visible growth (turbidity) was taken as the MIC. If no visible growth was seen, microorganisms were freshly prepared as stated above. Tubes were subjected to a second microorganism suspension inoculation (10 µL) after 20 days and incubated at 37°C overnight in a shaking incubator. For tubes still showing no visible growth, microorganisms were again freshly prepared as stated above. Tubes were subjected to a third microorganism suspension inoculation (10 µL) after 2 days and incubated at 37°C overnight in a shaking incubator.

#### 5.7.5 Determination of MBC

One sterilized loop from each clear (no growth) tube was cultured on an agar plate and incubated for 24 hours at 37°C. The smallest dimension of each silver dressing supporting no colony formation was taken as the MBC.

## CHAPTER VI

### CONCLUSION AND FUTURE DIRECTIONS

A series of (bis)NHC-silver(I) nitrate complexes were synthesized by varying the substituents on the 4- and 5-positions of the imidazole ring with hydrogen atoms, chlorine atoms or a combination of both. These complexes were evaluated for their stability in an aqueous environment and it was determined that the series increased in stability as  $H,H < H, Cl < Cl,Cl$  attributed to the presence of two electron withdrawing groups at the 4- and 5-position of the imidazole ring. Corresponding (bis)NHC-gold(I) nitrate complexes were synthesized from their silver(I) precursors. The gold complexes were also evaluated for their water stability with superiority in comparison to their silver precursors. The antimicrobial properties of both gold and silver complexes were determined and the silver precursors were found to be much more efficacious than corresponding gold analogs. The (bis)NHC-gold(I) complexes were found to have lower bacteriostatic activity and displayed bactericidal properties at higher concentrations than their silver(I) precursors. It has been shown that NHC-gold complexes have a selectivity for gram positive bacteria.<sup>16,89</sup> However, the

(bis)NHC-gold complexes synthesized within showed greater broad spectrum activity.

The major interest of medicinal applications for gold-containing compounds is centered around their potential as antitumor agents. However, the toxicity associated with gold(I) and gold(III) complexes may hinder their usefulness. The adverse effects to normal tissues could potentially be minimized by successfully targeting the gold complexes to tumors. *In vitro* testing has shown that gold nanoparticles noncovalently bound to folic acid have been successfully targeted to cancerous cells.<sup>77</sup> The incorporation of a folic acid moiety onto a nitrogen substituent of the imidazole ring of a gold-NHC complex could lead to increased targeting of cancerous cells. The encapsulation of a folic acid NHC-gold complex into nanoparticles may also reduce toxicity effects to healthy cells.

Silver acetate NHC complexes were also synthesized varying at the 1- and 3- positions of the imidazole ring and compared with our previously reported silver acetate NHC systems varying at the 4- and 5-positions of the imidazole ring. Water stability studies indicated enhanced stability for the dichloro analog attributed to its electron withdrawing capability.<sup>95</sup> These systems showed superior stabilities in comparison to (bis)NHC-silver analogs, with the exception of both dihydro silver systems being equally unstable. Early results would indicate that the (bis)NHC-gold complexes have the most stability in an aqueous environment with the dihydro gold system showing stability in D<sub>2</sub>O for approximately 3 years. The silver acetate NHC complexes were also evaluated

for their antimicrobial properties. The acetate systems showed superior results against the gold systems in terms of both bacteriostatic and bactericidal activity. They displayed equal bacteriostatic activity to the silver (bis)NHC systems but improved bactericidal activity.

Imidazolium salts with different substituents at the 1-, 3-, 4- and or 5-positions of the imidazole ring were synthesized and evaluated for antimicrobial activity. A salt bearing a carboxylic acid at one nitrogen position of the imidazole ring showed the greatest bacteriostatic activity. It has been shown that imidazolium salts bearing long alkyl chain substituents (12-14 carbons) at one nitrogen atom of the imidazole ring have excellent bacteriostatic activity.<sup>109,110,111</sup> The incorporation of a carboxylic acid or long alkyl chain substituents onto a nitrogen position of the imidazole ring of a silver acetate NHC complex could lead to enhanced antimicrobial activity. The addition of such substituents to the imidazole ring of gold-NHC complexes may also help to enhance their bacteriostatic activity as well.

## BIBLIOGRAPHY

1. Hermann, W. A. *Angewandte Chemie, International Edition in English* **1997**, 36, 2162-2187.
2. Arduengo, A. J. *Journal of the American Chemical Society* **1991**, 113, 361-363.
3. Garrison, J.; Tessier, C.; Youngs, W. *Chemical Reviews* **2005**, 105, 3978-4008.
4. Kuehl, O. *Chemical Society Reviews* **2007**, 36, 592-607.
5. Kuhn, N.; Al-Sheikh, A. *Coordination Chemistry Reviews* **2005**, 249, 829-857.
6. Hermann, W. A. *Angewandte Chemie, International Edition in English* **2001**, 41, 1290-1309.
7. Huaizhi, Z.; Yuantao, N. *Gold Bulletin* **2001**, 34, 24-29.
8. Shaw, C. III. *Chem. Rev.* **1999**, 99, 2589-2600.
9. Fricker, S. *Gold Bulletin* **1996**, 29, 53-60.
10. Barnard, P.; Berners-Price, S. *Coordination Chemistry Reviews* **2007**, 251, 1889-1902.
11. Lin, I.; Vasam, C. B. *Canadian Journal of Chemistry* **2005**, 83, 812-825.
12. Ruiz, J.; Perandones, B. *Journal of the American Chemical Society* **2007**, 129, 9298- 9299.
13. Raubenheimer, H.; Olivier, P.; Lindeque, L.; Desmet, M.; Hrušak, J.; Kruger, G. *Journal of Organometallic Chemistry* **1997**, 544, 91-100.
14. Cetinkaya, B.; Dixneuf, P.; Lappert, M. *Journal of the Chemical Society, Dalton Transactions: Inorganic Chemistry* **1974**, 16, 1591-1599.

15. Seckin, T.; Koytepe, S.; Ozdemir, I.; Cetinkaya, B. *Journal of Inorganic and Organometallic Polymers* **2003**, *13*, 9-20.
16. Özdemir, İ.; Denizci, A.; Öztürk, H.; Cetinkaya, B. *Applied Organometallic Chemistry* **2004**, *18*, 318-322.
17. De Frémont, P.; Scott, N.; Stevens, E.; Nolan, S. *Organometallics* **2005**, *24*, 2411-2418.
18. Herrmann, W.; Runte, O.; Artus, G. *Journal of Organometallic Chemistry* **1995**, *501*, C1-C4.
19. Fränkel, R.; Kniczek, J.; Ponikwar, W.; Nöth, H.; Polborn, K.; Fehlhammer, W. *Inorganica Chimica Acta* **2001**, *312*, 23-29.
20. Böhler, C.; Stein, D.; Donati, N.; Grützmacher, H. *New Journal of Chemistry* **2002**, *26*, 1291-1295.
21. Baker, M.; Barnard, P.; Berners-Price, S.; Brayshaw, S.; Hickey, J.; Skelton, B.; White, A. *Journal of Organometallic Chemistry* **2005**, *690*, 5625-5635.
22. Baker, M.; Barnard, P.; Berners-Price, S.; Brayshaw, S.; Hickey, J.; Skelton, B.; White, A. *Dalton Transactions* **2006**, *30*, 3708-3715.
23. Barnard, P.; Baker, M.; Berners-Price, S.; Skelton, B.; White, A. *Dalton Transactions* **2004**, *7*, 1038-1047.
24. Raubenheimer, H.; Lindeque, L.; Cronje, S. *Journal of Organometallic Chemistry* **1996**, *511*, 177-184.
25. Bovio, B.; Calogero, S.; Wagner, F.; Burini, A.; Pietroni, R. *Journal of Organometallic Chemistry* **1994**, *470*, 275-283.
26. Fischer, E.; Böck, M. *Monatshefte für Chemie* **1984**, *115*, 1159-1164.
27. Liu, S.; Hsieh, T.; Lee, G.; Peng, S. *Organometallics* **1998**, *17*, 993-995.
28. Ku, R.; Huang, J.; Cho, J.; Kiang, F.; Reddy, K.; Chen, Y.; Lee, K.; Lee, J.; Lee, G.; Peng, S.; Liu, S. *Organometallics* **1999**, *18*, 2145-2154.
29. Wang, H.; Lin, I. *Organometallics* **1998**, *17*, 972-975.



30. Wang, H.; Vasam, C.; Tsai, T.; Chen, S.; Chang, A.; Lin, I. *Organometallics* **2005**, *24*, 486-493.
31. Wang, H.; Chen, C.; Lin, I. *Organometallics* **1999**, *18*, 1216-1223.
32. Ray, L.; Katiyar, V.; Barman, S.; Mustafa, J.; Nanavati, H.; Shaikh, M.; Ghosh, P. *Journal of Organometallic Chemistry* **2007**, *692*, 4259-4269.
33. Baker, M.; Barnard, P.; Brayshaw, S.; Hickey, J.; Skelton, B.; White, A. *Dalton Transactions* **2005**, *1*, 37-43.
34. Samantaray, M.; Pang, K.; Shaikh, M.; Ghosh, P. *Inorganic Chemistry* **2008**, *47*, 4153-4165.
35. Catalano, V.; Moore, A. *Inorganic Chemistry* **2005**, *44*, 6558-6566.
36. Minghetti, G.; Bonati, F. *Journal of Organometallic Chemistry* **1973**, *54*, C62-C63.
37. Parks, J.; Balch, A. *Journal of Organometallic Chemistry* **1974**, *71*, 453-463.
38. Minghetti, G.; Bonati, F. *Journal of Organometallic Chemistry* **1974**, *73*, C43-C44.
39. Manojlovic-Muir, L. *Journal of Organometallic Chemistry* **1974**, *734*, C45-C46.
40. De Frémont, P.; Singh, R.; Stevens, E.; Petersen, J.; Nolan, S. *Organometallics* **2007**, *26*, 1376-1385.
41. Merchant, B. *Biologicals* **1998**, *26*, 49-59.
42. Carvajal, M.; Novoa, J.; Alvarez, S. *Journal of the American Chemical Society* **2004**, *126*, 1465-1477.
43. Shaw III, C.; Schraa, S.; Gleichmann, E.; Grover, Y.; Dunemann, L.; Jagarlamudi, A. *Metal-Based Drugs* **1994**, *1*, 351-362.
44. Schuhmann, D.; Kubicka-Muranyi, M.; Mirtschewa, J.; Günther, J.; Kind, P.; Gleichmann, E. *Journal of Immunology* **1990**, *145*, 2132-2139.

45. Aletaha, D.; Kapral, T.; Smolen, J. *Annals of the Rheumatic Diseases* **2003**, 62, 482-486.
46. Grootveld, M.; Blake, D.; Sahinoglu, T.; Claxson, A.; Mapp, P.; Stevens, C.; Allen, R.; Furst, A. *Free Rad. Res. Comms.* **1990**, 10, 199-220.
47. Forestier, J. *Journal of the Medical Society of New Jersey* **1935**, 32, 364-366.
48. Sharma, R.; Smillie, J.; Palmer, D. *Pharmacology* **1985**, 30, 115-120.
49. Elder, R.; Eidsness, M. *Chem. Rev.* **1987**, 87, 1027-1046.
50. Champion, G.; Graham, G.; Ziegler, J. *Baillière's Clinical Rheumatology* **1990**, 4, 491-534.
51. Xiao, J.; Shaw, C.; *Inorganic Chemistry* **1992**, 31, 3706-3710.
52. Snyder, R.; Mirabelli, C.; Crooke, S. *Biochemical Pharmacology* **1986**, 35, 923-932.
53. Isab, A.; Shaw, C.; Hoeschele, J.; Locke, J. *Inorganic Chemistry* **1988**, 27, 3406-3409.
54. Coffey, M.; Shaw, C.; Hormann, A.; Mirabelli, C.; Crooke, S. *J. Inorganic Biochemistry* **1987**, 30, 177-187.
55. Intoccia, A.; Flanagan, T.; Walz, D.; Gutzait, L.; Swagzdis, J.; Flagiello Jr.; J.; Hwang, B.; Dewey, R.; Noguchi, H. *The Journal of Rheumatology Supplement* **1982**, 8, 90-98.
56. Goebel, C.; Kubicka-Muranyi, M.; Tonn, T.; Gonzalez, J.; Gleichmann, E. *Archives of Toxicology* **1995**, 69, 450-459.
57. Elder, R.; Zhao, Z.; Zhang, Y.; Dorsey, J.; Hess, E.; Tepperman, K. *The Journal of Rheumatology* **1993**, 20, 268-272.
58. Graham, G.; Haavisto, T.; Jones, H.; Champion, G. *Biochemical Pharmacology* **1984**, 33, 1257-1262.
59. Tepperman, K.; Zhang, Y.; Roy, P.; Floyd, R.; Zhao, Z.; Dorsey, J.; Elder, R. *Metal Based Drugs* **1994**, 1, 433-443.

60. Rudkowski, R.; Graham, G.; Champion, G.; Ziegler, J. *Biochemical Pharmacology* **1990**, 39, 1687-1695.
61. Canumalla, A.; Schraa, S.; Isab, A.; Shaw, C. *Journal of Biological Inorganic Chemistry* **1998**, 3, 9-17.
62. Leibfarth, J.; Persellin, R. *Agents and Actions* **1981**, 11, 458-472.
63. Walz, D.; Dimartino, M.; Griswold, D. *The Journal of Rheumatology, Supplement* **1982**, 8, 32-36.
64. Best, S.; Sadler, P. *Gold Bulletin* **1996**, 29, 87-93.
65. Fries, J.; Williams, C.; Ramey, D.; Bloch, D. *Arthritis and Rheumatism* **1993**, 36, 297-306.
66. Fricker, Simon P. *Transition Metal Chemistry* **1996**, 21, 377-383.
67. Tiekink, E. *Critical Reviews in Oncology Hematology* **2002**, 42, 225-248.
68. Tiekink, E. *Gold Bulletin* **2003**, 36, 117-124.
69. Parish, R.; Howe, B.; Wright, J.; Mack, J.; Pritchard, R.; Buckley, R.; Elsome, A.; Fricker, S. *Inorganic Chemistry* **1996**, 35, 1659-1666.
70. Buckley, R.; Elsome, A.; Fricker, S.; Henderson, G.; Theobald, B.; Parish, R.; Howe, B.; Kelland, L. *Journal of Medicinal Chemistry* **1996**, 39, 5208-5214.
71. Parish, R.; Mack, J.; Hargreaves, L.; Wright, J.; Buckley, R.; Elsome, A.; Fricker, S.; Theobald, B. *Journal of the Chemical Society, Dalton Transactions* **1996**, 1, 69-74.
72. Hainfeld, J.; Slatkin, D.; Smilowitz, H. *Physics in Medicine and Biology* **2004**, 49, N309-N315.
73. Patra, H.; Banerjee, S.; Chaudhuri, U.; Lahiri, P.; Dasgupta, A. *Nanomedicine* **2007**, 3, 111-119.
74. Connor, E.; Mwamuka, J.; Gole, A.; Murphy, C.; Wyatt, M. *Small* **2005**, 1, 325-327.
75. Krpetic, Z.; Porta, F.; Scari, G. *Gold Bulletin* **2006**, 39(2), 66-68.

76. El-Sayed, I.; Huang, X.; El-Sayed, M. *Cancer Letters* **2006**, 239, 129-135.
77. Bhattacharya, R.; Patra, C.; Earl, A.; Wang, S.; Katarya, A.; Lu, L.; Kizhakkedathu, J.; Yaszemski, M.; Greipp, P.; Mukhopadhyay, D.; Mukherjee, P. *Nanomedicine* **2007**, 3, 224-238.
78. Hartung, E.; Cotter, J. *Journal of Laboratory and Clinical Medicine* **1941**, 26, 1274-1284.
79. Sabin, A. *Journal of Bacteriology* **1941**, 40, 823-856.
80. Pruzanski, W.; Leers, W.; Wardlaw, A. *Arthritis and Rheumatism* **1974**, 17, 207-217.
81. Dawson, M.; Hobby, G. *Journal of Pharmacology* **1940**, 69, 359-364.
82. Preston, W.; Block, W.; Freyberg, R. *Proceedings of the Society for Experimental Biology and Medicine* **1942**, 50, 253-256.
82. Rhodes, M.; Sadler, M.; Scawen, M.; Silver, S. *Journal of Inorganic Biochemistry* **1992**, 46, 129-142.
84. Fricker, Simon P. *Toxicology In Vitro* **1994**, 8, 879-881.
85. Elsome, A.; Hamilton-Miller, J.; Brumfitt, W.; Noble, W. *Journal of Antimicrobial Chemotherapy* **1996**, 37, 911-918.
86. Rigobello, M.; Scutari, G.; Boscolo, R.; Bindoli, A. *British Journal of Pharmacology* **2002**, 136, 1162-1168.
87. Barnard, P.; Baker, M.; Berners-Price, S.; Day, D. *Journal of Inorganic Biochemistry* **2004**, 98, 1642-1647.
88. Horvath, U.; Bentivoglio, G.; Hummel, M.; Schottenberger, H.; Wurst, K.; Nell, M.; van Rensburg, C.; Cronje, S.; Raubenheimer, H. I. *New Journal of Chemistry* **2008**, 32, 533-539.
89. Ray, S.; Mohan, R.; Singh, J.; Samantaray, M.; Shaikh, M.; Panda, D.; Ghosh, P. *Journal of the American Chemical Society* **2007**, 129, 15042-15053.
90. Emsley, J. *The Elements* **1999**, Oxford University Press Inc., Oxford NY, 88-89.

91. Takahashi, Y.; Funakoshi, T.; Shimada, H.; Kojima, S. *Toxicology* **1995**, *97*, 151-157.
92. Melaiye, A.; Simons, R.; Milsted, A.; Pingitore, F.; Wesdemiotis, C.; Tessier, C.; Youngs, W. *Journal of Medicinal Chemistry* **2004**, *47*, 973-977.
93. Kascatan-Nebioglu, A.; Melaiye, A.; Hindi, K.; Durmus, S.; Panzner, M.; Hogue, L.; Hovis, C.; Mallet, R.; Coughenour, M.; Crosby, S.; Milsted, A.; Ely, D.; Tessier, C.; Cannon, C.; Youngs, W. *Journal of Medicinal Chemistry* **2006**, *49*, 6811-6818.
94. Kascatan-Nebioglu, A.; Panzner, M.; Tessier, C.; Cannon, C.; Youngs, W. *Coordination Chemistry Reviews* **2007**, *251*, 884-895.
95. Hindi, K.; Siciliano, T.; Durmus, S.; Panzner, M.; Medvetz, D.; Reddy, D.; Hogue, L.; Hovis, C.; Hilliard, J.; Mallet, R.; Tessier, C.; Cannon, C.; Youngs, W. *Journal of Medicinal Chemistry* **2008**, *51*, 1577-1583.
96. Melaiye, A.; Sun, Z.; Hindi, K.; Milsted, A.; Ely, D.; Reneker, D.; Tessier, C.; Youngs, W. *Journal of the American Chemical Society* **2005**, *127*, 2285-2291.
97. Lee, K.; Wang, H.; Lin, I. *Journal of the Chemical Society, Dalton Transactions* **2002**, *14*, 2852-2856.
98. Schwerdtfeger, P.; Boyd, P.; Brienne, S.; Burrell, A. *Inorganic Chemistry* **1992**, *31*, 3411-3422.
99. Roulet, R.; Lan, N.; Mason, W.; Fenske, G. *Helvetica Chimica Acta* **1973**, *56*, 2405-2418.
100. Mohamed, A.; Kani, I.; Ramirez, A.; Fackler, J. *Inorganic Chemistry* **2004**, *43*, 3833-3839.
101. Viciano, M.; Mas-Marza, E.; Sanau, M.; Peris, E. *Organometallics* **2006**, *25*, 3063-3069.
102. Catalano, V.; Malwitz, M.; Etogo, A. *Inorganic Chemistry* **2004**, *43*, 5714-5724.
103. Catalano, V.; Horner, S. *Inorganic Chemistry* **2003**, *42*, 8430-8438.

104. Chen, W.; Liu, F.; You, X. *Journal of Solid State Chemistry* **2002**, *167*, 119-125.
105. Bruker (1997). SMART (Version 5.625), SAINT (Version 6.22) and SHELXTL (Version 6.10)
106. Sheldrick, G. M. (1997). SHELX-97. University of Göttingen, Germany
107. Guerret, O.; Sole, S.; Gornitzka, H.; Teichert, M.; Trinquier, G.; Bertrand, G. *Journal of the American Chemical Society* **1997**, *119*, 6668-6669.
108. Quezada, C.; Garrison, J.; Panzner, M.; Tessier, C.; Youngs, W. *Organometallics* **2004**, *23*, 4846-4848.
109. Pernak, J.; Skrzypczak, A. *European Journal of Medicinal Chemistry* **1996**, *31*, 901-903.
110. Pernak, J.; Sobaszekiewicz, K.; Mirska, I. *The Royal Society of Chemistry* **2003**, *5*, 52-56.
111. Dembereinyamba, D.; Kim, K.; Choi, S.; Park, S.; Lee, H.; Kim, C.; Yoo, I. *Bioinorganic and Medicinal Chemistry* **2004**, *12*, 853-857.
112. Denyer, S.; Stewart, G. *International Biodeterioration and Biodegradation* **1998**, *41*, 261-268.
113. Medvetz, D. *The Synthesis, Characterization and Antitumor Properties of Ag(I), Cu(II) and Rh(III) Metal Complexes* [dissertation]. Akron, Ohio: The University of Akron; **2008**.
114. Lansdown, A. *British Journal of Nursing* **2004**, *13*(Suppl. 6), S6-S19.
115. Hermans, M. *Advances in Skin & Wound Care* **2007**, *20*, 166-172.
116. Ballard, K. *British Journal of Nursing* **2002**, *11*, 206-211.
117. Yin, H.; Langford, R.; Burrell, R. *Journal of Burn Care & Rehabilitation* **1999**, *20*, 195-200.
118. Thomas, S.; McCubbin, P. *Journal of Wound Care* **2003**, *12*, 101-107.
119. Schaller, M.; Laude, J.; Bodewaldt, H.; Hamm, G.; Korting, H. *Skin Pharmacology and Physiology* **2004**, *17*, 31-36.

120. Castellano, J.; Shafii, S.; Ko, F.; Donate, G.; Wright, T.; Mannari, R.; Payne, W.; Smith, D.; Robson, M. *International Wound Journal* **2007**, *4*, 114-122.
121. Percival, S.; Bowler, P.; Dolman, J. *International Wound Journal* **2007**, *4*, 186-191.
122. Ip, M.; Lui, S.; Poon, V.; Lung, I.; Burd, A. *Journal of Medical Microbiology* **2006**, *55*, 59-63.

## APPENDICES



## APPENDIX A

### SUPPLEMENTARY MATERIAL FOR THE X-RAY CRYSTAL STRUCTURE OF

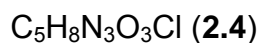


Table A. Crystal data and structure refinement for **2.4**.

Empirical formula	C <sub>5</sub> H <sub>8</sub> ClN <sub>3</sub> O <sub>3</sub>	
Formula weight	193.59	
Temperature	100(2) K	
Wavelength	0.71073 Å	
Crystal system	Monoclinic	
Space group	P2(1)/n	
Unit cell dimensions	a = 8.608(4) Å	α = 90°.
	b = 9.977(4) Å	β = 100.313(7)°.
	c = 9.726(4) Å	γ = 90°.
Volume	821.8(6) Å <sup>3</sup>	
Z	4	
Density (calculated)	1.565 Mg/m <sup>3</sup>	
Absorption coefficient	0.436 mm <sup>-1</sup>	
F(000)	400	
Crystal size	0.39 x 0.17 x 0.08 mm <sup>3</sup>	
Theta range for data collection	2.91 to 26.30°.	
Index ranges	-10 ≤ h ≤ 10, -12 ≤ k ≤ 12, -12 ≤ l ≤ 11	
Reflections collected	6398	
Independent reflections	1677 [R(int) = 0.0309]	
Completeness to theta = 26.30°	100.0 %	
Absorption correction	Semi-empirical from equivalents	
Max. and min. transmission	0.9659 and 0.8347	

Table A. Crystal data and structure refinement for **2.4** (continued).

Refinement method	Full-matrix least-squares on $F^2$ Data /
restraints / parameters	1677 / 0 / 111
Goodness-of-fit on $F^2$	1.064
Final R indices [ $I > 2\sigma(I)$ ]	$R1 = 0.0353$ , $wR2 = 0.0963$
R indices (all data)	$R1 = 0.0400$ , $wR2 = 0.0997$
Largest diff. peak and hole	0.392 and -0.212 e/ $\text{\AA}^3$

Table B. Atomic coordinates ( $\times 10^4$ ) and equivalent isotropic displacement parameters ( $\text{\AA}^2 \times 10^3$ ) for **2.4**.  $U(\text{eq})$  is defined as one third of the trace of the orthogonalized  $U_{ij}$  tensor.

	x	y	z	$U(\text{eq})$
Cl(1)	439(1)	4293(1)	6716(1)	26(1)
O(1)	7315(1)	6430(1)	9067(1)	22(1)
O(2)	6688(2)	7776(1)	10635(1)	25(1)
O(3)	8579(2)	8309(1)	9516(1)	28(1)
N(1)	3139(2)	5334(1)	8156(1)	17(1)
N(2)	2367(2)	6587(1)	9725(1)	18(1)
N(3)	7534(2)	7509(1)	9745(1)	19(1)
C(1)	4171(2)	4666(2)	7282(2)	17(1)
C(2)	2416(2)	7480(2)	10935(2)	26(1)
C(3)	3622(2)	6159(2)	9228(2)	18(1)
C(4)	1024(2)	6018(2)	8961(2)	19(1)
C(5)	1518(2)	5237(2)	7991(2)	17(1)

Table C. Bond lengths [Å] and angles [°] for **2.4**.

---

Cl(1)-C(5)	1.6957(17)
O(1)-N(3)	1.2585(19)
O(2)-N(3)	1.2560(18)
O(3)-N(3)	1.2522(19)
N(1)-C(3)	1.335(2)
N(1)-C(5)	1.379(2)
N(1)-C(1)	1.492(2)
N(2)-C(3)	1.330(2)
N(2)-C(4)	1.380(2)
N(2)-C(2)	1.471(2)
C(4)-C(5)	1.349(2)
C(3)-N(1)-C(5)	107.55(14)
C(3)-N(1)-C(1)	125.86(14)
C(5)-N(1)-C(1)	126.57(14)
C(3)-N(2)-C(4)	109.22(14)
C(3)-N(2)-C(2)	125.20(15)
C(4)-N(2)-C(2)	125.54(15)
O(3)-N(3)-O(2)	120.75(14)
O(3)-N(3)-O(1)	119.77(14)
O(2)-N(3)-O(1)	119.48(14)
N(2)-C(3)-N(1)	108.75(15)
C(5)-C(4)-N(2)	105.99(15)
C(4)-C(5)-N(1)	108.49(15)
C(4)-C(5)-Cl(1)	129.20(14)
N(1)-C(5)-Cl(1)	122.30(13)

---

Table D. Anisotropic displacement parameters ( $\text{\AA}^2 \times 10^3$ ) for **2.4**. The anisotropic displacement factor exponent takes the form:  $-2\pi^2 [h^2 a^{*2} U^{11} + \dots + 2 h k a^* b^* U^{12}]$

	U <sup>11</sup>	U <sup>22</sup>	U <sup>33</sup>	U <sup>23</sup>	U <sup>13</sup>	U <sup>12</sup>
Cl(1)	23(1)	26(1)	28(1)	-4(1)	1(1)	-4(1)
O(1)	21(1)	20(1)	25(1)	-4(1)	5(1)	-1(1)
O(2)	24(1)	31(1)	22(1)	-3(1)	9(1)	1(1)
O(3)	24(1)	27(1)	36(1)	-5(1)	11(1)	-9(1)
N(1)	16(1)	17(1)	18(1)	2(1)	4(1)	1(1)
N(2)	19(1)	19(1)	17(1)	-1(1)	3(1)	0(1)
N(3)	16(1)	22(1)	18(1)	1(1)	1(1)	2(1)
C(1)	17(1)	20(1)	15(1)	1(1)	5(1)	-1(1)
C(2)	28(1)	29(1)	19(1)	-7(1)	3(1)	3(1)
C(3)	17(1)	17(1)	18(1)	3(1)	3(1)	0(1)
C(4)	16(1)	20(1)	21(1)	2(1)	4(1)	1(1)
C(5)	16(1)	18(1)	18(1)	2(1)	3(1)	-2(1)

Table E. Hydrogen coordinates ( $\times 10^4$ ) and isotropic displacement parameters ( $\text{\AA}^2 \times 10^3$ ) for **2.4**.

	x	y	z	U(eq)
H(1A)	5273	4924	7617	26
H(1B)	3853	4945	6306	26
H(1C)	4066	3692	7350	26
H(2A)	2385	6943	11773	39
H(2B)	1504	8084	10768	39
H(2C)	3391	8008	11069	39
H(3A)	4687	6401	9578	21
H(4)	-33	6149	9091	23

## APPENDIX B

### SUPPLEMENTARY MATERIAL FOR THE X-RAY CRYSTAL STRUCTURE OF

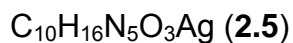


Table F. Crystal data and structure refinement for **2.5**.

Empirical formula	$\text{C}_{10}\text{H}_{16}\text{AgN}_5\text{O}_3$	
Formula weight	362.15	
Temperature	100(2) K	
Wavelength	0.71073 Å	
Crystal system	Monoclinic	
Space group	P2(1)/c	
Unit cell dimensions	$a = 13.7006(15)$ Å	$\alpha = 90^\circ$ .
	$b = 6.9793(8)$ Å	$\beta = 114.105(2)^\circ$ .
	$c = 15.8626(18)$ Å	$\gamma = 90^\circ$ .
Volume	$1384.5(3)$ Å <sup>3</sup>	
Z	4	
Density (calculated)	$1.737$ Mg/m <sup>3</sup>	
Absorption coefficient	$1.468$ mm <sup>-1</sup>	
F(000)	728	
Crystal size	$0.40 \times 0.32 \times 0.06$ mm <sup>3</sup>	
Theta range for data collection	$1.63$ to $28.30^\circ$ .	
Index ranges	$-17 \leq h \leq 18$ , $-8 \leq k \leq 9$ , $-20 \leq l \leq 21$	
Reflections collected	11417	
Independent reflections	3270 [R(int) = 0.0282]	
Completeness to theta = $26.30^\circ$	100.0 %	
Absorption correction	Semi-empirical from equivalents	
Max. and min. transmission	0.9171 and 0.5913	

Table F. Crystal data and structure refinement for **2.5** (continued).

Refinement method	Full-matrix least-squares on $F^2$
Data / restraints / parameters	3270 / 0 / 176
Goodness-of-fit on $F^2$	1.159
Final R indices [ $I > 2\sigma(I)$ ]	$R_1 = 0.0358$ , $wR_2 = 0.0770$
R indices (all data)	$R_1 = 0.0417$ , $wR_2 = 0.0792$
Largest diff. peak and hole	1.363 and -0.578 e/Å <sup>3</sup>

Table G. Atomic coordinates ( $\times 10^4$ ) and equivalent isotropic displacement parameters (Å<sup>2</sup> $\times 10^3$ ) for **2.5**.  $U(\text{eq})$  is defined as one third of the trace of the orthogonalized  $U_{ij}$  tensor.

	x	y	z	$U(\text{eq})$
Ag	2555(1)	2292(1)	9973(1)	21(1)
O(1)	1600(2)	53(3)	1957(2)	30(1)
O(2)	2366(2)	2671(3)	2633(2)	46(1)
O(3)	3316(2)	108(3)	2767(2)	30(1)
N(1)	3337(2)	-1541(4)	9554(2)	20(1)
N(2)	4462(2)	-570(4)	10863(2)	24(1)
N(3)	620(2)	5051(4)	9057(2)	23(1)
N(4)	1704(2)	6115(4)	10369(2)	20(1)
N(5)	2429(2)	943(4)	2448(2)	22(1)
C(1)	3527(2)	-88(4)	10158(2)	21(1)
C(2)	4131(3)	-2920(5)	9871(2)	27(1)
C(3)	4847(3)	-2283(5)	10703(2)	28(1)
C(4)	2409(2)	-1652(4)	8671(2)	23(1)
C(5)	4990(3)	569(5)	11701(2)	33(1)
C(6)	1556(2)	4643(4)	9776(2)	21(1)
C(7)	192(2)	6747(5)	9205(2)	27(1)
C(8)	880(3)	7425(5)	10029(2)	28(1)
C(9)	128(3)	3860(5)	8243(2)	32(1)
C(10)	2610(2)	6252(5)	11265(2)	25(1)

Table H. Bond lengths [Å] and angles [°] for **2.5**.

Ag-C(1)	2.073(3)	C(1)-N(2)-C(3)	111.6(3)
Ag-C(6)	2.077(3)	C(1)-N(2)-C(5)	124.4(3)
O(1)-N(5)	1.249(3)	C(3)-N(2)-C(5)	123.9(3)
O(2)-N(5)	1.253(3)	C(6)-N(3)-C(7)	111.0(3)
O(3)-N(5)	1.253(3)	C(6)-N(3)-C(9)	124.4(3)
N(1)-C(1)	1.346(4)	C(7)-N(3)-C(9)	124.5(3)
N(1)-C(2)	1.385(4)	C(6)-N(4)-C(8)	111.5(3)
N(1)-C(4)	1.459(4)	C(6)-N(4)-C(10)	123.6(3)
N(2)-C(1)	1.355(4)	C(8)-N(4)-C(10)	124.9(3)
N(2)-C(3)	1.372(4)	O(1)-N(5)-O(2)	119.5(3)
N(2)-C(5)	1.461(4)	O(1)-N(5)-O(3)	120.3(3)
N(3)-C(6)	1.354(4)	O(2)-N(5)-O(3)	120.1(3)
N(3)-C(7)	1.383(4)	N(1)-C(1)-N(2)	104.1(3)
N(3)-C(9)	1.450(4)	N(1)-C(1)-Ag	125.2(2)
N(4)-C(6)	1.350(4)	N(2)-C(1)-Ag	130.7(2)
N(4)-C(8)	1.380(4)	C(3)-C(2)-N(1)	105.9(3)
N(4)-C(10)	1.459(4)	C(2)-C(3)-N(2)	106.6(3)
C(2)-C(3)	1.358(5)	N(4)-C(6)-N(3)	104.3(3)
C(7)-C(8)	1.346(5)	N(4)-C(6)-Ag	126.5(2)
C(1)-Ag-C(6)	178.92(11)	N(3)-C(6)-Ag	129.2(2)
C(1)-N(1)-C(2)	111.7(3)	C(8)-C(7)-N(3)	106.7(3)
C(1)-N(1)-C(4)	124.2(2)	C(7)-C(8)-N(4)	106.5(3)
C(2)-N(1)-C(4)	124.0(3)		

Table I. Anisotropic displacement parameters ( $\text{\AA}^2 \times 10^3$ ) for **2.5**. The anisotropic displacement factor exponent takes the form:  $-2\pi^2 [h^2 a^{*2} U^{11} + \dots + 2 h k a^* b^* U^{12}]$ 

	U <sup>11</sup>	U <sup>22</sup>	U <sup>33</sup>	U <sup>23</sup>	U <sup>13</sup>	U <sup>12</sup>
Ag	19(1)	19(1)	23(1)	-1(1)	7(1)	0(1)
O(1)	21(1)	27(1)	33(1)	-5(1)	3(1)	0(1)

Table I. Anisotropic displacement parameters ( $\text{\AA}^2 \times 10^3$ ) for **2.5** (continued).

O(2)	51(2)	20(1)	56(2)	-10(1)	9(2)	0(1)
O(3)	19(1)	34(1)	32(1)	-3(1)	7(1)	-1(1)
N(1)	19(1)	19(1)	22(1)	4(1)	7(1)	2(1)
N(2)	17(1)	29(1)	22(1)	1(1)	4(1)	-2(1)
N(3)	16(1)	28(1)	21(1)	3(1)	4(1)	-4(1)
N(4)	18(1)	21(1)	19(1)	1(1)	7(1)	1(1)
N(5)	26(1)	21(1)	17(1)	-1(1)	6(1)	-3(1)
C(1)	18(1)	20(1)	21(1)	3(1)	5(1)	-1(1)
C(2)	27(2)	23(2)	30(2)	5(1)	11(1)	7(1)
C(3)	20(1)	32(2)	30(2)	9(1)	8(1)	7(1)
C(4)	22(2)	23(2)	20(1)	-1(1)	4(1)	-2(1)
C(5)	23(2)	44(2)	24(2)	-5(2)	3(1)	-7(1)
C(6)	19(1)	22(2)	22(1)	1(1)	8(1)	-4(1)
C(7)	20(1)	31(2)	30(2)	10(1)	11(1)	5(1)
C(8)	28(2)	28(2)	33(2)	9(1)	16(2)	9(1)
C(9)	25(2)	42(2)	22(2)	-1(1)	1(1)	-9(1)
C(10)	25(2)	27(2)	22(2)	-3(1)	8(1)	-2(1)

Table J. Hydrogen coordinates ( $\times 10^4$ ) and isotropic displacement parameters ( $\text{\AA}^2 \times 10^3$ ) for **2.5**.

	x	y	z	U(eq)
H(2)	4168	-4076	9569	32
H(3)	5489	-2903	11097	34
H(4A)	1813	-2253	8763	34
H(4B)	2588	-2418	8237	34
H(4C)	2202	-358	8422	34
H(5A)	4976	1925	11535	49
H(5B)	5733	145	12023	49
H(5C)	4614	401	12105	49



Table J. Hydrogen coordinates ( $\times 10^4$ ) and isotropic displacement parameters ( $\text{\AA}^2 \times 10^3$ ) for **2.5** (continued).

H(7)	-461	7323	8804	32
H(8)	812	8578	10319	34
H(9A)	622	2831	8258	48
H(9B)	-37	4642	7689	48
H(9C)	-533	3302	8233	48
H(10A)	2548	5257	11677	38
H(10B)	2612	7517	11534	38
H(10C)	3277	6073	11187	38

## APPENDIX C

### SUPPLEMENTARY MATERIAL FOR THE X-RAY CRYSTAL STRUCTURE OF

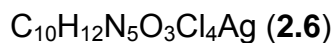


Table K. Crystal data and structure refinement for **2.6**.

Empirical formula	$\text{C}_{10}\text{H}_{12}\text{AgCl}_4\text{N}_5\text{O}_5$	
Formula weight	531.92	
Temperature	100(2) K	
Wavelength	0.71073 Å	
Crystal system	Triclinic	
Space group	P-1	
Unit cell dimensions	$a = 6.5183(12)$ Å	$\alpha = 72.205(3)^\circ$ .
	$b = 10.808(2)$ Å	$\beta = 79.989(3)^\circ$ .
	$c = 14.542(3)$ Å	$\gamma = 73.465(3)^\circ$ .
Volume	930.9(3) Å <sup>3</sup>	
Z	2	
Density (calculated)	1.898 Mg/m <sup>3</sup>	
Absorption coefficient	1.688 mm <sup>-1</sup>	
F(000)	524	
Crystal size	0.27 x 0.15 x 0.03 mm <sup>3</sup>	
Theta range for data collection	1.48 to 28.27°.	
Index ranges	$-8 \leq h \leq 8, -13 \leq k \leq 14, -19 \leq l \leq 19$	
Reflections collected	8161	
Independent reflections	4279 [R(int) = 0.0331]	
Completeness to theta = 26.30°	98.9 %	
Absorption correction	Semi-empirical from equivalents	
Max. and min. transmission	0.9511 and 0.6586	

Table K. Crystal data and structure refinement for **2.6** (continued).

Refinement method	Full-matrix least-squares on F <sup>2</sup> Data /
restraints / parameters	4279 / 0 / 230
Goodness-of-fit on F <sup>2</sup>	1.155
Final R indices [I>2sigma(I)]	R1 = 0.0574, wR2 = 0.1356
R indices (all data)	R1 = 0.0655, wR2 = 0.1401
Largest diff. peak and hole	2.085 and -1.549 e/Å <sup>3</sup>

Table L. Atomic coordinates ( $\times 10^4$ ) and equivalent isotropic displacement parameters ( $\text{\AA}^2 \times 10^3$ ) for **2.6**. U(eq) is defined as one third of the trace of the orthogonalized U<sub>ij</sub> tensor.

	x	y	z	U(eq)
Ag(1)	5078(1)	7078(1)	7330(1)	17(1)
Cl(1)	13325(2)	4043(1)	8758(1)	23(1)
Cl(2)	11629(2)	6875(1)	9642(1)	23(1)
Cl(3)	-1490(2)	7348(1)	4994(1)	26(1)
Cl(4)	-3144(2)	10153(1)	5879(1)	22(1)
O(1)	5348(6)	1413(4)	7813(2)	22(1)
O(2)	6755(6)	2935(4)	6770(3)	28(1)
O(3)	3751(6)	2648(4)	6529(3)	26(1)
O(4)	7565(7)	1504(4)	9238(3)	29(1)
O(5)	2002(7)	523(5)	9057(3)	43(1)
N(1)	9412(7)	5315(4)	8082(3)	18(1)
N(2)	8374(7)	7052(4)	8636(3)	18(1)
N(3)	1780(7)	7126(4)	6013(3)	19(1)
N(4)	746(7)	8857(4)	6582(3)	19(1)
N(5)	5290(7)	2349(4)	7027(3)	18(1)
C(1)	7795(8)	6420(5)	8077(3)	17(1)
C(2)	10994(8)	5257(5)	8619(3)	18(1)
C(3)	10364(8)	6350(5)	8959(4)	18(1)
C(4)	9381(9)	4271(5)	7644(4)	23(1)
C(5)	7024(9)	8281(5)	8860(4)	24(1)
C(6)	2376(8)	7744(5)	6572(3)	19(1)

Table L. Atomic coordinates ( $\times 10^4$ ) and equivalent isotropic displacement parameters ( $\text{\AA}^2 \times 10^3$ ) for **2.6** (continued).

C(7)	-194(8)	7842(5)	5686(4)	19(1)
C(8)	-831(8)	8920(5)	6031(3)	19(1)
C(9)	3110(9)	5946(5)	5742(4)	24(1)
C(10)	764(9)	9841(5)	7081(4)	23(1)

Table M. Bond lengths [ $\text{\AA}$ ] and angles [ $^\circ$ ] for <b>2.6</b> .		C(6)-Ag(1)-C(1)	179.51(19)
		C(1)-N(1)-C(2)	110.8(4)
		C(1)-N(1)-C(4)	124.0(4)
		C(2)-N(1)-C(4)	125.0(4)
Ag(1)-C(6)	2.074(5)	C(1)-N(2)-C(3)	110.0(4)
Ag(1)-C(1)	2.075(5)	C(1)-N(2)-C(5)	123.6(4)
Cl(1)-C(2)	1.697(5)	C(3)-N(2)-C(5)	126.3(4)
Cl(2)-C(3)	1.698(5)	C(6)-N(3)-C(7)	110.2(4)
Cl(3)-C(7)	1.700(5)	C(6)-N(3)-C(9)	124.5(4)
Cl(4)-C(8)	1.700(5)	C(7)-N(3)-C(9)	125.2(5)
O(1)-N(5)	1.272(5)	C(6)-N(4)-C(8)	109.9(4)
O(2)-N(5)	1.237(5)	C(6)-N(4)-C(10)	123.4(4)
O(3)-N(5)	1.249(5)	C(8)-N(4)-C(10)	126.7(4)
N(1)-C(1)	1.348(6)	O(2)-N(5)-O(3)	121.5(4)
N(1)-C(2)	1.375(7)	O(2)-N(5)-O(1)	119.6(4)
N(1)-C(4)	1.462(6)	O(3)-N(5)-O(1)	118.9(4)
N(2)-C(1)	1.365(6)	N(1)-C(1)-N(2)	105.2(4)
N(2)-C(3)	1.383(6)	N(1)-C(1)-Ag(1)	127.7(4)
N(2)-C(5)	1.464(6)	N(2)-C(1)-Ag(1)	127.0(4)
N(3)-C(6)	1.361(7)	C(3)-C(2)-N(1)	107.2(4)
N(3)-C(7)	1.379(6)	C(3)-C(2)-Cl(1)	128.3(4)
N(3)-C(9)	1.446(7)	N(1)-C(2)-Cl(1)	124.4(4)
N(4)-C(6)	1.361(7)	C(2)-C(3)-N(2)	106.8(4)
N(4)-C(8)	1.384(7)	C(2)-C(3)-Cl(2)	130.2(4)
N(4)-C(10)	1.462(7)	N(2)-C(3)-Cl(2)	123.0(4)
C(2)-C(3)	1.349(7)	N(3)-C(6)-N(4)	105.2(4)
C(7)-C(8)	1.339(7)	N(3)-C(6)-Ag(1)	127.7(4)

Table M. Bond lengths [Å] and angles [°] for **2.6** (continued).

N(4)-C(6)-Ag(1)	127.0(4)
C(8)-C(7)-N(3)	107.3(5)
C(8)-C(7)-Cl(3)	129.1(4)
N(3)-C(7)-Cl(3)	123.6(4)
C(7)-C(8)-N(4)	107.3(4)
C(7)-C(8)-Cl(4)	128.6(4)
N(4)-C(8)-Cl(4)	124.0(4)

Table N. Anisotropic displacement parameters ( $\text{\AA}^2 \times 10^3$ ) for **2.6**. The anisotropic displacement factor exponent takes the form:  $-2\pi^2 [h^2 a^{*2} U^{11} + \dots + 2 h k a^* b^* U^{12}]$

	U <sup>11</sup>	U <sup>22</sup>	U <sup>33</sup>	U <sup>23</sup>	U <sup>13</sup>	U <sup>12</sup>
Ag(1)	18(1)	18(1)	12(1)	-1(1)	-1(1)	-2(1)
Cl(1)	22(1)	20(1)	24(1)	-5(1)	-2(1)	0(1)
Cl(2)	28(1)	24(1)	19(1)	-7(1)	-2(1)	-11(1)
Cl(3)	29(1)	30(1)	20(1)	-10(1)	-3(1)	-7(1)
Cl(4)	20(1)	21(1)	21(1)	-5(1)	0(1)	1(1)
O(1)	25(2)	20(2)	13(2)	1(1)	-2(1)	-3(2)
O(2)	33(2)	24(2)	26(2)	-1(2)	-2(2)	-15(2)
O(3)	25(2)	28(2)	23(2)	-10(2)	-8(2)	1(2)
O(4)	37(2)	27(2)	23(2)	-9(2)	-7(2)	-4(2)
O(5)	42(3)	42(3)	36(3)	-2(2)	13(2)	-14(2)
N(1)	21(2)	15(2)	15(2)	-2(2)	2(2)	-5(2)
N(2)	23(2)	15(2)	15(2)	-5(2)	2(2)	-4(2)
N(3)	23(2)	16(2)	11(2)	0(2)	3(2)	-2(2)
N(4)	24(2)	18(2)	11(2)	-3(2)	1(2)	-5(2)
N(5)	21(2)	17(2)	13(2)	-6(2)	-3(2)	2(2)
C(1)	21(2)	17(2)	11(2)	-4(2)	4(2)	-6(2)
C(2)	22(2)	15(2)	14(2)	0(2)	1(2)	-4(2)

Table N. Anisotropic displacement parameters ( $\text{\AA}^2 \times 10^3$ ) for **2.6** (continued).

C(3)	21(2)	18(2)	15(2)	-2(2)	-1(2)	-9(2)
C(4)	28(3)	18(2)	23(3)	-11(2)	1(2)	-5(2)
C(5)	30(3)	15(2)	26(3)	-8(2)	2(2)	-2(2)
C(6)	23(2)	18(2)	12(2)	-2(2)	3(2)	-5(2)
C(7)	20(2)	19(2)	13(2)	1(2)	-2(2)	-4(2)
C(8)	20(2)	20(2)	12(2)	-1(2)	2(2)	-3(2)
C(9)	29(3)	21(3)	21(3)	-6(2)	1(2)	-4(2)
C(10)	26(3)	23(3)	19(3)	-9(2)	0(2)	-3(2)

Table O. Hydrogen coordinates ( $\times 10^4$ ) and isotropic displacement parameters ( $\text{\AA}^2 \times 10^3$ ) for **2.6**.

	x	y	z	U(eq)
H(4A)	9018	3507	8151	34
H(4B)	10801	3978	7312	34
H(4C)	8303	4629	7174	34
H(5A)	6838	9011	8260	36
H(5B)	7715	8519	9307	36
H(5C)	5617	8135	9163	36
H(9A)	3715	6205	5066	36
H(9B)	2236	5314	5812	36
H(9C)	4279	5520	6164	36
H(10A)	1204	9374	7735	34
H(10B)	-679	10432	7125	34
H(10C)	1780	10374	6717	34

## APPENDIX D

### SUPPLEMENTARY MATERIAL FOR THE X-RAY CRYSTAL STRUCTURE OF

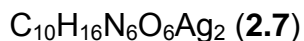


Table P. Crystal data and structure refinement for **2.7**.

Empirical formula	$\text{C}_{10}\text{H}_{16}\text{Ag}_2\text{N}_6\text{O}_6$	
Formula weight	532.03	
Temperature	100(2) K	
Wavelength	0.71073 Å	
Crystal system	Monoclinic	
Space group	P2(1)/m	
Unit cell dimensions	$a = 6.5678(9)$ Å	$\alpha = 90^\circ$ .
	$b = 15.329(2)$ Å	$\beta = 106.712(2)^\circ$ .
	$c = 8.2587(11)$ Å	$\gamma = 90^\circ$ .
Volume	796.35(18) Å <sup>3</sup>	
Z	2	
Density (calculated)	2.219 Mg/m <sup>3</sup>	
Absorption coefficient	2.501 mm <sup>-1</sup>	
F(000)	520	
Crystal size	0.35 x 0.17 x 0.03 mm <sup>3</sup>	
Theta range for data collection	2.57 to 28.28°.	
Index ranges	-8 ≤ h ≤ 8, -20 ≤ k ≤ 20, -10 ≤ l ≤ 10	
Reflections collected	6272	
Independent reflections	1983 [R(int) = 0.0519]	
Completeness to theta = 28.28°	97.1 %	
Absorption correction	Semi-empirical from equivalents	
Max. and min. transmission	0.9288 and 0.4748	

Table P. Crystal data and structure refinement for **2.7** (continued).

Refinement method	Full-matrix least-squares on $F^2$ Data /
restraints / parameters	1983 / 0 / 117
Goodness-of-fit on $F^2$	1.092
Final R indices [ $I > 2\sigma(I)$ ]	R1 = 0.0492, wR2 = 0.1549
R indices (all data)	R1 = 0.0509, wR2 = 0.1592
Largest diff. peak and hole	1.234 and -1.192 e/Å <sup>3</sup>

Table Q. Atomic coordinates ( $\times 10^4$ ) and equivalent isotropic displacement parameters (Å<sup>2</sup> $\times 10^3$ ) for **2.7**. U(eq) is defined as one third of the trace of the orthogonalized  $U_{ij}$  tensor.

	x	y	z	U(eq)
Ag(2)	12407(1)	2500	9049(1)	20(1)
Ag(1)	8186(1)	2500	8439(1)	15(1)
O(1)	15231(5)	3534(2)	9255(4)	24(1)
O(2)	12363(5)	4033(2)	7515(4)	31(1)
O(3)	15177(5)	4840(2)	8265(4)	29(1)
N(1)	10630(5)	3198(2)	12041(4)	17(1)
N(2)	6761(5)	3195(2)	4733(4)	21(1)
N(3)	14248(5)	4149(2)	8326(4)	19(1)
C(1)	10182(8)	2500	11000(7)	15(1)
C(2)	11305(6)	2942(3)	13700(5)	25(1)
C(3)	10319(8)	4104(3)	11463(6)	27(1)
C(4)	7126(8)	2500	5782(7)	19(1)
C(5)	6129(6)	2940(3)	3053(5)	24(1)
C(6)	7060(9)	4103(3)	5285(7)	37(1)



Table R. Bond lengths [Å] and angles [°] for **2.7**.

Ag(2)-O(1)	2.409(3)	C(4)-Ag(1)-C(1)	162.6(2)
Ag(2)-O(1)#1	2.409(3)	C(4)-Ag(1)-Ag(2)	102.18(14)
Ag(2)-C(1)	2.467(5)	C(1)-Ag(1)-Ag(2)	60.45(14)
Ag(2)-Ag(1)	2.6717(7)	N(3)-O(1)-Ag(2)	101.5(2)
Ag(1)-C(4)	2.102(5)	C(1)-N(1)-C(2)	110.9(3)
Ag(1)-C(1)	2.145(5)	C(1)-N(1)-C(3)	124.0(3)
O(1)-N(3)	1.269(4)	C(2)-N(1)-C(3)	125.0(4)
O(2)-N(3)	1.240(5)	C(4)-N(2)-C(5)	111.5(4)
O(3)-N(3)	1.230(4)	C(4)-N(2)-C(6)	124.7(4)
N(1)-C(1)	1.351(4)	C(5)-N(2)-C(6)	123.8(4)
N(1)-C(2)	1.371(5)	O(3)-N(3)-O(2)	122.1(4)
N(1)-C(3)	1.463(5)	O(3)-N(3)-O(1)	119.5(4)
N(2)-C(4)	1.350(5)	O(2)-N(3)-O(1)	118.4(3)
N(2)-C(5)	1.385(5)	N(1)-C(1)-N(1)#1	104.8(4)
N(2)-C(6)	1.460(6)	N(1)-C(1)-Ag(1)	125.9(2)
C(1)-N(1)#1	1.351(4)	N(1)#1-C(1)-Ag(1)	125.9(2)
C(2)-C(2)#1	1.354(10)	N(1)-C(1)-Ag(2)	110.7(3)
C(4)-N(2)#1	1.350(5)	N(1)#1-C(1)-Ag(2)	110.7(3)
C(5)-C(5)#1	1.349(9)	Ag(1)-C(1)-Ag(2)	70.41(15)
O(1)-Ag(2)-O(1)#1	82.32(13)	C(2)#1-C(2)-N(1)	106.7(2)
O(1)-Ag(2)-C(1)	122.87(10)	N(2)#1-C(4)-N(2)	104.2(5)
O(1)#1-Ag(2)-C(1)	122.87(10)	N(2)#1-C(4)-Ag(1)	127.9(2)
O(1)-Ag(2)-Ag(1)	138.56(6)	N(2)-C(4)-Ag(1)	127.9(2)
O(1)#1-Ag(2)-Ag(1)	138.56(7)	C(5)#1-C(5)-N(2)	106.4(2)
C(1)-Ag(2)-Ag(1)	49.14(12)		

---

Symmetry transformations used to generate equivalent atoms:  
#1 x, -y+1/2, z

Table S. Anisotropic displacement parameters ( $\text{\AA}^2 \times 10^3$ ) for **2.7**. The anisotropic displacement factor exponent takes the form:  $-2\pi^2 [h^2 a^{*2} U^{11} + \dots + 2 h k a^* b^* U^{12}]$

	U <sup>11</sup>	U <sup>22</sup>	U <sup>33</sup>	U <sup>23</sup>	U <sup>13</sup>	U <sup>12</sup>
Ag(2)	16(1)	22(1)	23(1)	0	7(1)	0
Ag(1)	14(1)	19(1)	11(1)	0	3(1)	0
O(1)	30(2)	24(2)	23(1)	8(1)	13(1)	9(1)
O(2)	26(2)	33(2)	29(2)	-2(1)	-1(1)	-1(1)
O(3)	42(2)	21(2)	29(2)	-3(1)	15(1)	-10(1)
N(1)	14(2)	20(2)	16(2)	-5(1)	4(1)	-2(1)
N(2)	18(2)	31(2)	13(2)	4(1)	5(1)	4(1)
N(3)	24(2)	20(2)	14(1)	-2(1)	9(1)	2(1)
C(1)	13(2)	13(2)	18(2)	0	3(2)	0
C(2)	17(2)	43(3)	17(2)	-7(2)	5(2)	-5(2)
C(3)	30(2)	14(2)	38(2)	-7(2)	9(2)	-9(2)
C(4)	17(3)	24(3)	16(2)	0	5(2)	0
C(5)	14(2)	43(2)	13(2)	3(2)	2(1)	7(2)
C(6)	55(3)	28(2)	29(2)	5(2)	12(2)	19(2)

Table T. Hydrogen coordinates ( $\times 10^4$ ) and isotropic displacement parameters ( $\text{\AA}^2 \times 10^3$ ) for **2.7**.

	x	y	z	U(eq)
H(6)	11696	3312	14663	31
H(5A)	11678	4415	11824	41
H(5B)	9293	4386	11952	41
H(5C)	9777	4116	10227	41
H(3)	5767	3311	2091	28
H(2A)	5671	4377	5142	56
H(2B)	7825	4416	4605	56
H(2C)	7886	4125	6480	56

## APPENDIX E

### SUPPLEMENTARY MATERIAL FOR THE X-RAY CRYSTAL STRUCTURE OF

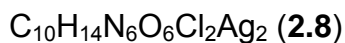


Table U. Crystal data and structure refinement for **2.8**.

Empirical formula	$\text{C}_{10}\text{H}_{14}\text{Ag}_2\text{Cl}_2\text{N}_6\text{O}_6$	
Formula weight	600.91	
Temperature	100(2) K	
Wavelength	0.71073 Å	
Crystal system	Monoclinic	
Space group	C2/c	
Unit cell dimensions	$a = 18.017(6)$ Å	$\alpha = 90^\circ$ .
	$b = 6.786(2)$ Å	$\beta = 122.812(5)^\circ$ .
	$c = 16.465(6)$ Å	$\gamma = 90^\circ$ .
Volume	$1692.0(10)$ Å <sup>3</sup>	
Z	4	
Density (calculated)	$2.359$ Mg/m <sup>3</sup>	
Absorption coefficient	$2.674$ mm <sup>-1</sup>	
F(000)	1168	
Crystal size	$0.09 \times 0.08 \times 0.07$ mm <sup>3</sup>	
Theta range for data collection	$2.71$ to $28.28^\circ$ .	
Index ranges	$-23 \leq h \leq 22$ , $-8 \leq k \leq 8$ , $-21 \leq l \leq 21$	
Reflections collected	7056	
Independent reflections	1978 [R(int) = 0.0277]	
Completeness to theta = $25.00^\circ$	99.5 %	
Absorption correction	Semi-empirical from equivalents	
Max. and min. transmission	0.8349 and 0.7948	

Table U. Crystal data and structure refinement for **2.8** (continued).

Refinement method	Full-matrix least-squares on F <sup>2</sup> Data /
restraints / parameters	1978 / 0 / 121
Goodness-of-fit on F <sup>2</sup>	1.075
Final R indices [I>2sigma(I)]	R1 = 0.0231, wR2 = 0.0568
R indices (all data)	R1 = 0.0271, wR2 = 0.0576Largest diff.
peak and hole	0.975 and -0.888 e/Å <sup>3</sup>

Table V. Atomic coordinates (x 10<sup>4</sup>) and equivalent isotropic displacement parameters (Å<sup>2</sup>x 10<sup>3</sup>) for **2.8**. U(eq) is defined as one third of the trace of the orthogonalized U<sub>ij</sub> tensor.

	x	y	z	U(eq)
Ag(1)	0	3832(1)	2500	15(1)
Ag(2)	0	7782(1)	2500	33(1)
Cl(1)	2971(1)	5537(1)	6375(1)	19(1)
O(1)	94(1)	10485(3)	3535(1)	28(1)
O(2)	-789(1)	8198(2)	3433(1)	23(1)
O(3)	-754(1)	11012(2)	4072(1)	27(1)
N(1)	1536(1)	4750(3)	4602(1)	15(1)
N(2)	2041(1)	4498(3)	3686(1)	14(1)
N(3)	-488(1)	9905(3)	3688(1)	17(1)
C(1)	1287(2)	4415(3)	3673(2)	15(1)
C(2)	2440(1)	5025(3)	5169(2)	15(1)
C(3)	2765(1)	4870(3)	4602(2)	15(1)
C(4)	936(2)	4764(4)	4941(2)	20(1)
C(5)	2083(2)	4325(3)	2828(2)	18(1)

Table W. Bond lengths [Å] and angles [°] for **2.8**.

Ag(1)-C(1)	2.100(2)	C(2)-N(1)-C(4)	125.87(19)
Ag(1)-C(1)#1	2.100(2)	C(1)-N(2)-C(3)	111.86(19)
Ag(1)-Ag(2)	2.6806(10)	C(1)-N(2)-C(5)	124.2(2)
Ag(2)-O(1)	2.446(2)	C(3)-N(2)-C(5)	123.9(2)
Ag(2)-O(1)#1	2.446(2)	O(3)-N(3)-O(2)	121.2(2)
Cl(1)-C(2)	1.708(2)	O(3)-N(3)-O(1)	120.4(2)
O(1)-N(3)	1.267(3)	O(2)-N(3)-O(1)	118.36(19)
O(2)-N(3)	1.251(3)	N(2)-C(1)-N(1)	105.12(19)
O(3)-N(3)	1.234(3)	N(2)-C(1)-Ag(1)	128.54(17)
N(1)-C(1)	1.360(3)	N(1)-C(1)-Ag(1)	126.32(17)
N(1)-C(2)	1.383(3)	C(3)-C(2)-N(1)	108.44(19)
N(1)-C(4)	1.459(3)	C(3)-C(2)-Cl(1)	129.81(18)
N(2)-C(1)	1.348(3)	N(1)-C(2)-Cl(1)	121.72(17)
N(2)-C(3)	1.381(3)	C(2)-C(3)-N(2)	105.2(2)
N(2)-C(5)	1.460(3)	C(2)-C(3)-H(3)	127.4
C(2)-C(3)	1.350(3)	N(2)-C(3)-H(3)	127.4
C(3)-H(3)	0.9500	N(1)-C(4)-H(4A)	109.5
C(4)-H(4A)	0.9800	N(1)-C(4)-H(4B)	109.5
C(4)-H(4B)	0.9800	H(4A)-C(4)-H(4B)	109.5
C(4)-H(4C)	0.9800	N(1)-C(4)-H(4C)	109.5
C(5)-H(5A)	0.9800	H(4A)-C(4)-H(4C)	109.5
C(5)-H(5B)	0.9800	H(4B)-C(4)-H(4C)	109.5
C(5)-H(5C)	0.9800	N(2)-C(5)-H(5A)	109.5
C(1)-Ag(1)-C(1)#1	158.29(12)	N(2)-C(5)-H(5B)	109.5
C(1)-Ag(1)-Ag(2)	79.14(6)	H(5A)-C(5)-H(5B)	109.5
C(1)#1-Ag(1)-Ag(2)	79.14(6)	N(2)-C(5)-H(5C)	109.5
O(1)-Ag(2)-O(1)#1	82.82(9)	H(5A)-C(5)-H(5C)	109.5
O(1)-Ag(2)-Ag(1)	138.59(4)	H(5B)-C(5)-H(5C)	109.5
O(1)#1-Ag(2)-Ag(1)	138.59(4)		
N(3)-O(1)-Ag(2)	98.81(14)		
C(1)-N(1)-C(2)	109.35(19)		
C(1)-N(1)-C(4)	124.76(19)		

---

Symmetry transformations used to  
generate equivalent atoms:  
#1 -x,y,-z+1/2

Table X. Anisotropic displacement parameters ( $\text{\AA}^2 \times 10^3$ ) for **2.8**. The anisotropic displacement factor exponent takes the form:  $-2\pi^2 [h^2 a^{*2} U^{11} + \dots + 2 h k a^* b^* U^{12}]$

	U <sup>11</sup>	U <sup>22</sup>	U <sup>33</sup>	U <sup>23</sup>	U <sup>13</sup>	U <sup>12</sup>
Ag(1)	14(1)	14(1)	14(1)	0	7(1)	0
Ag(2)	59(1)	16(1)	46(1)	0	44(1)	0
Cl(1)	23(1)	18(1)	12(1)	-1(1)	8(1)	1(1)
O(1)	27(1)	27(1)	40(1)	2(1)	24(1)	-3(1)
O(2)	28(1)	16(1)	23(1)	-2(1)	12(1)	-4(1)
O(3)	29(1)	26(1)	27(1)	-6(1)	17(1)	4(1)
N(1)	17(1)	14(1)	15(1)	1(1)	10(1)	0(1)
N(2)	16(1)	17(1)	12(1)	-2(1)	9(1)	-2(1)
N(3)	17(1)	17(1)	15(1)	1(1)	7(1)	1(1)
C(1)	18(1)	15(1)	13(1)	0(1)	9(1)	-1(1)
C(2)	16(1)	12(1)	13(1)	1(1)	6(1)	0(1)
C(3)	13(1)	14(1)	15(1)	-1(1)	5(1)	0(1)
C(4)	24(1)	24(1)	20(1)	-2(1)	16(1)	2(1)
C(5)	22(1)	20(1)	15(1)	-1(1)	13(1)	0(1)

Table Y. Hydrogen coordinates ( $\times 10^4$ ) and isotropic displacement parameters ( $\text{\AA}^2 \times 10^3$ ) for **2.8**.

	x	y	z	U(eq)
H(3)	3363	4991	4791	18
H(4A)	1118	3751	5438	31
H(4B)	334	4491	4398	31
H(4C)	954	6060	5214	31
H(5A)	1638	3377	2379	27
H(5B)	2671	3868	3016	27
H(5C)	1967	5613	2512	27

## APPENDIX F

### SUPPLEMENTARY MATERIAL FOR THE X-RAY CRYSTAL STRUCTURE OF

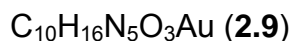


Table Z. Crystal data and structure refinement for **2.9**.

Empirical formula	$\text{C}_{10}\text{H}_{18}\text{AuN}_5\text{O}_4$	
Formula weight	469.26	
Temperature	100(2) K	
Wavelength	0.71073 Å	
Crystal system	Triclinic	
Space group	P-1	
Unit cell dimensions	$a = 6.9373(6)$ Å	$\alpha = 108.9990(10)^\circ$ .
	$b = 9.9372(9)$ Å	$\beta = 99.3050(10)^\circ$ .
	$c = 11.2032(10)$ Å	$\gamma = 97.1970(10)^\circ$ .
Volume	707.41(11) Å <sup>3</sup>	
Z	2	
Density (calculated)	2.203 Mg/m <sup>3</sup>	
Absorption coefficient	10.419 mm <sup>-1</sup>	
F(000)	448	
Crystal size	0.38 x 0.31 x 0.15 mm <sup>3</sup>	
Theta range for data collection	1.97 to 28.29°.	
Index ranges	$-9 \leq h \leq 8, -12 \leq k \leq 13, -14 \leq l \leq 14$	
Reflections collected	6044	
Independent reflections	3240 [R(int) = 0.0336]	
Completeness to theta = 28.29°	92.3 %	
Absorption correction	Semi-empirical from equivalents	
Refinement method	Full-matrix least-squares on F <sup>2</sup>	

Table Z. Crystal data and structure refinement for **2.9** (continued).

Data / restraints / parameters	3240 / 0 / 185
Goodness-of-fit on $F^2$	1.123
Final R indices [ $I > 2\sigma(I)$ ]	$R1 = 0.0311$ , $wR2 = 0.0793$
R indices (all data)	$R1 = 0.0322$ , $wR2 = 0.0801$
Largest diff. peak and hole	3.298 and -2.428 e/Å <sup>3</sup>

Table AA. Atomic coordinates ( $\times 10^4$ ) and equivalent isotropic displacement parameters (Å<sup>2</sup> $\times 10^3$ ) for **2.9**.  $U(\text{eq})$  is defined as one third of the trace of the orthogonalized  $U_{ij}$  tensor.

	x	y	z	$U(\text{eq})$
Au(1)	2478(1)	5132(1)	523(1)	13(1)
O(1)	2507(5)	2511(4)	3902(3)	21(1)
O(2)	-463(5)	2948(4)	4032(4)	25(1)
O(3)	240(6)	2002(5)	2159(4)	31(1)
O(4)	5585(6)	1655(4)	2518(4)	26(1)
N(1)	2178(6)	3525(5)	-2311(4)	14(1)
N(2)	2685(6)	2120(5)	-1244(4)	15(1)
N(3)	2475(6)	8201(5)	2240(4)	15(1)
N(4)	3026(6)	6880(5)	3387(4)	14(1)
N(5)	743(6)	2473(4)	3349(4)	17(1)
C(1)	2436(7)	3476(5)	-1102(5)	13(1)
C(2)	2259(8)	2188(6)	-3208(5)	19(1)
C(3)	2595(8)	1318(6)	-2523(5)	18(1)
C(4)	1902(8)	4798(5)	-2629(5)	18(1)
C(5)	3088(8)	1589(6)	-180(5)	22(1)
C(6)	2650(7)	6840(5)	2156(5)	14(1)
C(7)	3131(7)	8268(5)	4243(5)	17(1)
C(8)	2772(7)	9097(6)	3510(5)	18(1)
C(9)	2113(8)	8696(6)	1142(5)	19(1)
C(10)	3338(8)	5654(5)	3788(5)	17(1)



Table AB. Bond lengths [Å] and angles [°] for **2.9**.

Au(1)-C(1)	2.011(5)	C(2)-N(1)-C(4)	124.5(4)
Au(1)-C(6)	2.024(5)	C(1)-N(2)-C(3)	111.1(4)
O(1)-N(5)	1.269(5)	C(1)-N(2)-C(5)	124.2(4)
O(2)-N(5)	1.257(5)	C(3)-N(2)-C(5)	124.6(4)
O(3)-N(5)	1.234(5)	C(6)-N(3)-C(8)	110.9(4)
N(1)-C(1)	1.355(6)	C(6)-N(3)-C(9)	125.2(4)
N(1)-C(2)	1.395(7)	C(8)-N(3)-C(9)	123.8(4)
N(1)-C(4)	1.447(6)	C(6)-N(4)-C(7)	110.8(4)
N(2)-C(1)	1.342(6)	C(6)-N(4)-C(10)	125.4(4)
N(2)-C(3)	1.380(6)	C(7)-N(4)-C(10)	123.7(4)
N(2)-C(5)	1.454(7)	O(3)-N(5)-O(2)	120.8(4)
N(3)-C(6)	1.348(6)	O(3)-N(5)-O(1)	120.2(4)
N(3)-C(8)	1.376(6)	O(2)-N(5)-O(1)	119.0(4)
N(3)-C(9)	1.464(7)	N(2)-C(1)-N(1)	105.0(4)
N(4)-C(6)	1.348(6)	N(2)-C(1)-Au(1)	129.0(4)
N(4)-C(7)	1.385(6)	N(1)-C(1)-Au(1)	125.9(4)
N(4)-C(10)	1.457(6)	C(3)-C(2)-N(1)	105.9(4)
C(2)-C(3)	1.348(8)	C(2)-C(3)-N(2)	107.2(4)
C(7)-C(8)	1.357(7)	N(3)-C(6)-N(4)	105.2(4)
C(1)-Au(1)-C(6)	177.33(15)	N(3)-C(6)-Au(1)	126.8(4)
C(1)-N(1)-C(2)	110.7(4)	N(4)-C(6)-Au(1)	127.9(4)
C(1)-N(1)-C(4)	124.8(4)	C(8)-C(7)-N(4)	106.2(4)
		C(7)-C(8)-N(3)	106.8(4)

Table AC. Anisotropic displacement parameters ( $\text{\AA}^2 \times 10^3$ ) for **2.9**. The anisotropic displacement factor exponent takes the form:  $-2\pi^2 [h^2 a^{*2} U^{11} + \dots + 2 h k a^* b^* U^{12}]$

	U <sup>11</sup>	U <sup>22</sup>	U <sup>33</sup>	U <sup>23</sup>	U <sup>13</sup>	U <sup>12</sup>
Au(1)	16(1)	12(1)	12(1)	6(1)	1(1)	2(1)
O(1)	19(2)	20(2)	27(2)	13(2)	1(1)	4(1)
O(2)	23(2)	31(2)	24(2)	9(2)	9(1)	8(2)
O(3)	33(2)	42(2)	16(2)	7(2)	4(2)	9(2)
O(4)	27(2)	24(2)	26(2)	10(2)	3(2)	4(2)
N(1)	14(2)	15(2)	15(2)	9(2)	3(2)	3(2)
N(2)	20(2)	14(2)	13(2)	8(2)	2(2)	5(2)
N(3)	19(2)	13(2)	13(2)	7(2)	1(2)	2(2)
N(4)	14(2)	14(2)	14(2)	8(2)	2(1)	0(2)
N(5)	18(2)	15(2)	18(2)	9(2)	2(2)	3(2)
C(1)	12(2)	14(2)	15(2)	7(2)	1(2)	1(2)
C(2)	22(3)	20(3)	15(2)	6(2)	4(2)	5(2)
C(3)	25(3)	14(2)	16(2)	5(2)	5(2)	5(2)
C(4)	21(2)	16(2)	20(2)	11(2)	3(2)	2(2)
C(5)	29(3)	24(3)	21(3)	16(2)	8(2)	13(2)
C(6)	12(2)	13(2)	15(2)	7(2)	-1(2)	0(2)
C(7)	19(2)	15(2)	16(2)	5(2)	1(2)	0(2)
C(8)	19(2)	16(2)	17(2)	5(2)	4(2)	5(2)
C(9)	23(3)	19(3)	19(3)	12(2)	4(2)	6(2)
C(10)	22(2)	16(2)	15(2)	8(2)	0(2)	5(2)

Table AD. Hydrogen coordinates ( $\times 10^4$ ) and isotropic displacement parameters ( $\text{\AA}^2 \times 10^3$ ) for **2.9**.

	x	y	z	U(eq)
H(2)	2107	1941	-4116	22
H(3)	2742	336	-2857	22
H(4A)	889	5240	-2205	27
H(4B)	1468	4519	-3567	27
H(4C)	3162	5498	-2328	27
H(5A)	4481	1962	280	32
H(5B)	2841	527	-520	32
H(5C)	2215	1922	417	32
H(7)	3401	8577	5160	21
H(8)	2733	10102	3815	21
H(9A)	3371	9195	1063	28
H(9B)	1177	9364	1280	28
H(9C)	1549	7860	347	28
H(10A)	3154	4779	3021	26
H(10B)	2377	5508	4308	26
H(10C)	4692	5850	4304	26

## APPENDIX G

### SUPPLEMENTARY MATERIAL FOR THE X-RAY CRYSTAL STRUCTURE OF

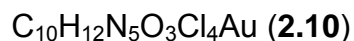


Table AE. Crystal data and structure refinement for **2.10**.

Empirical formula	$\text{C}_{10}\text{H}_{12}\text{AuCl}_4\text{N}_5\text{O}_3$	
Formula weight	589.01	
Temperature	100(2) K	
Wavelength	0.71073 Å	
Crystal system	Triclinic	
Space group	P-1	
Unit cell dimensions	$a = 7.656(3)$ Å	$\alpha = 98.774(6)^\circ$ .
	$b = 8.850(3)$ Å	$\beta = 96.074(6)^\circ$ .
	$c = 12.903(5)$ Å	$\gamma = 106.662(6)^\circ$ .
Volume	$817.4(5)$ Å <sup>3</sup>	
Z	2	
Density (calculated)	$2.393$ Mg/m <sup>3</sup>	
Absorption coefficient	$9.673$ mm <sup>-1</sup>	
F(000)	556	
Crystal size	$0.50 \times 0.22 \times 0.13$ mm <sup>3</sup>	
Theta range for data collection	$1.62$ to $26.30^\circ$ .	
Index ranges	$-9 \leq h \leq 9$ , $-11 \leq k \leq 11$ , $-15 \leq l \leq 16$	
Reflections collected	6542	
Independent reflections	3291 [ $R(\text{int}) = 0.0311$ ]	
Completeness to $\theta = 26.30^\circ$	99.0 %	
Absorption correction	Semi-empirical from equivalents	
Max. and min. transmission	0.2856 and 0.0667	

Table AE. Crystal data and structure refinement for **2.10** (continued).

Refinement method	Full-matrix least-squares on $F^2$ Data /
restraints / parameters	3291 / 0 / 212
Goodness-of-fit on $F^2$	1.064
Final R indices [ $I > 2\sigma(I)$ ]	R1 = 0.0248, wR2 = 0.0577
R indices (all data)	R1 = 0.0264, wR2 = 0.0584
Largest diff. peak and hole	1.322 and -1.067 e/Å <sup>3</sup>

Table AF. Atomic coordinates ( $\times 10^4$ ) and equivalent isotropic displacement parameters (Å<sup>2</sup> $\times 10^3$ ) for **2.10**. U(eq) is defined as one third of the trace of the orthogonalized  $U_{ij}$  tensor.

	x	y	z	U(eq)
Au(1)	4750(1)	48(1)	2316(1)	11(1)
Cl(1)	7730(2)	-2663(1)	5594(1)	17(1)
Cl(2)	9218(1)	1486(1)	6403(1)	16(1)
Cl(3)	577(1)	-1209(1)	-1844(1)	15(1)
Cl(4)	2041(1)	2946(1)	-936(1)	17(1)
O(1)	1011(4)	5375(4)	1732(2)	20(1)
O(2)	957(4)	4653(4)	3259(2)	17(1)
O(3)	-1530(4)	4885(4)	2402(2)	18(1)
N(1)	6210(4)	-1590(4)	3977(3)	11(1)
N(2)	7137(5)	1001(4)	4467(3)	11(1)
N(3)	2515(5)	-808(4)	111(3)	11(1)
N(4)	3371(5)	1760(4)	701(3)	14(1)
N(5)	142(5)	4969(4)	2465(3)	13(1)
C(1)	6105(5)	-201(5)	3660(3)	10(1)
C(2)	7290(5)	-1241(5)	4955(3)	12(1)
C(3)	7867(6)	358(5)	5262(3)	12(1)
C(4)	5374(6)	-3213(5)	3324(4)	17(1)
C(5)	7455(6)	2711(5)	4463(3)	15(1)
C(6)	3432(5)	358(5)	954(3)	12(1)
C(7)	1848(5)	-122(5)	-671(3)	12(1)

Table AF. Atomic coordinates ( $\times 10^4$ ) and equivalent isotropic displacement parameters ( $\text{\AA}^2 \times 10^3$ ) for **2.10** (continued).

C(8)	2390(6)	1475(5)	-309(3)	13(1)
C(9)	2301(6)	-2519(5)	24(4)	16(1)
C(10)	4082(6)	3335(5)	1400(3)	16(1)

---

Table AG. Bond lengths [Å] and angles [°] for **2.10**.

Au(1)-C(1)	2.001(4)	C(1)-N(2)-C(5)	124.1(3)
Au(1)-C(6)	2.028(4)	C(3)-N(2)-C(5)	126.1(4)
Cl(1)-C(2)	1.697(4)	C(6)-N(3)-C(7)	109.1(4)
Cl(2)-C(3)	1.694(4)	C(6)-N(3)-C(9)	125.6(4)
Cl(3)-C(7)	1.694(4)	C(7)-N(3)-C(9)	125.2(4)
Cl(4)-C(8)	1.702(4)	C(6)-N(4)-C(8)	109.3(4)
O(1)-N(5)	1.251(4)	C(6)-N(4)-C(10)	126.2(4)
O(2)-N(5)	1.253(5)	C(8)-N(4)-C(10)	124.4(4)
O(3)-N(5)	1.254(4)	O(1)-N(5)-O(2)	119.5(3)
N(1)-C(2)	1.373(5)	O(1)-N(5)-O(3)	120.0(4)
N(1)-C(1)	1.373(5)	O(2)-N(5)-O(3)	120.5(3)
N(1)-C(4)	1.474(5)	N(2)-C(1)-N(1)	104.9(3)
N(2)-C(1)	1.359(5)	N(2)-C(1)-Au(1)	126.5(3)
N(2)-C(3)	1.388(5)	N(1)-C(1)-Au(1)	128.6(3)
N(2)-C(5)	1.463(5)	C(3)-C(2)-N(1)	107.2(4)
N(3)-C(6)	1.350(5)	C(3)-C(2)-Cl(1)	129.3(3)
N(3)-C(7)	1.379(5)	N(1)-C(2)-Cl(1)	123.5(3)
N(3)-C(9)	1.462(5)	C(2)-C(3)-N(2)	107.7(4)
N(4)-C(6)	1.343(5)	C(2)-C(3)-Cl(2)	128.7(3)
N(4)-C(8)	1.382(6)	N(2)-C(3)-Cl(2)	123.6(3)
N(4)-C(10)	1.460(5)	N(4)-C(6)-N(3)	107.0(4)
C(2)-C(3)	1.337(6)	N(4)-C(6)-Au(1)	126.7(3)
C(7)-C(8)	1.345(6)	N(3)-C(6)-Au(1)	126.2(3)
C(1)-Au(1)-C(6)	178.43(15)	C(8)-C(7)-N(3)	107.3(4)
C(2)-N(1)-C(1)	110.4(3)	C(8)-C(7)-Cl(3)	129.6(3)
C(2)-N(1)-C(4)	125.1(4)	N(3)-C(7)-Cl(3)	123.0(3)
C(1)-N(1)-C(4)	124.4(4)	C(7)-C(8)-N(4)	107.2(4)
C(1)-N(2)-C(3)	109.8(3)	C(7)-C(8)-Cl(4)	128.8(4)
		N(4)-C(8)-Cl(4)	123.9(3)

Table AH. Anisotropic displacement parameters ( $\text{\AA}^2 \times 10^3$ ) for **2.10**. The anisotropic displacement factor exponent takes the form:  $-2\pi^2 [h^2 a^{*2} U^{11} + \dots + 2 h k a^* b^* U^{12}]$

	U <sup>11</sup>	U <sup>22</sup>	U <sup>33</sup>	U <sup>23</sup>	U <sup>13</sup>	U <sup>12</sup>
Au(1)	9(1)	13(1)	10(1)	3(1)	1(1)	4(1)
Cl(1)	19(1)	14(1)	21(1)	7(1)	0(1)	7(1)
Cl(2)	15(1)	16(1)	13(1)	1(1)	-2(1)	3(1)
Cl(3)	14(1)	17(1)	13(1)	3(1)	-1(1)	2(1)
Cl(4)	17(1)	14(1)	22(1)	8(1)	1(1)	6(1)
O(1)	20(2)	23(2)	19(2)	10(1)	7(1)	7(1)
O(2)	17(2)	16(2)	16(2)	6(1)	-6(1)	3(1)
O(3)	11(2)	21(2)	23(2)	3(1)	3(1)	7(1)
N(1)	8(2)	11(2)	13(2)	1(1)	-1(1)	3(1)
N(2)	11(2)	12(2)	13(2)	4(1)	1(1)	4(1)
N(3)	10(2)	11(2)	12(2)	3(1)	1(1)	4(1)
N(4)	10(2)	14(2)	16(2)	4(2)	-1(2)	2(1)
N(5)	13(2)	9(2)	16(2)	-1(2)	-3(2)	3(2)
C(1)	6(2)	15(2)	12(2)	6(2)	2(2)	5(2)
C(2)	10(2)	12(2)	12(2)	4(2)	-1(2)	3(2)
C(3)	11(2)	15(2)	11(2)	4(2)	1(2)	5(2)
C(4)	16(2)	13(2)	19(2)	-1(2)	-3(2)	2(2)
C(5)	17(2)	11(2)	16(2)	4(2)	1(2)	3(2)
C(6)	6(2)	12(2)	17(2)	0(2)	1(2)	2(2)
C(7)	9(2)	17(2)	12(2)	5(2)	3(2)	4(2)
C(8)	10(2)	12(2)	18(2)	4(2)	1(2)	3(2)
C(9)	18(2)	11(2)	19(2)	7(2)	5(2)	5(2)
C(10)	12(2)	15(2)	19(2)	-1(2)	0(2)	6(2)



Table AI. Hydrogen coordinates ( $\times 10^4$ ) and isotropic displacement parameters ( $\text{\AA}^2 \times 10^{-3}$ ) for **2.10**.

	x	y	z	U(eq)
H(4A)	4615	-3152	2680	26
H(4B)	4599	-3906	3732	26
H(4C)	6351	-3660	3128	26
H(5A)	8366	3066	4001	22
H(5B)	7918	3329	5187	22
H(5C)	6293	2882	4198	22
H(9A)	3120	-2673	609	23
H(9B)	2621	-2931	-655	23
H(9C)	1017	-3102	62	23
H(10A)	3049	3720	1574	23
H(10B)	4884	4095	1042	23
H(10C)	4792	3249	2055	23

## APPENDIX H

### SUPPLEMENTARY MATERIAL FOR THE X-RAY CRYSTAL STRUCTURE OF



Table AJ. Crystal data and structure refinement for **2.11**.

Empirical formula	$\text{C}_5\text{H}_9\text{AuCl}_4\text{N}_2$	
Formula weight	435.91	
Temperature	100(2) K	
Wavelength	0.71073 Å	
Crystal system	Monoclinic	
Space group	C2/c	
Unit cell dimensions	$a = 16.068(5)$ Å	$\alpha = 90^\circ$ .
	$b = 8.854(3)$ Å	$\beta = 101.700(4)^\circ$ .
	$c = 8.078(2)$ Å	$\gamma = 90^\circ$ .
Volume	$1125.5(6)$ Å <sup>3</sup>	
Z	4	
Density (calculated)	$2.573$ Mg/m <sup>3</sup>	
Absorption coefficient	$13.973$ mm <sup>-1</sup>	
F(000)	800	
Crystal size	$0.22 \times 0.11 \times 0.02$ mm <sup>3</sup>	
Theta range for data collection	$2.59$ to $26.29^\circ$ .	
Index ranges	$-20 \leq h \leq 20$ , $-11 \leq k \leq 11$ , $-10 \leq l \leq 10$	
Reflections collected	4105	
Independent reflections	1142 [ $R(\text{int}) = 0.0527$ ]	
Completeness to $\theta = 26.29^\circ$	99.7 %	
Absorption correction	Semi-empirical from equivalents	
Max. and min. transmission	0.7598 and 0.1475	

Table AJ. Crystal data and structure refinement for **2.11** (continued).

Refinement method	Full-matrix least-squares on $F^2$ Data /
restraints / parameters	1142 / 0 / 58
Goodness-of-fit on $F^2$	0.953
Final R indices [ $I > 2\sigma(I)$ ]	R1 = 0.0371, wR2 = 0.0907
R indices (all data)	R1 = 0.0471, wR2 = 0.0926
Largest diff. peak and hole	3.235 and -1.837 e/Å <sup>3</sup>

Table AK. Atomic coordinates ( $\times 10^4$ ) and equivalent isotropic displacement parameters (Å<sup>2</sup> $\times 10^3$ ) for **2.11**. U(eq) is defined as one third of the trace of the orthogonalized  $U_{ij}$  tensor.

	x	y	z	U(eq)
Au(1)	2500	2500	0	23(1)
Cl(1)	3933(2)	2943(2)	635(3)	29(1)
Cl(2)	2294(1)	4359(2)	1839(3)	30(1)
N(1)	5546(5)	2361(6)	8516(9)	24(2)
C(1)	5000	3229(12)	7500	27(3)
C(2)	5343(5)	863(8)	8126(10)	27(2)
C(3)	6255(6)	2880(9)	9838(11)	29(2)

Table AL. Bond lengths [Å] and angles [°] for **2.11**.

Au(1)-Cl(2)	2.2859(19)
Au(1)-Cl(2)#1	2.2860(19)
Au(1)-Cl(1)	2.288(2)
Au(1)-Cl(1)#1	2.288(2)
N(1)-C(1)	1.320(10)
N(1)-C(2)	1.386(9)
N(1)-C(3)	1.468(11)
C(1)-N(1)#2	1.320(10)
C(2)-C(2)#2	1.336(16)
Cl(2)-Au(1)-Cl(2)#1	180.00(7)
Cl(2)-Au(1)-Cl(1)	90.17(8)
Cl(2)#1-Au(1)-Cl(1)	89.83(8)
Cl(2)-Au(1)-Cl(1)#1	89.83(8)
Cl(2)#1-Au(1)-Cl(1)#1	90.17(8)
Cl(1)-Au(1)-Cl(1)#1	180.00(3)
C(1)-N(1)-C(2)	108.6(7)
C(1)-N(1)-C(3)	126.1(6)
C(2)-N(1)-C(3)	125.2(7)
N(1)#2-C(1)-N(1)	108.8(9)
C(2)#2-C(2)-N(1)	107.0(5)

Symmetry transformations used to generate equivalent atoms:

#1 -x+1/2,-y+1/2,-z #2 -x+1,y,-z+3/2

Table AM. Anisotropic displacement parameters (Å<sup>2</sup> × 10<sup>3</sup>) for **2.11**. The anisotropic displacement factor exponent takes the form:  $-2\pi^2 [h^2 a^{*2} U^{11} + \dots + 2 h k a^* b^* U^{12}]$

	U <sup>11</sup>	U <sup>22</sup>	U <sup>33</sup>	U <sup>23</sup>	U <sup>13</sup>	U <sup>12</sup>
Au(1)	30(1)	17(1)	26(1)	4(1)	12(1)	5(1)
Cl(1)	32(1)	22(1)	37(1)	2(1)	14(1)	4(1)
Cl(2)	38(1)	22(1)	33(1)	-2(1)	14(1)	6(1)

Table AM. Anisotropic displacement parameters ( $\text{\AA}^2 \times 10^3$ ) for **2.11** (continued).

N(1)	29(4)	17(3)	27(4)	1(2)	9(3)	3(3)
C(1)	47(8)	10(6)	28(6)	0	17(6)	0
C(2)	30(5)	14(4)	40(5)	3(3)	16(4)	3(3)
C(3)	26(5)	30(5)	28(4)	-3(3)	2(4)	-3(4)

Table AN. Hydrogen coordinates ( $\times 10^4$ ) and isotropic displacement parameters ( $\text{\AA}^2 \times 10^3$ ) for **2.11**.

	x	y	z	U(eq)
H(1)	5000	4302	7500	33
H(2)	5635	1	8650	32
H(3A)	6502	3796	9455	43
H(3B)	6690	2089	10070	43
H(3C)	6047	3101	10871	43

## APPENDIX I

### SUPPLEMENTARY MATERIAL FOR THE X-RAY CRYSTAL STRUCTURE OF

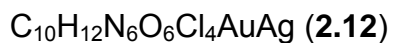


Table AO. Crystal data and structure refinement for **2.12**.

Empirical formula	$\text{C}_{10}\text{H}_{12}\text{AgAuCl}_4\text{N}_6\text{O}_6$	
Formula weight	758.89	
Temperature	100(2) K	
Wavelength	0.71073 Å	
Crystal system	Monoclinic	
Space group	C2/m	
Unit cell dimensions	$a = 37.071(8)$ Å	$\alpha = 90^\circ$ .
	$b = 6.2092(13)$ Å	$\beta = 100.532(4)^\circ$ .
	$c = 12.900(3)$ Å	$\gamma = 90^\circ$ .
Volume	$2919.4(11)$ Å <sup>3</sup>	
Z	6	
Density (calculated)	$2.590$ Mg/m <sup>3</sup>	
Absorption coefficient	$9.127$ mm <sup>-1</sup>	
F(000)	2136	
Crystal size	$0.27 \times 0.11 \times 0.09$ mm <sup>3</sup>	
Theta range for data collection	$1.12$ to $26.30^\circ$ .	
Index ranges	$-45 \leq h \leq 46$ , $-7 \leq k \leq 7$ , $-16 \leq l \leq 16$	
Reflections collected	11643	
Independent reflections	3231 [R(int) = 0.0458]	
Completeness to theta = $26.30^\circ$	99.4 %	
Absorption correction	Semi-empirical from equivalents	

Table AO. Crystal data and structure refinement for **2.12** (continued).

Max. and min. transmission	0.4939 and 0.1919
Refinement method	Full-matrix least-squares on F <sup>2</sup>
Data / restraints / parameters	3231 / 0 / 255
Goodness-of-fit on F <sup>2</sup>	1.074
Final R indices [I>2sigma(I)]	R1 = 0.0364, wR2 = 0.0835
R indices (all data)	R1 = 0.0423, wR2 = 0.0860
Largest diff. peak and hole	2.062 and -2.149 e/Å <sup>3</sup>

Table AP. Atomic coordinates (x 10<sup>4</sup>) and equivalent isotropic displacement parameters (Å<sup>2</sup> x 10<sup>3</sup>) for **2.12**. U(eq) is defined as one third of the trace of the orthogonalized U<sub>ij</sub> tensor.

	x	y	z	U(eq)
Au(1)	3262(1)	5000	8830(1)	11(1)
Au(2)	0	5000	5000	13(1)
Ag(1)	3349(1)	0	9107(1)	27(1)
Ag(2)	0	0	5000	19(1)
Cl(1)	4183(1)	5000	12917(2)	18(1)
Cl(2)	4745(1)	5000	11005(2)	20(1)
Cl(3)	2344(1)	5000	4728(2)	19(1)
Cl(4)	1784(1)	5000	6628(2)	24(1)
Cl(5)	1221(1)	5000	2847(2)	19(1)
Cl(6)	409(1)	5000	952(2)	21(1)
O(1)	3957(2)	0	10322(6)	26(2)
O(2)	3455(2)	0	10949(5)	21(1)
O(3)	3977(2)	0	12020(5)	29(2)
O(4)	2651(2)	0	8923(5)	29(2)
O(5)	2928(2)	0	7582(5)	20(1)
O(6)	2332(2)	0	7340(5)	26(2)
O(7)	578(2)	0	4869(5)	20(1)
O(8)	930(2)	0	3701(5)	24(2)
O(9)	331(2)	0	3205(5)	21(1)

Table AP. Atomic coordinates ( $\times 10^4$ ) and equivalent isotropic displacement parameters ( $\text{\AA}^2 \times 10^3$ ) for **2.12** (continued).

N(1)	3710(2)	5000	11062(5)	13(2)
N(2)	4051(2)	5000	9879(5)	13(2)
N(3)	2824(2)	5000	6596(5)	13(2)
N(4)	2470(2)	5000	7756(5)	14(2)
N(5)	3801(2)	0	11107(7)	20(2)
N(6)	2631(2)	0	7935(6)	23(2)
N(7)	680(2)	5000	3979(5)	10(1)
N(8)	182(2)	5000	2839(6)	12(2)
N(9)	612(2)	0	3885(5)	15(2)
C(1)	3702(2)	5000	10012(7)	16(2)
C(2)	4071(2)	5000	11579(7)	12(2)
C(3)	4281(2)	5000	10859(7)	14(2)
C(4)	3393(2)	5000	11572(7)	19(2)
C(5)	4158(3)	5000	8835(7)	22(2)
C(6)	2829(2)	5000	7631(6)	11(2)
C(7)	2459(2)	5000	6053(7)	16(2)
C(8)	2245(2)	5000	6773(7)	15(2)
C(9)	3144(2)	5000	6112(7)	20(2)
C(10)	2345(2)	5000	8769(7)	18(2)
C(11)	309(3)	5000	3884(7)	18(2)
C(12)	781(2)	5000	3019(6)	16(2)
C(13)	466(2)	5000	2282(7)	16(2)
C(14)	939(2)	5000	4986(7)	22(2)
C(15)	-211(2)	5000	2398(7)	19(2)



Table AQ. Bond lengths [Å] and angles [°] for **2.12**.

Au(1)-C(6)	2.016(8)	N(1)-C(2)	1.383(10)
Au(1)-C(1)	2.019(8)	N(1)-C(4)	1.450(11)
Au(1)-Ag(1)#1	3.1350(7)	N(2)-C(1)	1.335(11)
Au(1)-Ag(1)	3.1350(7)	N(2)-C(3)	1.389(10)
Au(2)-C(11)	1.997(9)	N(2)-C(5)	1.472(11)
Au(2)-C(11)#2	1.997(9)	N(3)-C(6)	1.332(11)
Au(2)-Ag(2)	3.1046(6)	N(3)-C(7)	1.403(11)
Au(2)-Ag(2)#1	3.1046(6)	N(3)-C(9)	1.439(11)
Ag(1)-O(5)	2.277(6)	N(4)-C(6)	1.370(11)
Ag(1)-O(2)	2.336(6)	N(4)-C(8)	1.385(10)
Ag(1)-O(1)	2.499(7)	N(4)-C(10)	1.463(11)
Ag(1)-O(4)	2.557(8)	N(7)-C(12)	1.357(11)
Ag(1)-Au(1)#3	3.1350(7)	N(7)-C(11)	1.359(11)
Ag(2)-O(7)	2.178(6)	N(7)-C(14)	1.467(10)
Ag(2)-O(7)#4	2.178(6)	N(8)-C(11)	1.346(11)
Ag(2)-Au(2)#3	3.1046(6)	N(8)-C(13)	1.380(11)
Cl(1)-C(2)	1.700(9)	N(8)-C(15)	1.464(10)
Cl(2)-C(3)	1.696(9)	C(2)-C(3)	1.314(12)
Cl(3)-C(7)	1.685(9)	C(7)-C(8)	1.327(13)
Cl(4)-C(8)	1.687(8)	C(12)-C(13)	1.363(11)
Cl(5)-C(12)	1.688(9)	C(6)-Au(1)-C(1)	179.0(3)
Cl(6)-C(13)	1.690(9)	C(6)-Au(1)-Ag(1)#1	97.958(16)
O(1)-N(5)	1.256(10)	C(1)-Au(1)-Ag(1)#1	82.055(16)
O(2)-N(5)	1.261(10)	C(6)-Au(1)-Ag(1)	97.958(16)
O(3)-N(5)	1.239(10)	C(1)-Au(1)-Ag(1)	82.055(16)
O(4)-N(6)	1.264(10)	Ag(1)#1-Au(1)-Ag(1)	164.02(3)
O(5)-N(6)	1.267(10)	C(11)-Au(2)-C(11)#2	180.0(4)
O(6)-N(6)	1.227(10)	C(11)-Au(2)-Ag(2)	90.0
O(7)-N(9)	1.299(9)	C(11)#2-Au(2)-Ag(2)	90.000(1)
O(8)-N(9)	1.242(9)	C(11)-Au(2)-Ag(2)#1	90.0
O(9)-N(9)	1.234(9)	C(11)#2-Au(2)-Ag(2)#1	90.000(1)
N(1)-C(1)	1.348(11)	Ag(2)-Au(2)-Ag(2)#1	180.0
		O(5)-Ag(1)-O(2)	147.1(2)
		O(5)-Ag(1)-O(1)	159.9(2)
		O(2)-Ag(1)-O(1)	53.0(2)

Table AQ. Bond lengths [Å] and angles [°] for **2.12** (continued).

O(5)-Ag(1)-O(4)	52.9(2)	C(6)-N(4)-C(8)	109.1(7)
O(2)-Ag(1)-O(4)	94.2(2)	C(6)-N(4)-C(10)	125.3(7)
O(1)-Ag(1)-O(4)	147.2(2)	C(8)-N(4)-C(10)	125.6(7)
O(5)-Ag(1)-Au(1)#3	82.034(15)	O(3)-N(5)-O(1)	121.7(8)
O(2)-Ag(1)-Au(1)#3	96.36(2)	O(3)-N(5)-O(2)	119.9(8)
O(1)-Ag(1)-Au(1)#3	97.682(17)	O(1)-N(5)-O(2)	118.4(8)
O(4)-Ag(1)-Au(1)#3	84.74(2)	O(6)-N(6)-O(4)	120.7(9)
O(5)-Ag(1)-Au(1)	82.034(15)	O(6)-N(6)-O(5)	121.4(8)
O(2)-Ag(1)-Au(1)	96.36(2)	O(4)-N(6)-O(5)	117.9(8)
O(1)-Ag(1)-Au(1)	97.682(17)	C(12)-N(7)-C(11)	111.1(7)
O(4)-Ag(1)-Au(1)	84.74(2)	C(12)-N(7)-C(14)	124.4(7)
Au(1)#3-Ag(1)-Au(1)	164.02(3)	C(11)-N(7)-C(14)	124.5(7)
O(7)-Ag(2)-O(7)#4	180.00(3)	C(11)-N(8)-C(13)	111.1(7)
O(7)-Ag(2)-Au(2)	90.0	C(11)-N(8)-C(15)	122.1(8)
O(7)#4-Ag(2)-Au(2)	90.0	C(13)-N(8)-C(15)	126.8(7)
O(7)-Ag(2)-Au(2)#3	90.0	O(9)-N(9)-O(8)	124.8(7)
O(7)#4-Ag(2)-Au(2)#3	90.0	O(9)-N(9)-O(7)	118.2(7)
Au(2)-Ag(2)-Au(2)#3	180.0	O(8)-N(9)-O(7)	116.9(7)
N(5)-O(1)-Ag(1)	90.5(5)	N(2)-C(1)-N(1)	106.6(7)
N(5)-O(2)-Ag(1)	98.1(5)	N(2)-C(1)-Au(1)	124.7(6)
N(6)-O(4)-Ag(1)	88.0(6)	N(1)-C(1)-Au(1)	128.7(6)
N(6)-O(5)-Ag(1)	101.2(5)	C(3)-C(2)-N(1)	107.7(8)
N(9)-O(7)-Ag(2)	110.5(5)	C(3)-C(2)-Cl(1)	130.7(7)
C(1)-N(1)-C(2)	109.0(7)	N(1)-C(2)-Cl(1)	121.6(7)
C(1)-N(1)-C(4)	125.8(7)	C(2)-C(3)-N(2)	107.5(8)
C(2)-N(1)-C(4)	125.2(7)	C(2)-C(3)-Cl(2)	129.7(7)
C(1)-N(2)-C(3)	109.2(7)	N(2)-C(3)-Cl(2)	122.8(7)
C(1)-N(2)-C(5)	123.2(7)	N(3)-C(6)-N(4)	106.4(7)
C(3)-N(2)-C(5)	127.6(7)	N(3)-C(6)-Au(1)	129.3(6)
C(6)-N(3)-C(7)	109.7(7)	N(4)-C(6)-Au(1)	124.4(6)
C(6)-N(3)-C(9)	124.9(7)	C(8)-C(7)-N(3)	107.2(7)
C(7)-N(3)-C(9)	125.4(7)	C(8)-C(7)-Cl(3)	129.4(7)
		N(3)-C(7)-Cl(3)	123.3(7)
		C(7)-C(8)-N(4)	107.7(7)

Table AQ. Bond lengths [Å] and angles [°] for **2.12** (continued).

C(7)-C(8)-Cl(4)	130.4(7)
N(4)-C(8)-Cl(4)	122.0(7)
N(8)-C(11)-N(7)	104.7(7)
N(8)-C(11)-Au(2)	125.4(7)
N(7)-C(11)-Au(2)	129.8(6)
N(7)-C(12)-C(13)	107.1(8)
N(7)-C(12)-Cl(5)	123.6(6)

C(13)-C(12)-Cl(5)	129.3(7)
C(12)-C(13)-N(8)	106.0(7)
C(12)-C(13)-Cl(6)	129.8(7)
N(8)-C(13)-Cl(6)	124.2(6)

Symmetry transformations used to generate equivalent atoms:

#1 x,y+1,z #2 -x,-y+1,-z+1 #3  
x,y-1,z #4 -x,-y,-z+1

Table AR. Anisotropic displacement parameters (Å<sup>2</sup> × 10<sup>3</sup>) for **2.12**. The anisotropic displacement factor exponent takes the form:  $-2\pi^2 [h^2 a^{*2} U^{11} + \dots + 2 h k a^* b^* U^{12}]$

	U <sup>11</sup>	U <sup>22</sup>	U <sup>33</sup>	U <sup>23</sup>	U <sup>13</sup>	U <sup>12</sup>
Au(1)	8(1)	13(1)	10(1)	0	-4(1)	0
Au(2)	11(1)	15(1)	12(1)	0	-1(1)	0
Ag(1)	30(1)	29(1)	19(1)	0	-3(1)	0
Ag(2)	15(1)	22(1)	19(1)	0	-1(1)	0
Cl(1)	17(1)	24(1)	12(1)	0	-4(1)	0
Cl(2)	8(1)	29(1)	22(1)	0	-2(1)	0
Cl(3)	28(1)	15(1)	10(1)	0	-6(1)	0
Cl(4)	10(1)	37(1)	22(1)	0	-6(1)	0
Cl(5)	11(1)	22(1)	23(1)	0	1(1)	0
Cl(6)	22(1)	28(1)	12(1)	0	0(1)	0
O(1)	24(4)	26(4)	35(4)	0	18(3)	0
O(2)	13(3)	29(4)	20(3)	0	1(3)	0
O(3)	21(4)	28(4)	28(4)	0	-18(3)	0
O(4)	40(4)	32(4)	14(3)	0	2(3)	0
O(5)	23(4)	24(3)	13(3)	0	4(3)	0
O(6)	26(4)	31(4)	17(3)	0	-10(3)	0
O(7)	20(3)	29(4)	9(3)	0	0(3)	0
O(8)	21(4)	30(4)	24(4)	0	8(3)	0

Table AR. Anisotropic displacement parameters ( $\text{\AA}^2 \times 10^3$ ) for **2.12** (continued).

O(9)	21(3)	21(3)	15(3)	0	-14(3)	0
N(1)	9(4)	18(4)	10(3)	0	-2(3)	0
N(2)	12(4)	18(4)	9(4)	0	-2(3)	0
N(3)	13(4)	14(4)	10(3)	0	-3(3)	0
N(4)	16(4)	15(4)	10(4)	0	-2(3)	0
N(5)	22(4)	9(4)	28(4)	0	0(4)	0
N(6)	41(5)	11(4)	20(4)	0	12(4)	0
N(7)	5(3)	10(3)	12(4)	0	-5(3)	0
N(8)	5(3)	6(3)	20(4)	0	-8(3)	0
N(9)	19(4)	15(4)	9(4)	0	-1(3)	0
C(1)	12(4)	15(4)	18(5)	0	-3(4)	0
C(2)	7(4)	11(4)	14(4)	0	-9(3)	0
C(3)	10(4)	18(5)	12(4)	0	-5(3)	0
C(4)	18(5)	27(5)	13(4)	0	4(4)	0
C(5)	20(5)	26(5)	21(5)	0	7(4)	0
C(6)	10(4)	12(4)	10(4)	0	-4(3)	0
C(7)	16(5)	18(5)	9(4)	0	-11(3)	0
C(8)	5(4)	15(4)	22(5)	0	-2(3)	0
C(9)	15(5)	28(5)	19(5)	0	6(4)	0
C(10)	13(4)	24(5)	14(4)	0	-2(3)	0
C(11)	22(5)	21(5)	12(4)	0	1(4)	0
C(12)	16(5)	20(5)	9(4)	0	-2(3)	0
C(13)	14(4)	17(4)	14(4)	0	-2(3)	0
C(14)	13(5)	35(6)	16(5)	0	-5(4)	0
C(15)	9(4)	27(5)	19(5)	0	-4(4)	0

Table AS. Hydrogen coordinates ( $\times 10^4$ ) and isotropic displacement parameters ( $\text{\AA}^2 \times 10^3$ ) for **2.12**.

	x	y	z	U(eq)
H(4A)	3168	5000	11035	29
H(4B)	3398	6289	12013	29
H(4C)	3398	3711	12013	29
H(5A)	3938	5000	8285	33
H(5B)	4304	3711	8763	33
H(5C)	4304	6289	8763	33
H(9A)	3365	5000	6661	30
H(9B)	3143	6289	5673	30
H(9C)	3143	3711	5673	30
H(10A)	2558	5000	9344	26
H(10B)	2197	3711	8820	26
H(10C)	2197	6289	8820	26
H(14A)	1191	5000	4853	33
H(14B)	899	3711	5390	33
H(14C)	899	6289	5390	33
H(15A)	-351	5000	2973	29
H(15B)	-273	3711	1963	29
H(15C)	-273	6289	1963	29

## APPENDIX J

### SUPPLEMENTARY MATERIAL FOR THE X-RAY CRYSTAL STRUCTURE OF

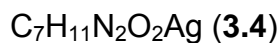


Table AT. Crystal data and structure refinement for **3.4**.

Empirical formula	C <sub>7</sub> H <sub>11</sub> AgN <sub>2</sub> O <sub>2</sub>	
Formula weight	263.05	
Temperature	100(2) K	
Wavelength	0.71073 Å	
Crystal system	Triclinic	
Space group	P-1	
Unit cell dimensions	a = 10.508(2) Å	α = 95.984(4)°.
	b = 10.521(2) Å	β = 96.090(4)°.
	c = 12.881(3) Å	γ = 93.974(4)°.
Volume	1403.7(5) Å <sup>3</sup>	
Z	6	
Density (calculated)	1.867 Mg/m <sup>3</sup>	
Absorption coefficient	2.117 mm <sup>-1</sup>	
F(000)	780	
Crystal size	0.11 x 0.05 x 0.04 mm <sup>3</sup>	
Theta range for data collection	1.60 to 26.29°.	
Index ranges	-13 ≤ h ≤ 13, -13 ≤ k ≤ 13, -16 ≤ l ≤ 16	
Reflections collected	11234	
Independent reflections	5611 [R(int) = 0.0320]	
Completeness to theta = 26.29°	98.7 %	
Absorption correction	Semi-empirical from equivalents	
Max. and min. transmission	0.9201 and 0.8005	

Table AT. Crystal data and structure refinement for **3.4** (continued).

Refinement method	Full-matrix least-squares on $F^2$ Data /
restraints / parameters	5611 / 0 / 344
Goodness-of-fit on $F^2$	1.015
Final R indices [ $I > 2\sigma(I)$ ]	R1 = 0.0486, wR2 = 0.1040
R indices (all data)	R1 = 0.0700, wR2 = 0.1091
Largest diff. peak and hole	1.001 and -0.787 e/Å <sup>3</sup>

Table AU. Atomic coordinates ( $\times 10^4$ ) and equivalent isotropic displacement parameters (Å<sup>2</sup> $\times 10^3$ ) for **3.4**. U(eq) is defined as one third of the trace of the orthogonalized  $U_{ij}$  tensor.

	x	y	z	U(eq)
Ag(1A)	4628(1)	1312(1)	3526(1)	25(1)
Ag(1B)	4014(1)	1689(1)	3092(1)	22(1)
Ag(2)	10438(1)	7053(1)	4819(1)	26(1)
Ag(3)	8526(1)	3467(1)	9619(1)	23(1)
O(1)	5141(4)	-327(4)	2506(3)	40(1)
O(2)	3763(4)	609(4)	1491(3)	38(1)
O(3)	11934(3)	6874(4)	6019(3)	29(1)
O(4)	10731(4)	8169(4)	6883(3)	31(1)
O(5)	7206(3)	4872(4)	9864(3)	27(1)
O(6)	6856(4)	4403(4)	8136(3)	30(1)
N(1)	4995(5)	2976(4)	5489(4)	34(1)
N(2)	3390(4)	3700(4)	4680(3)	25(1)
N(3)	8811(4)	6391(4)	2685(3)	27(1)
N(4)	8179(4)	8024(4)	3521(3)	26(1)
N(5)	10815(4)	1868(4)	10105(3)	20(1)
N(6)	9792(4)	1191(4)	8618(3)	26(1)
C(1)	4203(6)	2803(5)	4577(5)	38(2)
C(2)	4671(5)	3976(6)	6140(4)	32(1)
C(3)	3657(5)	4450(5)	5629(4)	25(1)
C(4)	6049(7)	2193(8)	5769(9)	93(4)
C(5)	2352(6)	3896(10)	3865(6)	72(3)

Table AU. Atomic coordinates ( $\times 10^4$ ) and equivalent isotropic displacement parameters ( $\text{\AA}^2 \times 10^3$ ) for **3.4** (continued).

C(6)	9056(5)	7162(5)	3575(4)	25(1)
C(7)	7792(5)	6736(6)	2057(4)	30(1)
C(8)	7404(5)	7770(6)	2580(5)	34(1)
C(9)	9571(6)	5299(5)	2399(4)	35(1)
C(10)	8077(6)	9110(6)	4291(5)	35(1)
C(11)	9803(5)	2087(5)	9452(4)	21(1)
C(12)	11434(5)	827(5)	9710(4)	26(1)
C(13)	10784(5)	392(5)	8772(4)	29(1)
C(14)	11175(5)	2567(5)	11154(4)	27(1)
C(15)	8830(6)	1014(6)	7701(4)	37(2)
C(16)	4471(5)	-287(5)	1634(4)	29(1)
C(17)	4526(5)	-1326(5)	777(4)	29(1)
C(18)	11708(5)	7561(5)	6838(4)	22(1)
C(19)	12690(5)	7602(6)	7796(4)	30(1)
C(20)	6630(5)	5003(5)	8966(4)	26(1)
C(21)	5611(5)	5926(6)	8922(5)	33(1)

Table AV. Bond lengths [ $\text{\AA}$ ] and angles [ $^\circ$ ] for **3.4**.

Ag(1A)-C(1)	2.068(6)	O(6)-C(20)	1.238(6)
Ag(1A)-O(1)	2.190(4)	N(1)-C(1)	1.354(8)
Ag(1B)-C(1)	2.120(6)	N(1)-C(2)	1.361(7)
Ag(1B)-O(2)	2.229(4)	N(1)-C(4)	1.462(8)
Ag(2)-C(6)	2.064(5)	N(2)-C(1)	1.322(7)
Ag(2)-O(3)	2.117(4)	N(2)-C(3)	1.375(7)
Ag(3)-C(11)	2.054(5)	N(2)-C(5)	1.473(7)
Ag(3)-O(5)	2.118(4)	N(3)-C(6)	1.324(7)
O(1)-C(16)	1.267(7)	N(3)-C(7)	1.366(7)
O(2)-C(16)	1.257(7)	N(3)-C(9)	1.482(7)
O(3)-C(18)	1.269(6)	N(4)-C(6)	1.339(7)
O(4)-C(18)	1.249(6)	N(4)-C(8)	1.377(7)
O(5)-C(20)	1.273(6)	N(4)-C(10)	1.450(7)



Table AV. Bond lengths [Å] and angles [°] for **3.4** (continued).

N(5)-C(11)	1.333(6)	C(11)-N(5)-C(12)	111.9(5)
N(5)-C(12)	1.391(6)	C(11)-N(5)-C(14)	124.3(4)
N(5)-C(14)	1.468(6)	C(12)-N(5)-C(14)	123.7(4)
N(6)-C(11)	1.352(7)	C(11)-N(6)-C(13)	111.1(4)
N(6)-C(13)	1.395(7)	C(11)-N(6)-C(15)	125.2(5)
N(6)-C(15)	1.458(7)	C(13)-N(6)-C(15)	123.6(5)
C(2)-C(3)	1.345(8)	N(2)-C(1)-N(1)	104.6(5)
C(7)-C(8)	1.331(8)	N(2)-C(1)-Ag(1A)	141.5(5)
C(12)-C(13)	1.342(8)	N(1)-C(1)-Ag(1A)	114.0(5)
C(16)-C(17)	1.479(7)	N(2)-C(1)-Ag(1B)	115.7(5)
C(18)-C(19)	1.518(7)	N(1)-C(1)-Ag(1B)	139.5(5)
C(20)-C(21)	1.496(7)	Ag(1A)-C(1)-Ag(1B)	26.02(8)
C(1)-Ag(1A)-O(1)	176.0(2)	C(3)-C(2)-N(1)	106.7(5)
C(1)-Ag(1B)-O(2)	176.8(2)	C(2)-C(3)-N(2)	106.1(5)
C(6)-Ag(2)-O(3)	175.97(18)	N(3)-C(6)-N(4)	105.2(5)
C(11)-Ag(3)-O(5)	177.35(17)	N(3)-C(6)-Ag(2)	128.4(4)
C(16)-O(1)-Ag(1A)	104.8(4)	N(4)-C(6)-Ag(2)	126.4(4)
C(16)-O(2)-Ag(1B)	100.8(4)	C(8)-C(7)-N(3)	105.4(5)
C(18)-O(3)-Ag(2)	107.5(3)	C(7)-C(8)-N(4)	107.8(5)
C(20)-O(5)-Ag(3)	106.8(3)	N(5)-C(11)-N(6)	104.5(4)
C(1)-N(1)-C(2)	110.9(5)	N(5)-C(11)-Ag(3)	129.3(4)
C(1)-N(1)-C(4)	125.6(7)	N(6)-C(11)-Ag(3)	126.2(4)
C(2)-N(1)-C(4)	123.4(6)	C(13)-C(12)-N(5)	106.3(5)
C(1)-N(2)-C(3)	111.7(5)	C(12)-C(13)-N(6)	106.2(5)
C(1)-N(2)-C(5)	124.1(6)	O(2)-C(16)-O(1)	121.3(5)
C(3)-N(2)-C(5)	124.2(6)	O(2)-C(16)-C(17)	120.0(5)
C(6)-N(3)-C(7)	112.0(5)	O(1)-C(16)-C(17)	118.7(5)
C(6)-N(3)-C(9)	123.8(5)	O(4)-C(18)-O(3)	123.3(5)
C(7)-N(3)-C(9)	124.1(5)	O(4)-C(18)-C(19)	120.3(5)
C(6)-N(4)-C(8)	109.5(5)	O(3)-C(18)-C(19)	116.3(5)
C(6)-N(4)-C(10)	126.5(5)	O(6)-C(20)-O(5)	123.8(5)
C(8)-N(4)-C(10)	123.9(5)	O(6)-C(20)-C(21)	118.6(5)
		O(5)-C(20)-C(21)	117.6(5)

Table AW Anisotropic displacement parameters ( $\text{\AA}^2 \times 10^3$ ) for **3.4**. The anisotropic displacement factor exponent takes the form:  $-2\pi^2 [h^2 a^{*2} U^{11} + \dots + 2 h k a^* b^* U^{12}]$

	U <sup>11</sup>	U <sup>22</sup>	U <sup>33</sup>	U <sup>23</sup>	U <sup>13</sup>	U <sup>12</sup>
Ag(1A)	33(1)	21(1)	21(1)	-3(1)	5(1)	6(1)
Ag(1B)	24(1)	21(1)	21(1)	-1(1)	4(1)	6(1)
Ag(2)	27(1)	30(1)	20(1)	0(1)	1(1)	4(1)
Ag(3)	22(1)	26(1)	23(1)	7(1)	3(1)	9(1)
O(1)	53(3)	38(3)	25(2)	-7(2)	-4(2)	7(2)
O(2)	31(2)	35(2)	46(3)	-14(2)	9(2)	10(2)
O(3)	31(2)	35(2)	23(2)	-1(2)	2(2)	14(2)
O(4)	30(2)	37(2)	28(2)	-1(2)	2(2)	16(2)
O(5)	27(2)	36(2)	19(2)	3(2)	3(2)	16(2)
O(6)	30(2)	33(2)	26(2)	6(2)	-3(2)	8(2)
N(1)	28(3)	25(3)	53(3)	17(2)	15(2)	12(2)
N(2)	24(2)	31(3)	17(2)	5(2)	-1(2)	-8(2)
N(3)	29(3)	27(3)	24(2)	7(2)	2(2)	-2(2)
N(4)	22(2)	26(3)	30(2)	9(2)	1(2)	-4(2)
N(5)	18(2)	14(2)	30(2)	6(2)	4(2)	3(2)
N(6)	25(2)	27(3)	26(2)	5(2)	5(2)	-4(2)
C(1)	48(4)	22(3)	46(4)	-4(3)	29(3)	-9(3)
C(2)	28(3)	49(4)	19(3)	6(3)	6(2)	-4(3)
C(3)	28(3)	20(3)	26(3)	-3(2)	8(2)	3(2)
C(4)	51(5)	82(6)	178(10)	91(7)	61(6)	48(5)
C(5)	32(4)	138(8)	47(4)	46(5)	-13(3)	-19(5)
C(6)	30(3)	20(3)	25(3)	7(2)	3(2)	-4(2)
C(7)	31(3)	36(3)	21(3)	10(2)	-2(2)	-8(3)
C(8)	23(3)	37(4)	42(4)	18(3)	-4(3)	-3(3)
C(9)	48(4)	25(3)	30(3)	1(3)	3(3)	1(3)
C(10)	37(3)	30(3)	41(4)	6(3)	11(3)	5(3)

Table AW Anisotropic displacement parameters ( $\text{\AA}^2 \times 10^3$ ) for **3.4** (continued).

C(11)	20(3)	18(3)	27(3)	8(2)	5(2)	0(2)
C(12)	26(3)	17(3)	37(3)	10(2)	11(2)	7(2)
C(13)	37(3)	16(3)	36(3)	2(2)	16(3)	3(2)
C(14)	19(3)	35(3)	24(3)	2(2)	-4(2)	2(2)
C(15)	40(4)	40(4)	29(3)	3(3)	7(3)	-8(3)
C(16)	24(3)	25(3)	36(3)	-5(2)	15(3)	-5(2)
C(17)	28(3)	27(3)	30(3)	-7(2)	3(2)	4(2)
C(18)	24(3)	23(3)	20(3)	7(2)	3(2)	1(2)
C(19)	26(3)	42(4)	21(3)	-3(2)	-1(2)	2(3)
C(20)	22(3)	23(3)	33(3)	3(2)	10(2)	1(2)
C(21)	25(3)	33(3)	45(4)	9(3)	7(3)	14(3)

Table AX. Hydrogen coordinates ( $\times 10^4$ ) and isotropic displacement parameters ( $\text{\AA}^2 \times 10^3$ ) for **3.4**.

	x	y	z	U(eq)
H(2)	5080	4281	6822	38
H(3)	3215	5160	5874	30
H(4A)	6225	1652	5142	139
H(4B)	5808	1650	6302	139
H(4C)	6819	2753	6050	139
H(5A)	1938	3063	3547	108
H(5B)	2710	4352	3322	108
H(5C)	1717	4404	4183	108
H(7)	7435	6325	1387	36
H(8)	6715	8247	2347	41
H(9A)	10450	5621	2322	52
H(9B)	9176	4827	1734	52
H(9C)	9590	4726	2953	52
H(10A)	8522	8961	4971	53
H(10B)	7169	9213	4363	53

Table AX. Hydrogen coordinates ( $\times 10^4$ ) and isotropic displacement parameters ( $\text{\AA}^2 \times 10^3$ ) for **3.4** (continued).

H(10C)	8470	9888	4061	53
H(12)	12171	491	10039	31
H(13)	10964	-317	8307	35
H(14A)	11148	3490	11111	40
H(14B)	12046	2387	11417	40
H(14C)	10573	2292	11633	40
H(15A)	8245	258	7741	55
H(15B)	9257	892	7062	55
H(15C)	8342	1774	7685	55
H(17A)	5356	-1236	498	44
H(17B)	3833	-1273	215	44
H(17C)	4426	-2158	1051	44
H(19A)	13336	8321	7799	45
H(19B)	13109	6798	7774	45
H(19C)	12259	7715	8434	45
H(21A)	5521	6236	8228	50
H(21B)	5850	6654	9463	50
H(21C)	4793	5494	9045	50

## APPENDIX K

### SUPPLEMENTARY MATERIAL FOR THE X-RAY CRYSTAL STRUCTURE OF

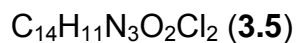


Table AY. Crystal data and structure refinement for **3.5**.

Empirical formula	$\text{C}_{14}\text{H}_{11}\text{Cl}_2\text{N}_3\text{O}_2$	
Formula weight	324.16	
Temperature	100(2) K	
Wavelength	0.71073 Å	
Crystal system	Triclinic	
Space group	P-1	
Unit cell dimensions	$a = 7.443(4)$ Å	$\alpha = 77.313(7)^\circ$ .
	$b = 7.880(4)$ Å	$\beta = 76.201(8)^\circ$ .
	$c = 12.360(6)$ Å	$\gamma = 84.818(8)^\circ$ .
Volume	$686.3(6)$ Å <sup>3</sup>	
Z	2	
Density (calculated)	1.569 Mg/m <sup>3</sup>	
Absorption coefficient	0.480 mm <sup>-1</sup>	
F(000)	332	
Crystal size	0.16 x 0.08 x 0.04 mm <sup>3</sup>	
Theta range for data collection	1.73 to 27.30°.	
Index ranges	$-9 \leq h \leq 9$ , $-10 \leq k \leq 10$ , $-15 \leq l \leq 15$	
Reflections collected	5725	
Independent reflections	2994 [R(int) = 0.0419]	
Completeness to theta = 27.30°	96.9 %	
Absorption correction	Semi-empirical from equivalents	
Max. and min. transmission	0.9810 and 0.9271	

Table AY. Crystal data and structure refinement for **3.5** (continued).

Refinement method	Full-matrix least-squares on F <sup>2</sup> Data /
restraints / parameters	2994 / 0 / 253
Goodness-of-fit on F <sup>2</sup>	1.000
Final R indices [I>2sigma(I)]	R1 = 0.0512, wR2 = 0.1339
R indices (all data)	R1 = 0.0638, wR2 = 0.1389
Largest diff. peak and hole	0.498 and -0.481 e/Å <sup>3</sup>

Table AZ. Atomic coordinates (x 10<sup>4</sup>) and equivalent isotropic displacement parameters (Å<sup>2</sup> x 10<sup>3</sup>) for **3.5**. U(eq) is defined as one third of the trace of the orthogonalized U<sub>ij</sub> tensor.

	x	y	z	U(eq)
Cl(1)	11867(1)	3201(1)	-623(1)	35(1)
Cl(2A)	7186(2)	3030(2)	-749(1)	28(1)
Cl(2B)	9470(5)	387(7)	1822(4)	26(1)
O(1)	4759(2)	6178(2)	2660(1)	28(1)
O(2)	2888(2)	1307(2)	5354(1)	28(1)
N(1)	4042(2)	3476(2)	3817(1)	21(1)
N(2A)	7464(4)	977(3)	1251(2)	22(1)
N(3A)	10415(5)	1055(4)	1332(3)	26(1)
N(2B)	6894(8)	1689(7)	611(4)	22(1)
N(3B)	8468(11)	3448(7)	-921(5)	29(2)
C(1)	3963(3)	5300(3)	3544(2)	21(1)
C(2)	3018(3)	2837(3)	4914(2)	22(1)
C(3)	2177(3)	4385(3)	5382(2)	21(1)
C(4)	2742(3)	5865(2)	4561(2)	20(1)
C(5)	2166(3)	7514(3)	4742(2)	24(1)
C(6)	994(3)	7632(3)	5794(2)	27(1)
C(7)	453(3)	6155(3)	6618(2)	25(1)
C(8)	1042(3)	4501(3)	6421(2)	24(1)
C(9)	5203(3)	2393(3)	3089(2)	25(1)
C(10)	4284(3)	1979(3)	2201(2)	24(1)
C(11)	5439(3)	657(3)	1564(2)	33(1)

Table AZ. Atomic coordinates ( $\times 10^4$ ) and equivalent isotropic displacement parameters ( $\text{\AA}^2 \times 10^3$ ) for **3.5** (continued).

C(12A)	8351(7)	2083(6)	279(4)	24(1)
C(13A)	10102(5)	2106(5)	345(3)	25(1)
C(14A)	8805(9)	379(14)	1877(10)	25(2)
C(12B)	8645(14)	1620(11)	735(8)	24(2)
C(13B)	9591(11)	2740(9)	-226(7)	27(2)
C(14B)	6690(20)	2850(20)	-388(11)	44(4)

Table BA. Bond lengths [ $\text{\AA}$ ] and angles [ $^\circ$ ] for **3.5**.

		C(3)-C(4)	1.390(3)
		C(4)-C(5)	1.380(3)
		C(5)-C(6)	1.398(3)
		C(5)-H(5)	0.9500
		C(6)-C(7)	1.387(3)
		C(6)-H(6)	0.9500
		C(7)-C(8)	1.392(3)
		C(7)-H(7)	0.9500
		C(8)-H(8)	0.9500
		C(9)-C(10)	1.527(3)
		C(9)-H(9A)	0.9900
		C(9)-H(9B)	0.9900
		C(10)-C(11)	1.523(3)
		C(10)-H(10A)	0.9900
		C(10)-H(10B)	0.9900
		C(11)-H(1)	0.94(3)
		C(11)-H(2)	0.98(3)
		C(12A)-C(13A)	1.327(7)
		C(14A)-H(14A)	0.9500
		C(12B)-C(13B)	1.392(11)
		C(14B)-H(14B)	0.9500
		C(13B)-Cl(1)-C(13A)	31.1(3)
		C(2)-N(1)-C(1)	111.77(17)
		C(2)-N(1)-C(9)	124.16(17)
		C(1)-N(1)-C(9)	123.80(17)
Cl(1)-C(13B)	1.697(8)		
Cl(1)-C(13A)	1.704(4)		
Cl(2A)-C(12A)	1.708(5)		
Cl(2B)-C(12B)	1.684(12)		
O(1)-C(1)	1.207(2)		
O(2)-C(2)	1.211(2)		
N(1)-C(2)	1.396(3)		
N(1)-C(1)	1.402(3)		
N(1)-C(9)	1.456(3)		
N(2A)-C(12A)	1.380(5)		
N(2A)-C(14A)	1.393(9)		
N(2A)-C(11)	1.494(4)		
N(3A)-C(14A)	1.321(8)		
N(3A)-C(13A)	1.373(6)		
N(2B)-C(12B)	1.343(12)		
N(2B)-C(14B)	1.397(16)		
N(2B)-C(11)	1.533(6)		
N(3B)-C(13B)	1.340(11)		
N(3B)-C(14B)	1.401(14)		
C(1)-C(4)	1.494(3)		
C(2)-C(3)	1.488(3)		
C(3)-C(8)	1.375(3)		

Table BA. Bond lengths [Å] and angles [°] for **3.5** (continued).

C(12A)-N(2A)-C(14A)	105.8(5)	N(1)-C(9)-C(10)	113.69(18)
C(12A)-N(2A)-C(11)	124.9(3)	N(1)-C(9)-H(9A)	108.8
C(14A)-N(2A)-C(11)	129.2(5)	C(10)-C(9)-H(9A)	108.8
C(14A)-N(3A)-C(13A)	105.5(6)	N(1)-C(9)-H(9B)	108.8
C(12B)-N(2B)-C(14B)	110.9(9)	C(10)-C(9)-H(9B)	108.8
C(12B)-N(2B)-C(11)	118.8(6)	H(9A)-C(9)-H(9B)	107.7
C(14B)-N(2B)-C(11)	130.1(8)	C(11)-C(10)-C(9)	111.82(19)
C(13B)-N(3B)-C(14B)	107.2(9)	C(11)-C(10)-H(10A)	109.3
O(1)-C(1)-N(1)	125.10(19)	C(9)-C(10)-H(10A)	109.3
O(1)-C(1)-C(4)	129.16(18)	C(11)-C(10)-H(10B)	109.3
N(1)-C(1)-C(4)	105.73(16)	C(9)-C(10)-H(10B)	109.3
O(2)-C(2)-N(1)	124.45(19)	H(10A)-C(10)-H(10B)	107.9
O(2)-C(2)-C(3)	129.27(19)	N(2A)-C(11)-C(10)	113.26(18)
N(1)-C(2)-C(3)	106.28(16)	N(2A)-C(11)-N(2B)	39.4(2)
C(8)-C(3)-C(4)	121.36(19)	C(10)-C(11)-N(2B)	106.3(2)
C(8)-C(3)-C(2)	130.61(18)	N(2A)-C(11)-H(1)	117.8(15)
C(4)-C(3)-C(2)	108.03(18)	C(10)-C(11)-H(1)	113.2(15)
C(5)-C(4)-C(3)	121.7(2)	N(2B)-C(11)-H(1)	88.9(14)
C(5)-C(4)-C(1)	130.13(18)	N(2A)-C(11)-H(2)	96.2(17)
C(3)-C(4)-C(1)	108.18(17)	C(10)-C(11)-H(2)	111.1(17)
C(4)-C(5)-C(6)	116.98(19)	N(2B)-C(11)-H(2)	131.4(17)
C(4)-C(5)-H(5)	121.5	H(1)-C(11)-H(2)	103(2)
C(6)-C(5)-H(5)	121.5	C(13A)-C(12A)-N(2A)	106.9(5)
C(7)-C(6)-C(5)	121.30(19)	C(13A)-C(12A)-Cl(2A)	132.8(4)
C(7)-C(6)-H(6)	119.3	N(2A)-C(12A)-Cl(2A)	120.3(4)
C(5)-C(6)-H(6)	119.3	C(12A)-C(13A)-N(3A)	111.4(4)
C(6)-C(7)-C(8)	121.0(2)	C(12A)-C(13A)-Cl(1)	128.2(4)
C(6)-C(7)-H(7)	119.5	N(3A)-C(13A)-Cl(1)	120.4(3)
C(8)-C(7)-H(7)	119.5	N(3A)-C(14A)-N(2A)	110.4(8)
C(3)-C(8)-C(7)	117.68(18)	N(3A)-C(14A)-H(14A)	124.8
C(3)-C(8)-H(8)	121.2	N(2A)-C(14A)-H(14A)	124.8
C(7)-C(8)-H(8)	121.2	N(2B)-C(12B)-C(13B)	105.1(10)
		N(2B)-C(12B)-Cl(2B)	126.1(7)
		C(13B)-C(12B)-Cl(2B)	128.8(8)
		N(3B)-C(13B)-C(12B)	111.2(8)



Table BA. Bond lengths [Å] and angles [°] for **3.5** (continued).

N(3B)-C(13B)-Cl(1)	119.3(5)
C(12B)-C(13B)-Cl(1)	129.5(8)

N(2B)-C(14B)-N(3B)	105.5(12)
N(2B)-C(14B)-H(14B)	127.2
N(3B)-C(14B)-H(14B)	127.3

Table BB. Anisotropic displacement parameters ( $\text{\AA}^2 \times 10^3$ ) for **3.5**. The anisotropic displacement factor exponent takes the form:  $-2\pi^2 [h^2 a^{*2} U^{11} + \dots + 2 h k a^* b^* U^{12}]$

	U <sup>11</sup>	U <sup>22</sup>	U <sup>33</sup>	U <sup>23</sup>	U <sup>13</sup>	U <sup>12</sup>
Cl(1)	33(1)	35(1)	36(1)	-16(1)	6(1)	-8(1)
Cl(2A)	33(1)	31(1)	22(1)	-9(1)	-7(1)	3(1)
Cl(2B)	34(2)	26(1)	21(1)	-12(1)	-3(2)	-2(2)
O(1)	35(1)	29(1)	20(1)	-5(1)	-3(1)	-4(1)
O(2)	37(1)	18(1)	28(1)	-6(1)	-6(1)	0(1)
N(1)	26(1)	20(1)	19(1)	-9(1)	-4(1)	1(1)
N(2A)	26(2)	23(1)	16(2)	-9(1)	1(1)	-1(1)
N(3A)	34(2)	25(2)	22(2)	-12(1)	-5(2)	5(2)
N(2B)	30(4)	22(3)	13(3)	-7(2)	-2(2)	0(2)
N(3B)	33(4)	23(3)	27(3)	-11(2)	1(3)	1(3)
C(1)	25(1)	24(1)	20(1)	-9(1)	-8(1)	-1(1)
C(2)	25(1)	23(1)	19(1)	-7(1)	-7(1)	-2(1)
C(3)	26(1)	20(1)	19(1)	-8(1)	-8(1)	-2(1)
C(4)	24(1)	21(1)	19(1)	-8(1)	-7(1)	-3(1)
C(5)	30(1)	20(1)	27(1)	-8(1)	-9(1)	-3(1)
C(6)	31(1)	23(1)	33(1)	-17(1)	-10(1)	0(1)
C(7)	27(1)	32(1)	22(1)	-15(1)	-5(1)	-1(1)
C(8)	30(1)	24(1)	19(1)	-7(1)	-6(1)	-4(1)
C(9)	26(1)	26(1)	26(1)	-14(1)	-4(1)	3(1)
C(10)	28(1)	27(1)	18(1)	-10(1)	-3(1)	0(1)
C(11)	33(1)	33(1)	35(1)	-22(1)	7(1)	-11(1)
C(12A)	37(3)	18(2)	16(2)	-9(2)	-1(2)	-1(2)

Table BB. Anisotropic displacement parameters ( $\text{\AA}^2 \times 10^3$ ) for **3.5** (continued).

C(13A)	31(2)	24(2)	21(2)	-14(2)	-1(2)	0(2)
C(14A)	34(5)	19(2)	20(2)	-9(2)	3(4)	-2(4)
C(12B)	39(6)	19(4)	12(5)	-8(3)	6(4)	-4(4)
C(13B)	29(4)	24(3)	24(4)	-7(3)	9(4)	-3(3)
C(14B)	45(7)	51(7)	34(8)	-28(7)	20(5)	-19(5)

Table BC. Hydrogen coordinates ( $\times 10^4$ ) and isotropic displacement parameters ( $\text{\AA}^2 \times 10^3$ ) for **3.5**.

	x	y	z	U(eq)
H(5)	2549	8524	4178	29
H(6)	561	8746	5946	32
H(7)	-332	6275	7328	30
H(8)	672	3487	6984	29
H(9A)	5536	1286	3571	30
H(9B)	6363	2993	2693	30
H(10A)	3049	1514	2583	29
H(10B)	4105	3065	1650	29
H(14A)	8592	-403	2595	30
H(14B)	5584	3171	-650	53
H(1)	4900(30)	400(30)	1010(20)	33(7)
H(2)	5530(40)	-470(40)	2070(20)	52(8)

## APPENDIX L

### SUPPLEMENTARY MATERIAL FOR THE X-RAY CRYSTAL STRUCTURE OF

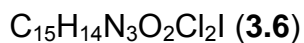


Table BD. Crystal data and structure refinement for **3.6**.

Empirical formula	$\text{C}_{15}\text{H}_{14}\text{Cl}_2\text{IN}_3\text{O}_2$	
Formula weight	466.09	
Temperature	100(2) K	
Wavelength	0.71073 Å	
Crystal system	Triclinic	
Space group	P-1	
Unit cell dimensions	$a = 8.056(2)$ Å	$\alpha = 108.092(4)^\circ$ .
	$b = 8.669(2)$ Å	$\beta = 96.705(4)^\circ$ .
	$c = 13.128(3)$ Å	$\gamma = 97.150(4)^\circ$ .
Volume	$852.9(4)$ Å <sup>3</sup>	
Z	2	
Density (calculated)	1.815 Mg/m <sup>3</sup>	
Absorption coefficient	2.202 mm <sup>-1</sup>	
F(000)	456	
Crystal size	0.17 x 0.08 x 0.04 mm <sup>3</sup>	
Theta range for data collection	1.65 to 28.27°.	
Index ranges	-10 ≤ h ≤ 10, -11 ≤ k ≤ 11, -16 ≤ l ≤ 17	
Reflections collected	7290	
Independent reflections	3843 [R(int) = 0.0231]	
Completeness to theta = 28.27°	90.6 %	
Absorption correction	Semi-empirical from equivalents	
Max. and min. transmission	0.916 and 0.6843	

Table BD. Crystal data and structure refinement for **3.6** (continued).

Refinement method	Full-matrix least-squares on $F^2$ Data /
restraints / parameters	3843 / 0 / 209
Goodness-of-fit on $F^2$	1.057
Final R indices [ $I > 2\sigma(I)$ ]	R1 = 0.0283, wR2 = 0.0731
R indices (all data)	R1 = 0.0340, wR2 = 0.0749
Largest diff. peak and hole	0.700 and -0.843 e/Å <sup>3</sup>

Table BE. Atomic coordinates ( $\times 10^4$ ) and equivalent isotropic displacement parameters (Å<sup>2</sup> $\times 10^3$ ) for **3.6**. U(eq) is defined as one third of the trace of the orthogonalized  $U_{ij}$  tensor.

	x	y	z	U(eq)
I(1)	3119(1)	2562(1)	6387(1)	23(1)
O(1)	5943(2)	9482(2)	7548(2)	20(1)
O(2)	945(2)	8639(2)	8780(2)	21(1)
N(1)	1243(3)	8114(3)	2960(2)	17(1)
N(2)	2470(3)	7455(3)	4290(2)	16(1)
N(3)	3286(3)	8723(3)	7923(2)	15(1)
C(1)	2016(4)	8692(3)	3991(2)	17(1)
C(2)	1191(3)	6427(3)	2596(2)	15(1)
C(3)	1966(3)	6013(3)	3420(2)	16(1)
C(4)	430(4)	9067(4)	2367(2)	20(1)
C(5)	3308(3)	7607(4)	5389(2)	17(1)
C(6)	2040(4)	6990(4)	6010(2)	19(1)
C(7)	2858(4)	7066(3)	7134(2)	18(1)
C(8)	4833(3)	9765(3)	8095(2)	17(1)
C(9)	4815(3)	11212(3)	9069(2)	15(1)
C(10)	3288(3)	10951(3)	9450(2)	16(1)
C(11)	2313(3)	9345(3)	8729(2)	16(1)
C(12)	6026(4)	12595(3)	9610(2)	19(1)
C(13)	5662(4)	13727(3)	10543(2)	19(1)
C(14)	4136(4)	13467(4)	10912(2)	19(1)
C(15)	2918(4)	12067(3)	10372(2)	18(1)

Table BE. Atomic coordinates ( $\times 10^4$ ) and equivalent isotropic displacement parameters ( $\text{\AA}^2 \times 10^3$ ) for **3.6** (continued).

Cl(1)	271(1)	5224(1)	1322(1)	20(1)
Cl(2)	2356(1)	4158(1)	3457(1)	20(1)

Table BF. Bond lengths [ $\text{\AA}$ ] and angles [ $^\circ$ ] for **3.6**.

		C(1)-N(2)-C(3)	108.6(2)
		C(1)-N(2)-C(5)	125.0(2)
		C(3)-N(2)-C(5)	126.3(2)
O(1)-C(8)	1.213(3)	C(8)-N(3)-C(11)	111.4(2)
O(2)-C(11)	1.211(3)	C(8)-N(3)-C(7)	124.3(2)
N(1)-C(1)	1.333(4)	C(11)-N(3)-C(7)	123.4(2)
N(1)-C(2)	1.383(4)	N(2)-C(1)-N(1)	109.3(2)
N(1)-C(4)	1.460(3)	C(3)-C(2)-N(1)	107.8(2)
N(2)-C(1)	1.328(4)	C(3)-C(2)-Cl(1)	129.9(2)
N(2)-C(3)	1.382(3)	N(1)-C(2)-Cl(1)	122.3(2)
N(2)-C(5)	1.479(3)	C(2)-C(3)-N(2)	106.6(2)
N(3)-C(8)	1.395(4)	C(2)-C(3)-Cl(2)	129.9(2)
N(3)-C(11)	1.403(3)	N(2)-C(3)-Cl(2)	123.4(2)
N(3)-C(7)	1.458(3)	N(2)-C(5)-C(6)	110.6(2)
C(2)-C(3)	1.352(4)	C(7)-C(6)-C(5)	112.5(2)
C(2)-Cl(1)	1.693(3)	N(3)-C(7)-C(6)	114.2(2)
C(3)-Cl(2)	1.691(3)	O(1)-C(8)-N(3)	124.9(3)
C(5)-C(6)	1.524(4)	O(1)-C(8)-C(9)	128.9(3)
C(6)-C(7)	1.523(4)	N(3)-C(8)-C(9)	106.2(2)
C(8)-C(9)	1.491(4)	C(12)-C(9)-C(10)	121.0(3)
C(9)-C(12)	1.383(4)	C(12)-C(9)-C(8)	131.0(3)
C(9)-C(10)	1.400(4)	C(10)-C(9)-C(8)	108.0(2)
C(10)-C(15)	1.385(4)	C(15)-C(10)-C(9)	121.7(3)
C(10)-C(11)	1.479(4)	C(15)-C(10)-C(11)	130.5(3)
C(12)-C(13)	1.399(4)	C(9)-C(10)-C(11)	107.8(2)
C(13)-C(14)	1.391(4)	O(2)-C(11)-N(3)	124.0(3)
C(14)-C(15)	1.395(4)	O(2)-C(11)-C(10)	129.4(3)
C(1)-N(1)-C(2)	107.6(2)	N(3)-C(11)-C(10)	106.6(2)
C(1)-N(1)-C(4)	125.7(2)	C(9)-C(12)-C(13)	117.6(3)
C(2)-N(1)-C(4)	126.3(2)	C(14)-C(13)-C(12)	121.1(3)

Table BF. Bond lengths [Å] and angles [°] for **3.6** (continued).

C(13)-C(14)-C(15) 121.4(3)

C(10)-C(15)-C(14) 117.2(3)

Table BG. Anisotropic displacement parameters ( $\text{\AA}^2 \times 10^3$ ) for **3.6**. The anisotropic displacement factor exponent takes the form:  $-2\pi^2 [h^2 a^{*2} U^{11} + \dots + 2 h k a^* b^* U^{12}]$

	U <sup>11</sup>	U <sup>22</sup>	U <sup>33</sup>	U <sup>23</sup>	U <sup>13</sup>	U <sup>12</sup>
I(1)	25(1)	17(1)	26(1)	4(1)	12(1)	-1(1)
O(1)	17(1)	26(1)	18(1)	8(1)	7(1)	3(1)
O(2)	16(1)	21(1)	26(1)	10(1)	6(1)	0(1)
N(1)	15(1)	19(1)	20(1)	9(1)	5(1)	3(1)
N(2)	15(1)	17(1)	15(1)	6(1)	4(1)	1(1)
N(3)	15(1)	16(1)	16(1)	7(1)	3(1)	2(1)
C(1)	18(1)	17(1)	17(1)	6(1)	4(1)	1(1)
C(2)	13(1)	17(1)	15(1)	7(1)	5(1)	-1(1)
C(3)	16(1)	17(1)	17(1)	8(1)	4(1)	1(1)
C(4)	17(1)	22(2)	27(2)	16(1)	4(1)	5(1)
C(5)	14(1)	24(2)	14(1)	8(1)	0(1)	-1(1)
C(6)	16(1)	23(1)	18(1)	8(1)	4(1)	-1(1)
C(7)	22(2)	14(1)	17(1)	5(1)	5(1)	-3(1)
C(8)	17(1)	21(1)	16(1)	12(1)	1(1)	3(1)
C(9)	15(1)	18(1)	15(1)	10(1)	2(1)	4(1)
C(10)	14(1)	19(1)	16(1)	9(1)	3(1)	1(1)
C(11)	14(1)	20(1)	17(1)	12(1)	1(1)	3(1)
C(12)	14(1)	26(2)	19(1)	12(1)	3(1)	1(1)
C(13)	20(2)	19(1)	17(1)	8(1)	1(1)	1(1)
C(14)	20(2)	21(1)	17(1)	8(1)	4(1)	4(1)
C(15)	15(1)	24(2)	18(1)	9(1)	4(1)	5(1)
Cl(1)	19(1)	23(1)	15(1)	6(1)	1(1)	-2(1)
Cl(2)	23(1)	17(1)	24(1)	10(1)	6(1)	3(1)

Table BH. Hydrogen coordinates ( $\times 10^4$ ) and isotropic displacement parameters ( $\text{\AA}^2 \times 10^3$ ) for **3.6**.

	x	y	z	U(eq)
H(1)	2210	9813	4442	21
H(4A)	-802	8828	2325	30
H(4B)	711	8769	1632	30
H(4C)	837	10245	2747	30
H(5A)	3802	8774	5791	21
H(5B)	4241	6957	5329	21
H(6A)	1128	7666	6086	23
H(6B)	1514	5838	5587	23
H(7A)	2074	6382	7413	22
H(7B)	3906	6579	7067	22
H(12)	7069	12771	9357	22
H(13)	6471	14689	10931	22
H(14)	3920	14258	11546	23
H(15)	1878	11887	10625	22

## APPENDIX M

### SUPPLEMENTARY MATERIAL FOR THE X-RAY CRYSTAL STRUCTURE OF

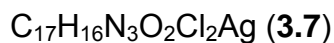


Table BI. Crystal data and structure refinement for **3.7**.

Empirical formula	$\text{C}_{17}\text{H}_{16}\text{AgCl}_2\text{N}_3\text{O}_4$	
Formula weight	505.10	
Temperature	100(2) K	
Wavelength	0.71073 Å	
Crystal system	Triclinic	
Space group	P-1	
Unit cell dimensions	$a = 11.897(4)$ Å	$\alpha = 78.521(6)^\circ$ .
	$b = 12.585(5)$ Å	$\beta = 68.000(6)^\circ$ .
	$c = 14.912(5)$ Å	$\gamma = 66.388(6)^\circ$ .
Volume	$1893.7(12)$ Å <sup>3</sup>	
Z	4	
Density (calculated)	$1.772$ Mg/m <sup>3</sup>	
Absorption coefficient	$1.375$ mm <sup>-1</sup>	
F(000)	1008	
Crystal size	$0.16 \times 0.12 \times 0.09$ mm <sup>3</sup>	
Theta range for data collection	$1.48$ to $26.30^\circ$ .	
Index ranges	$-14 \leq h \leq 14$ , $-15 \leq k \leq 15$ , $-18 \leq l \leq 18$	
Reflections collected	14988	
Independent reflections	7561 [ $R(\text{int}) = 0.0400$ ]	
Completeness to $\theta = 26.30^\circ$	98.3 %	
Absorption correction	Semi-empirical from equivalents	
Max. and min. transmission	0.884 and 0.820	
Refinement method	Full-matrix least-squares on $F^2$	



Table BI. Crystal data and structure refinement for **3.7**(continued).

Data / restraints / parameters	7561 / 0 / 491
Goodness-of-fit on $F^2$	1.135
Final R indices [ $I > 2\sigma(I)$ ]	$R1 = 0.0576$ , $wR2 = 0.1557$
R indices (all data)	$R1 = 0.0764$ , $wR2 = 0.1688$
Largest diff. peak and hole	1.610 and -1.008 e/Å <sup>3</sup>

Table BJ. Atomic coordinates ( $\times 10^4$ ) and equivalent isotropic displacement parameters (Å<sup>2</sup> $\times 10^3$ ) or **3.7**.  $U(eq)$  is defined as one third of the trace of the orthogonalized  $U_{ij}$  tensor.

	x	y	z	$U(eq)$
C(28)	11110(6)	1700(6)	5124(5)	29(1)
N(6)	8686(5)	672(4)	6988(4)	24(1)
O(6)	9613(5)	-1319(4)	6968(4)	43(1)
O(5)	8312(4)	2628(4)	6632(3)	32(1)
C(13)	2146(8)	4960(7)	4555(5)	42(2)
C(12)	3008(8)	3838(7)	4363(5)	42(2)
C(11)	3924(8)	3286(6)	4813(5)	35(2)
C(5)	4363(6)	4229(5)	8310(5)	28(1)
N(1)	2454(5)	4956(4)	9761(4)	23(1)
C(4)	2999(6)	5103(6)	8702(4)	28(1)
C(15)	1944(7)	5494(6)	12159(5)	35(2)
C(16)	5656(6)	7392(5)	8646(5)	27(1)
C(14)	2210(7)	5585(6)	5187(5)	35(2)
C(9)	3132(6)	5036(5)	5641(4)	26(1)
C(7)	4786(6)	3551(5)	6103(5)	29(1)
N(2)	1982(5)	5158(4)	11267(4)	27(1)
C(8)	3444(6)	5473(6)	6345(4)	28(1)
C(10)	3967(6)	3904(6)	5463(4)	29(1)
C(3)	1659(6)	4339(5)	10262(5)	26(1)
C(2)	1344(6)	4477(5)	11208(5)	28(1)
C(6)	5045(6)	4561(6)	7259(5)	28(1)
O(1)	5624(5)	2635(4)	6177(4)	40(1)

Table BJ. Atomic coordinates ( $\times 10^4$ ) and equivalent isotropic displacement parameters ( $\text{\AA}^2 \times 10^3$ ) or **3.7**(continued).

N(3)	4428(5)	4531(4)	6590(4)	26(1)
C(17)	6530(6)	8080(6)	8283(5)	34(2)
O(2)	2971(5)	6425(4)	6650(3)	35(1)
O(3)	5089(4)	7362(4)	9573(3)	30(1)
O(4)	5469(5)	6923(4)	8078(4)	39(1)
C(1)	2659(6)	5455(5)	10375(4)	26(1)
Ag(1)	3861(1)	6407(1)	9949(1)	29(1)
Ag(2)	9232(1)	1713(1)	9665(1)	28(1)
Cl(2)	1189(2)	3615(1)	9710(1)	33(1)
Cl(1)	316(2)	3993(2)	12174(1)	39(1)
Cl(3)	6045(2)	-1046(2)	10847(2)	42(1)
Cl(4)	5734(2)	38(2)	12961(1)	49(1)
N(4)	7651(5)	170(4)	10236(4)	24(1)
N(5)	7429(5)	859(5)	11526(4)	29(1)
C(18)	8065(6)	853(5)	10572(4)	24(1)
C(19)	6782(6)	-218(5)	10981(5)	30(1)
C(21)	8042(6)	-22(5)	9216(4)	26(1)
C(22)	7224(6)	1009(5)	8698(4)	27(1)
C(20)	6654(6)	213(6)	11797(5)	31(2)
C(23)	7399(6)	777(6)	7677(5)	30(1)
C(24)	9008(6)	1628(5)	6500(4)	23(1)
C(25)	9669(6)	-370(5)	6654(5)	26(1)
C(27)	10347(6)	1137(5)	5782(4)	23(1)
C(26)	10724(6)	-52(5)	5886(4)	25(1)
O(8)	10633(5)	1353(4)	7708(3)	36(1)
O(7)	10444(5)	2564(4)	8695(3)	36(1)
C(31)	11931(6)	-742(6)	5320(5)	32(2)
C(33)	10888(6)	2136(5)	7867(5)	28(1)
C(29)	12314(7)	1006(6)	4548(5)	35(2)
C(30)	12719(7)	-198(6)	4645(5)	37(2)
C(32)	7566(7)	1461(6)	12202(5)	38(2)
C(34)	11792(7)	2682(6)	7077(6)	44(2)

Table BK. Bond lengths [Å] and angles [°] for **3.7**.

C(28)-C(27)	1.364(9)	C(2)-Cl(1)	1.694(7)
C(28)-C(29)	1.388(9)	C(6)-N(3)	1.457(8)
N(6)-C(25)	1.389(8)	O(3)-Ag(1)	2.101(4)
N(6)-C(24)	1.392(8)	C(1)-Ag(1)	2.067(6)
N(6)-C(23)	1.460(8)	Ag(2)-C(18)	2.035(6)
O(6)-C(25)	1.212(8)	Ag(2)-O(7)	2.092(5)
O(5)-C(24)	1.203(7)	Cl(3)-C(19)	1.684(7)
C(13)-C(14)	1.381(10)	Cl(4)-C(20)	1.696(6)
C(13)-C(12)	1.382(11)	N(4)-C(19)	1.367(8)
C(12)-C(11)	1.372(10)	N(4)-C(18)	1.389(8)
C(11)-C(10)	1.384(9)	N(4)-C(21)	1.455(8)
C(5)-C(4)	1.517(8)	N(5)-C(18)	1.337(8)
C(5)-C(6)	1.531(9)	N(5)-C(20)	1.366(9)
N(1)-C(1)	1.346(8)	N(5)-C(32)	1.463(9)
N(1)-C(3)	1.373(8)	C(19)-C(20)	1.363(10)
N(1)-C(4)	1.470(7)	C(21)-C(22)	1.542(8)
C(15)-N(2)	1.454(8)	C(22)-C(23)	1.528(9)
C(16)-O(4)	1.249(8)	C(24)-C(27)	1.504(8)
C(16)-O(3)	1.291(7)	C(25)-C(26)	1.480(9)
C(16)-C(17)	1.496(9)	C(27)-C(26)	1.373(8)
C(14)-C(9)	1.381(9)	C(26)-C(31)	1.383(9)
C(9)-C(10)	1.380(9)	O(8)-C(33)	1.228(8)
C(9)-C(8)	1.493(9)	O(7)-C(33)	1.282(8)
C(7)-O(1)	1.203(7)	C(31)-C(30)	1.377(10)
C(7)-N(3)	1.391(8)	C(33)-C(34)	1.529(9)
C(7)-C(10)	1.496(9)	C(29)-C(30)	1.389(10)
N(2)-C(1)	1.342(8)	C(27)-C(28)-C(29)	116.5(6)
N(2)-C(2)	1.386(8)	C(25)-N(6)-C(24)	112.0(5)
C(8)-O(2)	1.201(8)	C(25)-N(6)-C(23)	124.8(5)
C(8)-N(3)	1.395(8)	C(24)-N(6)-C(23)	122.8(5)
C(3)-C(2)	1.345(9)	C(14)-C(13)-C(12)	121.0(7)
C(3)-Cl(2)	1.693(6)	C(11)-C(12)-C(13)	121.6(7)
		C(12)-C(11)-C(10)	117.3(7)
		C(4)-C(5)-C(6)	111.5(5)
		C(1)-N(1)-C(3)	110.7(5)

Table BK. Bond lengths [Å] and angles [°] for **3.7** (continued).

C(1)-N(1)-C(4)	122.9(5)	C(16)-O(3)-Ag(1)	109.8(4)
C(3)-N(1)-C(4)	126.4(5)	N(2)-C(1)-N(1)	105.8(5)
N(1)-C(4)-C(5)	111.8(5)	N(2)-C(1)-Ag(1)	129.8(5)
O(4)-C(16)-O(3)	123.6(6)	N(1)-C(1)-Ag(1)	124.3(4)
O(4)-C(16)-C(17)	121.4(6)	C(1)-Ag(1)-O(3)	177.7(2)
O(3)-C(16)-C(17)	115.0(6)	C(18)-Ag(2)-O(7)	178.1(2)
C(9)-C(14)-C(13)	117.6(7)	C(19)-N(4)-C(18)	110.8(5)
C(10)-C(9)-C(14)	121.0(6)	C(19)-N(4)-C(21)	125.9(6)
C(10)-C(9)-C(8)	108.7(6)	C(18)-N(4)-C(21)	123.2(5)
C(14)-C(9)-C(8)	130.3(6)	C(18)-N(5)-C(20)	111.7(6)
O(1)-C(7)-N(3)	125.2(6)	C(18)-N(5)-C(32)	124.3(6)
O(1)-C(7)-C(10)	128.9(6)	C(20)-N(5)-C(32)	124.0(6)
N(3)-C(7)-C(10)	105.9(5)	N(5)-C(18)-N(4)	104.1(5)
C(1)-N(2)-C(2)	109.9(5)	N(5)-C(18)-Ag(2)	133.2(5)
C(1)-N(2)-C(15)	124.6(6)	N(4)-C(18)-Ag(2)	122.4(4)
C(2)-N(2)-C(15)	125.5(6)	C(20)-C(19)-N(4)	106.0(6)
O(2)-C(8)-N(3)	125.9(6)	C(20)-C(19)-Cl(3)	129.6(5)
O(2)-C(8)-C(9)	128.8(6)	N(4)-C(19)-Cl(3)	124.3(5)
N(3)-C(8)-C(9)	105.3(5)	N(4)-C(21)-C(22)	111.1(5)
C(9)-C(10)-C(11)	121.4(6)	C(23)-C(22)-C(21)	114.1(5)
C(9)-C(10)-C(7)	107.6(5)	C(19)-C(20)-N(5)	107.4(6)
C(11)-C(10)-C(7)	130.9(6)	C(19)-C(20)-Cl(4)	129.5(6)
C(2)-C(3)-N(1)	106.6(6)	N(5)-C(20)-Cl(4)	123.1(5)
C(2)-C(3)-Cl(2)	130.4(5)	N(6)-C(23)-C(22)	113.2(5)
N(1)-C(3)-Cl(2)	123.0(5)	O(5)-C(24)-N(6)	125.2(6)
C(3)-C(2)-N(2)	107.1(6)	O(5)-C(24)-C(27)	129.2(6)
C(3)-C(2)-Cl(1)	128.6(5)	N(6)-C(24)-C(27)	105.6(5)
N(2)-C(2)-Cl(1)	124.3(5)	O(6)-C(25)-N(6)	124.1(6)
N(3)-C(6)-C(5)	113.0(5)	O(6)-C(25)-C(26)	129.9(6)
C(7)-N(3)-C(8)	112.3(5)	N(6)-C(25)-C(26)	106.0(5)
C(7)-N(3)-C(6)	123.1(5)	C(28)-C(27)-C(26)	123.0(6)
C(8)-N(3)-C(6)	124.6(5)	C(28)-C(27)-C(24)	129.5(6)
		C(26)-C(27)-C(24)	107.5(5)
		C(27)-C(26)-C(31)	120.5(6)
		C(27)-C(26)-C(25)	108.9(5)

Table BK. Bond lengths [Å] and angles [°] for **3.7** (continued).

C(31)-C(26)-C(25)	130.6(6)
C(33)-O(7)-Ag(2)	107.9(4)
C(30)-C(31)-C(26)	117.8(6)
O(8)-C(33)-O(7)	124.0(6)

O(8)-C(33)-C(34)	122.0(6)
O(7)-C(33)-C(34)	113.9(6)
C(28)-C(29)-C(30)	121.5(6)
C(31)-C(30)-C(29)	120.7(6)

Table BL. Anisotropic displacement parameters ( $\text{\AA}^2 \times 10^3$ ) for **3.7**. The anisotropic displacement factor exponent takes the form:  $-2\pi^2 [h^2 a^{*2} U^{11} + \dots + 2 h k a^* b^* U^{12}]$

	U <sup>11</sup>	U <sup>22</sup>	U <sup>33</sup>	U <sup>23</sup>	U <sup>13</sup>	U <sup>12</sup>
C(28)	29(3)	21(3)	29(3)	-3(3)	-2(3)	-7(3)
N(6)	26(3)	25(3)	22(3)	-5(2)	-4(2)	-12(2)
O(6)	34(3)	31(3)	54(3)	0(2)	-5(2)	-12(2)
O(5)	34(3)	22(2)	32(2)	-7(2)	-8(2)	-3(2)
C(13)	59(5)	47(4)	32(4)	8(3)	-20(4)	-31(4)
C(12)	64(5)	48(5)	24(3)	4(3)	-15(3)	-33(4)
C(11)	55(5)	27(3)	25(3)	-1(3)	-9(3)	-20(3)
C(5)	29(3)	26(3)	29(3)	-4(3)	-11(3)	-7(3)
N(1)	22(3)	25(3)	21(3)	-2(2)	-4(2)	-10(2)
C(4)	28(3)	30(3)	20(3)	-2(2)	-5(3)	-8(3)
C(15)	41(4)	35(4)	23(3)	-8(3)	-9(3)	-6(3)
C(16)	21(3)	20(3)	30(3)	-1(3)	-8(3)	1(3)
C(14)	46(4)	32(4)	26(3)	2(3)	-10(3)	-17(3)
C(9)	33(3)	26(3)	16(3)	-1(2)	-4(3)	-11(3)
C(7)	26(3)	24(3)	25(3)	-5(3)	-1(3)	-3(3)
N(2)	28(3)	25(3)	25(3)	-6(2)	-9(2)	-3(2)
C(8)	25(3)	33(4)	18(3)	-2(3)	-3(2)	-7(3)
C(10)	34(4)	33(4)	17(3)	-2(3)	-1(3)	-15(3)
C(3)	24(3)	23(3)	31(3)	-7(3)	-10(3)	-3(3)
C(2)	28(3)	23(3)	28(3)	-2(3)	-5(3)	-8(3)
C(6)	28(3)	30(3)	27(3)	-2(3)	-11(3)	-11(3)

Table BL. Anisotropic displacement parameters ( $\text{\AA}^2 \times 10^3$ ) for **3.7** (continued).

O(1)	39(3)	30(3)	40(3)	-13(2)	-10(2)	0(2)
N(3)	22(3)	26(3)	23(3)	-6(2)	-2(2)	-5(2)
C(17)	22(3)	26(3)	42(4)	6(3)	-4(3)	-5(3)
O(2)	41(3)	26(2)	33(3)	-7(2)	-15(2)	-2(2)
O(3)	34(3)	32(2)	26(2)	-3(2)	-8(2)	-16(2)
O(4)	45(3)	41(3)	34(3)	-2(2)	-16(2)	-15(2)
C(1)	28(3)	27(3)	22(3)	3(2)	-7(3)	-11(3)
Ag(1)	31(1)	30(1)	28(1)	-2(1)	-9(1)	-14(1)
Ag(2)	27(1)	34(1)	26(1)	-4(1)	-6(1)	-14(1)
Cl(2)	28(1)	28(1)	45(1)	-11(1)	-12(1)	-8(1)
Cl(1)	30(1)	36(1)	39(1)	4(1)	0(1)	-11(1)
Cl(3)	29(1)	31(1)	62(1)	2(1)	-9(1)	-14(1)
Cl(4)	34(1)	47(1)	32(1)	10(1)	6(1)	-4(1)
N(4)	19(3)	24(3)	26(3)	-4(2)	-3(2)	-7(2)
N(5)	25(3)	28(3)	26(3)	-4(2)	-7(2)	-2(2)
C(18)	24(3)	24(3)	19(3)	-1(2)	-7(2)	-2(3)
C(19)	22(3)	22(3)	34(4)	4(3)	-5(3)	-5(3)
C(21)	28(3)	24(3)	23(3)	-2(2)	-5(3)	-8(3)
C(22)	22(3)	28(3)	27(3)	-5(3)	-5(3)	-6(3)
C(20)	22(3)	27(3)	26(3)	1(3)	2(3)	-1(3)
C(23)	20(3)	40(4)	31(3)	-1(3)	-6(3)	-15(3)
C(24)	29(3)	23(3)	21(3)	-6(2)	-9(2)	-9(3)
C(25)	29(3)	25(3)	29(3)	-2(3)	-9(3)	-13(3)
C(27)	28(3)	25(3)	17(3)	-3(2)	-7(2)	-9(3)
C(26)	31(3)	21(3)	24(3)	-2(2)	-9(3)	-11(3)
O(8)	46(3)	33(3)	31(3)	-5(2)	-10(2)	-18(2)
O(7)	36(3)	39(3)	36(3)	-15(2)	1(2)	-21(2)
C(31)	29(3)	27(3)	33(4)	-7(3)	-3(3)	-8(3)
C(33)	20(3)	24(3)	30(3)	2(3)	-6(3)	-3(3)
C(29)	30(4)	38(4)	31(4)	-3(3)	2(3)	-16(3)
C(30)	28(4)	40(4)	35(4)	-10(3)	-3(3)	-9(3)
C(32)	45(4)	37(4)	27(4)	-5(3)	-11(3)	-8(3)
C(34)	38(4)	29(4)	47(5)	7(3)	-4(3)	-10(3)

Table BM. Hydrogen coordinates ( $\times 10^4$ ) and isotropic displacement parameters ( $\text{\AA}^2 \times 10^3$ ) for **3.7**.

	x	y	z	U(eq)
H(28)	10831	2523	5063	35
H(13)	1502	5306	4249	50
H(12)	2964	3438	3906	50
H(11)	4507	2511	4685	43
H(5A)	4321	3451	8344	33
H(5B)	4875	4185	8717	33
H(4A)	3017	5899	8524	33
H(4B)	2433	5012	8401	33
H(15A)	2568	4860	12422	53
H(15B)	1069	5658	12632	53
H(15C)	2170	6191	12025	53
H(14)	1638	6366	5304	42
H(6A)	5049	5353	7225	33
H(6B)	5959	4020	7054	33
H(17A)	7179	7804	7657	52
H(17B)	6969	7983	8749	52
H(17C)	6015	8903	8202	52
H(21A)	7934	-742	9154	32
H(21B)	8971	-126	8901	32
H(22A)	6296	1208	9094	33
H(22B)	7460	1691	8659	33
H(23A)	7248	51	7706	37
H(23B)	6737	1419	7442	37
H(31)	12206	-1566	5395	38
H(29)	12875	1363	4078	43
H(30)	13549	-650	4240	44
H(32A)	7935	892	12664	57
H(32B)	6711	2003	12552	57
H(32C)	8143	1892	11841	57
H(34A)	12560	2534	7252	65

Table BM. Hydrogen coordinates ( $\times 10^4$ ) and isotropic displacement parameters ( $\text{\AA}^2 \times 10^3$ ) for **3.7** (continued).

H(34B)	11334	3522	7012	65
H(34C)	12062	2340	6460	65



## APPENDIX N

### SUPPLEMENTARY MATERIAL FOR THE X-RAY CRYSTAL STRUCTURE OF

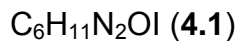


Table BN. Crystal data and structure refinement for **4.1**.

Empirical formula	$\text{C}_6\text{H}_{11}\text{IN}_2\text{O}$	
Formula weight	254.06	
Temperature	100(2) K	
Wavelength	0.71073 Å	
Crystal system	Monoclinic	
Space group	P2(1)	
Unit cell dimensions	$a = 7.5518(11)$ Å	$\alpha = 90^\circ$ .
	$b = 7.2999(11)$ Å	$\beta = 106.635(2)^\circ$ .
	$c = 8.6033(13)$ Å	$\gamma = 90^\circ$ .
Volume	$454.43(12)$ Å <sup>3</sup>	
Z	2	
Density (calculated)	1.849 Mg/m <sup>3</sup>	
Absorption coefficient	3.467 mm <sup>-1</sup>	
F(000)	242	
Crystal size	0.35 x 0.12 x 0.10 mm <sup>3</sup>	
Theta range for data collection	2.47 to 28.29°.	
Index ranges	-9 ≤ h ≤ 10, -9 ≤ k ≤ 9, -11 ≤ l ≤ 11	
Reflections collected	4006	
Independent reflections	2022 [R(int) = 0.0244]	
Completeness to theta = 28.29°	95.9 %	
Absorption correction	Semi-empirical from equivalents	
Max. and min. transmission	0.7231 and 0.3767	

Table BN. Crystal data and structure refinement for **4.1** (continued).

Refinement method	Full-matrix least-squares on $F^2$ Data /
restraints / parameters	2022 / 1 / 93
Goodness-of-fit on $F^2$	1.109
Final R indices [ $I > 2\sigma(I)$ ]	R1 = 0.0277, wR2 = 0.0663
R indices (all data)	R1 = 0.0286, wR2 = 0.0669
Absolute structure parameter	0.07(4)
Largest diff. peak and hole	1.837 and -1.042 e/Å <sup>3</sup>

Table BO. Atomic coordinates ( $\times 10^4$ ) and equivalent isotropic displacement parameters (Å<sup>2</sup> $\times 10^3$ ) for **4.1**. U(eq) is defined as one third of the trace of the orthogonalized  $U_{ij}$  tensor.

	x	y	z	U(eq)
I(1)	2946(1)	3032(1)	8193(1)	18(1)
O(1)	4808(5)	4707(5)	3466(4)	25(1)
N(1)	8718(5)	3449(4)	977(4)	17(1)
N(2)	8275(5)	2925(16)	3295(4)	18(1)
C(1)	8342(7)	3801(8)	-769(6)	26(1)
C(2)	10406(6)	3659(6)	2122(6)	21(1)
C(3)	10116(6)	3356(6)	3587(6)	22(1)
C(4)	7453(5)	2987(16)	1706(4)	18(1)
C(5)	7306(7)	2541(6)	4503(6)	22(1)
C(6)	6223(7)	4174(7)	4855(6)	24(1)

Table BP. Bond lengths [Å] and angles [°] for **4.1**.

		N(2)-C(4)	1.330(4)
		N(2)-C(3)	1.376(7)
		N(2)-C(5)	1.459(6)
O(1)-C(6)	1.411(6)	C(1)-H(1A)	0.9800
O(1)-H(1)	0.8400	C(1)-H(1B)	0.9800
N(1)-C(4)	1.328(6)	C(1)-H(1C)	0.9800
N(1)-C(2)	1.379(6)	C(2)-C(3)	1.358(7)
N(1)-C(1)	1.469(6)	C(2)-H(2)	0.9500

Table BP. Bond lengths [Å] and angles [°] for **4.1** (continued).

C(3)-H(3)	0.9500	C(3)-C(2)-N(1)	106.5(4)
C(4)-H(4)	0.9500	C(3)-C(2)-H(2)	126.8
C(5)-C(6)	1.525(7)	N(1)-C(2)-H(2)	126.8
C(5)-H(5A)	0.9900	C(2)-C(3)-N(2)	106.9(4)
C(5)-H(5B)	0.9900	C(2)-C(3)-H(3)	126.6
C(6)-H(6A)	0.9900	N(2)-C(3)-H(3)	126.6
C(6)-H(6B)	0.9900	N(1)-C(4)-N(2)	107.9(4)
C(6)-O(1)-H(1)	109.5	N(1)-C(4)-H(4)	126.1
C(4)-N(1)-C(2)	109.5(4)	N(2)-C(4)-H(4)	126.1
C(4)-N(1)-C(1)	125.0(4)	N(2)-C(5)-C(6)	113.5(5)
C(2)-N(1)-C(1)	125.4(4)	N(2)-C(5)-H(5A)	108.9
C(4)-N(2)-C(3)	109.3(4)	C(6)-C(5)-H(5A)	108.9
C(4)-N(2)-C(5)	123.8(4)	N(2)-C(5)-H(5B)	108.9
C(3)-N(2)-C(5)	126.8(4)	C(6)-C(5)-H(5B)	108.9
N(1)-C(1)-H(1A)	109.5	H(5A)-C(5)-H(5B)	107.7
N(1)-C(1)-H(1B)	109.5	O(1)-C(6)-C(5)	111.5(4)
H(1A)-C(1)-H(1B)	109.5	O(1)-C(6)-H(6A)	109.3
N(1)-C(1)-H(1C)	109.5	C(5)-C(6)-H(6A)	109.3
H(1A)-C(1)-H(1C)	109.5	O(1)-C(6)-H(6B)	109.3
H(1B)-C(1)-H(1C)	109.5	C(5)-C(6)-H(6B)	109.3
		H(6A)-C(6)-H(6B)	108.0

Table BQ. Anisotropic displacement parameters ( $\text{\AA}^2 \times 10^3$ ) for **4.1**. The anisotropic displacement factor exponent takes the form:  $-2\pi^2 [h^2 a^{*2} U^{11} + \dots + 2 h k a^* b^* U^{12}]$

	U <sup>11</sup>	U <sup>22</sup>	U <sup>33</sup>	U <sup>23</sup>	U <sup>13</sup>	U <sup>12</sup>
I(1)	20(1)	18(1)	18(1)	0(1)	9(1)	0(1)
O(1)	20(2)	32(2)	25(2)	6(2)	11(1)	-1(1)
N(1)	18(2)	17(3)	19(2)	0(1)	10(1)	1(1)
N(2)	25(1)	14(2)	17(1)	4(2)	7(1)	0(3)

Table BQ. Anisotropic displacement parameters ( $\text{\AA}^2 \times 10^3$ ) for **4.1** (continued).

C(1)	24(2)	43(3)	18(2)	0(2)	14(2)	1(2)
C(2)	16(2)	22(2)	25(2)	-2(2)	6(2)	1(2)
C(3)	24(2)	16(4)	22(2)	0(2)	2(2)	2(2)
C(4)	21(2)	16(2)	17(2)	1(3)	8(1)	1(5)
C(5)	34(2)	18(3)	19(2)	4(2)	15(2)	2(2)
C(6)	31(3)	24(3)	20(2)	-3(2)	12(2)	-1(2)

Table BR. Hydrogen coordinates ( $\times 10^4$ ) and isotropic displacement parameters ( $\text{\AA}^2 \times 10^3$ ) for **4.1**.

	x	y	z	U(eq)
H(1)	5242	5426	2906	37
H(1A)	7147	3265	-1352	40
H(1B)	9319	3247	-1158	40
H(1C)	8311	5125	-962	40
H(2)	11547	3957	1925	25
H(3)	11012	3428	4617	26
H(4)	6186	2743	1186	21
H(5A)	8219	2154	5525	26
H(5B)	6444	1507	4118	26
H(6A)	5672	3849	5733	29
H(6B)	7076	5216	5235	29

## APPENDIX O

### SUPPLEMENTARY MATERIAL FOR THE X-RAY CRYSTAL STRUCTURE OF

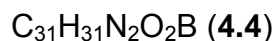


Table BS. Crystal data and structure refinement for **4.4**.

Empirical formula	$C_{31}H_{31}BN_2O_2$	
Formula weight	474.39	
Temperature	100(2) K	
Wavelength	0.71073 Å	
Crystal system	Monoclinic	
Space group	P2(1)/n	
Unit cell dimensions	$a = 9.2523(10)$ Å	$\alpha = 90^\circ$ .
	$b = 9.2082(10)$ Å	$\beta = 98.149(2)^\circ$ .
	$c = 30.191(3)$ Å	$\gamma = 90^\circ$ .
Volume	$2546.2(5)$ Å <sup>3</sup>	
Z	4	
Density (calculated)	1.238 Mg/m <sup>3</sup>	
Absorption coefficient	0.076 mm <sup>-1</sup>	
F(000)	1008	
Crystal size	0.43 x 0.17 x 0.05 mm <sup>3</sup>	
Theta range for data collection	2.23 to 28.32°.	
Index ranges	$-11 \leq h \leq 11, -11 \leq k \leq 12, -39 \leq l \leq 39$	
Reflections collected	22051	
Independent reflections	6111 [R(int) = 0.0925]	
Completeness to theta = 28.32°	96.0 %	
Absorption correction	Semi-empirical from equivalents	
Refinement method	Full-matrix least-squares on F <sup>2</sup>	

Table BS. Crystal data and structure refinement for **4.4** (continued).

Data / restraints / parameters	6111 / 0 / 449
Goodness-of-fit on $F^2$	0.979
Final R indices [ $I > 2\sigma(I)$ ]	R1 = 0.0598, wR2 = 0.1019
R indices (all data)	R1 = 0.1006, wR2 = 0.1147
Largest diff. peak and hole	0.265 and -0.223 e/Å <sup>3</sup>

Table BT. Atomic coordinates ( $\times 10^4$ ) and equivalent isotropic displacement parameters (Å<sup>2</sup> $\times 10^3$ ) for **4.4**. U(eq) is defined as one third of the trace of the orthogonalized  $U_{ij}$  tensor.

	x	y	z	U(eq)
O(1)	10225(2)	6575(2)	301(1)	33(1)
O(2)	8184(2)	5536(2)	-38(1)	28(1)
N(1)	8500(2)	7503(2)	1112(1)	22(1)
N(2)	9212(2)	5957(2)	1635(1)	23(1)
C(1)	9663(2)	6904(2)	1352(1)	23(1)
C(2)	7263(2)	6916(2)	1249(1)	27(1)
C(3)	7706(2)	5955(2)	1572(1)	28(1)
C(4)	10165(3)	5107(3)	1968(1)	33(1)
C(5)	8552(2)	8532(2)	740(1)	26(1)
C(6)	7973(2)	7839(2)	295(1)	27(1)
C(7)	8875(2)	6567(2)	185(1)	23(1)
C(8)	4678(2)	1890(2)	1803(1)	18(1)
C(9)	6195(2)	1737(2)	1916(1)	23(1)
C(10)	6993(2)	2426(2)	2278(1)	28(1)
C(11)	6296(2)	3324(2)	2549(1)	29(1)
C(12)	4806(2)	3490(2)	2454(1)	30(1)
C(13)	4021(2)	2775(2)	2091(1)	23(1)
C(14)	3901(2)	-688(2)	1408(1)	17(1)
C(15)	4371(2)	-1377(2)	1814(1)	22(1)
C(16)	4250(2)	-2870(2)	1876(1)	24(1)
C(17)	3691(2)	-3746(2)	1522(1)	23(1)
C(18)	3235(2)	-3116(2)	1109(1)	22(1)

Table BT. Atomic coordinates ( $\times 10^4$ ) and equivalent isotropic displacement parameters ( $\text{\AA}^2 \times 10^3$ ) for **4.4** (continued).

C(19)	3322(2)	-1610(2)	1058(1)	19(1)
C(20)	4678(2)	1666(2)	935(1)	17(1)
C(21)	5300(2)	789(2)	634(1)	18(1)
C(22)	5987(2)	1348(2)	291(1)	21(1)
C(23)	6085(2)	2824(2)	230(1)	21(1)
C(24)	5506(2)	3740(2)	523(1)	23(1)
C(25)	4838(2)	3167(2)	866(1)	22(1)
C(26)	2105(2)	1520(2)	1276(1)	18(1)
C(27)	1420(2)	2484(2)	959(1)	25(1)
C(28)	-61(2)	2810(2)	918(1)	28(1)
C(29)	-931(2)	2185(2)	1200(1)	24(1)
C(30)	-289(2)	1226(2)	1522(1)	26(1)
C(31)	1181(2)	902(2)	1554(1)	25(1)
B(1)	3850(2)	1092(2)	1351(1)	17(1)

Table BU. Bond lengths [ $\text{\AA}$ ] and angles [ $^\circ$ ] for **4.4**.

		C(9)-C(10)	1.384(3)
		C(10)-C(11)	1.384(3)
		C(11)-C(12)	1.376(3)
O(1)-C(7)	1.249(2)	C(12)-C(13)	1.391(3)
O(2)-C(7)	1.280(2)	C(14)-C(15)	1.394(2)
N(1)-C(1)	1.329(2)	C(14)-C(19)	1.401(2)
N(1)-C(2)	1.381(2)	C(14)-B(1)	1.648(3)
N(1)-C(5)	1.475(2)	C(15)-C(16)	1.395(3)
N(2)-C(1)	1.330(2)	C(16)-C(17)	1.378(3)
N(2)-C(3)	1.379(2)	C(17)-C(18)	1.387(3)
N(2)-C(4)	1.466(3)	C(18)-C(19)	1.399(2)
C(2)-C(3)	1.339(3)	C(20)-C(21)	1.400(2)
C(5)-C(6)	1.515(3)	C(20)-C(25)	1.409(2)
C(6)-C(7)	1.503(3)	C(20)-B(1)	1.647(3)
C(8)-C(13)	1.393(2)	C(21)-C(22)	1.388(2)
C(8)-C(9)	1.404(2)	C(22)-C(23)	1.376(3)
C(8)-B(1)	1.641(3)	C(23)-C(24)	1.383(3)

Table BU. Bond lengths [Å] and angles [°] for **4.4** (continued).

C(24)-C(25)	1.383(3)	C(12)-C(13)-C(8)	122.86(19)
C(26)-C(27)	1.390(3)	C(15)-C(14)-C(19)	115.21(17)
C(26)-C(31)	1.401(2)	C(15)-C(14)-B(1)	122.98(16)
C(26)-B(1)	1.646(3)	C(19)-C(14)-B(1)	121.46(16)
C(27)-C(28)	1.391(3)	C(14)-C(15)-C(16)	123.07(18)
C(28)-C(29)	1.379(3)	C(17)-C(16)-C(15)	120.09(19)
C(29)-C(30)	1.383(3)	C(16)-C(17)-C(18)	119.01(18)
C(30)-C(31)	1.382(3)	C(17)-C(18)-C(19)	119.94(18)
C(1)-N(1)-C(2)	108.37(17)	C(18)-C(19)-C(14)	122.63(18)
C(1)-N(1)-C(5)	124.81(17)	C(21)-C(20)-C(25)	114.00(16)
C(2)-N(1)-C(5)	126.66(17)	C(21)-C(20)-B(1)	126.07(16)
C(1)-N(2)-C(3)	108.39(17)	C(25)-C(20)-B(1)	119.91(15)
C(1)-N(2)-C(4)	125.29(18)	C(22)-C(21)-C(20)	123.01(18)
C(3)-N(2)-C(4)	126.28(18)	C(23)-C(22)-C(21)	120.75(18)
N(1)-C(1)-N(2)	108.64(18)	C(22)-C(23)-C(24)	118.60(18)
C(3)-C(2)-N(1)	107.25(18)	C(25)-C(24)-C(23)	119.94(19)
C(2)-C(3)-N(2)	107.35(18)	C(24)-C(25)-C(20)	123.65(18)
N(1)-C(5)-C(6)	111.01(17)	C(27)-C(26)-C(31)	114.49(17)
C(7)-C(6)-C(5)	112.80(17)	C(27)-C(26)-B(1)	126.14(16)
O(1)-C(7)-O(2)	123.88(18)	C(31)-C(26)-B(1)	119.35(16)
O(1)-C(7)-C(6)	119.84(18)	C(26)-C(27)-C(28)	123.12(18)
O(2)-C(7)-C(6)	116.26(18)	C(29)-C(28)-C(27)	120.60(19)
C(13)-C(8)-C(9)	114.67(17)	C(28)-C(29)-C(30)	118.03(19)
C(13)-C(8)-B(1)	125.94(17)	C(31)-C(30)-C(29)	120.50(18)
C(9)-C(8)-B(1)	119.36(16)	C(30)-C(31)-C(26)	123.24(19)
C(10)-C(9)-C(8)	123.26(18)	C(8)-B(1)-C(26)	109.93(14)
C(9)-C(10)-C(11)	120.0(2)	C(8)-B(1)-C(20)	106.07(14)
C(12)-C(11)-C(10)	118.6(2)	C(26)-B(1)-C(20)	111.81(15)
C(11)-C(12)-C(13)	120.56(19)	C(8)-B(1)-C(14)	110.85(14)
		C(26)-B(1)-C(14)	105.41(14)
		C(20)-B(1)-C(14)	112.84(14)



Table BV. Anisotropic displacement parameters ( $\text{\AA}^2 \times 10^3$ ) for **4.4**. The anisotropic displacement factor exponent takes the form:  $-2\pi^2 [h^2 a^{*2} U^{11} + \dots + 2 h k a^* b^* U^{12}]$

	U <sup>11</sup>	U <sup>22</sup>	U <sup>33</sup>	U <sup>23</sup>	U <sup>13</sup>	U <sup>12</sup>
O(1)	24(1)	41(1)	33(1)	-9(1)	-2(1)	7(1)
O(2)	29(1)	25(1)	31(1)	1(1)	5(1)	-3(1)
N(1)	21(1)	23(1)	23(1)	-1(1)	2(1)	2(1)
N(2)	23(1)	26(1)	21(1)	-2(1)	2(1)	2(1)
C(1)	22(1)	26(1)	21(1)	-2(1)	4(1)	4(1)
C(2)	20(1)	31(1)	30(1)	-4(1)	2(1)	2(1)
C(3)	23(1)	33(1)	30(1)	-3(1)	8(1)	-3(1)
C(4)	34(1)	35(1)	27(1)	7(1)	-1(1)	6(1)
C(5)	26(1)	22(1)	29(1)	1(1)	3(1)	4(1)
C(6)	26(1)	28(1)	26(1)	2(1)	-1(1)	7(1)
C(7)	24(1)	27(1)	16(1)	5(1)	1(1)	1(1)
C(8)	20(1)	16(1)	18(1)	6(1)	5(1)	2(1)
C(9)	21(1)	26(1)	21(1)	-1(1)	4(1)	-1(1)
C(10)	23(1)	32(1)	27(1)	3(1)	2(1)	-5(1)
C(11)	42(1)	24(1)	20(1)	-1(1)	-4(1)	-5(1)
C(12)	45(1)	24(1)	23(1)	-3(1)	4(1)	9(1)
C(13)	25(1)	21(1)	22(1)	2(1)	4(1)	5(1)
C(14)	14(1)	18(1)	20(1)	2(1)	6(1)	2(1)
C(15)	26(1)	21(1)	20(1)	-3(1)	4(1)	2(1)
C(16)	28(1)	24(1)	21(1)	5(1)	5(1)	4(1)
C(17)	22(1)	17(1)	30(1)	1(1)	8(1)	2(1)
C(18)	18(1)	24(1)	24(1)	-4(1)	5(1)	-2(1)
C(19)	17(1)	21(1)	20(1)	4(1)	5(1)	2(1)
C(20)	14(1)	19(1)	19(1)	1(1)	-1(1)	0(1)
C(21)	15(1)	17(1)	22(1)	0(1)	2(1)	0(1)
C(22)	19(1)	24(1)	20(1)	-3(1)	5(1)	0(1)
C(23)	19(1)	26(1)	20(1)	4(1)	4(1)	-4(1)
C(24)	25(1)	18(1)	27(1)	4(1)	5(1)	-1(1)
C(25)	25(1)	19(1)	23(1)	-3(1)	7(1)	1(1)

Table BV. Anisotropic displacement parameters ( $\text{\AA}^2 \times 10^3$ ) for **4.4** (continued).

C(26)	19(1)	17(1)	17(1)	-4(1)	3(1)	0(1)
C(27)	24(1)	31(1)	22(1)	5(1)	8(1)	4(1)
C(28)	23(1)	35(1)	25(1)	7(1)	1(1)	8(1)
C(29)	17(1)	27(1)	27(1)	-5(1)	2(1)	4(1)
C(30)	21(1)	26(1)	31(1)	5(1)	10(1)	0(1)
C(31)	23(1)	25(1)	27(1)	8(1)	4(1)	6(1)
B(1)	16(1)	17(1)	17(1)	1(1)	3(1)	1(1)

Table BW. Hydrogen coordinates ( $\times 10^4$ ) and isotropic displacement parameters ( $\text{\AA}^2 \times 10^3$ ) for **4.4**.

	x	y	z	U(eq)
H(1)	10717(19)	7149(18)	1334(6)	20(5)
H(2)	6290(20)	7260(20)	1118(7)	39(6)
H(3)	7180(20)	5330(20)	1736(7)	35(6)
H(9)	6735(19)	1100(20)	1722(6)	29(5)
H(10)	8070(20)	2260(20)	2338(6)	32(6)
H(11)	6860(20)	3860(20)	2796(7)	37(6)
H(12)	4310(19)	4130(19)	2634(6)	24(5)
H(13)	2959(19)	2859(18)	2036(6)	17(5)
H(15)	4764(19)	-803(19)	2060(6)	23(5)
H(16)	4537(19)	-3320(20)	2172(6)	27(5)
H(17)	3620(20)	-4790(20)	1568(7)	39(6)
H(18)	2840(20)	-3690(20)	837(6)	31(5)
H(19)	2947(18)	-1171(19)	772(6)	21(5)
H(21)	5250(18)	-300(20)	677(6)	24(5)
H(22)	6401(19)	701(19)	98(6)	24(5)
H(23)	6522(18)	3208(18)	-13(6)	18(5)
H(24)	5595(19)	4730(20)	499(6)	26(5)
H(25)	4442(19)	3830(20)	1067(6)	26(5)
H(27)	2030(20)	2980(20)	768(6)	29(5)

Table BW. Hydrogen coordinates ( $\times 10^4$ ) and isotropic displacement parameters ( $\text{\AA}^2 \times 10^3$ ) for **4.4** (continued).

H(28)	-500(20)	3470(20)	696(7)	34(6)
H(29)	-1960(20)	2380(19)	1167(6)	26(5)
H(30)	-840(20)	750(20)	1727(7)	37(6)
H(31)	1586(17)	204(18)	1775(6)	15(5)
H(2')	8900(30)	4700(40)	-164(11)	141(13)
H(4A)	9930(30)	4050(30)	1938(8)	71(8)
H(5A)	7942(18)	9395(19)	796(6)	19(5)
H(6A)	6960(20)	7530(20)	278(7)	44(7)
H(4B)	10050(30)	5430(30)	2268(9)	74(9)
H(5B)	9600(20)	8842(19)	774(6)	26(5)
H(6B)	8020(20)	8520(20)	53(7)	35(6)
H(4C)	11150(30)	5230(30)	1924(8)	73(9)

## APPENDIX P

### SUPPLEMENTARY MATERIAL FOR THE X-RAY CRYSTAL STRUCTURE OF

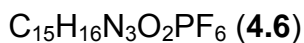


Table BX. Crystal data and structure refinement for **4.6**.

Empirical formula	$\text{C}_{15}\text{H}_{16}\text{N}_3\text{O}_2\text{PF}_6$	
Formula weight	415.27	
Temperature	100(2) K	
Wavelength	0.71073 Å	
Crystal system	Orthorhombic	
Space group	Pbca	
Unit cell dimensions	$a = 8.1750(19)$ Å	$\alpha = 90^\circ$ .
	$b = 12.680(3)$ Å	$\beta = 90^\circ$ .
	$c = 32.223(7)$ Å	$\gamma = 90^\circ$ .
Volume	$3340.2(13)$ Å <sup>3</sup>	
Z	8	
Density (calculated)	1.652 Mg/m <sup>3</sup>	
Absorption coefficient	0.246 mm <sup>-1</sup>	
F(000)	1696	
Crystal size	0.41 x 0.26 x 0.05 mm <sup>3</sup>	
Theta range for data collection	2.53 to 28.38°.	
Index ranges	$-10 \leq h \leq 10$ , $-16 \leq k \leq 16$ , $-42 \leq l \leq 42$	
Reflections collected	27461	
Independent reflections	4099 [R(int) = 0.0765]	
Completeness to theta = 28.38°	98.0 %	
Absorption correction	Semi-empirical from equivalents	
Refinement method	Full-matrix least-squares on F <sup>2</sup>	

Table BX. Crystal data and structure refinement for **4.6** (continued).

Data / restraints / parameters	4099 / 0 / 297
Goodness-of-fit on $F^2$	1.034
Final R indices [ $I > 2\sigma(I)$ ]	R1 = 0.0553, wR2 = 0.1338
R indices (all data)	R1 = 0.0947, wR2 = 0.1491
Largest diff. peak and hole	0.400 and -0.351 e/Å <sup>3</sup>

Table BY. Atomic coordinates ( $\times 10^4$ ) and equivalent isotropic displacement parameters (Å<sup>2</sup> $\times 10^3$ ) for **4.6**. U(eq) is defined as one third of the trace of the orthogonalized  $U_{ij}$  tensor.

	x	y	z	U(eq)
P(1)	4061(1)	1919(1)	1785(1)	28(1)
F(1)	2683(2)	1869(1)	1437(1)	43(1)
F(2)	4252(3)	3151(2)	1708(1)	64(1)
F(3)	2694(3)	2130(2)	2124(1)	60(1)
F(4)	5423(3)	1963(2)	2133(1)	74(1)
F(5)	3854(2)	680(1)	1859(1)	47(1)
F(6)	5398(2)	1691(2)	1442(1)	72(1)
O(1)	7679(2)	479(1)	725(1)	29(1)
O(2)	10600(2)	2651(1)	-129(1)	32(1)
N(1)	9227(2)	1731(2)	384(1)	23(1)
N(2)	8499(3)	3874(2)	1670(1)	27(1)
N(3)	6735(3)	4861(2)	1971(1)	31(1)
C(1)	9681(3)	1953(2)	-25(1)	23(1)
C(2)	8824(3)	1168(2)	-288(1)	20(1)
C(3)	8820(3)	1039(2)	-712(1)	25(1)
C(4)	7869(3)	222(2)	-871(1)	29(1)
C(5)	6948(3)	-421(2)	-613(1)	29(1)
C(6)	6962(3)	-292(2)	-183(1)	24(1)
C(7)	7922(3)	513(2)	-29(1)	18(1)
C(8)	8192(3)	862(2)	406(1)	21(1)
C(9)	9916(3)	2269(3)	745(1)	34(1)
C(10)	8683(3)	2879(2)	1001(1)	25(1)

Table BY. Atomic coordinates ( $\times 10^4$ ) and equivalent isotropic displacement parameters ( $\text{\AA}^2 \times 10^3$ ) for **4.6** (continued).

C(11)	9569(4)	3436(4)	1349(1)	56(1)
C(12)	7415(3)	4628(2)	1613(1)	27(1)
C(13)	7416(4)	4248(2)	2270(1)	39(1)
C(14)	8512(4)	3633(2)	2086(1)	39(1)
C(15)	5441(5)	5638(3)	2030(1)	67(1)

Table BZ. Bond lengths [ $\text{\AA}$ ] and angles [ $^\circ$ ] for **4.6**.

		C(5)-C(6)	1.393(4)
		C(5)-H(1)	0.92(3)
		C(6)-C(7)	1.380(3)
		C(6)-H(2)	0.93(3)
		C(7)-C(8)	1.485(3)
		C(9)-C(10)	1.516(4)
		C(9)-H(8)	0.97(4)
		C(9)-H(9)	0.97(4)
		C(10)-C(11)	1.511(4)
		C(10)-H(3)	0.95(3)
		C(10)-H(4)	0.94(3)
		C(11)-H(11)	0.86(4)
		C(11)-H(12)	1.03(5)
		C(12)-H(5)	0.89(3)
		C(13)-C(14)	1.327(4)
		C(13)-H(13)	0.89(3)
		C(14)-H(10)	0.89(3)
		C(15)-H(15A)	0.9800
		C(15)-H(15B)	0.9800
		C(15)-H(15C)	0.9800
		F(4)-P(1)-F(6)	90.90(14)
		F(4)-P(1)-F(3)	90.08(13)
		F(6)-P(1)-F(3)	178.75(13)
		F(4)-P(1)-F(2)	90.43(11)
		F(6)-P(1)-F(2)	90.13(13)
		F(3)-P(1)-F(2)	90.63(12)
		F(4)-P(1)-F(1)	179.60(12)
P(1)-F(4)	1.5806(18)		
P(1)-F(6)	1.5815(19)		
P(1)-F(3)	1.5864(19)		
P(1)-F(2)	1.589(2)		
P(1)-F(1)	1.5918(16)		
P(1)-F(5)	1.5980(19)		
O(1)-C(8)	1.212(3)		
O(2)-C(1)	1.207(3)		
N(1)-C(8)	1.390(3)		
N(1)-C(1)	1.398(3)		
N(1)-C(9)	1.462(3)		
N(2)-C(12)	1.316(3)		
N(2)-C(14)	1.376(4)		
N(2)-C(11)	1.464(4)		
N(3)-C(12)	1.314(3)		
N(3)-C(13)	1.357(4)		
N(3)-C(15)	1.459(4)		
C(1)-C(2)	1.482(3)		
C(2)-C(3)	1.379(3)		
C(2)-C(7)	1.389(3)		
C(3)-C(4)	1.392(4)		
C(3)-H(6)	0.91(3)		
C(4)-C(5)	1.388(4)		
C(4)-H(7)	0.92(3)		

Table BZ. Bond lengths [Å] and angles [°] for **4.6** (continued).

F(6)-P(1)-F(1)	89.36(11)	C(7)-C(6)-C(5)	116.7(2)
F(3)-P(1)-F(1)	89.65(11)	C(7)-C(6)-H(2)	118.0(18)
F(2)-P(1)-F(1)	89.87(10)	C(5)-C(6)-H(2)	125.2(18)
F(4)-P(1)-F(5)	90.20(11)	C(6)-C(7)-C(2)	121.8(2)
F(6)-P(1)-F(5)	89.90(12)	C(6)-C(7)-C(8)	130.2(2)
F(3)-P(1)-F(5)	89.33(11)	C(2)-C(7)-C(8)	108.0(2)
F(2)-P(1)-F(5)	179.37(11)	O(1)-C(8)-N(1)	124.8(2)
F(1)-P(1)-F(5)	89.50(9)	O(1)-C(8)-C(7)	129.0(2)
C(8)-N(1)-C(1)	111.69(19)	N(1)-C(8)-C(7)	106.16(19)
C(8)-N(1)-C(9)	124.3(2)	N(1)-C(9)-C(10)	114.6(2)
C(1)-N(1)-C(9)	123.6(2)	N(1)-C(9)-H(8)	104(2)
C(12)-N(2)-C(14)	107.7(2)	C(10)-C(9)-H(8)	114(2)
C(12)-N(2)-C(11)	125.4(3)	N(1)-C(9)-H(9)	109(2)
C(14)-N(2)-C(11)	126.8(3)	C(10)-C(9)-H(9)	111(2)
C(12)-N(3)-C(13)	108.8(2)	H(8)-C(9)-H(9)	104(3)
C(12)-N(3)-C(15)	125.0(3)	C(11)-C(10)-C(9)	108.9(2)
C(13)-N(3)-C(15)	126.2(3)	C(11)-C(10)-H(3)	106.5(19)
O(2)-C(1)-N(1)	125.0(2)	C(9)-C(10)-H(3)	112.6(18)
O(2)-C(1)-C(2)	128.9(2)	C(11)-C(10)-H(4)	109.5(17)
N(1)-C(1)-C(2)	106.0(2)	C(9)-C(10)-H(4)	110.1(18)
C(3)-C(2)-C(7)	121.6(2)	H(3)-C(10)-H(4)	109(2)
C(3)-C(2)-C(1)	130.3(2)	N(2)-C(11)-C(10)	114.5(2)
C(7)-C(2)-C(1)	108.0(2)	N(2)-C(11)-H(11)	107(3)
C(2)-C(3)-C(4)	117.0(2)	C(10)-C(11)-H(11)	113(3)
C(2)-C(3)-H(6)	122.0(19)	N(2)-C(11)-H(12)	103(3)
C(4)-C(3)-H(6)	120.9(19)	C(10)-C(11)-H(12)	112(3)
C(5)-C(4)-C(3)	121.3(2)	H(11)-C(11)-H(12)	106(4)
C(5)-C(4)-H(7)	117.4(17)	N(3)-C(12)-N(2)	108.9(2)
C(3)-C(4)-H(7)	121.3(17)	N(3)-C(12)-H(5)	125.3(17)
C(4)-C(5)-C(6)	121.5(2)	N(2)-C(12)-H(5)	125.6(17)
C(4)-C(5)-H(1)	119.0(17)	C(14)-C(13)-N(3)	107.3(2)
C(6)-C(5)-H(1)	119.5(17)	C(14)-C(13)-H(13)	131.6(19)
		N(3)-C(13)-H(13)	121.2(19)
		C(13)-C(14)-N(2)	107.4(3)

Table BZ. Bond lengths [Å] and angles [°] for **4.6** (continued).

C(13)-C(14)-H(10)	135(2)	N(3)-C(15)-H(15B)	109.5
N(2)-C(14)-H(10)	117(2)	H(15A)-C(15)-H(15B)	109.5
N(3)-C(15)-H(15A)	109.5	N(3)-C(15)-H(15C)	109.5
		H(15A)-C(15)-H(15C)	109.5
		H(15B)-C(15)-H(15C)	109.5

Table CA. Anisotropic displacement parameters ( $\text{\AA}^2 \times 10^3$ ) for **4.6**. The anisotropic displacement factor exponent takes the form:  $-2\pi^2 [h^2 a^{*2} U^{11} + \dots + 2 h k a^* b^* U^{12}]$

	U <sup>11</sup>	U <sup>22</sup>	U <sup>33</sup>	U <sup>23</sup>	U <sup>13</sup>	U <sup>12</sup>
P(1)	25(1)	37(1)	21(1)	3(1)	-3(1)	-6(1)
F(1)	44(1)	47(1)	37(1)	-10(1)	-20(1)	8(1)
F(2)	98(2)	43(1)	52(1)	12(1)	-26(1)	-26(1)
F(3)	69(1)	71(1)	41(1)	-24(1)	23(1)	-10(1)
F(4)	64(1)	95(2)	63(1)	38(1)	-43(1)	-41(1)
F(5)	57(1)	37(1)	45(1)	7(1)	-2(1)	1(1)
F(6)	46(1)	105(2)	65(1)	24(1)	31(1)	16(1)
O(1)	31(1)	35(1)	20(1)	3(1)	3(1)	4(1)
O(2)	25(1)	26(1)	46(1)	-2(1)	7(1)	-6(1)
N(1)	19(1)	27(1)	21(1)	-6(1)	0(1)	0(1)
N(2)	26(1)	31(1)	25(1)	-10(1)	0(1)	-2(1)
N(3)	36(1)	32(1)	25(1)	-8(1)	1(1)	2(1)
C(1)	18(1)	21(1)	29(1)	-3(1)	2(1)	5(1)
C(2)	17(1)	19(1)	24(1)	0(1)	1(1)	5(1)
C(3)	25(1)	28(1)	23(1)	1(1)	2(1)	6(1)
C(4)	30(1)	36(2)	20(1)	-7(1)	-2(1)	10(1)
C(5)	26(1)	26(1)	35(2)	-11(1)	-4(1)	1(1)
C(6)	23(1)	20(1)	29(1)	-2(1)	2(1)	3(1)
C(7)	16(1)	18(1)	21(1)	0(1)	0(1)	6(1)
C(8)	17(1)	25(1)	20(1)	-1(1)	-2(1)	7(1)



Table CA. Anisotropic displacement parameters ( $\text{\AA}^2 \times 10^3$ ) for **4.6** (continued).

C(9)	22(1)	47(2)	33(2)	-19(1)	-2(1)	1(1)
C(10)	24(1)	27(1)	23(1)	-4(1)	2(1)	1(1)
C(11)	28(2)	79(3)	60(2)	-47(2)	5(2)	-3(2)
C(12)	35(1)	28(1)	17(1)	0(1)	-1(1)	-6(1)
C(13)	55(2)	45(2)	17(1)	0(1)	4(1)	-7(2)
C(14)	49(2)	32(2)	36(2)	4(1)	-10(1)	3(1)
C(15)	67(2)	64(3)	69(2)	-28(2)	-3(2)	33(2)

Table CB. Hydrogen coordinates ( $\times 10^4$ ) and isotropic displacement parameters ( $\text{\AA}^2 \times 10^3$ ) for **4.6**.

	x	y	z	U(eq)
H(15A)	5381	6099	1786	100
H(15B)	5679	6062	2277	100
H(15C)	4392	5276	2067	100
H(1)	6350(40)	-960(20)	-727(8)	34(8)
H(2)	6370(30)	-700(20)	5(9)	34(8)
H(3)	8140(40)	3410(30)	845(9)	44(9)
H(4)	7900(40)	2420(20)	1113(9)	35(8)
H(5)	7130(30)	4900(20)	1369(8)	25(7)
H(6)	9420(40)	1460(20)	-883(9)	39(8)
H(7)	7830(30)	80(20)	-1152(8)	26(7)
H(8)	10790(50)	2700(30)	629(11)	60(11)
H(9)	10490(40)	1760(30)	914(11)	54(10)
H(10)	9250(40)	3160(30)	2172(10)	52(10)
H(11)	10280(50)	3040(30)	1472(12)	69(13)
H(12)	10200(60)	4090(40)	1247(14)	112(17)
H(13)	7110(40)	4310(20)	2534(9)	37(8)

## APPENDIX Q

### ABBREVIATIONS AND ACCRONYMS

Å Angstrom	calcd. Calculated
Anal. analysis	d doublet (NMR spectra)
$\alpha$ crystallographic unit-cell angle between axes <i>b</i> and <i>c</i>	lattice spacing (crystallographic)
$\beta$ crystallographic unit-cell angle between axes <i>a</i> and <i>c</i>	DMF dimethylformamide
$\gamma$ crystallographic unit-cell angle between axes <i>a</i> and <i>b</i>	DMSO dimethylsulfoxide
$\delta$ scale (NMR) ppm	ed edition
$\sigma$ bond referring to bonding between sigma orbitals	Ed. editor
$\pi$ bond referring to bonding between pi orbitals	ESI electro spray ionization
<i>a</i> crystallographic unit cell axis <i>a</i>	et. al. and others
<i>b</i> crystallographic unit cell axis <i>b</i>	<i>F</i> (000) scaling coefficient for structure
C celcius	factors
<i>c</i> crystallographic unit cell axis <i>c</i>	Fc calculated structure factor
	Fo observed structure factor
	h hour
	Hz hertz
	L general ligand

<i>J</i> nuclear spin-spin coupling	s singlet (spectrum)
constant through bonds	sat. saturated
m multiplet	t triplet (spectrum)
MeCN acetonitrile	t <sub>1/2</sub> half-life
MeOH methanol	THF tetrahydrofuran
min minutes	U temperature factor
mL milliliter	unsat. unsaturated
mmol millimole	wR <sub>2</sub> weighted residual based on I
m/z mass-to-charge ratio	
Nap naphthalene	
<i>n</i> -Bu <i>n</i> -butyl	
NHC N-heterocyclic carbene	
nm nanometer	
NMR nuclear magnetic resonance	
p page	
Ph phenyl	
pp pages	
ppm parts per million	
q quartet (spectral)	
R organic group	
<i>R</i> , <i>R</i> residual based on Fo	
ROP ring opening polymerization	
RT room temperature	